UNIVERSITY OF CALIFORNIA, MERCED

The Role of Heart Rate, Temperature, and Autonomic Nervous System Regulation Over Calcium Alternans in the Intact Mouse Heart

A dissertation submitted in partial satisfaction of the requirements for the degree of

DOCTOR OF PHILOSOPHY

in

Quantitative Systems Biology

by

Yuriana Aguilar

Committee in charge:

Dr. Nestor Oviedo, Chair

Dr. Ariel L. Escobar, Advisor

Dr. Jing Xu

Dr. Maria-Elena Zoghbi

2016

The Dissertation of Yuriana Aguilar is approved by, and it is acceptable in quality and form for publication on microfilm and electronically:

Dr. Nestor Oviedo, Chair Date

Dr. Ariel L. Escobar, Advisor Date

Dr. Jing Xu Date

Dr. Maria-Elena Zoghbi Date

University of California, Merced

2016

DEDICATION

I would like to dedicate this dissertation to my family. Thank you, Ana and Arturo Aguilar, for being the best supportive parents and bringing me from Mexico to get a better life. I know this degree is a fulfillment of the American Dream you envisioned. Thank you, Ismael Sanchez, for the love and patience you have shown and the years you have endured a messy home and cold meals while your wife spent hours in the lab. To Victoria Irene and the children to come, this hard work was to give you a better life.

TABLE OF CONTENTS

LIST OF FIGURES

LIST OF TABLES

ACKNOWLEDGEMENTS

The studies performed in this dissertation were funded by NIH grants (R01 HL-084487) to Dr. Ariel L. Escobar. Additional funding to Yuriana Aguilar includes: University of California Merced Fletcher Jones Fellowship (2015-2016), Quantitative Systems Biology Summer Research Fellowship (2014, 2015, 2016), Miguel Velez Fellowship (2014), and Rose R Ruiz Fellowship (2015, 2016).

I would like to thank Dr. Ariel L Escobar for investing his time, energy, and efforts into teaching me on a daily basis. I am so thankful that he opened the doors of his lab, his office, and his home to me at any time. I am very grateful for all the patience and guidance. The dynamic environment with the development of new techniques every year and new researchers from other labs in the United States and outside the states including Argentina, Spain, Uruguay, Mexico, and Brazil played an important role in my development as a young investigator. Even though I could not leave the United States, Dr. Escobar provided me with an international experience that showed me science is without borders. I could have never obtained this experience in any other lab. In addition, I am grateful for the instrumental diversity he provided within the lab allowing me to learn various techniques under one roof.

I would like to acknowledge and thank our collaborators for including me in their innovative projects: Josefina Ramos-Franco, M.D/Ph.D at the department of Molecular Biophysics and Physiology at Rush University, Chicago, Illinois, USA; Alicia Mattiazzi, M.D/Ph.D at Centro de Investigaciones Cardiovasculares at Universidad de La Plata, La Plata, Argentina; Julio A. Copello, Ph.D at the department of Pharmacology at Southern Illinois University School of Medicine, Springfield, Illinois, USA; Ye Chen-Izu, Ph.D at the department of Pharmacology, Biomedical Engineering and Medicine at University of California, Davis, Davis, California, USA.

I would like to thank the committee for their support and guidance over the years: Dr. Nestor Oviedo (Chair), Dr. Jing Xu, and Dr. Maria-Elena Zoghbi.

I am grateful to Dr. Marcela Ferreiro, Dr. Azade Voolstra, Dr. Mariana Argenziano, Micaela Lopez Alarcon, Gabriela Mazzocchi, Dr. Carlos Valverde, Dr. Juan Felice and Bernardo Zepeda for their help, guidance, and cheers.

Thank you to all the undergraduates for your amazing help and for keeping me company: Victoria To, Myriam Zavalza, Raveena Heer, Caryl Trisha Catacutan, Mira Patel, Morris Saravia, Sarah Butler, Andrew Cardozo, Matthew DiPietro, and Osman Farhad.

The Revival Center of Merced for the friendship and prayers. I've never done it alone.

YURIANA AGUILAR
yaguilar0207@gmail.com
yaguilar@ucmerced.edu

Education

PhD, University of California, Merced — Merced, CA 2012-2016
Quantitative and Systems Biology
Advisor: Dr. Ariel L. Escobar

B.S, University of California, Merced — Merced, CA 2007-2011
Biological Sciences
Emphasis: Human Biology

Internships and Research Experience

Ariel L. Escobar Laboratory, 2012-2016
Research: Explore the electrophysiology of an intact mouse heart and the development of T-wave alternans by focusing on two physiological variables: $[Ca^{2+}]$ and membrane potential.

Monica Medina Laboratory, 2009-2012
Research: Assessed the increasing ocean temperature's effect on coral health and their symbiotic organisms.

UC LEADS Internship, 2009-2010
Research: A two summer research experience engaged in innovative research with hands on training on various laboratory techniques. The first summer was at UC Merced studying corals. The second summer focused on biomedical science at a UC Davis atherosclerosis lab.

Community Scholars Internship, 2009-2010
Research: Evaluated health disparities in Merced and developed project to address them.

Conferences/Presentations

Biophysical Society, *Platform Presenter* — Los Angeles, CA 2016
Aguilar-Sanchez, Y., Saravia, M., Millet, J., Escobar, AL. *Fluorescence Local Field Optical Mapping (FLOM) of Ca^{2+} alternanses temperature dependency in intact perfused mouse hearts.*

Biophysical Society, *Poster Presenter* — Los Angeles, CA 2016
Aguilar-Sanchez, Y., Zavalza, M., To, V., Ramos-Franco, J., Escobar, AL. *L-type calcium and NCX currents during ischemia and reperfusion in intact mouse hearts.*

GradSlam Competition, *Platform Presenter* Merced, CA 2016
Runner up winner. *Towards predicting sudden cardiac death.*
QSB retreat, *Poster Presenter* Merced, CA 2014
Aguilar-Sanchez, Y., Zavalza, M., Escobar, AL. *Transmural autonomic regulation of ventricular action potentials and calcium signalling in intact mouse hearts.*
Biophysical Society, *Poster Presenter* San Francisco, CA 2014
Aguilar-Sanchez, Y., Zavalza, M., Escobar, AL. *Transmural autonomic regulation of ventricular action potentials and calcium signaling in intact mouse hearts.*
UC Merced Research Week, *Poster Presenter* Merced, CA 2013,2014
American Heart Association, *Attendant* Los Angeles, CA 2012
UC Davis UC LEADS, *Platform Presenter* Davis, CA 2010
University of California's Leadership Excellence through Advanced Degrees
UC LEADS Research Symposium, *Poster Presenter* Irvine, CA 2009
UC Merced Researh Week, *Poster Presenter* Merced, CA 2009
UC Merced UC LEADS, *Platform Presenter* Merced, CA 2009

Publications

Aguilar-Sanchez, Y., Fainstein, D., Mejia-Alvarez, R., Escobar, A. L. Local field fluorescence microscopy: imaging cellular signals in intact hearts. *J. Vis. Exp.* In press.

Ramos-Franco, J., Aguilar-Sanchez, Y. & Escobar, A. L. Intact heart loose patch photolysis reveals ionic current kinetics during ventricular action potentials. *Circ. Res.* **118**, 203–215 (2016).

Mattiazzi, A., Argenziano, M., Aguilar-Sanchez, Y., Mazzocchi, G. & Escobar, A. L. Ca2+ Sparks and Ca2+ waves are the subcellular events underlying Ca2+ overload during ischemia and reperfusion in perfused intact hearts. *J. Mol. Cell. Cardiol.* **79**, 69–78 (2015).

Awards and Distinctions

- UC Merced Fletcher Jones Fellowship, 2015-2016
- Rose R. Ruiz Fellowship, 2015, 2016
- UC Merced Quantitative Systems Biology Summer Research Fellowship, 2016
- UC Merced Quantitative Systems Biology Summer Research Fellowship, 2015
- Miguel Velez Fellowship, 2014
- UC Merced Quantitative Systems Biology Summer Research Fellowship, 2014
- UC Merced Quantitative Systems Biology Summer Research Fellowship, 2013
- UC Merced Grossman Award in Molecular Cell Biology, 2011
- Donald A. Strauss 10K Scholarship, 2010
- Chancellor's Honor List, 2007-2008, 2008-2009, 2009-2010, 2010-2011
- UC LEADS Internship, Summer 2009, 2010

- Community Scholars Internship, 2009-2010
- UC Merced Student of Excellence Award, 2008
- Lead Peer Health Educator Award, 2008
- County Bank/Community Foundation of Merced Scholarship, 2008
- Kim and Harold Louie Foundation Scholarship, 2007
- Comcast Leaders and Achievers Scholarship, 2007

Community and University Service

Teaching Assistant,
Physiology for Engineers Lab, Spring 2015
Preparatory Chemistry 001 Discussion, Spring 2014, Fall 2014
Contemporary Biology 1 Lab, Fall 2013
Introduction to Molecular Biology 2 Discussion, Spring 2013

SACNAS Chapter Grad Student Advisor, 2012-2013
Society for Advancement of Chicanos and Native Americans in Science

Technical Skills

Experienced in:
Fluorescent microscopy (pulse local field), conducting whole organ experiments in Langendorff setting, sharp glass microelectrode measurements of membrane potential, culturing bacteria and induction of protein expression, PCR, Genotyping mice and corals, Extracting DNA, NanoDrop Spectrophotometer, ELISA, Centrifugating blood samples, Micropipette puller
Programs: OriginPro, ImagingSource, ImageJ, Microsoft Excel/Word, ChemiDocs, LabView, Axon

Familiar with:
RT-PCR, Western Blotting, Protein cloning, Cell culturing, Pulse Electroporation
Programs: ELISA Analysing program

Beginning in:
Cell sorting via FACS, Microarrays
Programs: FACS (analysing FACS data)

ABSTRACT:

THE ROLE OF HEART RATE, TEMPERATURE, AND AUTONOMIC NERVOUS SYSTEM REGULATION OVER CALCIUM ALTERNANS IN THE INTACT MOUSE HEART

Yuriana Aguilar

Doctorate of Philosophy in Quantitative Systems Biology, with an emphasis in Cardiac Electrophysiology at the University of California, Merced, 2016

T-wave alternans are alternating beat-to-beat changes in the morphology of the electrocardiographic T-wave. Despite being the only indicator of ventricular fibrillation leading to sudden cardiac death (SCD), the molecular mechanisms of alternans remain unclear. At the cellular level, the beat-to-beat changes in the T-wave are paralleled with beat-to-beat changes in the electrical repolarization duration (action potential duration (APD) alternans) and in the myoplasmic Ca^{2+} levels (Ca^{2+} alternans). The study presented in this thesis aimed to understand how T-wave alternans are generated by assessing how the two cardiac properties, electrical (measured as the action potential) and contractile (Ca^{2+} dynamics, measured as Ca^{2+} transients), change under conditions favoring alternans. Research has pointed to the mishandling of Ca^{2+} as the source of T-wave alternans. However, the precise cause of this mishandling has not been established. In this thesis, we assessed three variables that modulate the handling of intracellular Ca^{2+}: heart rate (HR), temperature, and autonomic nervous system (ANS) regulation. Studying these variables will allow us to determine what mishandling occurs in the presence of Ca^{2+} alternans. Tachycardia, or increased HRs, is a condition that favors the genesis of T-wave alternans. Thus, HR was used to induce alternans and to study what changes occur in the cardiac properties as the HR is increased. Since temperature dramatically affects the handling of intracellular Ca^{2+} content, we also assessed how temperature modulates Ca^{2+} alternans. In addition, the role of the ANS on Ca^{2+} alternans was studied because it is the body's primary method of changing the HR and it also modulates Ca^{2+} cycling that may affect alternans. We hypothesized that insufficient Ca^{2+} re-uptake by the sarcoplasmic reticulum (Ca^{2+} storage sites inside the cell) during increased HRs, hypothermia, or ANS dysfunction produces Ca^{2+} alternans. Consequently, Ca^{2+} alternans cause beat-to-beat alternations in the AP repolarization leading to T-wave alternans. The major conclusion from this thesis is that increases in the HR and colder temperatures (conditions favoring alternans) primarily affect the Ca^{2+} transient relaxation. These results point to the importance of the SR re-uptake mechanisms in the genesis of Ca^{2+} alternans. The ANS, in particular the sympathetic nervous system, is capable of reducing Ca^{2+} alternans by improving the re-sequestering of intracellular Ca^{2+} into the SR. Thus, targeting SR-Ca^{2+} reuptake may be a possible intervention method in the treatment of T-wave alternans before SCD occurs.

Graduate Advisor: Dr. Ariel L. Escobar
Committee Chair: Dr. Nestor Oviedo

LIST OF ABREVIATIONS

Symbol	Definition
Ca^{2+}	Calcium
Na^{+}	Sodium
K^{+}	Potassium
Cl^{-}	Chlorine
ECC	Excitation Contraction Coupling
CICR	Calcium Induced Calcium Released
RyR	Ryanodine Receptor
SERCA	Sarcoendoplasmic reticulum Ca^{2+}-ATPase
PLN	Phospholamban
SR	Sarcoplasmic Reticulum
T-tube	Transverse tubule
AP	Action Potential
APD	Action Potential Duration
APD30	Action Potential Duration at 30% Repolarization
APD70	Action Potential Duration at 70% Repolarization
APD90	Action Potential Duration at 90% Repolarization
ECG	Electrocardiogram
ANS	Autonomic Nervous System
NS	Nervous System
PKA	Protein Kinase A
AC	Adenylyl Cyclase
β-AR	Beta-adrenergic Receptor
cAMP	Cyclic Adenosine Monophosphate
ATP	Adenosine Triphosphate
I_{Ca}	Ca^{2+} current
I_{Na}	Na^{+} current
I_{K}	K^{+} current
I_{to}	Transient outward K^{+} current
ACh	Acetylcholine
M2	Muscarinic receptor 2
I_{KACh}	ACh-sensitive K^{+} current
NCX	Sodium Calcium Exchanger
TP	Time to Peak
RT	Rise Time
DT	Decay Time
HD	Half Duration
HR	Heart Rate
Ry	Ryanodine
Tg	Thapsigargin
FLOM	Fluorescence Local Field Optical Mapping
LPP	Loose Patch Photolysis
PLFFM	Pulsed Local Field Fluorescence Microscopy

PREFACE:

Sudden cardiac death (SCD) is defined as a natural death that occurs less than 1 hour after the onset of cardiopathic symptoms.[1] It is responsible for 12% of all natural deaths in the United States killing between 250,000 to 450,000 people each year.[2] SCD is sudden and, unfortunately, a precise way to predict a fatal episode is not available. However, a pathological electrocardiogram caused by alterations of ventricular electrical repolarization can be an increased risk predictor for cardiac arrhythmias leading to SCD.

Cardiac arrhythmias are a set of pathological conditions in which the heart rate (HR) varies in a broad range leading to a defective mechanical function of the organ. A subset of arrhythmias can be triggered by an increase in the HR named tachycardia. During tachycardia, the heart's electrical properties can be dramatically modified. Some of the changes in the organ's electrical properties include changes in the repolarization that affect the T-wave of the electrocardiogram and can lead to ventricular fibrillation. The T-wave depicts the underlying electrical repolarization phase of the action potential in the ventricular wall. Specifically, the T-wave is defined by the difference in the repolarization between the endocardium and epicardium of the ventricle.

Tachycardia can induce changes in the T-wave morphology termed T-wave alternans. T-wave alternans are beat-to-beat alternations in the amplitude of the T-wave. T-wave alternans are induced by transmural alternations in the repolarization of the ventricular action potential (AP). Drastic changes in the HR are directly associated with the T-wave alternans. The rhythmicity of the heart is highly regulated by the activity of the two branches of the autonomic nervous system (ANS): sympathetic nervous system (NS) and parasympathetic NS. While the sympathetic NS increases the HR, the parasympathetic NS decreases it. However, the molecular regulation of key cardiac properties across the ventricular wall, where T-wave alternans manifest, is not very clear. Since HR is associated with the genesis of T-wave alternans, it is likely that the ANS affects the appearance of alternans.

The fact that T-wave alternans are very temperature dependent has led researchers to speculate that T-wave alternans are triggered by a highly metabolic demanding process. In the heart the cycling of intracellular Ca^{2+} is highly metabolic and temperature dependent because it relies in ATP hydrolysis to reuptake the Ca^{2+} released from Ca^{2+} storage sites (sarcoplasmic reticulum, SR). Indeed, alternans in the intracellular Ca^{2+} dynamics can be easily observed in hypothermic scenarios. The central focus of this thesis is to understand why alternans have a strong temperature dependency and how changes in the intracellular Ca^{2+} dynamics can be coupled to the electrical properties of the membrane to affect AP duration alternans. The central **hypothesis of this thesis is that insufficient Ca^{2+} uptake by the sarcoplasmic reticulum during increased HRs, hypothermia, or autonomic nervous system dysfunction produces Ca^{2+} alternans. Ca^{2+} alternans produce beat-to-beat alterations in the AP repolarization leading to T-wave alternans.**

In this thesis, we used a whole series of innovative *ex vivo* experimental tools recently developed by our lab to study both the membrane ionic currents underlying T-wave alternans and the thermodynamics of these fatal arrhythmias. The multidisciplinary experimental approach presented in this dissertation will help us to elucidate how HR, temperature, and ANS regulation modulate cardiac properties in the intact heart, and could serve as a framework to study the molecular mechanisms of T-wave alternans leading to ventricular arrhythmias and SCD.

Chapter 1: Background and significance.

This chapter delves into the electromechanical function of the heart. It provides a background for understanding the molecular mechanisms behind the electrical and contractile properties at the cellular level with focus on intracellular Ca^{2+} and action potential signals. The heterogeneous nature of the heart is explored and the differences between the two layers of the ventricular wall is highlighted because it is the origin of T-wave alternans. Finally, the HR, temperature, and ANS regulation are assessed as variables that may influence the genesis of T-wave alternans by altering the intracellular Ca^{2+} dynamics.

Chapter 2: Innovative experimental approaches.

This chapter explicitly describes the novel tools used to address the questions in this project. Commonly used molecular fluorescent probes (Rhod 2 for Ca^{2+} and di-8-ANEPPS for membrane potential) were complemented with innovative set-ups such as Pulsed Local Field Fluorescence Microscopy (PLFFM), Loose Patch Photolysis (LPP) which can also measure membrane currents, and Fluorescence Local Field Optical Mapping (FLOM) that together allow the dissection of underlying molecular events at the intact heart level. The work was done on intact, isolated whole hearts from mice. All of the experiments in this thesis were conducted under physiological settings in the intact organ. Using the intact heart allowed us to assess cellular changes, but in cells that continue to be electrically, mechanically, and metabolically coupled.

Chapter 3: Effects of HR over AP and Ca^{2+} alternans across the ventricular wall.

Since HR is associated with the genesis of T-wave alternans, we explored the effects of HR over two cardiac properties, electrical and contractile, by measuring AP and Ca^{2+} transient (the transient increase in cytosolic $[Ca^{2+}]$), respectively. In this chapter, we aimed to test the hypothesis that HR affects the morphology of the AP and Ca^{2+} transients unevenly across the ventricular wall and this leads the heart to develop T-wave alternans. We assessed any differential effects produced by changes in the HR across the ventricular wall by recording AP and Ca^{2+} transients at the epicardium and endocardium with the PLFFM technique. Additionally, general transmural differences (without changes in the HR) in the AP and intracellular Ca^{2+} dynamics were quantified to unveil the causes of any differential regulation. Finally, in order to understand the molecular bases underlying heterogeneities of AP and Ca^{2+} dynamics in the epicardium and endocardium regions, we used RT-PCR to measure the expression level of genes coding for key Ca^{2+} handling proteins.

Chapter 4: Temperature dependency of intracellular Ca^{2+} dynamics and alternans.
The genesis of T-wave alternans is dependent on the intracellular Ca^{2+} handling, which affects the electrical repolarization, and consequently changes the T-wave from beat-to-beat. Many of the functions of key proteins involved in the cycling of intracellular Ca^{2+} are temperature dependent. In this chapter, we aimed to test the hypothesis that hypothermia promotes Ca^{2+} alternans by impairing Ca^{2+} re-sequestering. We induced cold temperatures with a cooling unit attached to the FLOM apparatus and measured changes in the Ca^{2+} transients at a constant HR and also at increasing HRs. The assessment of temperature on the Ca^{2+} transient was used to shed light on which mechanism (Ca^{2+} release/reuptake) are critical in the genesis of Ca^{2+} alternans which are more prevalent at colder temperatures. The simultaneous measurement of temperature and HR allowed us to evaluate the temperature dependency of Ca^{2+} alternans.

Chapter 5: Regulation of sympathetic NS on AP and Ca^{2+} dynamics across the ventricular wall and its effect on alternans.
In the body, the increases in the HR are mediated by stimulation from the sympathetic NS. Since increased HR predisposes the tissue to generate alternans, we wanted to understand how the sympathetic NS regulates the AP and Ca^{2+} dynamics across the ventricular wall. The cascade of events triggered by beta-adrenergic stimulation leads to the phosphorylation of multiple key Ca^{2+} handling proteins. In this chapter, we aimed to test the hypothesis that beta-adrenergic stimulation reduces Ca^{2+} alternans by accelerating Ca^{2+} re-uptake into the SR. We assessed changes in the Ca^{2+} transients (by using the PLFFM) upon beta-adrenergic stimulation to decipher if there is a differential sympathetic NS regulation across the ventricular wall and exactly how this affects the Ca^{2+} dynamics. Finally, in this chapter, we determined if the changes produced by beta-adrenergic stimulation, mimicking sympathetic NS activation, affected Ca^{2+} alternans.

Chapter 6: Regulation of parasympathetic NS on AP and Ca^{2+} dynamics across the ventricular wall and its effect on alternans.
The parasympathetic NS closely regulates effects produced by the stimulation of the sympathetic NS including changes in HR and Ca^{2+} dynamics. In addition, the parasympathetic NS can have an effect over the K^+ conductance at the myocyte level. It is well known that upon parasympathetic stimulation, acetylcholine interacts with muscarinic receptors associated with a G_i protein that inhibits adenylyl cyclase and affects Ca^{2+} dynamics by blocking protein kinase A activation. However, the G_i βγ-subunit can also dissociate and interact with an heteromeric K^+ channel (I_{KACh}).[3–5] In this chapter, we aimed to test the hypothesis that parasympathetic NS (by muscarinic stimulation) reduces the duration of the AP by activating a K_{ACh} channel and not by Ca^{2+} dynamics. We assessed the effects of muscarinic receptor stimulation on the AP and Ca^{2+} dynamics (using PLFFM) across the ventricular wall. We also measured Ca^{2+} currents (using LPP) and Ca^{2+} alternans after muscarinic stimulation. We finally blocked I_{KACh} with the bee venom tertiapin[6] and evaluated the changes in AP morphology.

CHAPTER 1: Background and Significance

The heart is only the size of the fist, but vital to our existence. It was once viewed as the source of our soul. After extensive years of research, it's unveiled to be an impressively well-coordinated electromechanical pump that dictates the nourishment of the rest of the body by the circulation of blood. The body is highly dependent on the function of the heart. Therefore, it is imperative to understand the physiological molecular processes in this dynamic organ in order to shed light on dysfunctions occurring during pathophysiologies that compromise the circulation of blood. In this chapter, we will delve into the historical advances in research associated with the heart, review its mechanism of action, understand the molecular basis and intricate interaction of the two key cardiac properties, electrical and contractile. Finally, we will study a pathological condition in which the electrical signal changes from beat-to-beat. We will assess how the role of heart rate, temperature, and autonomic nervous system modulates this arrhythmogenic phenomenon.

1.1 Research revealed the anatomy and functioning of an electrical pump

Interest in the heart began around 500BC when it was thought as the keeper of the soul. The heart was believed to be the center of conscious and control, instead of the brain. It was and continues to be a symbol of love and emotions. In 1628, William Harvey simply stated that the function of the heart was the propulsion of blood.[7] Although it may seem that Harvey had reduced the heart's image, he actually opened the door to the discovery of the central organ in circulation.

Dissections of the heart, such as those drawn by Leonardo Da Vinci (1452-1519) from 1511-1513 revealed the anatomical structures of the organ. Davinci's drawing "Heart of an ox" (1513)[8] is more vivid than many diagrams in today's physiology textbooks (**Fig. 1.1**). Although Da Vinci's meticulous dissections showed the heart is divided into right and left sections, he was unable to grasp circulation beyond the flow of blood through the valves.[9] Harvey correctly concluded that the right side of the heart connected with the left through the lungs and the left to the right through body tissues.[7]

Fig. 1.1

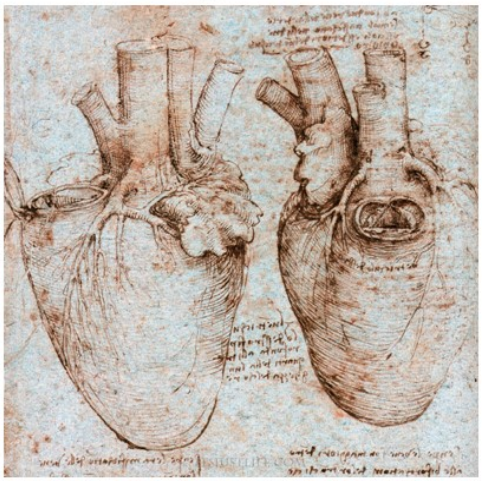

Fig. 1.1 Da Vinci (1513). Heart of an Ox. Acquired from Royal Collection.

Over the years, the sum of anatomical evaluations have revealed that, in pairs, the four chambers (two left/right ventricles and two left/right atriums) of the heart are connected by two atrioventricular (mitral and tricuspid) valves. The mitral valve acts between the left atrium and ventricle, while the tricuspid valve connects the right atrium

and ventricle. In addition, there are two more valves in the ventricles: pulmonary and aortic. The pulmonary valve is located in between the right ventricle and the pulmonary artery. The aortic valve is in the ventricle at the base of the aorta.

The heart's primary function is the propulsion of blood

The anatomy and structure of the heart led to speculations of its mechanism of action. Physiologists would speculate how the organ functioned inside the body, but it was through vivisections that people actually saw it in action. Vivisection was a method used in which the individual would have their chests open while they were still alive and conscious.[10] It was performed on animals and humans, particularly prisoners. Despite the horrific methods, the functioning of the heart was revealed as an impressive muscular pump.

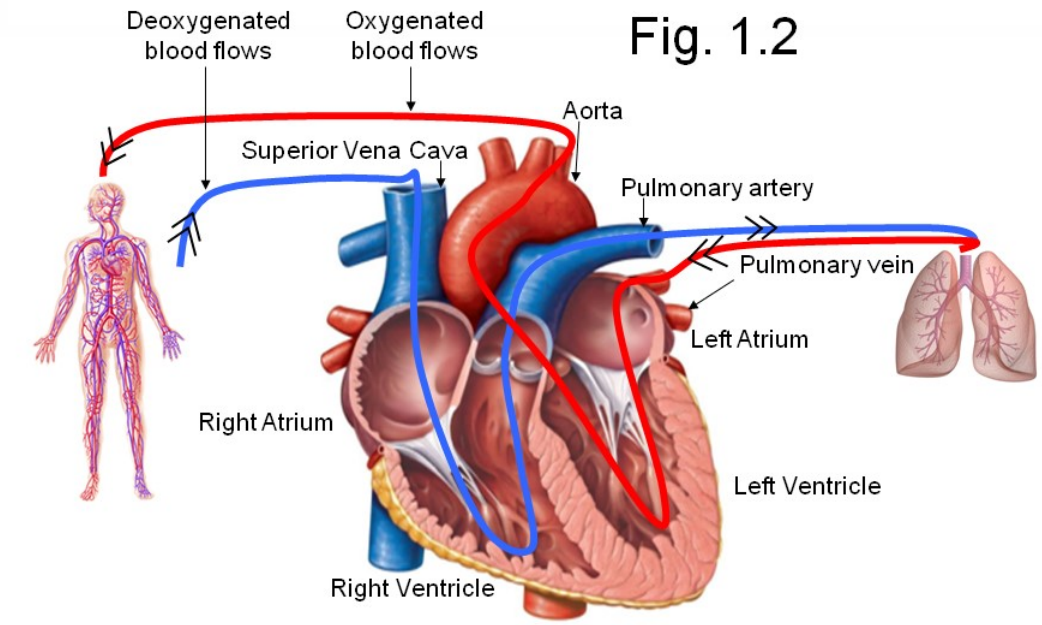

Fig. 1.2 The heart is the central organ in circulation, pumping deoxygenated blood through the lungs to get oxygenated and then returning it to the body. Double arrows indicate the direction of blood flow. (Heart acquired from online source).

The pump is the central organ in circulation that contracts in a well-coordinated manner pumping blood to the rest of the body. During Harvey's times, it was thought that blood was pumped from the heart and absorbed by the body.[7] However, Harvey discerned that this implied that the body had to produce and absorb a very large volume, continuously. He postulated that it had to be a circular flow. Now, it is well known that the body produces and circulates the same blood for a couple of days before regenerating new blood.[11,12] The circular flow of blood consists of deoxygenated blood coming from the body into the right atrium through the superior and inferior vena cava (**Fig. 1.2**). When the right atrium

contracts, blood gets pumped into the right ventricle and then ejected, through the pulmonary valve, into the pulmonary artery towards the lungs, where it gets oxygenated. From the lungs, oxygenated blood returns through the pulmonary veins into the left atrium. When the left atrium contracts, blood goes into the left ventricle and is then pumped into the aorta to the rest of the body.

Interestingly, when the blood is ejected through the aorta, blood enters the left and right coronary arteries that branch from the base of the aorta. This permits blood to flow through vasculature beds within the myocardium. The anatomy of the central organ in the circulatory system is interesting because not only is the heart circulating blood with every beat, but it is simultaneously able to supply itself with richly oxygenated blood. This network of vasculature is the basis of our intact mouse studies presented in this thesis (described in **Methods**).

The heart is an electromechanical pump

The heart is capable of serving as the leader in the propulsion of blood by functioning as a pump. It is an electrically-driven electromechanical pump by the action of its intrinsic electrical activity. Luigi Galvani, 1791, discovered that it was the electrical stimulation that caused a frog heart to contract.[13] In 1842, Carlo Matteucci showed that, even at rest, the heart possessed electrical activity and that each heart beat consisted of an electrical stimulation.[13,14] Gabriel Lippman made it possible to record the overall electrical signal in the heart when he built a capillary electrometer in 1872, which Augusto Waller (1887) used, producing the beginning electrocardiograms (ECGs). The ECG is now a part of the basic equipment of any medical facility. It can help in the diagnosis of many cardiac pathologies which present unique ECG waveform abnormalities associated with specific illnesses.[15–18]

The heart is able to work as a pump by the coupling of two very important properties: electrical and contractile. Its paced contraction is controlled by the generation of electrical signals that propagate through different regions of the organ in a highly coordinated manner. As the signal travels through the organ, it produces a cascade of cellular events allowing contraction. When the coordination of the electrical signal is lost, it is the basis of multiple pathologies.

The electrical stimulus originates in the sinoatrial (SA) node, which is the dominant pacemaking region of the heart.[19] The SAN cells are located within the right atrium. These electrical waves travel first to the right atrium and then to the left atrium (**Fig. 1.3**). As the electrical wave reaches the atrioventricular node, there is a delay to allow the ventricles to completely fill before contracting. Afterwards, the electrical signal propagates to the Bundle of His and then follows two branches called the Bundle Branches along the ventricle. These branches then innervate the ventricular walls and are referred to as Purkinje Fibers. The ventricular wall consists of three layers: the epicardium is the outermost, endocardium is the innermost, and midmyocardium is in between the epicardium and endocardium.[20–22] The Purkinje Fibers allow the propagation of the electrical stimulus in an inward-outward fashion across the ventricular wall by stimulating

first the endocardium and then the epicardium region. Contraction of the ventricles is then initiated resulting in the ejection of blood from the ventricles into either, the aorta and the rest of the body or the pulmonary artery and towards the lungs. For this thesis, we focus on the electrical propagation between the epicardium and endocardium region.

Fig. 1.3

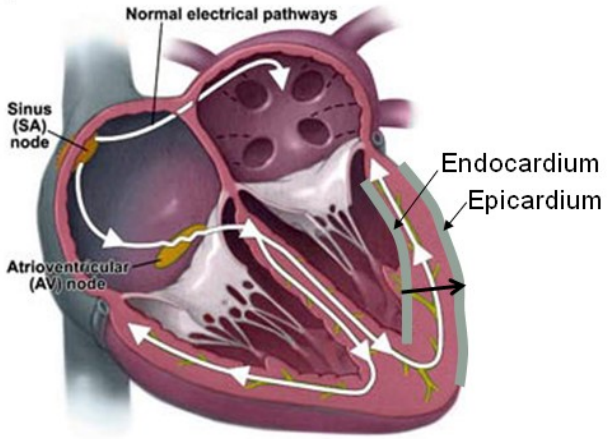

Fig. 1.3: The heart propagates the electrical signal from the SA node to the ventricular region to initiate contraction. (Heart acquired from online source.)

1.2 Molecular basis underlying the electrical activity of the pump

The electrical property of the heart is critical in defining its function at the organ level. At the cellular level, this electrical activity is measured as the action potential (AP). The AP is a signal produced by the transient change in membrane voltage over a short period of time. This change in voltage is a result of the movement of charges arising from charge-bearing ions (Na^+, K^+, Ca^{2+}) across the plasma membrane of a cell. The membrane acts like a capacitor and is able to separate charges such that the voltage difference across is the membrane potential (V_m). When the cell is in an unexcited state, the voltage difference is the resting membrane potential.[23]

The AP is caused by the transient change in charge distribution induced by the movement of ions across the membrane. This movement of ions is due to the activation of voltage-sensitive proteins that act as channels allowing the temporary permeability of very specific ions. The electrical stimulus propagates through the heart and when it reaches these voltage-gated channels it induces a change in their conformation such that their open state is more stable and the probability of staying open increases. This results in the subsequent movement of ions across the plasma membrane.

However, the opening of the channels is not enough to move the ions across the membrane. The movement of ions is driven by the charge separation across the membrane. This creates an electric potential in which the inside of the cell is more negative and the outside more positive, thus attracting positively charged ions into the cells. Additionally, the intra- and extracellular space have different ion concentrations producing a chemical gradient for each ion. Therefore, the ions move to produce the AP due to their electrochemical gradient when voltage-sensitive channels are activated. The ions involved

in the AP and their concentrations in the intra- and extracellular space are shown in **Table 1.1**.

Ion	Intracellular [mM]	Extracellular [mM]	Equilibrium potential (mV)
Na^+	14	140	60
K^+	155	4	-95
Ca^{2+}	$1x10^{-4}$ (100nM)	2	130

Table 1. Intracellular and extracellular concentration of ions

The AP has a depolarization segment in which the V_m becomes rapidly positive and a repolarization segment where it is returning to the resting membrane potential (~ -80mV).[24,25] These two segments can be divided into five distinct phases produced by specific ions moving across the membrane. **Fig. 1.4** shows the five phases of the AP and thoroughly represents all the underlying currents in the formation of the AP obtained by simulated experiments in human ventricular myocytes.

Phases of the action potential

The first phase (phase 0) of the AP is due to the rapid influx of Na^+ ions through voltage-gated Na^+ channels ($NaV_{1.5}$). The influx of positive ions moves the V_m towards the Na^+ equilibrium potential (60mV). The equilibrium potential for Na^+ (E_{Na}) refers to the V_m where there is an equilibrium of ions in the intra- and extracellular space such that the net movement is zero. At these potentials, the influx of Na^+ is decreased. Also, the voltage-gated Na^+ channels enter an inactive phase and are unable to pass Na^+ current (I_{Na}).[26]

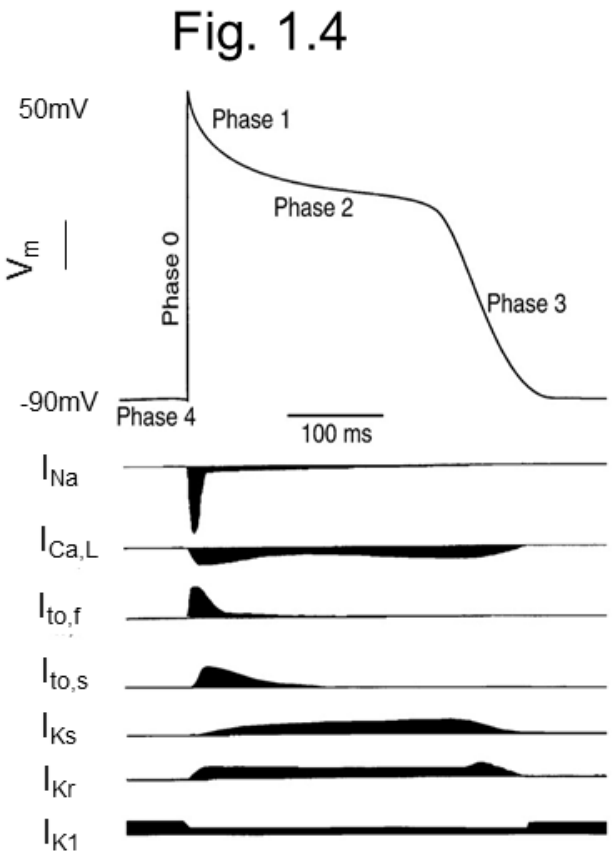

Fig. 1.4: Simulated underlying ionic currents during a human ventricular AP. (Modified from Nerbonne & Kass, 2005).

The repolarization segment of the AP has multiple phases. There is a rapid repolarization during phase 1 produced by the opening of fast, voltage-gated K^+ channels (K_v). Specifically, these channels produce the fast transient outward current of K^+ (I_{to}), which can be divided into a fast inactivating current, $I_{to,f}$, and a slow inactivating current, $I_{to,s}$.[27–29] These channels are formed from Kv4.2/4.3 subunits for $I_{to,f}$ [27,28] and Kv1.4 for $I_{to,s}$.[27,28,30] The change in voltage, caused by the rapid depolarization of I_{Na}, opens these K^+ channels. The movement of K^+ ions out of the cell, driven by the electrochemical gradient, lead to the repolarization of the AP. Thus far, phase 1 constitutes the inactivation of voltage-gated Na^+ channels and the consequent rapid activation and inactivation of an outward K^+ current.

Interestingly, phase 1 has solely been associated with I_{to}, but recently, voltage-gated Ca^{2+} channels (L-type, $CaV_{1.2}$) have been shown as active during this phase.[31] They open in phase 0, but the current is minimal due to the low driving force when the V_m is closer to the Ca^{2+} equilibrium potential (130mV). However, during phase 1, as the V_m moves away from the equilibrium potential the driving force increases and there is a rapid increase in the current through these L-type Ca^{2+} channels ($I_{Ca,L}$) right before closing by voltage-dependent deactivation.[31] It was thought that $I_{Ca,L}$ was mainly involved during phase 2 and the genesis of Ca^{2+}-induced-Ca^{2+}-release (CICR), described below.[32,33] However, Ferreiro et al. [34] showed that, in mice, phase 2 occurs at membrane potentials more negative than -40mV. These L-type Ca^{2+} channels are inactive at -40mV in mice,[35,36] therefore they cannot be part of phase 2.

Nevertheless, phase 2 is affected by the $I_{Ca,L}$ during phase 1. The influx of Ca^{2+} through the L-type channels activates proteins (ryanodine receptors, RyR) located in the membrane of intracellular Ca^{2+} storing organelles (Sarcoplasmic Reticulum, SR). This Ca^{2+} influx that triggers the SR to release Ca^{2+} is referred to as CICR. [37–39] CICR is the primary process behind contraction (described below) and greatly affects the AP morphology in phase 2.

The increase of intracellular [Ca^{2+}] due to the massive Ca^{2+} release from the SR activates a protein in the sarcolemma called the Na^+-Ca^{2+} exchanger (NCX). This exchanger uses the energy stored in the electromechanical gradient of Na^+ to exchange 3 Na^+ ions from outside the cell for 1 Ca^{2+} ion from the cytosol.[26] The net influx of a positive charge across the membrane into the cell produces an electrogenic effect and shifts the voltage towards a positive potential. As a result of this non-electro-neutral exchange, the membrane depolarizes. However, the membrane does not spike like in phase 0 because K^+ currents are also being activated. The balance between the two currents, I_K and I_{NCX} (not shown in **Fig. 1.4**), is what causes the phase 2 dome or plateau.

During phase 3 and 4, multiple K^+ currents come into play in order to repolarize the membrane towards the resting potential. There are two main classes of K^+ currents, outward and inward rectifiers referred to as I_K and I_{K1}, respectively. Both of these allow the efflux of K^+ from the cell due to its high intracellular K^+ concentration. However, these are activated during different phases of the AP at different V_m values. When the membrane

potential is more positive than the resting potential, outward rectifiers have an increase in current while the inward rectifiers only have a small outward current.[26] On the contrary, the inward rectifiers have an increase in inward current at potentials more negative than the resting membrane or hyperpolarized potentials. The delayed outward I_K consists of rapid and slow components, I_{Kr} and I_{Ks}, respectively. The activation of these currents move the membrane potential near the K^+ equilibrium potential.

Finally, during phase 4, the primary current is the inward rectifier K^+ current, I_{K1}.[26] This current maintains the resting membrane potential.

1.3 The propagation of the electrical signal produces changes in intracellular [Ca^{2+}] that lead to contraction of the heart

The electrical activity of the pump is coordinated with a force-generating mechanical action that contracts the heart. This coordination is referred to as Excitation Contraction Coupling (ECC) (**Fig. 1.5**).[40] In essence, ECC is what makes the heart an electromechanical organ. Overall, ECC consists of the propagation of an electrical signal

Fig. 1.5

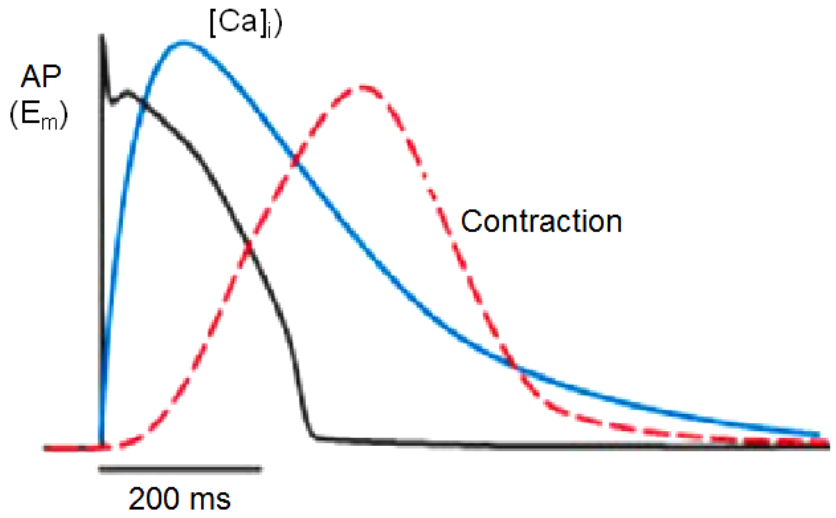

Fig. 1.5: ECC showing the time course between an electrical signal and the consequent increase in intracellular Ca^{2+} followed by the contraction. (Acquired from Bers, 2002).

that causes an increase in intracellular [Ca^{2+}] which, consequently, produces a mechanical contraction. **Fig. 1.6** shows the molecular events underlying ECC.

During ECC the propagation of an excitatory stimulus increases the open probability of voltage gated L-type Ca^{2+} channels such that there is an increase in the Ca^{2+} current ($I_{Ca,L}$). ECC happens primarily at T-tubules, which are invaginations of the surface

sarcolemma (seen in **Fig. 1.6**). T-tubules contain nine times more Ca^{2+} channels than the surface sarcolemma.[41] The sarcolemma is the plasma membrane of myocytes and the surface sarcolemma is all the sarcolemma excluding T-tubules.[41] These L-type Ca^{2+} channels are co-localized with RyRs[41] which are activated by Ca^{2+}. RyRs are proteins in the membrane of intracellular Ca^{2+} storing organelles known as the sarcoplasmic reticulum (SR). The small influx of Ca^{2+} through the L-type Ca^{2+} channels activates the co-localized RyRs to release Ca^{2+} into the cytosol.[42] This Ca^{2+} influx that triggers the SR to release Ca^{2+} is referred to as CICR.[37–39]

CICR is the link between electrical and contractile stimulation. When the cell undergoes CICR, there is a transient increase in cytosolic Ca^{2+} (100nM at diastole to 1µM at systole) due to the massive Ca^{2+} release from the SR.[43] The free Ca^{2+} interacts with sarcomeric proteins to produce contraction. The sarcomeres are the units involved in contraction and consist of thin and thick filaments. Thin filaments are made of actin and regulatory proteins, such as Troponin C, and thick filaments are made of myosin. The Ca^{2+} binds to regulatory proteins on the thin filament inducing a conformational change, which reveals the myosin binding sites on the actin enabling the myosin heads on the thick filament to bind.[41]

Fig. 1.6

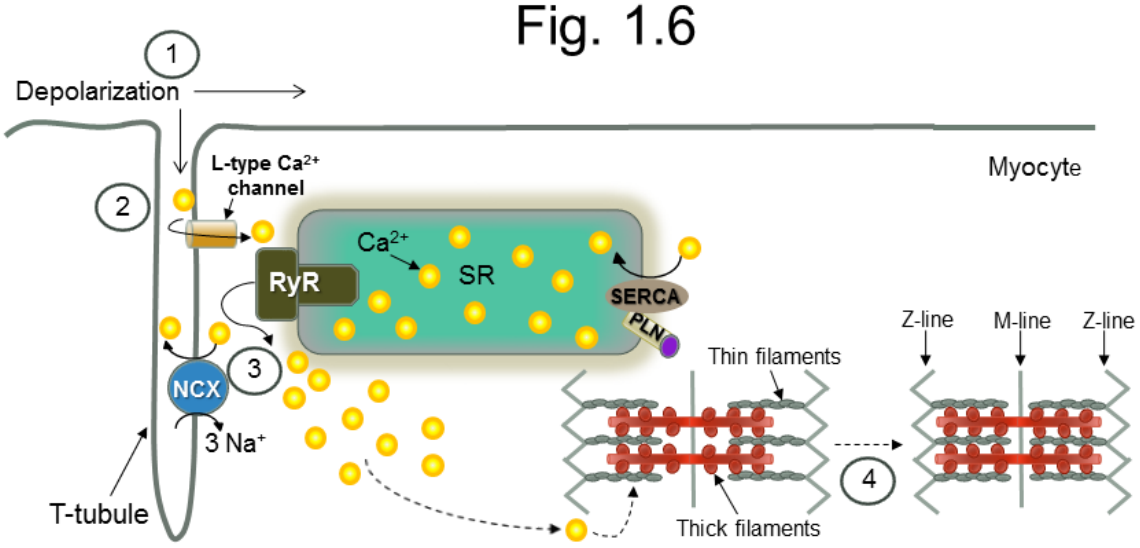

Fig. 1.6: ECC initiates when the (1) depolarization of the membrane opens the voltage-gated L-type Ca^{2+} channels that allow the influx of Ca^{2+} into the myocyte (2). The small influx of Ca^{2+} triggers the massive release of Ca^{2+} from the SR (3), producing a drastic increase in intracellular [Ca^{2+}]. This Ca^{2+}, consequently, binds to troponin C on the thin filaments to begin contraction (4).

A contraction occurs when the thick filaments pull the thin filaments. This is done by forming crossbridges and undergoing the cross bridge cycle. The cross bridge cycle is initiated in the presence of Ca^{2+} to produce a contraction. During this cycle, the bound

myosin hydrolyzes ATP to generate a stroke, sliding the actin filaments closer together.[26,41] Specifically, the myosin head releases actin when it binds ATP. The hydrolysis of ATP causes the myosin to move into a cocked-state. In this cocked-state, the myosin head is able to bind to actin. After binding to actin, myosin releases the phosphate to produce the power stroke. This causes the sliding of the actin filament over the myosin filaments towards the M-line (seen in **Fig. 1.6**). After the power stroke, myosin releases the ADP and is then ready for ATP to produce another cycle resuling in the sliding of the filaments.

Overall, contraction is the shortening of the distance between the Z-lines in a sarcomere in response to the transient increase in intracellular Ca^{2+}. The phase in which the heart contracts is known as systole.

Contraction is stopped when the heart's intracellular cytosolic Ca^{2+} concentration decays. There are a series of proteins whose purpose is to either expel Ca^{2+} from the cytosol across the sarcolemma (NCX) or across the sarcolemma reticulum into the SR (Sarcoendoplasmic Reticulum Ca^{2+}-ATPase (SERCA)). The cytosolic Ca^{2+} concentration is reduced by the action of the SERCA pump. It uses 1 molecule of ATP to pump 2 Ca^{2+} into the SR.[26,44,45] The activity of this pump is tightly regulated by phospholamban (PLN) and PLN is regulated by Protein Kinase A (PKA). When PKA phosphorylates PLN, the inhibition over SERCA is removed and SERCA is able to pump Ca^{2+} into the SR.[26] Free intracellular cytosolic Ca^{2+} is also reduced by the extrusion of Ca^{2+} through the action of NCX. The Ca^{2+}-ATPase pump removes Ca^{2+} from the cytosol into the extracellular space.[41] It also diffuses to other regions of the cell and binds to other proteins, such that there is less free cytosolic Ca^{2+}. The relaxation phase of the heart in which there is no force-generation is referred to as diastole.

1.4 Different AP morphologies throughout the heart

Different regions of the heart have varying electrical signals and consequently, the AP waveforms are very dissimilar.[28] This is attributed to the non-homogeneous distribution of proteins involved in the movement of ions across the membrane of individual cardiac cells. According to the specialized function of the region, the expression level of the genes coding for these proteins increases or decreases. **Fig. 1.7** shows the AP waves for the different regions of the heart. The AP at the SA node has a more triangular waveform than the ventricle, which presents a plateau phase.

Even within the same region there are different AP waveforms for subcategorized layers, which is the case for the ventricular wall. The endocardium has a slower repolarization in comparison with the epicardium waveform. This is a result of the varying density of ion channels producing changes in the membrane potential. In the case of the ventricle, the epicardium has a higher density of potassium channels producing a larger I_{to},[46] which results in a faster repolarization of phase 1. However, the density of these ion channels is the only clearly known distinction between the epicardium and endocardium. A thorough comparison of the kinetic differences in the repolarization has been performed by researchers, but on wedges or isolated cells.[20] Thus, these experiments may not be a precise representation of what happens in the intact heart because in the organ, the cells are

Fig. 1.7

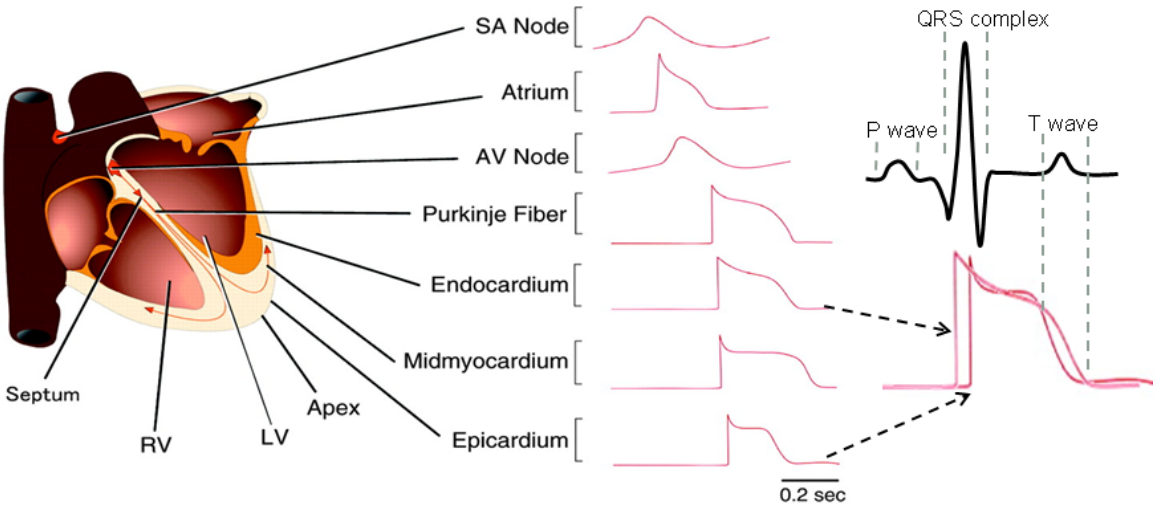

Fig. 1.7: The propagation of the electrical activity in the heart is characterized, at the cellular level, by the AP. The AP waveform presents very diverse morphologies in the different regions of the heart. (Modified from Nerbonne & Kass, 2005).

electrically, mechanically and metabolically coupled. In this thesis, we thoroughly assess electrical activity and Ca^{2+} handling differences between the epicardium and endocardium. Additionally, we complement electrophysiological experiments with molecular biology to unveil if there are any heterogeneities in the expression of Ca^{2+} handling proteins.

The AP is a measure of the membrane voltage changes over a small period of time caused by the movement of ions in a cardiomyocyte. Thus, the AP reports the electrical activity in one cell. However, the electrocardiographic signal can depict the overall electrical activity in the whole organ. This global-like view of the organ's electrical activity is an important tool in assessing cardiac pathologies associated with dysfunctions in specific regions of the heart. The different waves in the ECG signal indicate the electrical

activity depolarizing and repolarizing the organ tissues (**Fig. 1.7**). The P-wave represents the electrical depolarizing signal in the atrium. The QRS-complex represents the depolarization of the ventricular region. Finally, the T-wave is representative of the repolarization of the ventricles. More specifically, the T-wave is generated from the difference in repolarization between the epicardium and endocardium layer of the ventricular wall (shown overlapping in **Fig. 1.7**).

1.5 T-wave alternans as an indicator of SCD

Many pathologies are associated with particular wave patterns in the ECG.[15–18] For example, distinct changes in the T-wave have been linked to abnormal ventricular rhythms or ventricular fibrillation leading to sudden cardiac death (SCD).[47–52] It is used as a medical prognosis for an episode of SCD. Specifically, when the T-wave alternates from high to low amplitudes from beat-to-beat, it is referred to as T-wave alternans. The presence of T-wave alternans has been correlated to an increase risk for abnormal rhythms or arrhythmias.[53–55] Since the T-wave is the repolarization differences between the layers of the ventricular wall, then this implies that the electrical activity is changing from beat-to-beat. The rhythm of the organ is critical to its function and any changes from beat-to-beat can compromise its ability to circulate blood.

T-wave alternans are known to be frequency dependent and appear at higher HRs.[55,56] This implies that increases in the HR changes the dynamics of the electrical activity in the ventricular wall. Actually, experiments conducted by Verrier et al.[57] suggested that higher HRs amplify the repolarization heterogeneity across the ventricular wall and since the T-wave is a representation of this difference, it is affected. However, the precise mechanism by which the repolarization changes is unknown. Recording transmural APs can shed light on what is causing the changes in the repolarization in the different regions. The morphology of the recorded AP signal depicts the underlying movement of ions. The frequency induced changes in the AP phases may make it possible to decipher the cellular events leading to the genesis of alternans as the frequency is increased.

Ca^{2+} mishandling underlies T-wave alternans

Recent findings have shown that an underlying cause of T-wave alternans is the mishandling of intracellular Ca^{2+}.[58–62] Specifically, experiments conducted by Lab and Lee[62] in isolated ferret papillary muscles were the first to measure and observe that free intracellular [Ca^{2+}] alternated at the same time as the pressure changed from beat-to-beat (mechanical alternans). Their studies suggested that Ca^{2+} was behind the mechanical alternans. The mishandling of intracellular Ca^{2+} is reflected as beat-to-beat changes in the myoplasmic Ca^{2+} levels such that there is a Ca^{2+} transient with a high amplitude followed by one with a lower amplitude. These changes from beat-to-beat dramatically affect the contraction of the heart producing a strong contraction followed by a weaker one.

In addition, the Ca^{2+} mishandling also affects the AP waveform. Indeed, changes in the Ca^{2+} dynamics affect the AP due to their interconnectivity, specifically by NCX activity. If there is a high concentration of myoplasmic Ca^{2+}, this will facilitate the NCX

to exchange Ca^{2+} because the gradient between the extracellular and intracellular [Ca^{2+}] is less. When there is a low cytosolic Ca^{2+} level, the NCX will continue to work but less efficiently due to the large [Ca^{2+}] gradient. During Ca^{2+} alternans, the intracellular [Ca^{2+}] alternates between a high and low concentration resulting in different levels of NCX exchange. Since NCX activity produces an electrogenic effect, the AP repolarization duration changes from beat-to-beat (AP duration alternans).

Thus, in trying to understand T-wave alternans, the real question to be addressed is what is causing the changes in the myoplasmic Ca^{2+} levels from beat-to-beat. The Ca^{2+} handling is highly regulated in the heart by key proteins part of the CICR process. Together, these proteins cycle the intracellular Ca^{2+}. The L-type Ca^{2+} channel allows Ca^{2+} into the cell. The RyR releases Ca^{2+} from the SR. SERCA re-sequesters Ca^{2+} into the SR and NCX extrudes Ca^{2+} from the cell. For every beat, these proteins are responsible for Ca^{2+} handling. This thesis aims to understand how increases in the HR change the Ca^{2+} transient in order to decipher which part of the Ca^{2+} cycling becomes mishandled at increasing HRs.

Temperature affects Ca^{2+} handling

The heart's function can be altered by metabolic stresses which can consequently affect the generation of T-wave alternans.[63] Metabolic impairments can occur during hypothermia causing the heart to go into cardiac arrest.[63–67] Many physiological processes are temperature-dependent, including E-C coupling and CICR. Intracellular Ca^{2+} dynamics, aside from being frequency-dependent, are also temperature-dependent.[68] L-type Ca^{2+} channels,[69,70] the NCX,[34,71,72] and SERCA[45] have all been shown to be affected by temperature. As previously mentioned, these proteins are involved in the shuffling of Ca^{2+}. Consequently, temperature may affect Ca^{2+} content in the regions where these proteins govern.

Since Ca^{2+} dynamics are the underlying causes of AP duration (APD) alternans and T-wave alternans, then temperature may be critical in the generation of alternans. In order to further understand which molecular players are critical in the mishandling of Ca^{2+} that produces alternans, it is important to evaluate Ca^{2+} transient kinetic changes under conditions that increase the risk for alternans: HR and temperature. In this thesis, we aim to evaluate the temperature dependency of intracellular Ca^{2+} dynamics during normal and alternating conditions to thoroughly assess where and how Ca^{2+} mishandling occurs.

1.6 The Autonomic Nervous System affects Ca^{2+} cycling

Although the heart can act as an independent organ with its own pacemaker activity and contraction, it is highly regulated by the Autonomic Nervous System (ANS). The innervation by the ANS and the local or systemic releases of neurotransmitters modulate the cardiac properties, Ca^{2+} dynamics and electrical activity. The effects over these properties induced by the ANS can be further specified and subdivided into: HR (chronotropism), contractility (inotropism), mechanical relaxation of the organ (lusitropism) and velocity of electrical signal propagation (dromotropism). These are all

variables that may be involved in the development of T-wave alternans by modulating Ca^{2+} dynamics.

The ANS is divided into two branches: parasympathetic NS and sympathetic NS. The sympathetic NS produces a positive effect in the chronotropism, inotropism, lusitropism, and dromotropism while the parasympathetic NS has a negative effect. This thesis studies the ANS control across the ventricular wall over the cardiac properties, Ca^{2+} dynamics and electrical activity, in order to gain insights over the modulation of these properties and any possible effects on alternans.

Sympathetic NS affects Ca^{2+} dynamics by PKA activation

The sympathetic NS acts by releasing neurotransmitters (epinephrine, norepinephrine) systemically through the adrenal medulla or locally via neuron terminals. The heart has Beta-1-Adrenergic Receptors (β-AR) throughout the different regions (SA node, AV node, ventricles) that allow it to respond intracellularly by the binding of extracellular epinephrine or norepinephrine. At the cellular level, the sympathetic NS stimulation affects the intracellular Ca^{2+} handling by activating protein kinase A.

The binding of epinephrine or norepinephrine to β-ARs leads to the activation of the Guanyl protein (G-protein) G_s which is then able to dissociate into an $G\alpha_s$ and $G\beta\gamma_s$ subunit. $G\alpha_s$ then binds to and activates Adenylyl Cyclase (AC). AC converts adenosine triphosphate (ATP) into cyclic adenosine monophosphate (cAMP). The increased levels of cAMP in the cell leads to the binding of cAMP to the regulatory subunit of PKA, liberating the catalytic subunit to start phosphorylating multiple proteins inside the cell.[73]

It is by the activation of PKA and its subsequent phosphorylation of several key Ca^{2+} handling proteins (**Fig. 1.8**) that the sympathetic stimulation modulates the CICR signaling and affects the inotropicity, chronotropicity, and lusitropism. PKA phosphorylates L-type Ca^{2+} channels increasing their open probability (P_O) (inotropism). Since it is open for a longer time, more Ca^{2+} enters promoting CICR[74]. In addition, PKA phosphorylates the Ca^{2+} release channel (RyR) in the SR and increases the time the channel is open, thus more Ca^{2+} is released. In particular, PKA can phosphorylate two residues, S-2030 and S-2808. S-2808 phosphorylation increases RyR P_O, promoting a SR Ca^{2+} leak that finally decreases CICR.[75,76,77] To compensate for this release, PKA also phosphorylates PLN (S-16). Phosphorlyated, PLN cannot inhibit SERCA anymore allowing SERCA to uptake more Ca^{2+} into the SR (lusitropism).

In addition, PKA can also phosphorylate hyperpolarization-activated cyclic neuclotide-sensitive (HCN) channels responsible for the funny current (I_f).[78] In the SA node, this current is particularly important in modulating the HR (chronotropism) by changing the slope of the diastolic depolarization. During sympathetic NS stimulation, the slope of the depolarization becomes steeper, requiring less time to reach a threshold and fire an AP such that there is an increase in AP firing rate (increase in HR). [79]

In summary, the sympathetic NS's cascade of events affects three key proteins involved in the cycling of intracellular Ca^{2+} (L-type Ca^{2+} channel, RyR and SERCA). Together, the phosphorylations by PKA due to a sympathetic NS stimulation affect the Ca^{2+} handling and HR. Specifically, it helps in the cycling of intracellular Ca^{2+}. If alternans are due to the mishandling of the Ca^{2+} dynamics, then sympathetic NS stimulation may improve the efficiency of the shuffling of intracellular Ca^{2+} and thus eliminate alternans. Some researchers have shown this is true in canine[80] and cat myocytes.[81,82] However, others have shown that blocking sympathetic NS stimulation is protective against alternans. Thus, there is no consensus in the field.

The role of sympathetic regulation over electrical properties and Ca^{2+}signaling is well established in isolated myocytes.[83,84] Callewaert et al. measured Ca^{2+} transients in isolated rat ventricular myocytes in the presence of epinephrine. Their experiments suggested that epinephrine produces a greater CICR by increasing: the influx of Ca^{2+}, SR Ca^{2+} release, and SR Ca^{2+} reuptake. However, little is known about the catecholaminergic regulation of Ca^{2+} transients and electrical activity across the ventricular wall under

Fig. 1.8

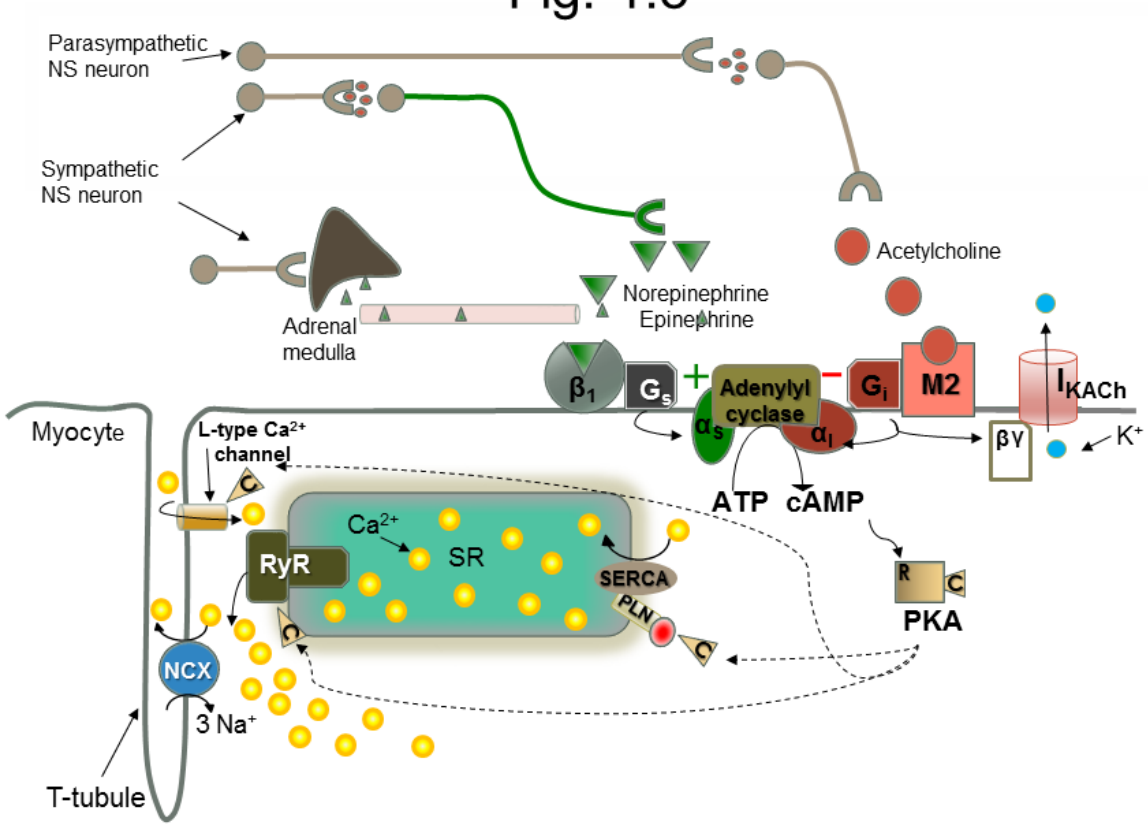

Fig. 1.8: The sympathetic and parasympathetic NS pathways intersect at adenylyl cyclase, while one activates, the other inactivates, respectively. PKA activation phosphorylates multiple Ca^{2+} regulatory proteins involved in ECC.

physiological conditions in the intact heart. Since Ca^{2+} handling is being implied as the underlying cause of T-wave alternans, we will assess how the sympathetic NS modifies the Ca^{2+} handling and its effects over alternans.

Parasympathetic NS affects Ca^{2+} dynamics by PKA inhibition and K^+ conductance

The parasympathetic NS produces opposite effects than those produced by the sympathetic NS branch. It causes a negative lusitropic, ionotropic, and chronotropic effect. In addition, parasympathetic NS acts only by releasing its neurotransmitters locally through terminal endings in the tissue. Preganglionic parasympathetic neurons release ACh to stimulate nicotinic receptors in the post-ganglionic parasympathetic neurons. The post-ganglionic neurons locally release acetylcholine which binds to muscarinic 2 (M2) receptors (**Fig. 1.8**).

At the cellular level, the binding of ACh to M2 receptors produces a cascade of events to inhibit PKA activation.[85] M2 receptors are associated with a G_i protein. When bound by ACh, G_i dissociates into $G\alpha_i$ and $G\beta\gamma_i$ subunits. The $G\alpha_i$ subunit binds to AC and inhibits its action so that ATP is not turned into cAMP and PKA is unable to get activated. If PKA is not active, then there is no phosphorylation of key Ca^{2+} handling proteins. Also, the $G\beta\gamma_i$ can interact with a K^+ channel (I_{KACh}) and increase its open state to produce an outward K^+ current.[4,5,86] In the SA node, the activation of these channels causes the resting membrane potential to become hyperpolarized. The hyperpolarization results in a decrease in the HR because it takes longer for the cell to reach the threshold to fire an AP. This effect of I_{KACh} over HR is in addition to those produced by the activity of HCN channels. Under parasympathetic NS stimulation, PKA activation is inhibited and is therefore unable to phosphorylate the HCN channels. This results in a decrease in I_f such that the slope of the diastolic depolarization is decreased producing a lower HR.

The regulatory effect of the parasympathetic NS stimulation over the HR and I_{KACh} is well accepted in the atrial region. However, the parasympathetic NS, and its regulation over the ventricular region is very obscure. This is due to the low innervation of parasympathetic NS neurons present in the ventricular region. Recently, it was shown that vagal innervation exists in the ventricle, but it is 80% less innervated than the atrium.[87] Due to the low innervation, some researchers have proposed non-specific inhibition of the parasympathetic NS in the heart because they believe it will only affect the innervation of the atriums. [87]

Although the parasympathetic and sympathetic NS each have direct innervation and thus regulation of the heart, their pathways intersect at AC. The sympathetic regulation acts via a G_s protein stimulating the AC while the parasympathetic regulation acts via a G_i protein inhibiting AC. Vagal inhibition over sympathetic NS activity is relatively strong such that a small vagal stimulation can really block sympathetic NS activity of greater magnitude.[88] Since the parasympathetic NS regulation is inhibitory, it can only inhibit what is already active. In the research presented here, we use an intact mouse heart that has been extracted from the body and no longer has the circulation of catecholamines. We assess

what happens when we restore the circulation of the catecholamines in the intact hearts. Specifically, in this thesis, we aim to evaluate how Ca^{2+} dynamics and the AP are affected under parasympathetic NS and sympathetic NS stimulation through ACh receptor or β-ARs agonists, respectively.

In summary, the ANS affects the HR in the body by affecting the current through HCN channels in the SA node. The sympathetic NS increases HR, while the parasympathetic NS decreases it. Since HR is a variable affecting the genesis of T-wave alternans, we want to evaluate how the ANS is capable of modifying the HR without producing alternans in nonpathological situations. This will be done by assessing effects of sympathetic and parasyampthetic NS stimulation over AP and Ca^{2+} transients under constant HR conditions in the absence of alternans. In addition, alternans will be induced by increasing the HR and then evaluating the effect of sympathetic and parasympathetic NS stimulation. These experiments will help us to understand how the ANS interacts with ECC and CICR processes. The effects of ANS regulation on AP and intracellular Ca^{2+} dynamics will be evaluated. Finally, since the ANS interacts with and modulates the handling of intracellular Ca^{2+}, in this thesis we will evaluate how stimulating these regulatory pathways affects the Ca^{2+} alternans.

SIGNIFICANCE:

The heart is the central organ in the circulatory system. Malfunctions in the organ have the potential to produce systemic damage throughout the body due to its critical role in circulating oxygen rich blood and removing waste. The heart is able to work as a pump by two properties: electrical (AP) and contractile (Ca^{2+} dynamics). The electrical is measured as the AP and the contractile is produced by the rise and fall of intracellular Ca^{2+} levels. These two properties are strictly coordinated to enable the activity of this electromechanical pump. Since the function of this organ entails the precise timing of complex processes at the cellular lever, there are multiple places where problems can arise in the cascade of events involved in every beat. For example, changes in the Ca^{2+} dynamics can affect both the mechanical and electrical activity of the organ, which in turn modify the circulation.

T-wave alternans, or beat-to-beat alternations of the amplitude of the electrocardiographic T-wave, is one scenario in which the underlying cause is the mishandling of intracellular Ca^{2+}.[60,89] It is characterized by a large myoplasmic Ca^{2+} level followed by one of smaller amplitude. These alternans are highly arrhythmogenic and can cause ventricular fibrillations, leading to sudden cardiac death (SCD). Every year, SCD kills between 250,000 to 450,000 people in the United States.[1] Since SCD is sudden, a clinical method to predict a fatal episode and intervene is imperative to saving lives. Recent research points to T-wave alternans as the warning signals for cardiac arrhythmias leading to SCD.[47–52] However, the molecular mechanisms of T-wave alternans have not been significantly unveiled to develop clinical interventions.

The main significance of this project is that the research suggests that the re-sequestering of Ca^{2+} into the SR is an important factor in the development of T-wave alternans in the ventricular wall, where T-wave alternans occur. The scope of this thesis provides physiological recordings (AP and Ca^{2+} transients) and molecular biological experiments (mRNA expression) to fully capture heterogeneities involved in Ca^{2+} handling in the ventricular wall. The results presented here explicitly compare the intracellular Ca^{2+} handling differences between the epicardium and endocardium layers of the ventricular wall under conditions favoring the genesis of alternans. Consequently, these experiments may provide significant insights on how these two layers handle Ca^{2+} differently. Since Ca^{2+} mishandling is the cause of alternans, then these experiments may help guide the development of tissue-specific therapeutic agents for treating and preventing T-wave alternans.

This thesis significantly evaluates three unique variables that affect T-wave alternans including: heart rate (HR), temperature, and the ANS's regulation of the heart. Tachycardia, or increased heart rates (HRs), predisposes the heart to develop T-wave alternans. Temperature dramatically affects the handling of intracellular Ca^{2+} content,[68] which is attributed to be the underlying cause of alternans.[58–61] The ANS modulates the Ca^{2+} cycling and changes the HR. This thesis will allow us to understand how the ANS can modify the AP and Ca^{2+} transient under constant HR (non-alternating) and when the HR is

increased to produce alternans. Together, these three variables and their effects on cardiac properties may reveal key proteins responsible for the development of T-wave alternans leading to SCD.

From the technical point of view, this dissertation presents significant advances in electrophysiological techniques. The project employed the use of innovative techniques developed by our lab to assess specific properties that conventional tools used in the field were unable to do, especially for the intact heart. These techniques enabled us to evaluate cardiac properties from whole hearts, but with resolutions at the myocyte level. In this thesis, we present results that have been published using these techniques. This provides the unique opportunity to introduce new tools with multiple applications in various research areas including the cardiovascular field. Aside from the techniques developed, using the intact organ was a more sophisticated model in studying T-wave alternans than experiments conducted on wedges or isolated cells. All the recordings presented here are an accurate representation of cellular activity because myocytes continued to be electrically, mechanically, and metabolically coupled in the intact mouse heart. In addition, this study shows the susceptibility of mice hearts to develop T-wave alternans, *ex vivo*, revealing their utility as fine models to study this phenomenon.

CHAPTER 2: Materials and Methods

The heart is an organ where the main contracting cells, the cardiomyocytes, are mechanically, electrically, and metabolically coupled.[31,90–93] This functional and structural connectivity critically defines the electromechanical driven pumping activity of the organ. Thus, any study that aims to test mechanistic hypothesis within a physiological framework needs to consider these unique interactions. It has been shown that multiple cardiac properties including spontaneous releases of Ca^{2+} are different when comparing isolated cells to whole heart experiments.[94] Therefore, in this doctoral thesis, an intact perfused heart approach was used as the main experimental model to test the central hypothesis of the dissertation.

Intact beating hearts were functionally maintained using a Langendorff perfusion apparatus. This approach allowed us to study molecular and cellular events at the whole organ level. By using this approach, the cardiomyocytes were kept in a physiological environment within the syncytium of the heart. The two key physiological properties studied were $[Ca^{2+}]$ and membrane potential. These properties are critical in defining the function of the organ. In order to monitor these properties at the cellular level, fluorescent molecular probes were perfused through the coronary vessels to enter the cells of the heart. These fluorescent probes change the rate at which they emit photons as a function of the magnitude of the AP or Ca^{2+} transient.

These emitted photons were then detected with three state-of-the art innovative techniques that allowed us to evaluate the excitability and Ca^{2+} dynamics on an intact perfused heart. The pulsed local field fluorescence microscopy (PLFFM) technique has been used by our lab to assess physiological parameters by exciting exogenous probes and detecting the light emitted by these fluorescent indicators present in the tissue.[34,95–97] In the PLFFM technique, the excitation and emitted light propagates through a multimode fiber optic placed on the surface of the heart. In this thesis, a beam splitter allowed us to use two fiber optics which facilitated the recording of fluorescence from two distinct anatomical regions of the heart. The recording of two regions allowed us to do a comparative study of physiological properties, $[Ca^{2+}]$ and membrane potential, in different places within the intact heart.

The PLFFM technique permitted us to evaluate how dissimilar molecular properties in different histological layers influence the underlying dynamics of $[Ca^{2+}]$ and membrane potential in the intact heart. The PLFFM detected a spatial average fluorescence emitted by the fluorescent probes within a region defined by the fiber optic diameter. Some physiological processes require the assessment of how the signal propagates from one region of the tissue to another. In order to study the temporal propagation and/or spatial distribution of physiological signals, the fluorescence from multiple sites needed be recorded simultaneously.

For the simultaneous study of multiple sites we used a recently engineered fluorescent local field optical mapping (FLOM) imaging technique. This technique

allowed us to detect the fluorescence emitted from the fluorescent indicators and evaluate [Ca^{2+}] and membrane potential at various locations. FLOM is very similar to PLFFM, but instead of using a fiber optic, the excitation and emitted light from the exogenous probes travels through an optical conduit. An optical conduit is a solid bundle of many optical fibers fused together in a cylindrical form. The bundle transmits a fluorescent image produced by the conduit in contact with the tissue. This back transmitted image is finally refocused onto a fast recording camera. Since the spatial distribution of some physiological processes including the Ca^{2+} transient kinetics, action potential propagation and Ca^{2+} alternans are affected by temperature, a device to generate a temperature gradient was fabricated on top of the FLOM apparatus. This attachment consists of a Peltier-controlled metallic cold finger that was positioned around the optical conduit. The cool site of the attachment can be positioned in contact with the epicardial layer of the heart. This procedure induced a temperature gradient on the tissue that can define the kinetic properties of Ca^{2+} transients that finally were recorded by FLOM.

The assessment of intracellular [Ca^{2+}] and membrane potential gives only a reduced view of the biophysical picture of ECC at the whole heart level. To expand this view, it is necessary to understand how Ca^{2+} fluxes across the plasma membrane define both the changes in intracellular [Ca^{2+}] and the time course of the ventricular AP. This essential piece of information was obtained by measuring, for the first time, transmembrane ionic currents at the intact heart level. With this in mind, we developed a third state-of-the-art technique, the loose-patch photolysis (LPP). The LPP technique can assess the electrophysiological properties of transmembrane currents during a self-generated AP at the whole organ level.[31]

The LPP set-up consisted of an epifluorescence arrangement like PLFFM that facilitated the simultaneous measurement of intracellular [Ca^{2+}] or membrane potential optically at the same time as ionic currents. In addition, the LPP set-up employs a UV laser to break UV-sensitive exogenous caged-compounds that can be selected to either activate or inhibit ionic currents flowing through specific types of ionic channels. The macroscopic current across the plasma membrane is measured through a loose patch glass pipette positioned on the surface of the heart. The selected UV sensitive caged-compounds are highly specific in activating/inhibiting the current through a single type of ionic channel. Therefore, the difference between the recorded current from a control trace that has not been exposed to a UV pulse and one where the caged-compound has been broken with the UV light pulses is proportional to the current produced by the activation/inhibition of a specific type of ionic channel under the loose patch pipette. In this thesis, the LPP technique was used to assess the underlying Ca^{2+} mediated currents through the L-type Ca^{2+} channel and NCX activated by photosensitive compounds in intact hearts.

Finally, this methodology chapter explains how the hearts were extracted from the thoracic cavity, how they were maintained in the Langendorff set-up using retro-perfusion, and how recordings were obtained and processed. It describes in detail the three innovative tools that have been developed and can be the future standard for assessing cardiac function at the cellular level using an intact organ.

2.1 Intact mice hearts were stabilized in a Langendorff perfusion apparatus

All of the experiments in this thesis were completed using mouse as the animal model. The use of mice as a model for studying cardiac physiology and pathophysiology presents several advantages and disadvantages. The mouse heart rate is one order of magnitude higher than human. The disparity in HR between humans and mouse affects many physiological parameters in the organ. This makes it difficult to directly extrapolate results obtained in mice to human. In spite of the HR differences, the mouse ventricular AP morphology presents a very remarkable similitude when compared with those obtained from cats,[98] dogs,[99,100] and humans.[101] Specifically, mice epicardial AP presents a stereotypic spike and dome morphology also present in the human heart's AP.[34,101] Nevertheless, the use of mice as the model limits research studies to focus on basic function of underlying molecular phenomena during health and disease. However, the use of mice makes it possible to biologically engineer transgenic models explicitly expressing or knocking-out proteins to test function in the intact heart under disease states. Researchers using human hearts are limited to studying small pieces of tissue, not the intact organ. One advantage of using mice hearts is that experimenting with their hearts is more feasible due to their heart's size. The small size facilitated the *ex vivo* functional maintaining of the organ with less perfusate required than a larger mammal's heart. Also, using a smaller heart with fluorescent molecular indicators is more cost-effective.

The mice used were Balb/c 8 week-old males purchased from Charles River Labs (Wilmington, MA) and were maintained in accordance with the National Institutes of Health Guide for the Care and Use of Laboratory Animals (NIH Publication No. 85–23, Revised 1996). The hearts were extracted after cervical dislocation was employed. This euthanization method avoided the use of anesthetics which could cause side effects on the heart. The Institutional Animal Care and Use Committee of the University of California Merced approved this euthanization method (# 2008–201).

Working with the intact organ is difficult due to the precautions taken to not damage any structure of the whole heart. During the dissection of the heart, the blood tends to clot which can cause irreversible tissue damage. Therefore, in order to prevent any tissue damage due to blood clots in the capillaries, mice were injected intraperitoneally with sodium heparin 15 min prior to euthanization. Sodium heparin is a blood thinner. Mice were injected 15,000 USP units per Kg using 1000USP/mL Heparin Sodium based on the mass of the mouse. The mice all weighed around 20 g. Therefore, they were injected with 20 units or 200 µL of 1000USP/mL heparin. After the mouse was euthanized, the heart was quickly extracted and cannulated onto a Langendorff-perfusion apparatus (**Fig. 2.1**). It was important to be quick in the extraction and cannulation to prevent ischemic damage. The stopping of blood flow or ischemic conditions can produce multiple side effects such as increases in intracellular Na^+ ,[102,103] cytosolic $[Ca^{2+}]$,[104–106] depolarization of the membrane and a drop in the ATP levels.[107,108]

The Langendorff system has been used since 1895 to maintain mammalian hearts *ex vivo*.[109] It was essential to use this method in this thesis because it keeps intact hearts vital for hours. In addition, the cardiomyocytes are in a more physiological setting within the syncytium of the organ and continue to be electrically, mechanically, and metabolically coupled. Therefore, the assessment of cellular variables such as [Ca^{2+}] and membrane potential presents results that are not affected by a harsh enzymatic dissociation process and loss of coupling.

The Langendorff set-up involves the retro-perfusion of Tyrode solution equilibrated with 100% O_2. The retro-perfusion of Tyrode solution is not mediated via the physiological direction of blood flow in the heart. Normally, when the heart contracts, there is an efflux of blood through the aorta and pulmonary artery. However, in the Langendorff set-up, Tyrode solution enters through the aorta. Although this is a non-physiological flow, retro-perfusion allowed Tyrode solution to enter via the coronary arteries originating at the base of the aorta. Retro-perfusion is critical in maintaining the cardiac tissue alive. The

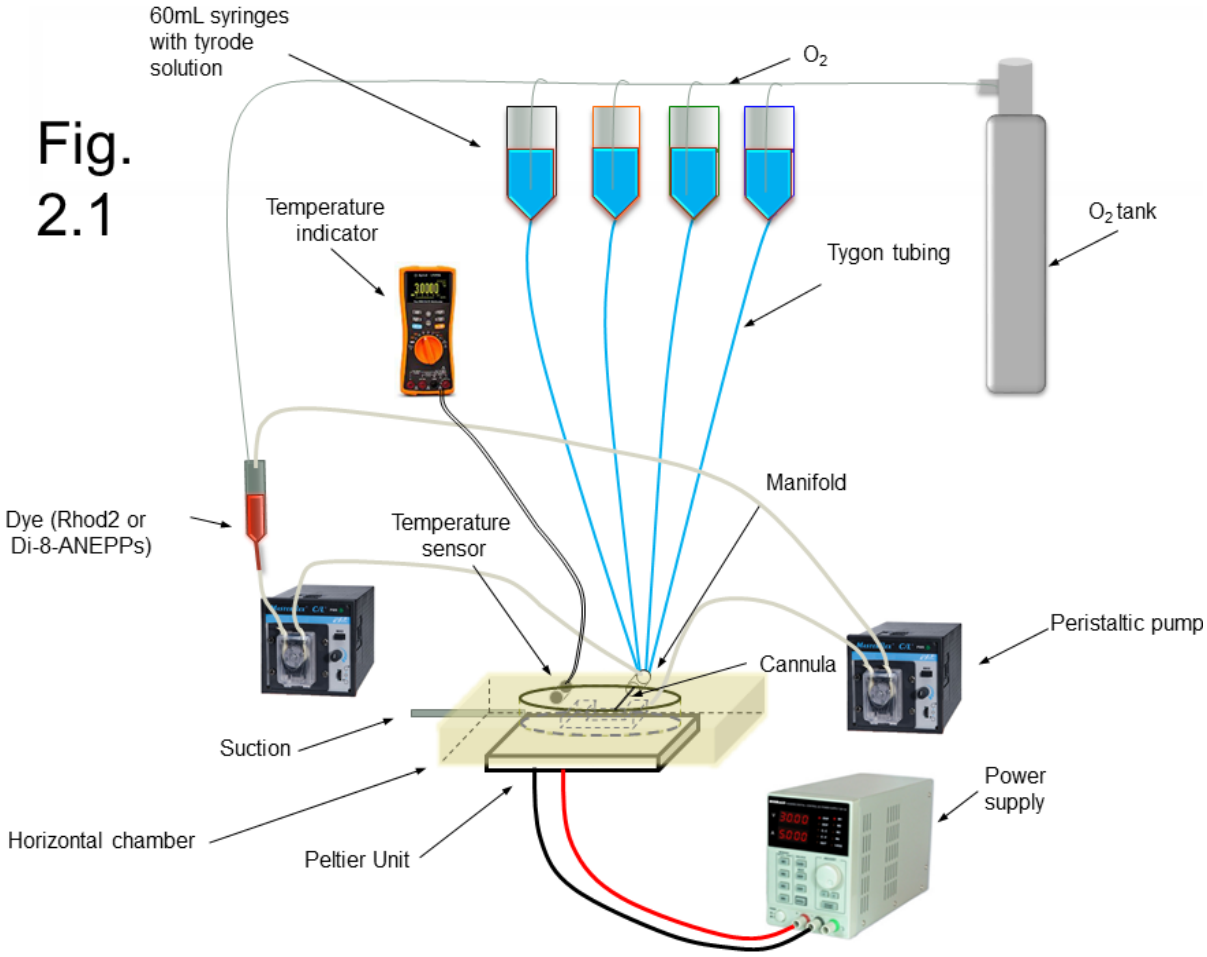

Fig. 2.1: The Langendorff perfusion apparatus was used to retroperfuse Tyrode solution into mice hearts. The Peltier unit below set the temperature of the bath.

heart was held in place with a non-absorbable surgical suture tied around the aorta onto a cannulation needle so the flow of the Tyrode would not cause it to slide off. The constant retro-perfusion of Tyrode allowed the removal of byproduct produced by the metabolic processes of the heart into the perfusion, which was discarded using a suction vacuum system.

Tyrode solution contained ionic concentrations equivalent to those found in blood serum. **Table 2.1** lists the solute concentrations used to make Tyrode solution. The osmolarity was between 285 and 295 to maintain the organ in isotonic conditions and prevent any hypertonicity. To simulate blood conditions, the pH of the solution was adjusted to 7.4 with NaOH. However, unlike blood, the Langendorff system lacked the circulation of proteins, antibodies, and neurotransmitters, which can be a limitation affecting the results. Tyrode solution was saturated with 100% O_2 using submerged "air stones" connected to an O_2 tank. Since our interest was focused on maintaining flow to the cardiac tissue, at times, a small 23Ga needle was pinched through the apex of the heart. This relieved pressure from the ventricles to avoid swelling. It was important to prevent the expansion of the ventricles because this inhibits proper retro-perfusion through the capillaries.

Compound	Concentration (mM)	Molecular Weight (g/mol)	Amount for 1L (g)
NaCl	140	58.44	8.1816
KCl	5.4	74.55	0.4025
$CaCl_2$	2	147.02	0.2940
$MgCl_2$	1	203.3	0.2033
$NaPO_4H_2$	0.33	138	0.0455
HEPES	10	238.31	2.3831
Glucose	10	16	1.8106

Table 2.1: Tyrode solution concentrations used to perfuse the heart. To simulate a physiological blood serum at pH 7.4, sodium hydroxide was added to the Tyrode solution at 37°C or at the specific temperature used in the experiment.

Once the retro-perfusion was initiated, the heart was allowed to stabilize for about 10 min with Tyrode solution at room temperature. The stabilization time allowed the heart to recover from the ischemic insult it suffered during the extraction and receive the necessary O_2. Since we wanted to understand the temperature dependency of Ca^{2+} dynamics, the external temperature of the solution surrounding the heart was controlled. A Peltier unit was used to change the temperature of the Tyrode solution in the horizontal chamber (**Fig. 2.1**). Most experiments were conducted at 32˚C or at physiological temperature of 37˚C, unless stated otherwise. Conducting experiments at 32˚C had the big advantage of maintaining the hearts loaded with the fluorescence-based dyes during the whole term of the experiment. At this temperature the extrusion of fluorescent indicators by the activity of ATP-binding cassette (ABC) transporters, whose role is to remove exogenous molecules from the cytosol, can be prevented. In addition, many physiological variables including membrane potential and intracellular [Ca^{2+}] and alternans are

temperature dependent. Therefore, to assess their temperature dependency, we conducted experiments in which the temperature varied.

A big experimental problem that occurs in muscular cells is the artifacts produced by the mechanical contraction. In order to record from the intact beating heart, blebbistatin (Sigma, St. Louis, MO) was used to stop the mechanical activity. The constant movement of the heart due to the mechanical contractions posed a problem for the multiple probes placed at the surface. A mechanical contraction could break the glass microelectrodes used to measure the AP (described in section 2.2) and also cause noise artifacts in the laser recordings. Blebbistatin inhibits the actin-myosin interaction[110] without affecting the electrical activity or influx through the L-type Ca^{2+} channels.[97,111,112] Therefore, before any recordings were initiated, the heart was retro-perfused with 10μM blebbistatin.

In order to maintain consistency in our experimental approach, all hearts went through similar protocols including: stabilization after cannulating with 10 min of Tyrode retro-perfusion, loading of dyes for 30 min (described in section 2.3), washing of dye with Tyrode solution for 10 min, increasing temperature with the Peltier, retro-perfusion of Tyrode solution with blebbistatin, and finally retro-perfusion with different pharmacological agents used to activate/inhibit molecular pathways and any consecutive washes. The techniques used to excite and record the emission of the dyes varied between the different set of experiments, but all the hearts went through the standard procedures mentioned here after being cannulated onto the Langendorff set-up.

2.2 Electrical measurements using sharp microelectrodes and ECG

The tissular electrical activity of the ventricular syncytium is a key property that defines several aspects of the cardiac function. For example, the coordinated propagation of the electrical activity is critical in defining the function of this electromechanical pump. At the cellular level, the dynamics of the electrical activity are usually assessed by measuring action potentials. Action potentials are transient changes in membrane voltage over a short period of time. These changes in membrane potential are due to the activation of voltage-gated channels and the subsequent movement of ions across the plasma membrane driven by the electrochemical gradient of the ions. The different regions of the heart have dissimilar APs waveforms. These diverse waveforms are a result of the different density and molecular types of ion channels in the tissue. Therefore, it is important to measure the AP as a way to do an overall assessment of the activity of the different channels in a certain anatomical region in the tissue. When the morphology of the AP changes after administering a certain agonist, its effect on specific channels can be deciphered by assessing which phase of the AP was affected.

All the electrical recordings of the action potentials were obtained by means of sharp glass microelectrodes filled with 3M KCl that were connected to an electrometric amplifier (World Precision Instruments (WPI), Sarasota, FL). Glass microelectrodes were pulled with Micropipette Puller (Flaming/Brown Micropipette Puller, Sutter Instrument Co., CA) and kept overnight in 3M KCl to remove any air bubbles that could cause

additional resistance or noise. These microelectrodes had an outer/inner diameter of 1/0.58 mm and resistance of 10-20 MΩ. Microelectrodes were connected to a high input impedance differential amplifier (Duo 773 Electrometer, WPI, USA). They were positioned at the surface of the heart using a manual mechanical micromanipulator. Before impaled in the tissue, the microelectrode readout was adjusted to zero in the bath in reference to an accompanying grounding AgCl electrode pellet (WPI, Sarasota, FL). The optically recorded APs were calibrated with the recordings from the microelectrodes.

The overall electrical activity of the heart can be assessed by an ECG. The different waves of the ECG depict the depolarization or repolarization of the different tissues or regions. The P-wave defines the depolarization of the atrium, while the QRS complex shows the depolarization of the ventricle. The T-wave, is associated with the repolarization of the ventricle. This thesis aimed at understanding the underlying mechanisms leading to T-wave abnormalities by assessing the Ca^{2+} transient and action potential durations. In addition, measuring the overall electrical activity across the ventricular wall was essential in detecting the generation of the T-wave alternans. ECG recordings were made possible by a homemade miniature ECG with two reference electrodes (**Fig. 2.2**). To measure a transmural ECG, one electrode of the ECG was placed inside the ventricle through the mitral valve and the other close to the epicardial surface of the left ventricle. Since this was a transmural ECG placed in the ventricle, all the recordings lacked a P-wave.

Fig. 2.2

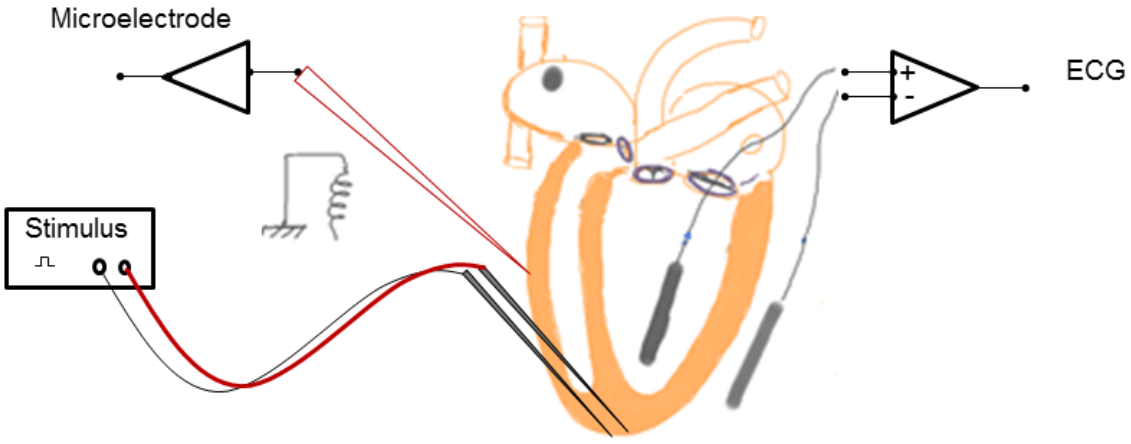

Fig. 2.2 Electrophysiological measurements were performed with ECG and a sharp glass microelectrode. The transmural ECG was placed in the left ventricle through the mitral valve. The glass microelectrode is placed on the epicardium. The HR was set using a stimulator connected to acupuncture needles placed on the apex of the heart.

HR is a critical variable in understanding T-wave and Ca^{2+} alternans. During high HRs, alternans are produced. For this thesis, we induced alternans by increasing the HR. It was also important to assess how AP and Ca^{2+} transients changed as a function of HR. In addition, keeping this variable (HR) constant was critical in evaluating how the ANS affects the two cardiac properties. Thus, throughout the study presented in this thesis, HR was an important variable to control. This was done by externally pacing the heart with acupuncture needles placed in the apex of the heart (seen in **Fig. 2.2**). These needles were connected to a wave generator that produced square current pulses of 1ms. Although the heart is naturally stimulated from the SA node, this stimulation method followed the pattern of depolarizations in the ventricular region by propagating from the apex to the base and from the inward (endocardium) to outward (epicardium) region.

2.3 Detecting cellular events: calcium and potentiometric dye loading

The use of fluorescent probes and the instruments to detect the light emitted by them have promoted the advancement of the understanding of underlying molecular events behind physiological processes. In this thesis, fluorescent molecular indicators were employed to monitor key cardiac intracellular events at the whole organ level of intact beating hearts. The physiological properties assessed include the membrane potential and intracellular [Ca^{2+}]. These two properties are critical in defining the function of the organ. They were assessed together because they are interconnected during the ECC process. Intracellular Ca^{2+} levels are critical in defining many physiological variables such as pressure, contractility, and APD.

Although the AP morphology can reflect changes in the Ca^{2+} dynamics (phase 1 and 2),[31,34] measuring Ca^{2+} transients reveals the Ca^{2+} cycling and kinetics in a more direct way. All of these variables were assessed with exogenous fluorescent indicators. Upon binding Ca^{2+} or detecting changes in the membrane's electric field, the fluorescent properties change and emit at different wavelengths. These fluorescent probes were retro- perfused through the coronary vessels using the Langendorff set-up to facilitate the reuptake into the cardiomyocytes.

Di-8-ANEPPS: Potentiometric signals

Usually, the electrical activity of excitable cells has been recorded with glass microelectrodes. Indeed, we already described the use of sharp glass microelectrodes to assess the electrical activity in cardiac tissue. Unfortunately, if an intact perfused heart is used as an experimental model, recordings with sharp microelectrodes are limited to epicardial measurements. However, in this project we planned to address how the differences between the epicardial and endocardial APs impact the behavior of the T-wave. Microelectrodes can easily break when attempting to record APs from the endocardial layer of the ventricular wall. Therefore, a fast-response potentiometric dye was used to optically measure the membrane potential in the endocardium and epicardium. More specifically, Di-8-ANEPPS dye is fast enough to detect millisecond changes in membrane potential and convey it as changes in fluorescence. For every 100mV changes in potential, there is a 10% change in fluorescence.[113]

Di-8-ANEPPS is a hydrophobic florescent indicator that can accumulate in biological membranes. Once in the membrane it spectral properties change as a result of the huge magnitude of the intramembrane electric field. Indeed, although the membrane potential only changes ~100 mV during an AP, the change in electric field can be larger than 10^7 V/m. This enormous electric field change is produced by the extremely low thickness of the membrane (50 Å). Thus, this huge electric field will not only affect the light absorption of the dye but also its fluorescent properties. As shown in **Fig. 2.3**, the dye anchors to the membrane by two hydrophobic carbon tails and aligns to the polar heads with its sulphonate hydrophilic group.[114] This structure permits the dye's chromophore to be parallel to the intramembrane electric field which can induce changes in the fluorescence.[114]

Di-8-ANEPPS is excited from the ground state with a green 532 nm YAG laser using the Pulsed Local Field Fluorescence Microscopy (PLFFM) technique, which will be described in section 2.4. In the excited stated, there is an electron cloud shift from the aniline group to the pyridinium (**Figure 2.3 a**).[114] The energy difference between the ground and excited state is what changes based on the membrane's electric field. When the membrane is repolarized (**Fig 2.3 b**), phase 4, it lowers the difference between the ground and excited state of the Di-8-ANEPPS molecule. According to $E=hc/\lambda$, where E is the energy, if the E is lower, then the wavelength (λ) is larger. Thus, PLFFM, records long, low energy wavelengths around 630 nm (**Fig. 2.3 c**). Therefore, at the resting membrane potential, it has a steady fluorescence above our 610 nm filter.

However, during the depolarization and repolarization phases of the action potential, the electric field increases the difference between the ground and excited state and thus there is a shift toward higher energy wavelengths (**Fig. 2.3 d**). Since the PLFFM records with a filter of 610 nm, the shift towards a lower wavelength in the emission spectrum decreases the amount of signal detected within our filtering window (**Fig. 2.3 e**). The resulting signal is an inverted AP as diagrammed in **Fig. 2.3 f**.

Fig. 2.3

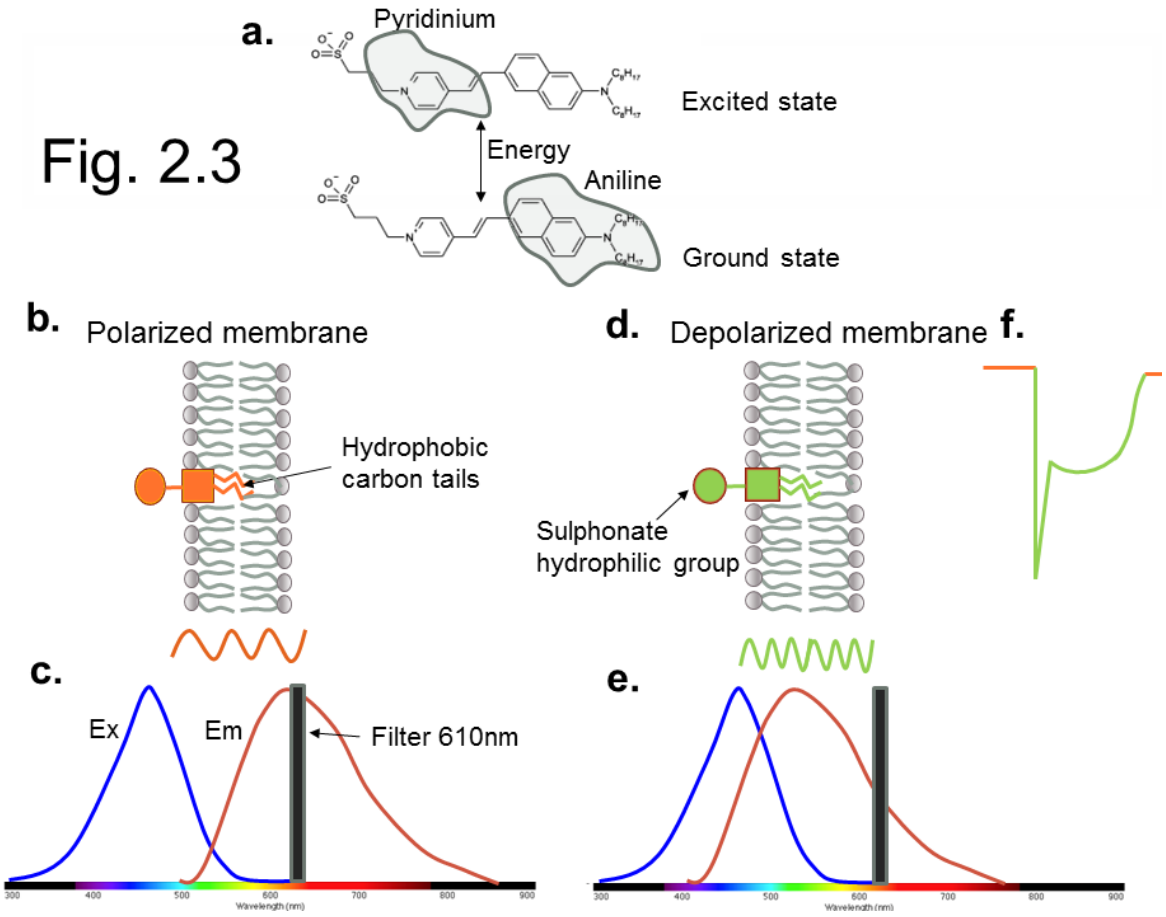

Fig. 2.3 Di-8-ANEPPS fluorescence is induced by changes in the membrane's electric field. a) There is a shift in electron cloud between the aniline and pyridinium groups when the dye molecule goes from the ground to the excited state, respectively. b) The dye orients itself parallel to the membrane's electric field with the aid of the hydrophobic carbon tails and sulphonate hydrophilic group. c) When the membrane is polarized, the energy between the dye's two states is low, producing long, low energy wavelengths. d) In the depolarized membrane, the difference between the ground and excited states is greater. This produces short, high energy wavelengths. e) The shift towards higher energy wavelengths leads to smaller detection due to the 610nm filter that only allows the recording of wavelengths above this number. f) The recorded signal is consequently an inverted AP.

Rhod-2AM: Intracellular Ca^{2+} signals

The rise and fall of cytosolic Ca^{2+} is essential to define the function of the organ as an electromechanical pump.[37,115–117] This rise and fall is referred to as the Ca^{2+} transient. Each cardiomyocyte tightly regulates the cytosolic [Ca^{2+}]. Ca^{2+} levels are important in defining the pressure, contractility, and APD. Most of the rise in intracellular Ca^{2+} is caused by the release of Ca^{2+} from the SR. This Ca^{2+} then binds to Troponin C and initiates the contractile machinery. The reuptake, as well as the release, process are also highly regulated. Assessing the Ca^{2+} transient kinetics is critical in understanding any effect on E-C coupling and CICR mechanisms, which ultimately affect the function of the organ.

In order to monitor the intracellular Ca^{2+} cycling that occurs during the systolic phase, Ca^{2+} transients were obtained by the fluorescence of Rhod-2-Acetoxymethyl (Rhod-2AM) (Life Technologies, Carlsbad, CA). Inside the cell, the membrane-permeant esters are cleaved by esterases [118]. Once hydrolyzed from the compound, Rhod-2 uses the 1,2-bis(o-aminophenoxy ether)ethan-N,N,N',N'-tetraacetic acid (BAPTA) structure to bind Ca^{2+}. BAPTA has a much higher selectivity for Ca^{2+} than Mg^{2+} [119]. Upon binding Ca^{2+}, Rhod-2 has a 100 fold increase in fluorescence that can be recorded using PLFFM, which is described in section 2.4. Using PLFFM, the dye is excited with a 532nm wavelength and if Ca^{2+} is bound, it fluoresces at a larger wavelength (**Fig. 2.4**).

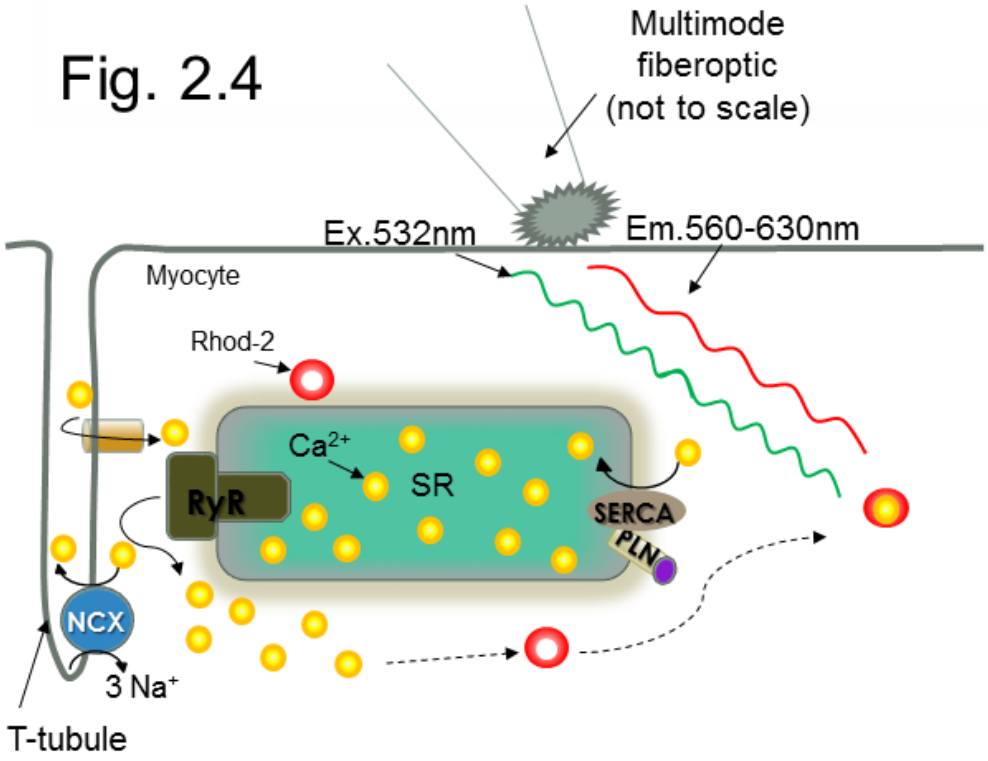

Fig. 2.4 The increase in intracellular Ca^{2+} caused by CICR can be assessed with the Ca^{2+} binding dye Rhod-2. When bound to Ca^{2+}, Rhod-2 fluoresces at higher wavelengths. The excitation and emission is mediated by a multimode fiber optic, described in the next section.

Fluorophore loading of Di-8-ANEPPS and Rhod-2AM

Di-8-ANEPPS or Rhod-2AM were perfused for 30 minutes after the hearts were stabilized in the Langendorff set-up. Di-8-ANEPPS (10µg) was prepared with 20uL of 20% pluronic in 5 mL of Tyrode solution. Rhod-2AM (50µg) was prepared with 20µL of 20% pluronic (Biotium, Hayward, CA) in 500µl of Tyrode solution. All dyes were sonicated (FS20 Ultrasonic Cleaner; Fisher Scientific, Pittsburgh, PA) for 20 mins and then perfused into the heart for 30 minutes at room temperature using peristaltic pumps (Masterflex C/L, Cole-Parmer, Vernon Hills, IL).

2.4 Pulsed Local Field Fluorescence Microscopy used to excite and record emission from dyes

The fluorescent molecular probes used to record key cardiac properties can be electromagnetically excited and the emission recorded with the Pulsed Local Field Fluorescence Microscopy (PLFFM) setup (**Fig. 2.5**). The PLFFM use epifluorescence in conjunction with fluorescent probes to visualize cellular events at the whole organ level.[95] These florescent probes molecules change fluorescent properties upon binding and this allows us to "visualize" cellular processes. The light source is a green, 532nm, solid-state neodymium-doped yttrium aluminum garnet (Nd-YAG) laser (Enlight Technologies, New Jersey, USA) for Rhod-2 and Di-8-ANEPPS excitation. For transmural measurements, this light was split with a beam splitter to allow two 200µm multimode optical fibers (0.67 NA) to illuminate the two layers of the ventricular wall. The beam was opened using a beam expander or aspheric lens. It was reflected with the aid of a dichroic mirror onto a microscope objective. The objective focused the light into an optical fiber that is in contact with the tissue. In order to facilitate the placement of the fiber onto the endocardium, a small incision was made on the surface of the ventricular free wall (seen in **Fig. 2.5**).

The laser light excites the fluorescent probes present in the tissue which then emit light at a different wavelength. The emission then traveled back through the multimode fiber optic. This light was filtered with a dichroic mirror which allowed the longer wavelength to pass, but reflected the excitation light back to the laser. The longer wavelength passing through the dichroic mirror was further spectrally filtered by an emission filter that eliminated any wavelengths bellow 610nm, reducing any light contamination coming from the excitation light. The emitted light was then focused onto an avalanche photodiode (Perkin Elmer, Waltham, MA) by an objective. The avalanche photodiode converts light photons into a current, which is amplified using a resistive feedback element. Finally, the signal is digitized by an A/D converter (National instrument) and is acquired by a PC.

Fig. 2.5

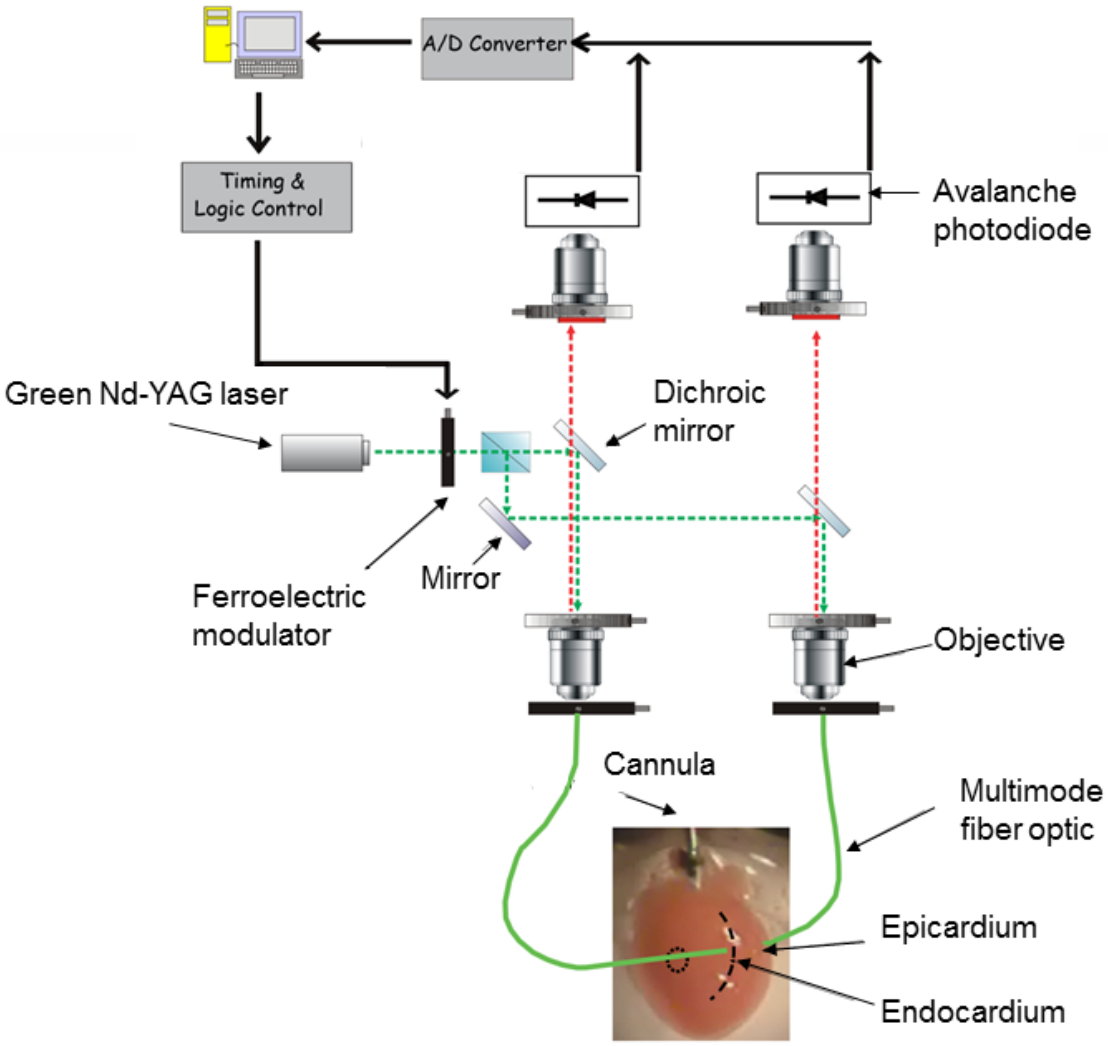

Fig. 2.5 PLFFM consists of a laser driven epifluorescence arrangement. Light travels through a beam splitter, expanded by an aspheric lens, reflected onto the back of a microscope objective and focused onto a fiber. The fibers are positioned in the endocardium or epicardium.

2.5 Loose-patch photolysis (LPP) to detect membrane currents at intact heart level

In this thesis project, we also seek to understand the molecular bases responsible for the ionic current underlying an action potential. Specifically, we wanted to determine how activation of certain pathways can modify ionic currents at the whole organ level. In this thesis work we present for the first time data on ionic currents at the intact organ by using the loose-patch photolysis (LPP) technology.[31] Unlike other techniques, the LPP allows the measurement of currents in an intact tissue during a triggered physiological AP. This technique brought together into one set-up other previously used tools including: PLFFM,[34,95–97] photo-breaking compounds with ultraviolet (UV) pulsing,[120–124] microelectrode measuring, and loose-patch recordings.[125,126] An illustration of LPP can be seen in **Fig. 2.6**.[31] The integration of multiple set-ups into one enables the LPP tool to measure ionic currents induced by photo-breaking of UV sensitive compounds at the same

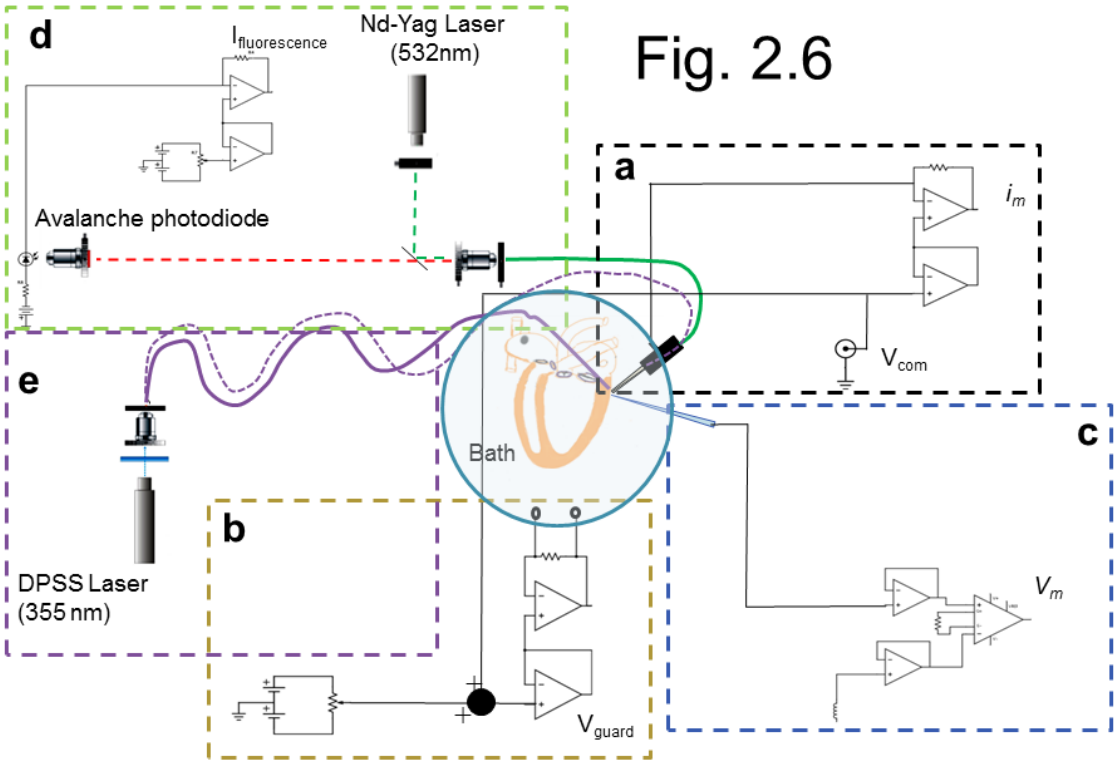

Fig. 2.6 LPP set-up consisting of various parts. a. Loose patch pipette records the membrane current on the surface of the heart. b. A reference electrode clamps the voltage of the inside of the pipette to the same potential as the surrounding bath. c. Glass microelectrodes connected to an amplifier record the membrane potential, electrically. d. PLFFM component enables the simultaneous recording of fluorescent probes at the pipette location on the surface of the heart. e. A UV illuminating component allows the breakage of photosensitive compounds to record immediate currents upon UV pulses at the loose patch site. This figure has been published by Ramos-Franco et al.[31]

as Ca^{2+} transients and membrane potential (**Fig. 2.7**). It is the only tool that can record membrane currents in the intact heart during a physiological AP.

Fig. 2.7

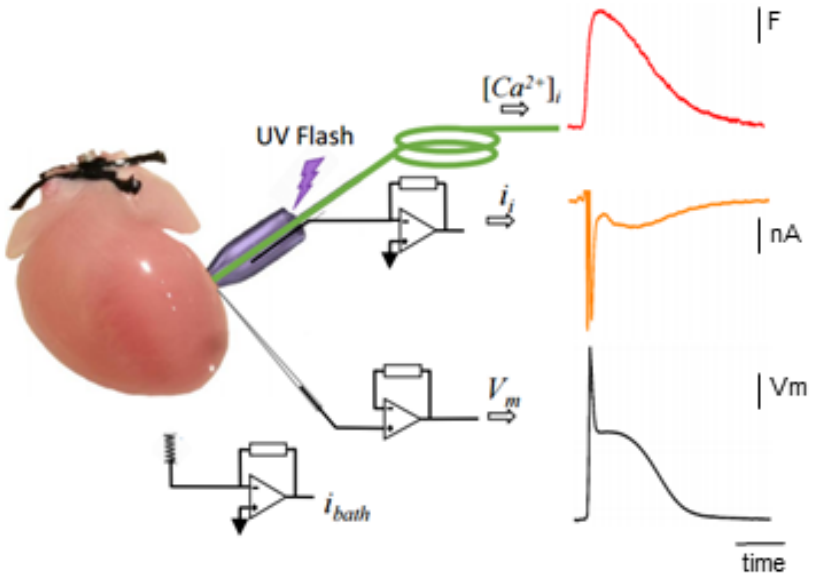

Fig. 2.7 The LPP technique is the only tool that can be used to measure membrane currents (orange trace) in the intact heart at the same time as a physiological AP (black trace) and Ca^{2+} transients (red trace). This figure has been published by Ramos-Franco et al.[31]

The loose patch was made with a giant glass patch pipette using capillary tubes (WPI, Sarasota, FL) with outer/inner diameter of 1.0/0.58mm. These glass capillaries were cut in half and heat was applied with a torch to decrease the diameter size of one end to approximately 200 µm. This allowed the tip of the capillary to be filled by a fiber optic placed in the interior and used to record intracellular Ca^{2+} or potentiometric signals at the loose patch location or to provide small UV pulses to break photosensitive compounds and assess immediately resulting membrane currents.[31] The patch pipette was filled with Tyrode solution and held by a microelectrode holder half-cell (WPI, Sarasota, FL). A micromanipulator was used to place the patch pipette on the surface of the ventricle. The interior of the giant glass patch pipette was voltage clamped to the same potential of the surrounding bath.

When the epicardial layer of the heart is patched, the current through the pipette (i_p) is the addition of the current leaking through the seal (i_{seal}) and the transmembrane current (i_m). Therefore,

$$V_o = -R_f \cdot i_p$$
$$= -R_f \cdot (i_{seal} + i_m)$$

where V_o is the output voltage of the current-to-voltage converter and R_f is the feedback resistor. If i_m. and i_{seal} are

$$i_m = \frac{V_m}{r_m}$$

$$i_{seal} = \frac{V_A - V_{bath}}{r_{seal}}$$

Then i_p is

$$i_p = \frac{V_m}{r_m} + \frac{V_A - V_{bath}}{r_{seal}}$$

where V_m and r_m are the potential and resistance of the membrane, respectively. V_A and V_{bath} are the potential inside the pipette and outside the heart, respectively, and r_{seal} is the seal resistance.

Zeroing the potential difference between the pipette and the bath, causes

$$i_{seal} = \frac{0}{r_{seal}} = 0$$

Thus, i_{seal} cancelled leaving

$$i_p = \frac{V_m}{r_m} = i_m$$

And consequently

$$V_o = -R_f \cdot i_m$$

as we previously described by Ramos-Franco et al.[31] Therefore, the output voltage of the current-to-voltage converter (V_o) directly measures the membrane current during a physiological AP. **Fig. 2.8** illustrates the different currents, voltages, and resistances in the loose patch.

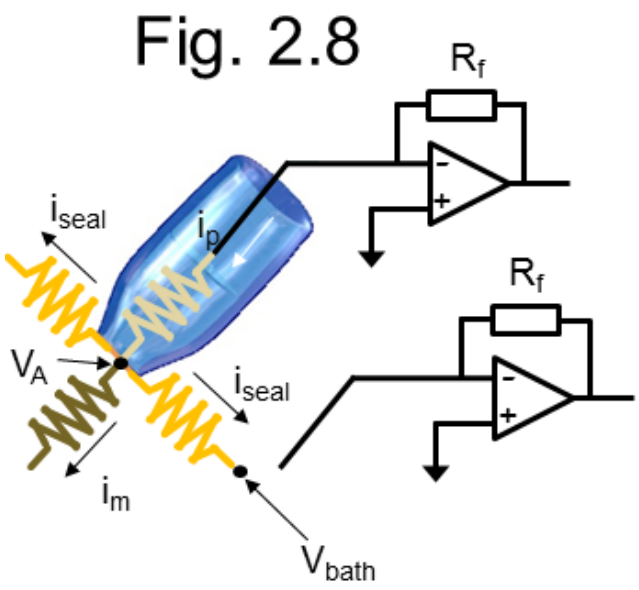

Fig. 2.8 Illustration of the loose patch and the currents measured with the pipette. The inside of the patch pipette is clamped to the same potential as the bath. This figure has been published by Ramos-Franco et al.[31]

However, during an action potential there are two different types of currents through the membrane. A displacement current (capacitive current) and a conduction current produced by the summation of all the ionic currents permeating through the membrane at any time. Thus, i_m will be the addition of all the ionic (i_i) and capacitive (i_c) currents. Then

$$i_m = i_c + \sum i_i$$

where i_i is each of the ionic currents occurring during the AP. In other words, the pipette was able to measure i_m as a complex signal, which consisted of a capacitive and the sum of all the ionic currents.[31] In order to evaluate the capacitive current, the membrane potential needed to be measured very close to the place where the membrane current was evaluated. This was done by positioning a sharp microelectrode a few micrometers away from the patch pipette. Interestingly, the capacitive current is dependent on the rate at which the V_m changes

$$i_c = C_m \frac{dV_m}{dt}$$

where C_m is the membrane capacitance. Previous experiments using the LPP technique showed that V_m does not change with the activation of local currents induced by releasing inhibition of channels with UV-sensitive compounds.[31] This is believed to be due to the electrotone imposed by the surrounding tissue on the small local 200µm site of UV pulse.

In order to dissect the UV-induced current, two traces were recorded using this technique where one is before a 10 ms UV flash and the other after the photolysis. Since the potential does not change during the UV flash, i_c is the same for the two recordings. Thus, i_c subtracts out when we subtract the two traces before and after the pulse. So, our equation reduces to

$$i_m = \sum i_i$$

such that the current measured by the pipette will be the addition of all the ionic currents occurring during the AP.

In order to dissect specific currents, photosensitive compounds were used to block/inhibit certain channels and a UV pulse was used to activate the current at the pipette location. In this thesis, we used the UV sensitive caged compound, nifedipine (10μM) as an immediate way to activate currents through the L-type Ca^{2+} channel. Current through the L-type Ca^{2+} channel is critical in CICR, which is very important in ECC.[40] In order to dissect the specific current through the locally activated L-type Ca^{2+} channels, we recorded two traces, one with no UV flash and the other with the UV flash. We then subtract the recorded currents, before ($i_{m\ no\ UV}$) and after ($i_{m\ UV}$) the UV flash,

$$i_{m\ no\ UV} - i_{m\ UV} = \sum i_{i\ no\ UV} - \sum i_{i\ UV}$$

If we express each sum as the individual currents during a physiological AP, then

$$= [i_{Ca\ no\ UV} + i_{Cl\ no\ UV} + i_{K\ no\ UV} \dots] - [i_{Ca\ UV} + i_{Cl\ UV} + i_{K\ UV} \dots]$$

where $i_{Ca\ no\ UV}$, $i_{Cl\ no\ UV}$, $i_{K\ no\ UV}$ are the Ca^{2+}, Cl^-, and K^+ currents, respectively, without the UV pulse. $i_{Ca\ UV}$, $i_{Cl\ UV}$, $i_{K\ UV}$ are the Ca^{2+}, Cl^-, and K^+ currents, respectively, after the UV pulse. Since no other pharmacos were used to change other ionic currents (i_{Cl}, i_K, etc.), the subtraction of the two recorded currents with the pipette, i_m before ($i_{m\ no\ UV}$) and i_m after ($i_{m\ UV}$) the UV flash, solely represented the currents induced by the photolysis break. In this case, the current only changed for Ca^{2+} ($i_{Ca\ UV}$) that was activated with the UV flash and thus the other currents were unchanged and this caused them to subtract out such that the difference in current is

$$i_{m\ no\ UV} - i_{m\ UV} = i_{Ca\ UV}$$

The PLFFM component in the LPP was used to optically record any changes in Ca^{2+} transients or AP using Rhod-2AM or di-8-ANEPPS, respectively. Finally, the sharp microelectrode was used to calibrate any optically measured electrical signal at the pipette surface and to reaffirm that dV_m/dt=0 due to the electrotone imposed by the tissue.[31]

2.6 Fluorescence local field optical mapping (FLOM)

In the heart, the propagation of various signals is important for its coordinated electromechanical activity. The evaluation of how physiological variables change in space and time all over the ventricular wall is critical to define the timing at which different anatomical areas are electrically activated. This is not only important to understand the function of the organ during the cardiac cycle but also to address the origin of arrhythmogenic events such as reentry arrhythmias. Historically, this has been addressed using the optical mapping technique.

Optical mapping is a fast imaging technique that allows the monitoring of physiological variables that change in space and time such as the propagation of the AP, Ca^{2+} transients, and alternans.[127–129] In addition, many disease states may alter the properties of these variables in specific regions. Reentrant arrhythmias, extrasystolic APs, and other highly arrhythmogenic events are unlikely to be recorded due to their random appearances in the tissue of the heart. Although optical mapping has been extremely useful to determine the spatio-temporal distribution of epicardial variables, it lacks the optical spatial resolution to measure subcellular signals. On the other hand, local field optical measurement of the AP and Ca dynamics is usually limited to single site measurements. PLFFM, for example, was adapted to optically measure AP and Ca^{2+} transients at two locations, epicardium and endocardium. However, this method was unable to detect regional differences beyond two 200μm regions.

In this thesis, we plan to understand how local variables are distributed under normal and stress conditions. For example, how Ca^{2+} transient and membrane potential spatially change as function of a gradual metabolic impairment. One way of imposing a metabolic challenge is by introducing a temperature perturbation on the intact tissue. In order to understand the temperature dependency as well as the spatial distribution of alternans, we developed the Fluorescence Local Field Optical Mapping (FLOM) apparatus. This new technique allowed us to simultaneously evaluate the influence of temperature and HR on the Ca^{2+} transient properties at various locations in the heart.

FLOM is a contact fluorescence imaging technique consisting of three main elements: a laser driven epifluorescence arrangement, an optical conduit that is in contact with the tissue, and a fast detection camera that images the surface that is in contact with the tip of the conduit (**Fig. 2.9**). A conduit is a solid bundle of many imaging fibers fused together into a cylindrical form. The optical fibers within the conduit transmit an image where the emitted light changes based on Ca^{2+} and dye interactions. The acquisition was performed by the camera's software (IC Capture, Imaging Source, Charlotte, North Carolina) and processed using ImageJ.

Fig. 2.9

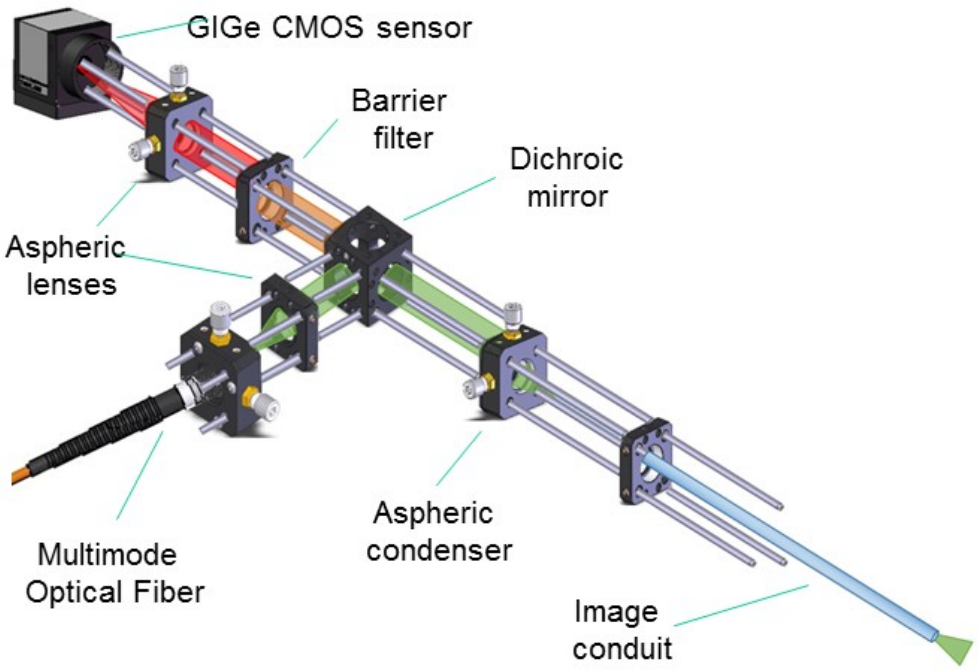

Fig. 2.9 FLOM consists of a laser driven epifluorescence arrangement that uses an optical conduit in contact with the tissue. Fluorescence is detected with a fast recording CMOS camera. (Figure was provided by A. L. Escobar)

For visualization purposes the images were color mapped using a lookup table. The color scale was set in which blue indicates low fluorescence from the dye interacting with intracellular Ca^{2+} and red is high fluorescence. The series of images can be reproduced in time and space (**Fig. 2.10 a**). These images depict changes in the intracellular Ca^{2+} over time as frames in a recorded movie (**Fig. 2.10 b**). When we plot these images as fluorescence over time, it results in intracellular Ca^{2+} transients with the Ca^{2+} sensing dye, Rhod-2, or even AP with the potentiometric dye, di-8-ANEPPS (**Fig. 2.10 c**). For this thesis, we wanted to assess the spatial distribution of Ca^{2+} transients; thus, we only used Rhod-2.

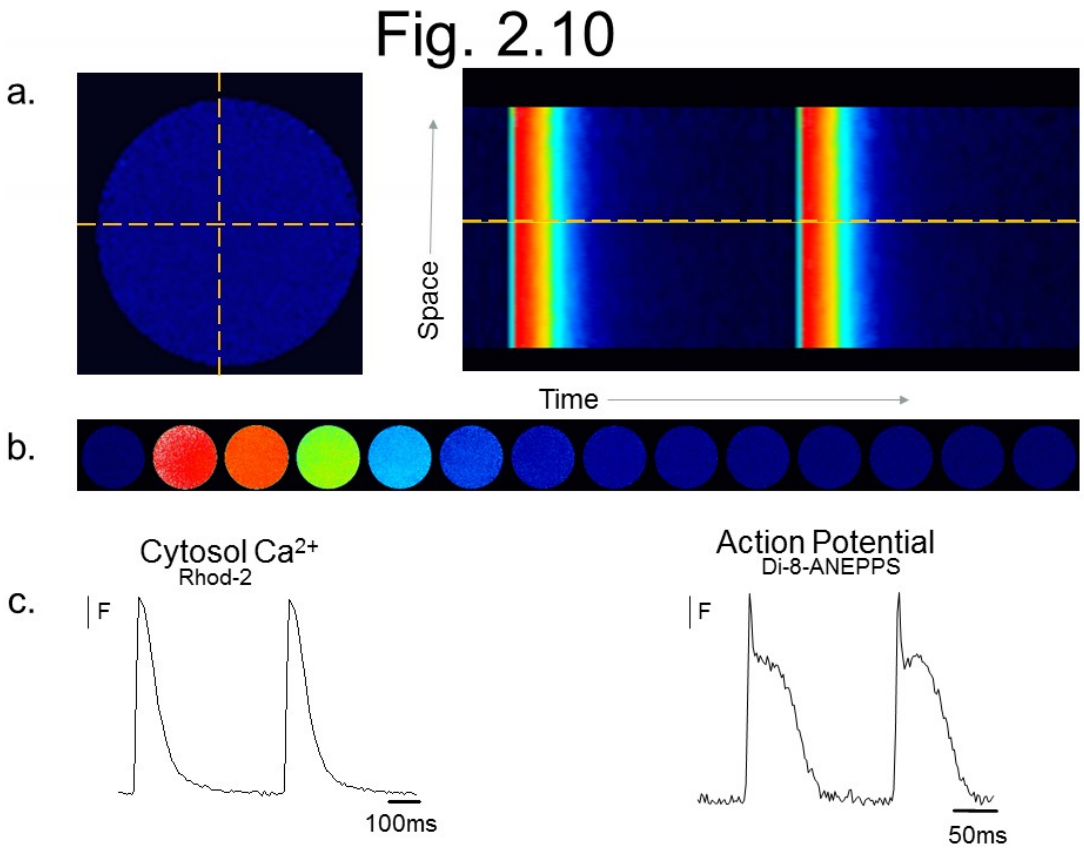

Fig. 2.10 a. FLOM recorded images can be reproduced in time and space. The color scale is set where blue indicates low fluorescence and red is high fluorescence. b. Montages of the frames in the recorded movie show changes in fluorescence over time. c. From the FLOM images, intracellular Ca^{2+} transients or APs can be computed, when using Rhod-2 or di-8-ANEPPS, respectively.

The construction of the light path using filters, expanders, dichroic mirrors, and microscope objectives is exactly the same for FLOM as the PLFFM.[95] The main difference is that instead of using a 200µm optical fiber, the light is focused onto a 3.2 mm optical conduit. It has a spatial resolution of 3 to 11 µm allowing us to record fluorescence from multiple sites within the same cell. The PLFFM records one average fluorescence from the fluorescent probes under the 200µm range, but FLOM is capable of recording about 1000 averages from within the 3.2mm conduit contact region. In addition, the emission is recorded by a camera instead of an avalanche photodiode. Together, these two features allow the recording of 2D images, which can also be depicted as line scan surface plots.

Since the spatial distribution of Ca^{2+} transients are affected by temperature, a device to generate a temperature gradient was fabricated on top of the FLOM apparatus (**Fig. 2.11**). The cooling is mediated by a Peltier-controlled metallic cold finger. The metallic cold finger is simply a metallic tube that is sandwiched between a metallic plate on the

bottom and a water block on top. The metallic tube is filed down towards the end so that only a half-moon is in contact with the tissue. Small Peltiers were sandwiched together to maximize the cooling of the metallic plate and the tube. The role of the water block is to circulate water with a pump in order to dissipate the heat produced by the cooling Peltier units. The conduit was positioned through the metallic tube. The conduit and the half-moon cold finger were in contact with the epicardial layer of the heart. This attachment was designed to locally change the temperature at the contact area between the conduit and the tissue. This generated a temperature gradient where the tissue closest to the cold half-moon was coldest (simulating hypothermic conditions) and the tissue farthest away was warmer based on the temperature of the bath (32ºC) in the horizontal chamber. The temperature gradient was assessed in Chapter 4.

Fig. 2.11

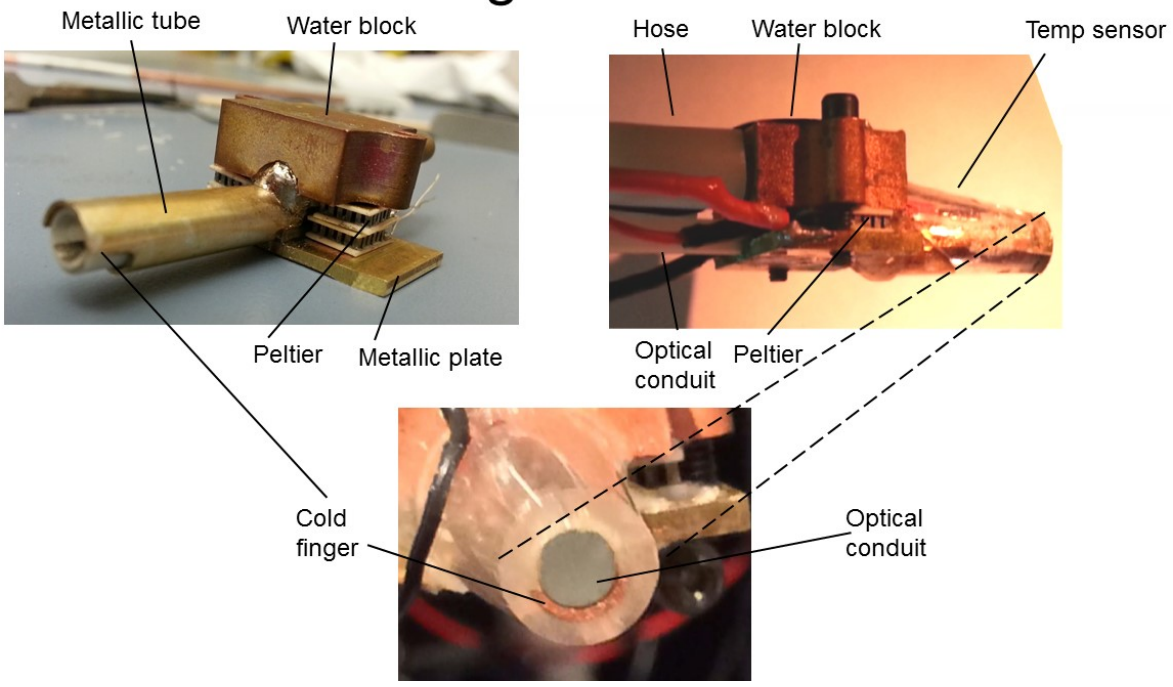

Fig. 2.11 The Peltier-mediated cold finger was built around the optical conduit. The cold metallic tube is filed down so only a half-moon reached the tip of the conduit where it is in contact with the surface of the heart.

2.7 Real Time Polymerase Chain Reaction (RT-PCR)

It is well known that the heart is a very intricate organ. Although coupled, each region presents distinct characteristics in the AP morphology and Ca^{2+} properties. Even the ventricular wall is very different in its epicardium, endocardium and midmyocardium regions.[22,130] The AP morphology disparities are due to the underlying differences in ionic channel distribution. Specifically, at the cellular level, the expression levels of proteins responsible for ion channels and the permeation of ions of across the plasma membrane are different for the various regions in the heart. For example, the gene Kv4.3 responsible for the I_{to} is more prevalent in the epicardium than endocardium. This correlates with the higher I_{to} in epicardium. [29,131]

In addition to ionic channel differences, the proteins involved in regulating key cardiac properties like Ca^{2+} handling may have different expression levels. Since the environment at the cellular level affects the function of the intact organ, it is important to assess the differences in expression of these key Ca^{2+} handling proteins. In this thesis, we wanted to test if the proteins involved in Ca^{2+} handling had different expression levels across the ventricular wall in the epicardium and endocardium. Specifically, to assess SR Ca^{2+} release differences across the ventricular wall, we assessed the transcription levels of RyR, SERCA, and PLN in the epicardium and endocardium. These proteins play critical roles, as already mentioned, in the cycling of Ca^{2+} inside myocytes and thus affect E-C coupling and CICR.

Additionally, CICR may be affected by the cascade of events resulting from the stimulation of receptors in the plasma membrane of cardiomyocytes. The expression level of receptors may not be homogeneous in the ventricular wall. These proteins that play the role of receptors are also important in Ca^{2+} cycling and AP morphology.

In order to assess the transcription level of key proteins involved in Ca^{2+} handling or as receptors in the membrane, we used Real Time Polymerase Chain Reaction (RT-PCR). RT-PCR amplifies and detects specific mRNA based on primer sequences. The reverse and forward primers used are listed in **Table 2.2**. RT-PCR compares transcription levels relative to a housekeeping gene or a gene whose expression is conserved and does not change based on different tissues. For these mRNA assessments, transcription levels were relative to glyceraldehyde 3-phosphate dehydrogenase (GAPDH).

Hearts were extracted from the mouse and maintained functional with Tyrode solution retro-perfusion as previously described. After the heart was stabilized and the blood completely washed out, the hearts were retro-perfused with RNA*later* (Qiagen) solution for 5 mins using peristaltic pumps. This solution prevented RNAse degradation and helped preserve the tissue. Small 4x4mm pieces of the left ventricle were placed in 0.6% agarose to facilitate the cutting of the epicardium and endocardium. The pieces submerged in agarose were placed on a vibratomic slicer (Leica VT1000S, Leica Inc) and sliced into 200 μm slices which were placed in Trizol. The first slice was always discarded

from the epicardium and endocardium to ensure that the epithelial region was not in the sample.

Instead of homogenizing the whole heart, these epicardial and endocardial slices were separately homogenized using an ultrasonic cell disruptor and incubated for 5 min at room temperature with 0.2mL of chloroform/mL Trizol. This ensured that the mRNA transcription levels detected was originating from the endocardium or epicardium tissue, specifically. The homogenate was centrifuged at 12000g 15 mins at 4°C and afterwards the supernatant was discarded. One mL of 75% ethanol/mL Trizol was added to the sample and then centrifuged at 7500g for 5 min at 4°C. Finally, the sample was dried for 15-30 mins and the pellet resuspended in 30µL RNAse free water to preserve the RNA, which was quantified using the Nanodrop. Only 2µg of the RNA was used in the reverse transcription reaction with 1µL of random primers (200ng/µL) and up to a final volume of 12.5µL with RNAse free water. In order to obtain the cDNA, a MIX (for reverse transcriptase) solution was added to the tube before the thermocycling began. The MIX solution contained 4µL of reaction buffer, 0.5µL of RNAse free water, 2µL dNTPs and 1µL of RevertAid to help with the cDNA reaction.

Gene	**Forward**
	Reverse
CHRM2	Forward: 5'-GGCCCCAGCCATTCTCTTCT-3'
	Reverse: 5'-AGGGACTGTGCACCCAGGAA-3'
GAPDH	Forward: 5'-TGCATCCTGCACCACCAACT-3'
	Reverse: 5'-CTTGGCAGCACCAGTGGATG-3'
ADRB1	Forward: 5'-GACTTCCGCAAGGCTTTCCA-3'
	Reverse: 5'-GTCCAGGCTCGAATCGCTGT-3'
RyR2	Forward: 5'-CCCTTGGGATGCATGAGACA-3'
	Reverse: 5'-AGCTGCGGCCACGTCTAAAG-3'
SERCA2	Forward: 5'-CCCGCTGTTTTGCTCGAGTT-3'
	Reverse: 5'-GTAGATGGCTCGCCCCTCCT-3'
PLN	Forward: 5'-TGACGATCACCGAAGCCAAG-3'
	Reverse: 5'-CGTGCTTGCTGAGGCATTTC-3'
KV4.3	Forward: 5'-ACCTGCTGCTCCCGTCGTAG-3'
	Reverse: 5'-GGCCGTGGTAATCTGGGATG-3'

Table 2.2 DNA sequences of the forward and reverse primers used in RT-PCR to produce the amplification of genes.

Finally, for the RT-PCR reaction, the cDNA samples were diluted with RNAse free water and 6.25uL of Mix (FastStart Roche, for PCR), 4.5uL of RNAse free water, 0.37uL of forward primer, and 0.37uL of reverse primer. The PCR conditions were as follows: a denaturing step of 2 min at 95°C, followed by 40 PCR cycles (95°C for 15 s; 60°C for 1 min, 72°C for 15 s), and a melting curve (55°C for 1 min and a step cycle starting at 55°C, up to 94.5°C). The protocol for this RT-PCR was published by our lab.[94]

2.8 Methods of analysis and statistics employed

The physiological recordings of the AP, Ca^{2+} transients, alternans and ionic currents were assessed based on well-established parameters in the field of cardiac electrophysiology. In order to compare between recordings before and after drug retro-perfusion, the AP and Ca^{2+} transient traces were normalized between 0 and 1. The traces analyzed for the electrically recorded APs were a result of the average from approximately 30 traces, to eliminate noise artifacts. Potentiometrically recorded APs were averaged from approximately 50 traces, since these present more noise. At times, traces were filtered at 0.2kHz. In this thesis, all AP traces shown are average traces.

The average AP trace for each set of experiments was evaluated at certain repolarization times. Specifically, the time it takes for the AP to reach 30%, 70%, or 90% repolarization was assessed and referred to APD 30, 70, or 90, respectively (**Fig. 2.12 a**). The repolarization times between control and non-control experiments were then evaluated and normalized to the control values for each heart used. Only after this normalization were values compiled from five experiments (N=5 hearts, or otherwise noted) and statistical analysis was performed in Origin 8 using one way ANOVA test.

Intracellular Ca^{2+} transients presented in this thesis are from an average of approximately 30 traces. The average was then adjusted between 0 and 1 and kinetic properties were measured. The parameters of Ca^{2+} transient kinetics measured were the rise time (RT), time-to-peak (TP), half duration (HD), and decay time (DT) (**Fig. 2.12 b**). RT is the time it takes the transient to rise between 10% and 90% of the rise. The time to peak is the time it takes the transient to reach a maximum in the amplitude. HD is the time taken for half of the Ca^{2+} transient to be complete. DT is the time taken for the transient to fall between 90% and 10% of the relaxation. Each of these parameters recorded in control and non-control experiments were evaluated and normalized to the control values for each heart used. After this normalization, five experiments (N=5 hearts, or stated otherwise) were compiled and statistical analysis was performed in Origin 8 with a one-way ANOVA test.

The APD and Ca^{2+} transient alternans are defined as alternating beat-to-beat changes in the durations or amplitudes in the APD or Ca^{2+} transient, respectively. In order to quantify the degree of alternans, the APD or Ca^{2+} transient amplitude was compared to the preceding trace. For the AP traces, there is a long AP followed by a short duration AP. The APD alternans is quantified as the difference between the long duration and the short duration at a particular point which can be APD30, 70, half phase 2, or 90 (**Fig. 2.12 c**). This difference is divided by the long duration.

During Ca^{2+} transient alternans, one of the transients has a higher amplitude (AH), while the next amplitude is low (AL). The alternans is quantified as the difference between the high amplitude and the low amplitude divided by the high amplitude (**Fig. 2.12 d**). For recordings comparing control to non-controls of the epicardium and endocardium, each non-control was compared to its respective region.

Fig. 2.12

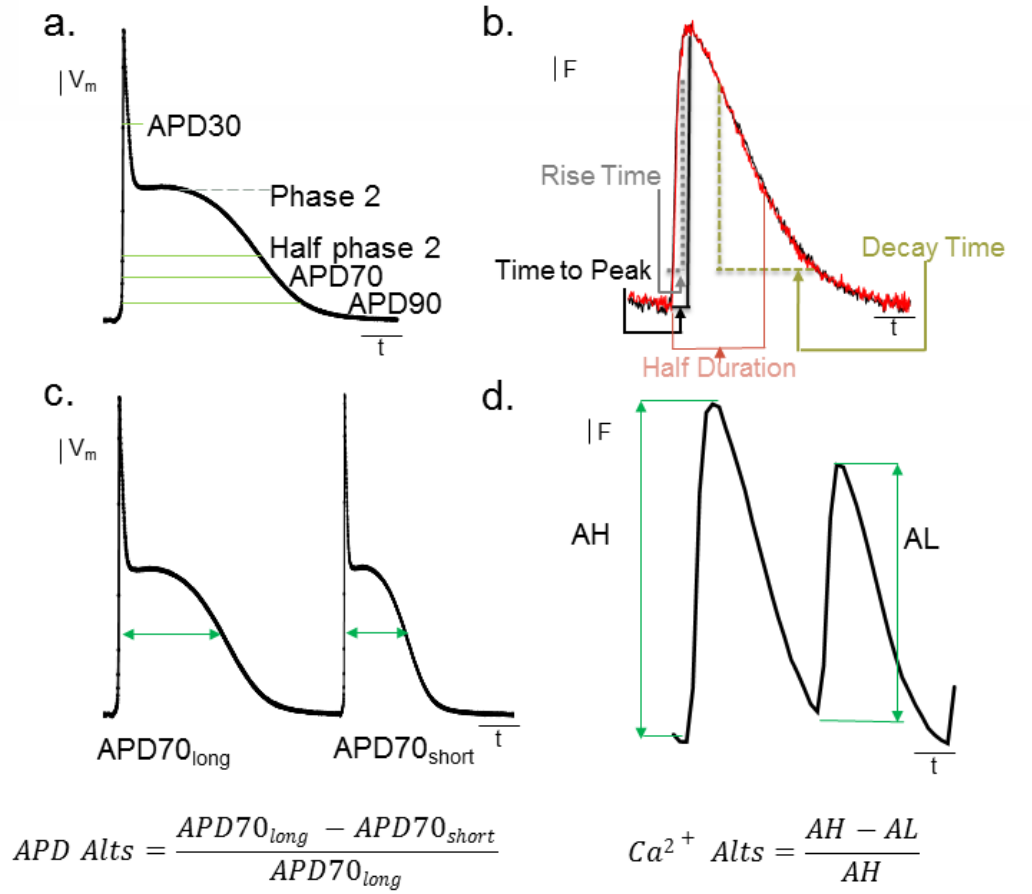

$$APD\ Alts = \frac{APD70_{long} - APD70_{short}}{APD70_{long}}$$

$$Ca^{2+}\ Alts = \frac{AH - AL}{AH}$$

Fig. 2.12 a. The action potential duration (APD) 30, half phase 2, 70, and 90 is the time taken for the AP to repolarize 30%, half phase 2, 70% or 90%, respectively. b. The Ca^{2+} transient was normalized between 0 and 1 and the rise time, time-to-peak, half duration and decay time were assessed. c. APD alternans was quantified as the long duration minus the short duration divided by the long duration at a particular repolarization percentage (shown APD70%). d. Ca^{2+} transient alternans was quantified as the high amplitude (AH) transient minus the low amplitude (AL) transient divided by the amplitude of the high transient.

In order to determine how alternans are spatially distributed, we used images from the FLOM. We spatially mapped Ca^{2+} alternans based on the amplitude of the Ca^{2+} transients in the region under the conduit. Since FLOM is an imaging technique, its camera records a series of images where each pixel records the fluorescence emitted by the fluorescent indicators. In addition to recording the fluorescence simultaneously at different locations in the heart, we can also take multiple images (as fast as 500 frames per second)

allowing us to create a video of the changes in fluorescence over time. We selected the images at the peak of the high and at the peak of the low transient and we processed them according to the equation used to calculate alternans (**Fig. 2.13**). This computed a map of the alternans distribution where some regions alternated more than others.

All the data in this thesis was expressed as means ± standard error (SEM) or standard deviation (SD). As previously described, ANOVA one way was used for statistical significance between control and non-control groups. Data was considered significant if $P<0.05$. N indicates the number of hearts used.

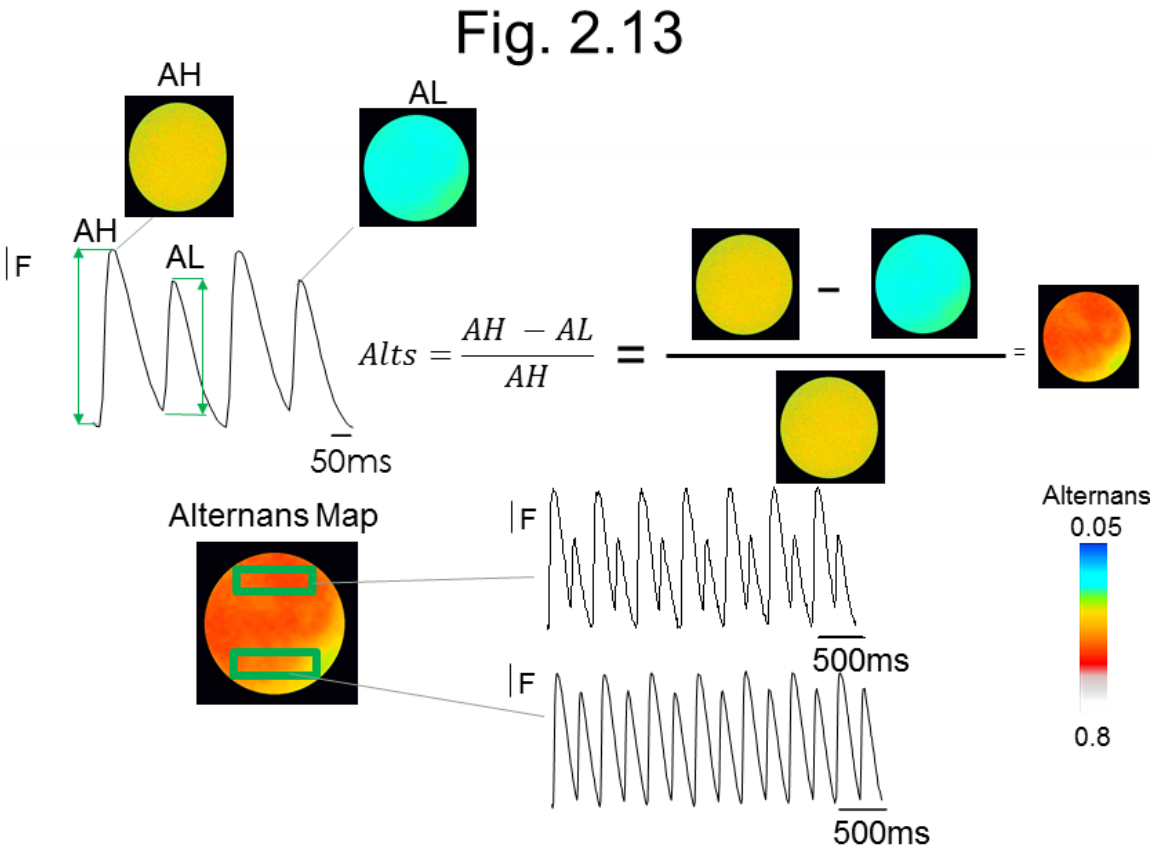

Fig. 2.13: From the series of images recorded using the FLOM apparatus, the images at the peak of the high Ca^{2+} and the low Ca^{2+} transient are processed. The resulting image is a map of Ca^{2+} transient alternans distribution where some regions alternate more (red colors) than others (yellow colors).

CHAPTER 3:

The effect of increasing the heart rate on AP morphology and intracellular [Ca^{2+}] dynamics

The heart is an electrically controlled mechanical pump. This electrical control occurs periodically at a frequency defined as heart rate (HR).[132] The stability of this cardiac frequency is essential for the normal function of the organ. The mechanism involved in the regulation of the cardiac frequency is called chronotropism.[133] A positive chronotropic effect is one in which the HR increases, while a negative chronotropic effect is a decrease in the HR. Both local and global alterations of the HR can lead to pathological conditions. When the periodicity of the HR changes from beat-to-beat, it defines a condition named cardiac arrhythmia.[132] Cardiac arrhythmias can be triggered by multiple factors such as ischemia,[134–137] inflammation,[138–141] changes in the basal HR, local activation/inhibition of the autonomic nervous system,[142,143] hypothermia,[144] etc. For example, both increase (tachycardia) and/or decrease of the heart rate (bradycardia) can trigger arrhythmias.[89,145–147] In particular, tachycardia can lead to a proarrhythmic scenario that is determined by a beat-to-beat alternation of the electrocardiographic T-wave, T-wave alternans. [52,148]

The T-wave seen in the ECG is produced by the repolarization of the ventricles.[149] Alterations in the ventricular electrical repolarization can be a risk predictor for the onset of ventricular fibrillation leading to SCD.[150] Increasing the HR promotes the generation of T-wave alternanses.[62] Our research group has shown that these T-waves alternans are produced by a Ca^{2+} driven differential alternation of the AP repolarization (APD alternans).[58] However, little is known about the transmural heterogeneities in the AP morphology and intracellular Ca^{2+} transients during T-wave alternanses. Thus, it is important to assess the AP and intracellular [Ca^{2+}] dynamics in the ventricular wall because differences in the repolarization between epicardium and endocardium leads to the generation to T-wave alternans. In this chapter, we will explore how increasing the HR of an isolated mouse heart affects the AP morphology and intracellular [Ca^{2+}] dynamics across the ventricular wall.

The function of the organ under physiological and pathological situations such as T-wave alternans is ultimately governed by proteins involved in the transport and buffering of ions at the cellular level. The heart is a highly heterogeneous organ and this is reflected in the non-homogeneous morphology of the AP.[28,40]

Even in the 1 mm mouse left ventricular wall where the T-wave alternans manifest, the AP morphology is very dissimilar due to the underlying molecular differences.[94] Intrestingly, these functional differences are not only present in rodents but also in larger animals that have an electrophysiological profile very similar to the human.[20,29] Therefore, in addition to measuring intracellular [Ca^{2+}] and membrane potential in the epicardium and endocardium, we want to understand molecular differences in these two regions. Unveiling molecular heterogeneities can help us

decipher what proteins are important for AP morphological and intracellular [Ca^{2+}] transient kinetic differences across the ventricular wall. Also, it can help us understand if there is any particular protein that plays a critical role in the generation of T-wave alternans.

3.1 How do the ventricular electrical properties respond to an increase in the HR?

The ECG signal is an overall depiction of the electrical signaling in the heart. The different waves in the ECG represent the depolarization or repolarization in the various regions of the organ. In order to see if the fast heart rhythm affects the electrical signaling in any particular region of an isolated mouse heart, we assessed the ECG during increasing HRs. Mice hearts were maintained at 32˚C and pacing frequency was increased using an external stimulator (see **Methods**).

Fig. 3.1 shows how the QRS complex does not change morphology at increasing HRs, but the T-wave does. In particular, the T-wave changes from beat-to-beat. When the

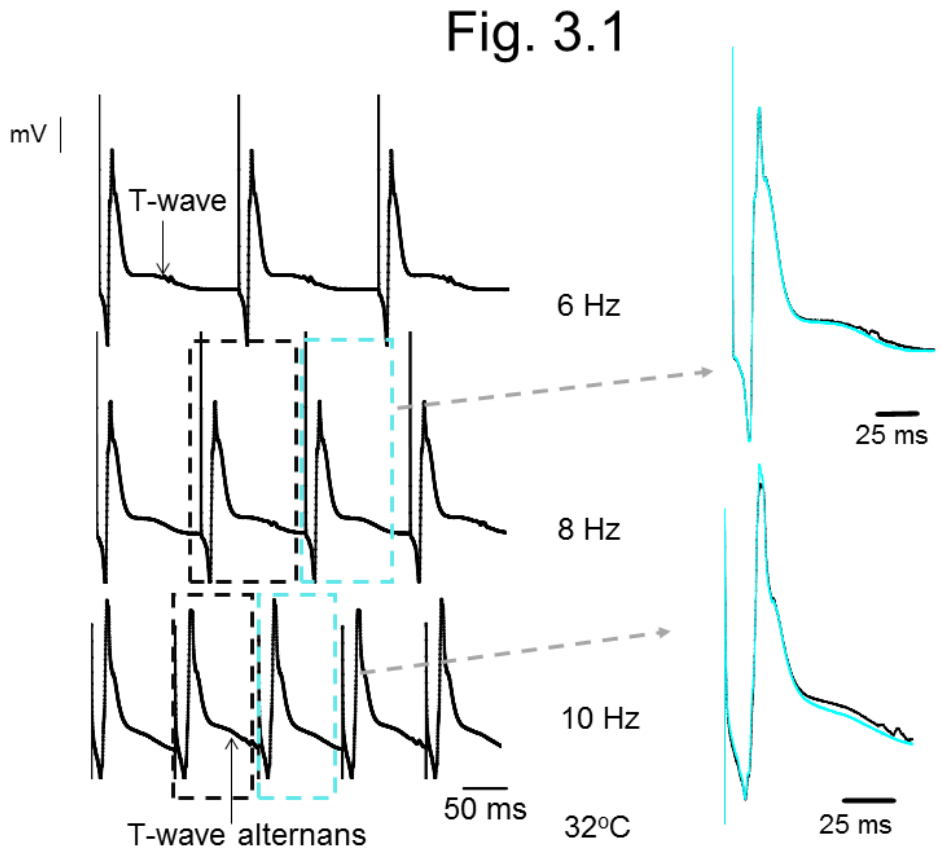

Fig. 3.1 Transmural ECGs from intact mice hearts maintained at 32°C. The pacing HR was increased until T-wave alternans developed. Sliding the trace in the cyan box over the trace in the black box shows the alternans in the T-wave appeared slightly at 8Hz and more drastically at 10Hz.

HR was set to 10Hz, the ECG's T-wave alternated between a high amplitude followed by a lower amplitude. In order to depict the changes in the T-wave between two consecutive traces, the alternating traces were overlapped. In **Fig. 3.1** the trace in the cyan dashed box was overlapped with the trace in the black dashed box. Sliding two consecutive traces such that the alternans are discordant allows us to clearly see the amplitude difference of the T-wave. Interestingly, increasing the HR made these T-wave alternans even more drastic.

As it was already stated, the T-wave is associated with the repolarization of the membrane in the ventricular cells. Therefore, at higher HRs, it is expected that there will be changes in the electrical repolarization of the ventricle. Hence, we wanted to understand what precise changes occur in the ventricular AP morphology when the HR increases and quantify them.

In order to assess the kinetics of AP at different HRs, intact mice hearts were cannulated and the epicardial AP was recorded at various HRs by using sharp glass microelectrodes (**Fig. 3.2**). It is interesting to observe that at a stimulation of 10Hz, there are very clear action potential duration (APD) alternans. These are indicated by an arrow

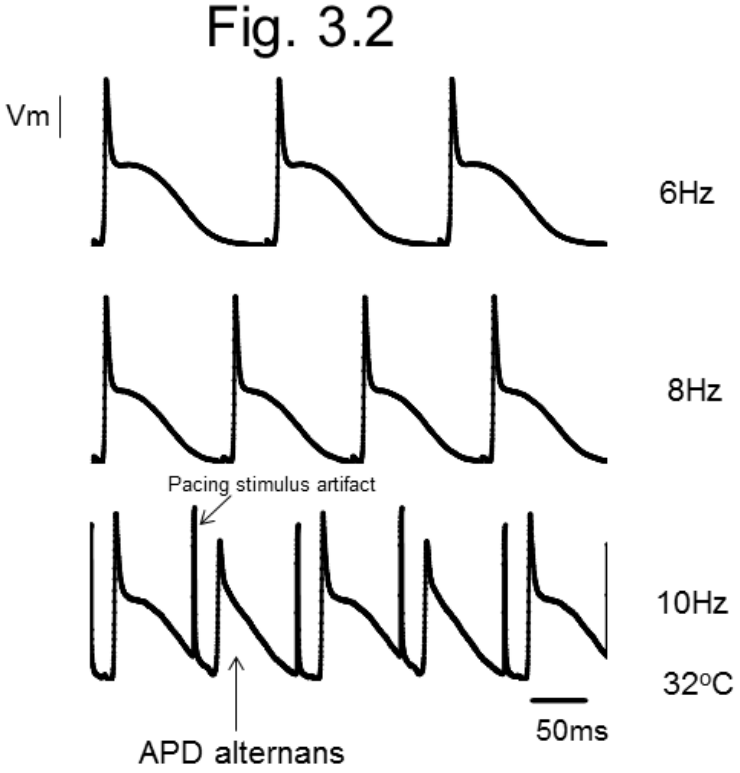

Fig. 3.2 Electrically recorded APs from the LV at increasing HR (controlled by external stimulation seen as the spikes in between consecutive APs). Intact mice hearts were maintained at 32°C in the Langendorff set-up. The APD clearly alternated (arrow) at 10Hz.

in **Fig. 3.2.** Aside from having a faster repolarization, the amplitude of phase 0 also dropped every-other beat (**Fig. 3.2**). This could be due to the lack of recovery of Na^+ channels from an inactivated state.

The epicardial APD alternans appear at a HR where the T-wave alternans are very pronounced. However, at 8Hz, where the ECGs showed a very slight alternans, the electrically recorded APs do not alternate. Nonetheless, the APD alternans may be present at 8Hz, but are not clearly visible. Thus, in order to quantify the APDs, we measured the APD in which the AP repolarizes 90% (APD 90) at increasing HRs (controlled by external stimulation).

During APD alternans, the durations alternate between a long and a short AP. Therefore, measuring APD 90 will indicate if there are differences in the duration between consecutive traces. **Fig. 3.3 a** shows AP traces at 6Hz, 7Hz, 8Hz, and 9Hz overlapped to assess morphological changes in the AP at increasing HRs. The two lines represent the duration of the long and short APs alternating during APD alternans. There is a clear shortening of the AP repolarization of phase 3 with increasing HRs. Measuring APD90 showed a clear trend of a faster repolarization time as the pacing HR increased (**Fig. 3.3 b**). The APD90 was normalized to the duration at 6Hz. At 7Hz, the APD90 was shorter

Fig. 3.3

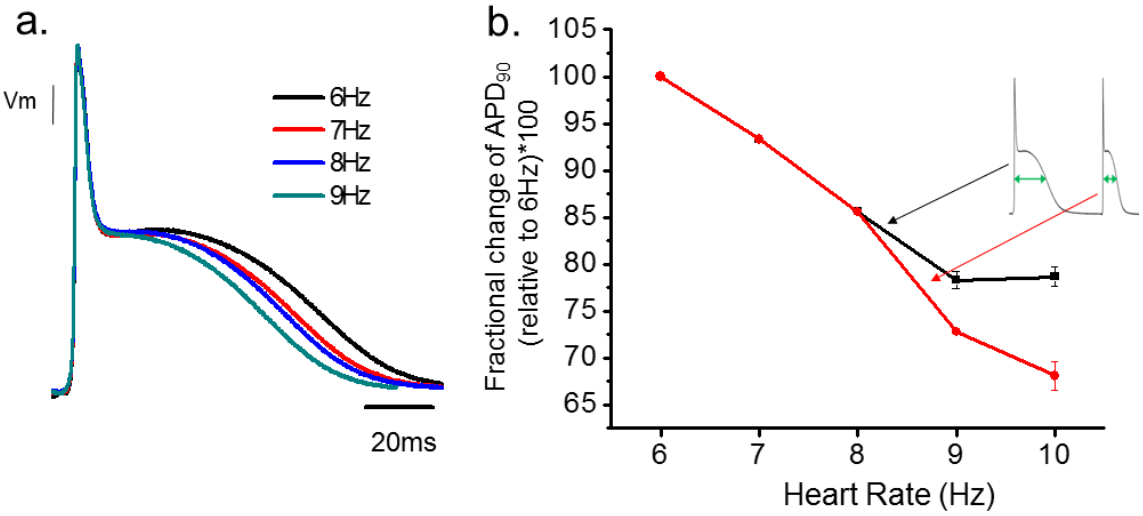

Fig. 3.3 a Electrically recorded APs from hearts externally paced at increasing stimulation HRs. When APD alternans were detected, the trace selected and shown was the AP with the long duration. b. The time taken for the AP to repolarize 90% (APD90) is faster for increasing frequencies. Hearts were maintained at 32°C. N=7 for the long APD recorded at all HRs. For the short APD, N=2 for 9Hz, N=6 for 10Hz. Mean ±SEM.

than 6Hz. It repolarized in 93% (±0.33 SEM) of the time in comparison to 6Hz (100% ± 0.05 SEM). At 8Hz, it was even faster and repolarized in 85.6% (±0.3 SEM) of the time.

It is interesting to see that at 9Hz, the APD90 varied more in duration such that the difference between the long and short APs (characterizing APD alternans) increased. There was a n AP with a long and short duration which alternate, referred to as action potential duration (APD) alternans. Out of seven experiments, only two showed alternans at 9Hz. The duration of the long AP was 78% (±0.88% SEM), while the short AP was 72.8% (±0.18% SEM) of the duration seen at 6Hz.

At 10Hz, the recorded APD90 had a long (78.6%±1.01 SEM) and short (68%±1.5 SEM) duration. At this higher HR, six hearts out of seven experiments showed alternans. **Fig. 3.2** shows this same phenomena at 10Hz, where a long AP is followed by another AP with a faster repolarization or shorter APD. Interestingly, the difference in duration between the long and short AP is greater at increasing HR as indicated by the difference between the two lines in **Fig. 3.3 b**. Therefore, the difference between the long and the short AP is greater for 10Hz than 9Hz.

The electrically recorded epicardial APD alternans occurred at frequencies in which the ECG's T-wave alternated. However, there are HRs where the ECG alternates with no indication of epicardial APD alternans. This suggest that other regions across the ventricular wall could be alternating at lower heart rates.

3.2 How do the tissular electrical properties change in response to an increase in the HR across the ventricular wall?

The T-wave is a result of transmural repolarization differences between the epicardium and endocardium. Therefore, it is possible that the endocardial APD alternates at lower heart rates in comparison to the epicardial AP. Thus, it is important to evaluate the transmural electrical activity by measuring the AP in both layers of the ventricular wall. To assess the electrical signaling in the endocardium and epicardium, we used the potentiometric dye, Di-8-ANEPPS. Since sharp glass microelectrodes easily break when recording from the inside of the ventricular wall, recording the AP optically was more efficient in accessing difficult regions. A 200μm fiber optic was positioned in the endocardium of an intact heart through a small incision. The **Methods** section thoroughly explains this set of experiments.

Despite being within close anatomical proximity (~1mm thick in mice), the epicardial and endocardial layers of the ventricular wall present very distinct morphological differences. Historically, the primary difference between the epicardium and endocardium has been associated with the longer AP duration of the endocardium and slower phase 1 repolarization rate.[20,46] Our optically recorded APs presented were in agreement with previous findings in that the endocardium depolarized earlier and also had a phase 1 that was slower than the epicardium (**Fig. 3.4 a**). **Fig. 3.4 b** shows the epicardium

and endocardium with different morphologies. Phase 1 occurs within 30% of the AP repolarization or APD30. Therefore, measuring the duration of APD30 (**Fig. 3.4 c**) is a standard way to assess phase 1. Thus, the APD30 of optically recorded APs from the epicardium (3±0.6ms) and endocardium (8±2.5ms) were quantified and were found to be significantly different ($P<0.05$). However, as opposed to other researchers,[20,46] the repolarization of phase 2 and 3 were not longer in the endocardium which may be due to

Fig. 3.4

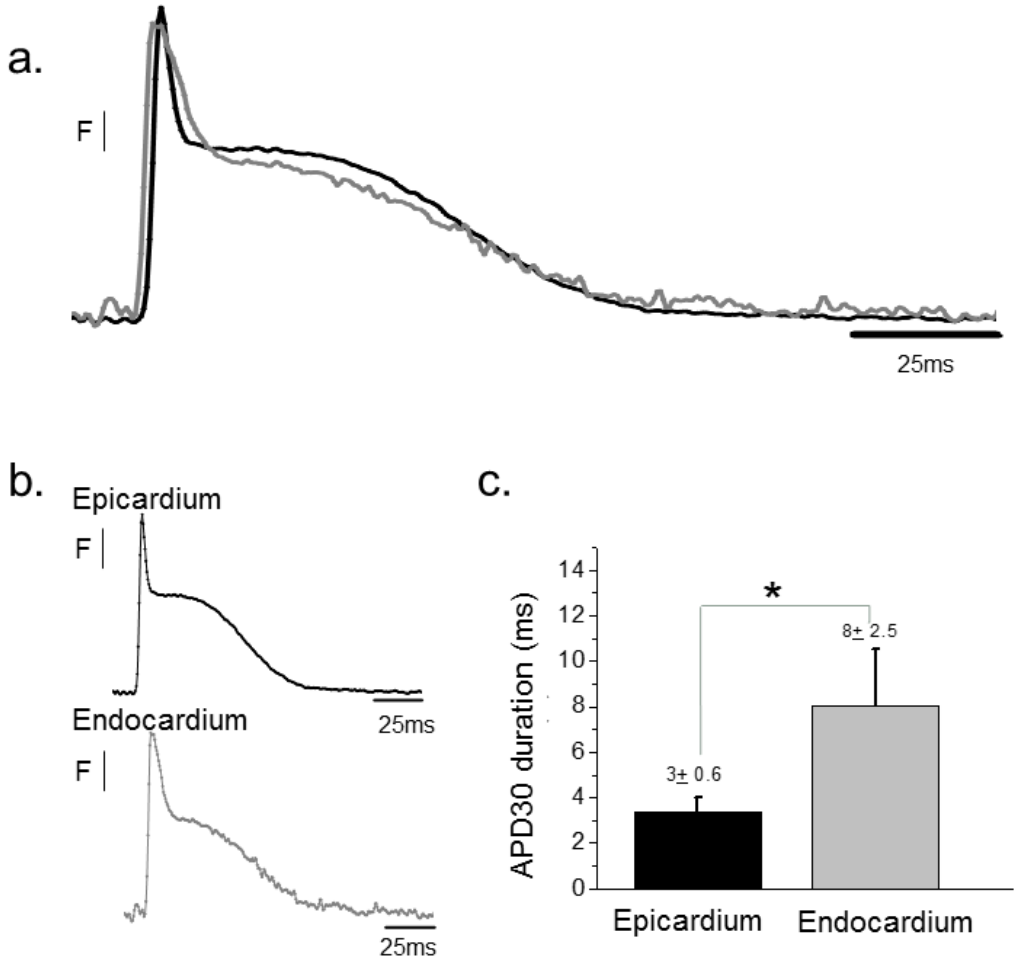

Fig. 3.4 a. Optically recorded APs from the epicardium (black) and endocardium (grey) show the endocardium depolarizes approximately 1 ms earlier than the epicardium in the ventricular layer of hearts loaded with di-8-ANEPPs. b. Sample traces of the epicardium and endocardium have distinct morphologies in the repolarization. c. The duration of APD 30 was the greatest difference between the epicardium and endocardium. Hearts were maintained at 34°C and externally paced at 6Hz. N=5. Mean ± SEM. *P<0.05. These results are in Press for publication (Aguilar-Sanchez et al 2016).

the dye used and our measurement (high noise that required filtering) in the intact heart instead of the common wedge preparation.

Since alternans are known to be dependent on the HR, it was important to understand how the two layers of the ventricular wall responded to increases in the HR. The increase in HR may affect the propagation of the electrical signal across the ventricular wall. In order to understand any differential changes induced by increases in the HR, we quantified APDs in the epicardium and endocardium at different frequencies.

To perform this set of experiments, the hearts were loaded with di-8-ANEPPS and externally paced using acupunctured needles placed in the apex of the heart (see **Methods**). As previously stated, a modified version of the PLFFM employing two fiber optics were used to simultaneously record from the endocardium and epicardium layer (in press for publication Aguilar-Sanchez et al., 2016).

The optically recorded APs from the epicardium showed a very similar HR dependency trend like the one seen in **Fig. 3.3** where the AP was measured electrically. The repolarization in phase 3 of optically recorded APs became faster with increasing HR (**Fig. 3.5 a**). Measuring the APD70 (**Fig. 3.5 a**) and APD90 (**Fig. 3.5 b**) of the potentiometric signals shows a duration that decreases with increasing HR. This was expected because at increasing HRs the cardiac cycle length decreases. As a consequence,

Fig. 3.5

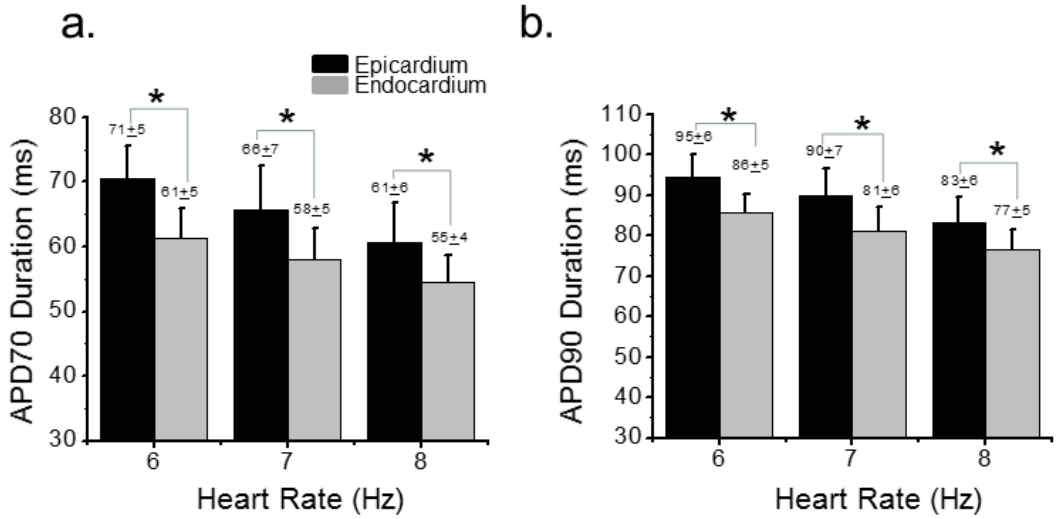

Fig. 3.5 a. The APD 70, unnormalized, from optically recorded APs from the epicardium and endocardium ventricular layer of hearts loaded with di-8-ANEPPs. b. APD90 from the epicardium and endocardium layers shorten with increasing frequencies. Hearts were maintained at 32°C and externally paced at 6Hz, 7Hz, and 8Hz. N=4 epicardium, N=3 endocardium. Mean ±SD. *P<0.05.

the overall duration of the AP must repolarize faster to be ready for the next, rapidly approaching electrical stimulus. Interestingly and unexpectedly, the endocardium presented durations shorter than the epicardium (except in phase 1) which may be a result of fiber optic positioning and the use of filtering due to the high noise when using potentiometric dyes.

The trend in the AP morphology shortening at increasing HRs is shown in **Fig. 3.6**. It is apparent that phase 3 presents HR-dependent differences. In order to quantify this, the APD90 was recorded at 6-10Hz and normalized to the duration at 6Hz. The optically recorded epicardial APD90s were graphed as a function of HR and resulted in a very similar graph seen from APD90 of *electrically* recorded APs. The two lines represent the duration of the long and short APs that occur during APD alternans. The optically recorded endocardial APs presented similar changes as the epicardium in the shortening of the APD at increasing HRs (**Fig. 3.6 c**). Additionally, the duration of phase 1 of the endocardial layer presented a strong HR dependency (seen in **Fig. 3.6 c**). This HR dependency was not observed in the duration of phase 1 in optical recordings obtained from the epicardial layer (**Fig. 3.6 a**), probably because this phase occurs too fast in this region making it difficult to observe changes.

Overall, the epicardium and endocardium signals respond very similar to increases in HR. Despite the morphological dissimilarities, both regions of the ventricular wall present the same pattern of faster phase 3 repolarization as the HR was increased. **Table 3.1** compares the epicardial and endocardial APD90s. Interestingly, phase 1 also changed during increases in the HR, but this was only apparent in the endocardium perhaps because this phase is slower in this region. Taken together, these results indicate that HR affects the repolarization of the AP. Thus, the key to understanding APD alternans across the ventricular wall is to assess the molecular events occurring during these repolarization phases.

Fig. 3.6

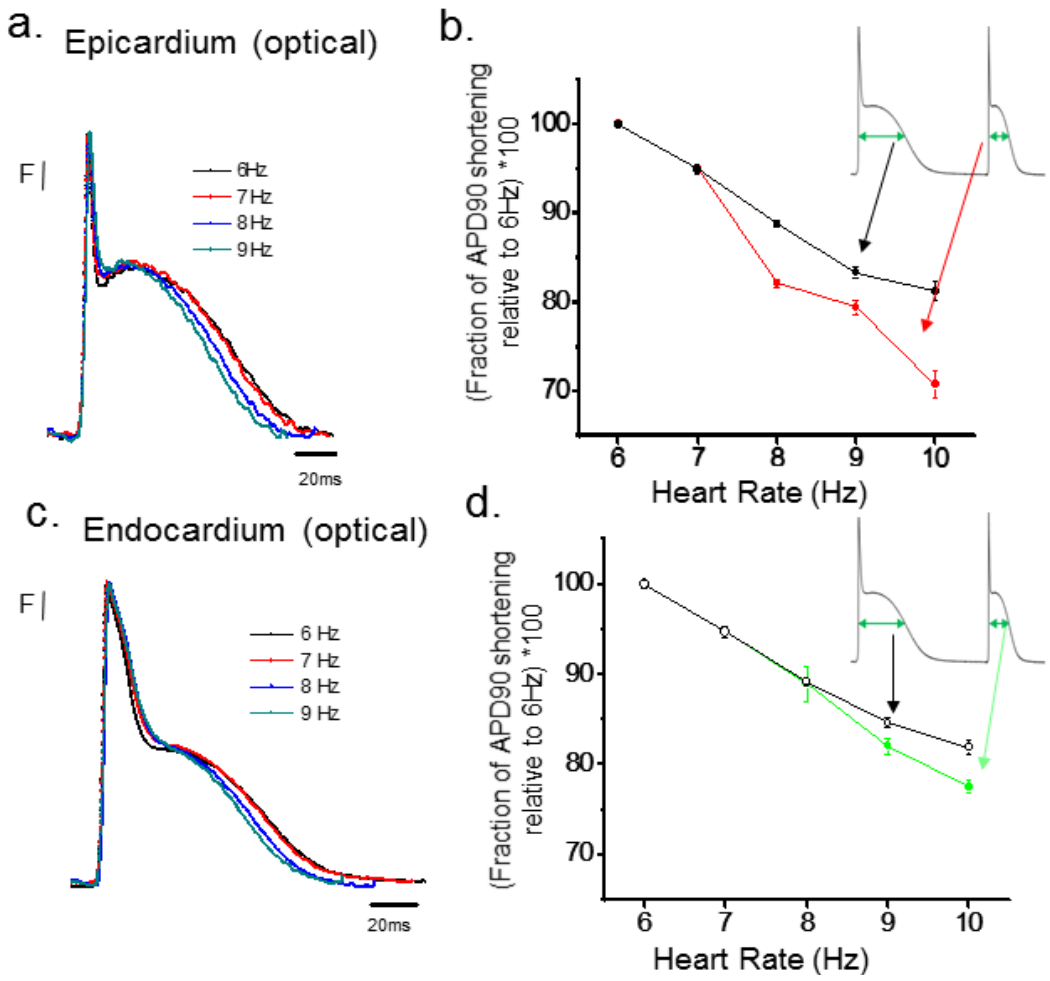

Fig. 3.6 a. Optically recorded APs from the epicardium of hearts externally paced at increasing HRs. b. The fraction of APD90 shortening relative to 6Hz of the optically recorded epicardial APs repolarize faster for increasing HRs. The two lines represent the duration of the long (black) and short (red) APs alternating during APD alternans. c. Optically recorded APs from the endocardium region show faster repolarization at increasing frequencies. d. The fraction of APD90 shortening relative to 6Hz of the optically recorded endocardial APs show a long duration (black) followed by a shorter duration (green) as HR was increased. Hearts were maintained at 32°C. N=4 for the long APD recorded at all HRs. For the short APD, N=1 for 8Hz, N=2 for 9Hz, N=3 for 10Hz. Mean ±SEM.

Frequency (Hz)	Epicardium APD90 shortening (relative to 6Hz)*100	SEM	Endocardium APD90 shortening (relative to 6Hz)*100	SEM
6	100	0.35618	100	0.43131
7	94.96376	0.52111	94.71884	0.66702
8	88.85841	0.32672	89.17564	0.44578
	82.08876	0.39539	88.96002	1.93793
9	83.43066	0.68927	84.62237	0.53393
	79.39211	0.72575	82.04535	0.91642
10	81.32975	1.02937	81.91536	0.77369
	70.74071	1.54726	77.49798	0.71501

Table 3.1 The fraction of APD90 shortening releative to 6Hz (multiplied by 100) of the optically recorded APs from the epicardium and the endocardium at different HRs. At 8-10Hz, the top value refers to the long duration AP while the value below is the short duration AP occurring during APD alternans.

3.3 Are intracellular Ca $^{2+}$ transients different in the epicardial and endocardial layers of the ventricular wall?

The repolarization morphology of the AP is greatly defined by the underlying handling of intracellular Ca^{2+} which contributes to activate membrane conductances that define phase 2.[34] In the last section, we saw that the APs recorded from the endocardium were more triangular (less phase 2) than those optically recorded from the epicardium. Since phase 2 is associated with high cytosolic [Ca^{2+}] during systole and its effect on NCX activity, it was important to assess the intracellular Ca^{2+} transients from both regions of the ventricular wall. This can shed light on differential handling of intracellular Ca^{2+} in the epicardium and endocardium.

Epicardial and endocardial intracellular Ca^{2+} transients were recorded with the aid of two fiber optics in the modified PLFFM set-up and using the Ca^{2+} sensing dye Rhod-2. **Fig. 3.7 a** depicts the intracellular Ca^{2+} transients recorded by measuring Rhod-2 fluorescence from the epicardium and endocardium of intact hearts. It is clear that the endocardium Ca^{2+} transient begins to rise sooner, but is slower at reaching a maximum than the epicardium Ca^{2+} transient. This was an expected result since the endocardial layer is the first to be depolarized during the transmural propagation of the AP and thus initiate CICR by the opening of voltage-gated L-type Ca^{2+} channels. This feature (the earlier and slower rising of the Ca^{2+} transient) helped to confirm that the fiber optic was positioned in the endocardium. If we shift these Ca^{2+} transients to start at the same time (**Fig. 3.7 b**), then we can confirm that the duration of the endocardial Ca^{2+} transient is longer.

In order to understand if there are any differential characteristics in the intracellular Ca^{2+} handling across the ventricular wall, we quantified the kinetics of the Ca^{2+} transients. The kinetic parameters measured were the rise time (RT), time to peak (TP), half duration (HD) and decay time (DT). As previously mentioned in the **Methods**, the RT is the time it takes the Ca^{2+} transient to rise between 10 and 90% of the rise. A summary of the results in presented in **Fig. 3.7 c**. We found that the RT of the endocardium vs. the epicardium (9 ± 1.8 ms vs. 7 ± 1.1 ms) was significantly slower ($P<0.05$) (**Fig. 3.7 c**). This may correlate with the endocardium having a slower SR Ca^{2+} release. The time taken the Ca^{2+} transient to reach a maximum is the TP. The TP was also found to be significantly slower for Ca^{2+} transients from the endocardium than the epicardium. This may also correlate with a slower Ca^{2+} release from the SR. The endocardium Ca^{2+} transient also had a longer HD, with a slower DT than those recorded from the epicardium.

Overall, these results indicate that the time course of the Ca^{2+} transients in the epicardium are not the same as those in the endocardium. This implies that the intracellular [Ca^{2+}] handling in both regions is different which may consequently affect Ca^{2+} alternans.

Fig. 3.7

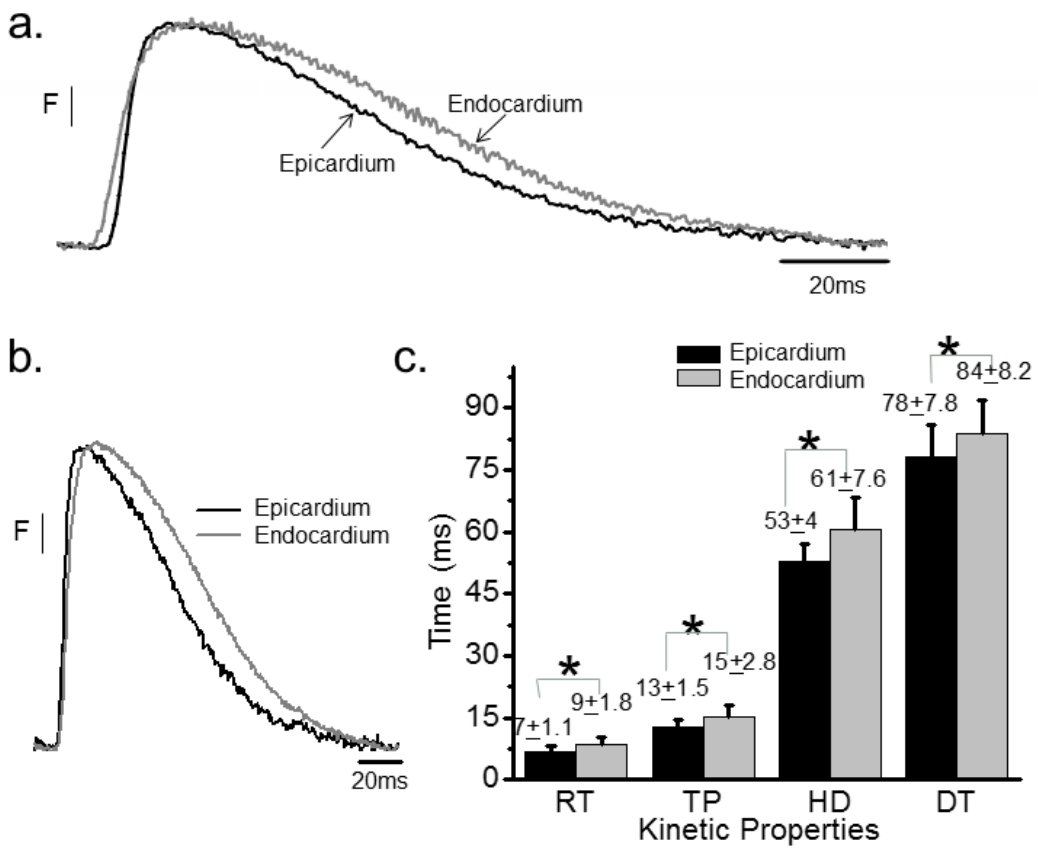

Fig. 3.7 a. Normalized, but un-shifted, Ca^{2+} transients recorded from the epicardial (black) and endocardial (grey) layer of the ventricular wall of hearts loaded with Rhod-2 at 37°C show the endocardium starts to rise earlier (and is slower) than the epicardium. b. Ca^{2+} transients that have been normalized and shifted to start rising at the same time show clear differences in the duration. c. The assessment of the Ca^{2+} transient kinetics show the endocardium is significantly slower (N=4 hearts, *P<0.05, ± SD) than the epicardium in RT, TP, HD, and DT. (These results are modified from an in press publication Aguilar-Sanchez et al. *J Vis Exp*. 2016).

3.4 Does heart rate modify differentially the kinetics of Ca^{2+} transients across the ventricular wall?

In the last section, we saw that intracellular Ca^{2+} handling across the ventricular wall is not identical. Both regions of the ventricular wall, epicardium and endocardium, have different Ca^{2+} dynamics. Since T-wave alternans are thought to be due to the mishandling of intracellular [Ca^{2+}] at the cellular level,[58–61] then the differential handling of Ca^{2+} across the ventricular wall may be critical in understanding the origin of alternans.

Generally, higher HRs increase the probability of T-wave alternans. When the HR increases, the heart changes its Ca^{2+} dynamics by increasing or decreasing the Ca^{2+} release/reuptake according to the HR. In order to understand how the intracellular Ca^{2+} may become mishandled during alternans, we assessed Ca^{2+} transients in the epicardium and endocardium at increasing HRs. This can reveal some details of what type of Ca^{2+} mishandling (release/reuptake) may be playing a critical role in producing alternans.

Specifically, we wanted to understand how the ventricular wall adapts to the increase in HR. Thus, we recorded intracellular Ca^{2+} transients from the epicardium (**Fig. 3.8 a**) and endocardium (**Fig. 3.8 b**) layer of intact mice hearts loaded with Rhod-2 using the modified PLFFM set-up. The hearts were externally paced at 6Hz, 7Hz, and 8Hz (HRs in which the kinetics are expected to change without generating alternans). By using these low HRs and selecting hearts that did not alternate, we ensured that the Ca^{2+} transient kinetics assessed were not influenced by alternans. We measured the RT and DT of the transients to quantify any kinetic differences that may occur during the time course of the Ca^{2+} transients at increasing HR.

Fig. 3.8 c showed that increasing the HR did not impose a significant effect ($P<0.05$) on the RT of Ca^{2+} transients recorded both in the epicardium and the endocardium implying no effects over the rising kinetics. However, the epicardium DT decreased with increasing HR significantly ($P<0.05$) (**Fig. 3.8 d**). The endocardium DT also decreased with increasing HR, but was only significant between 6Hz and 8Hz and between 7Hz and 8Hz. This implies that HR affects the relaxation kinetics.

Increasing the HR reduced the duration of the intracellular Ca^{2+} transients. This is in accordance to the cycle length decreasing when the HR increases (the time course of the Ca^{2+} transient occurs faster). However, these kinetic changes do not provide a quantitative measure of how much intracellular Ca^{2+} is released/reuptaken. RT and DT are measures of the kinetics, which are how fast the release and reuptake occur.

Fig. 3.8

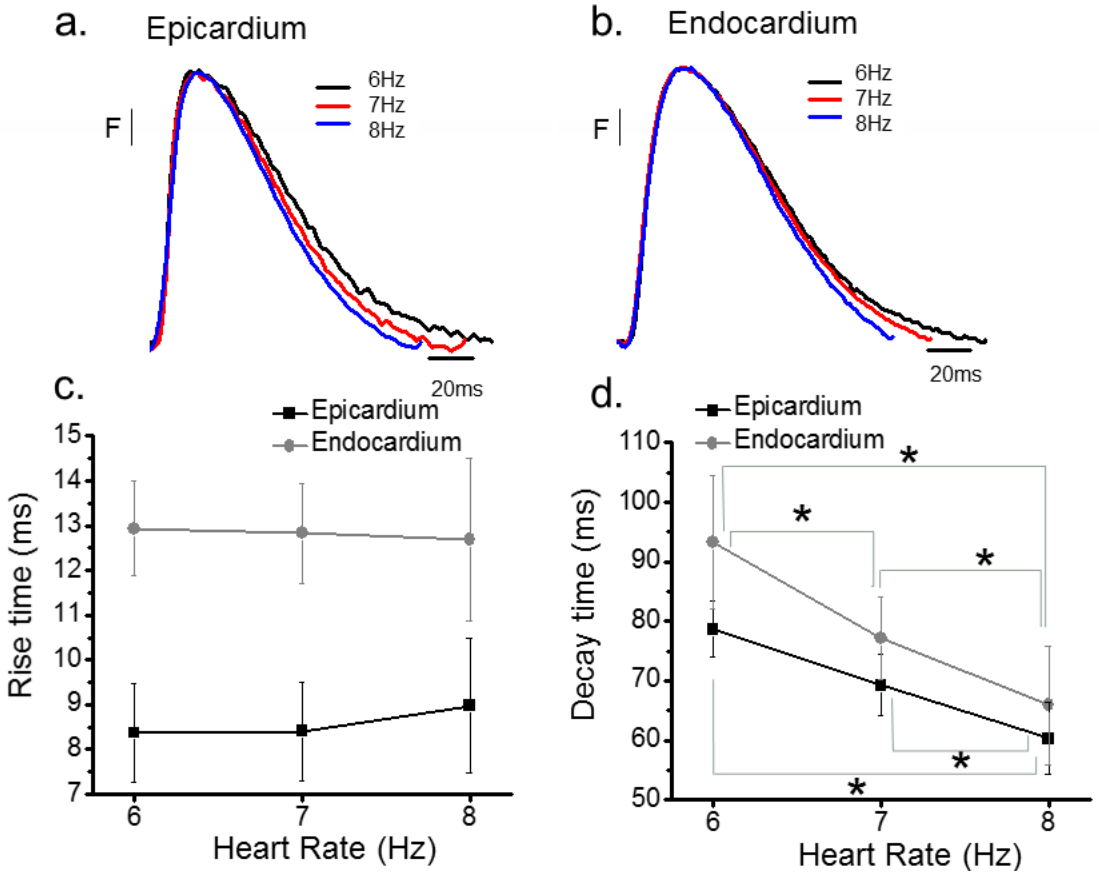

Fig. 3.8 a. Intracellular Ca^{2+} transients recorded from the epicardial and (b) endocardial layer of the ventricular wall externally paced at increasing HRs. These hearts were selected from those that did not present Ca^{2+} alternans so that alternans did not influence the kinetics assessed. c. Although Ca^{2+} transients from the endocardium and epicardium have different RT kinetics, these did not change during increased HRs. d. The DT decreased as the HR increased for both layers of the ventricular wall. Hearts were maintained at 32°C and loaded with Rhod-2. N=3 hearts, *P<0.05, mean ± SEM.

In order to measure if the Ca^{2+} transient kinetic changes are due to alterations in the SR Ca^{2+} release process, we assessed the amplitude of the Ca^{2+} transients. We quantified the amplitude of intracellular Ca^{2+} transients at different frequencies. Hearts were loaded with the Ca^{2+}-sensing dye, Rhod 2 and externally paced at 6-10Hz. We measured the epicardial and endocardial intracellular Ca^{2+} transients using two fiber optics, one was positioned in the epicardium and the other in the endocardium surface. **Fig. 3.9** shows epicardial intracellular Ca^{2+} transients that have not been normalized between zero and one. It is apparent that the intracellular Ca^{2+} transients at different HR have very dissimilar amplitudes. The amplitude decreases with increasing HR. This same pattern of decreasing amplitude was observed for the endocardium.

Fig. 3.9

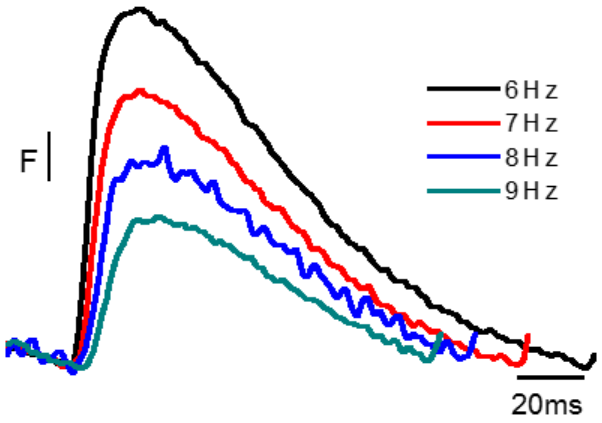

Fig. 3.9 Intracellular Ca^{2+} transients recorded from the epicardium of hearts externally paced at increasing HRs. Hearts were loaded with Rhod-2 and maintained at 32°C.

Fig. 3.10

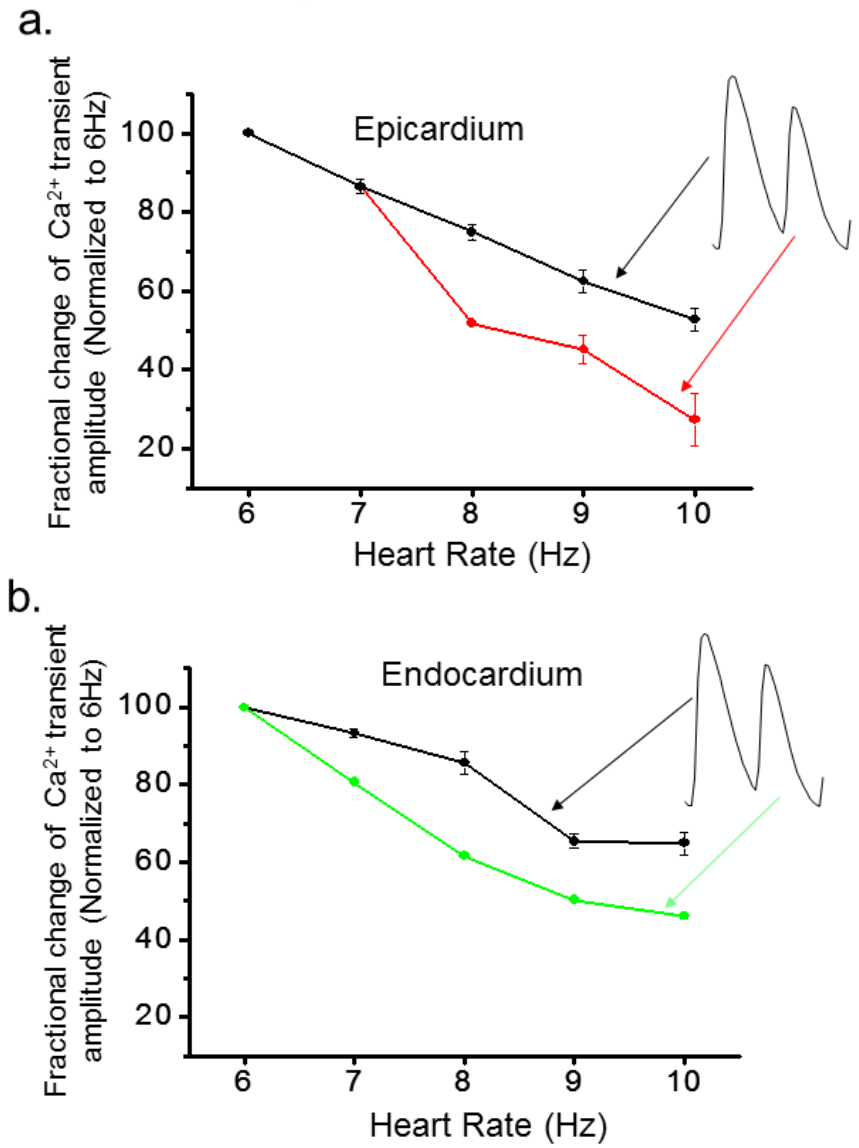

Fig. 3.10 a. The amplitude of intracellular Ca^{2+} transients recorded from the epicardium of intact hearts at increasing HRs show that alternans appear at 8Hz. The amplitude drops significantly with increasing HRs relative to 6Hz amplitude. B. Amplitude of intracellular Ca^{2+} transients recorded form the endocardium show alternans at lower HRs. Transient amplitudes were normalized to the amplitude at 6Hz. The fractional change of Ca^{2+} transient amplitudes are significantly different relative to the amplitude at 6Hz, *P<0.05. N=3 for the Ca^{2+} transient with the high amplitude recorded at 6-9Hz and N=2 for 10Hz. For the Ca^{2+} transient with low amplitude N=1 for 7Hz-8Hz and N=2 for 9Hz-10Hz. Mean ±SEM.

In order to quantify the amplitude changes, we recorded Ca^{2+} transients and normalized the amplitude to the amplitude at the lowest HR (6Hz). Increasing the heart rate to 7Hz resulted in an amplitude decrease for both the epicardium (86.5%$\pm$1.77 StErr) and the endocardium (93.2%$\pm$1.11 StErr). However, the amplitude dropped more for the epicardium than the endocardium. Interestingly, the endocardium showed alternans at lower frequencies than the epicardium.

It was surprising to see that the amplitude of the epicardial Ca^{2+} transients decreased more than the transients recorded from the endocardium when the HR was increased (**Fig 3.10 a** and **b**). This may suggest that the epicardium decreases its SR Ca^{2+} release when the HR increases and may play a protective role against Ca^{2+} alternans. The endocardium Ca^{2+} transient amplitudes do not drop as fast indicating that the Ca^{2+} dynamics are not changing at the same magnitude as those in the epicardium. Thus, the endocardium may have difficulty adjusting the Ca^{2+} dynamics at increasing HRs and could be the tissue to blame for the genesis of T-wave alternans.

Indeed, when we measured Ca^{2+} transients at increasing HRs, we saw that the endocardium began to alternate at lower HRs (arrow) than the epicardium (**Fig. 3.11)**. The degree of alternans as a function of HR for the epicardium and endocardium are seen in **Fig. 3.12**. The Ca^{2+} transient alternans (by measuring amplitude ratios based on equation) are higher and appear sooner in the endocardium. Again, this implies that the endocardium is unable to handle intracellular Ca^{2+} at increasing HRs.

In order to understand why the endocardium is more susceptible to alternating at lower HRs, we assessed which are the molecular differences underlying the ventricular wall. We assessed the mRNA expression levels of various key Ca^{2+} handling proteins in the endocardium and epicardium (**Fig. 3.12**).

Fig. 3.11

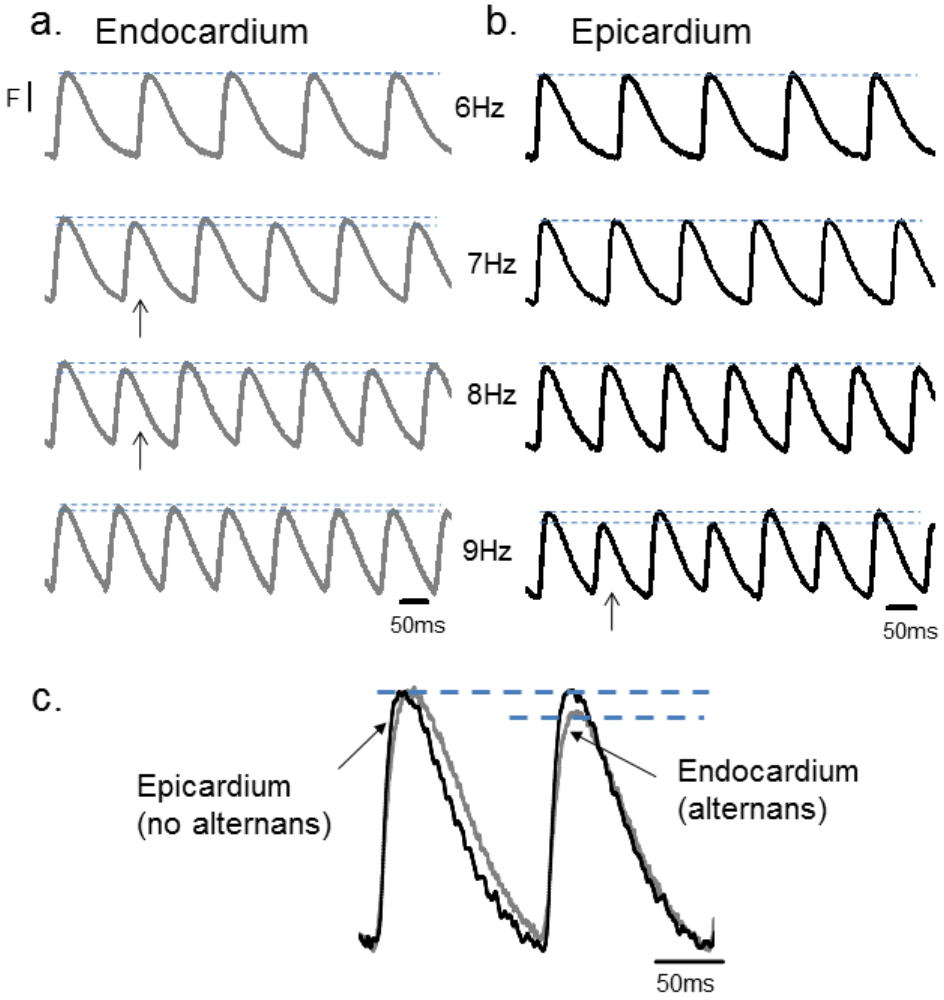

Fig. 3.11 a. Endocardial Ca^{2+} transients at various frequencies show alternans appearing at 7Hz (arrow). b. Epicardial Ca^{2+} transients show alternans appearing at higher HRs (9Hz). c. At 8Hz, the endocardium (grey) alternates while the epicardium does not (black).

Fig. 3.12

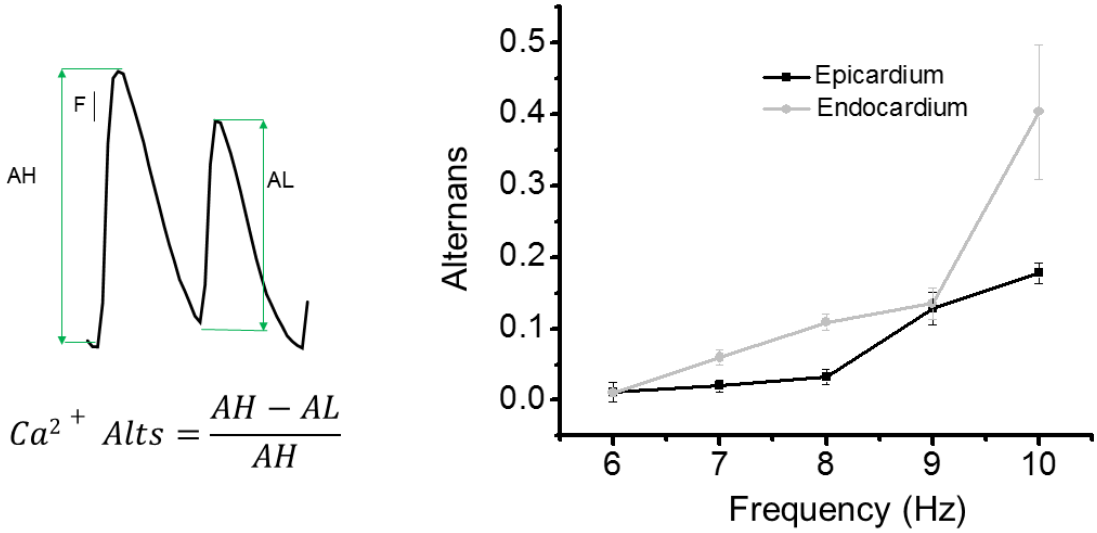

Fig. 3.12 Alternans computed (based on the Ca^{2+} transient amplitudes) from the epicardium (black) and endocardium (grey) at various HR. The endocardium presented a greater degree of Ca^{2+} alternans at lower HRs than the epicardium. Hearts were maintained at 32°C and externally paced. Frequencies 7, 8, and 10Hz are significantly different between the two layers. P<0.05. N=4. Mean ±SEM.

The proteins assessed were RyR2, SERCA, PLN, and Kv4.3. RyR2 regulates the Ca^{2+} release from the SR. Results showed lower levels of mRNA coding for RyR2 in the endocardium, which correlates with the longer time to peak seen in **Fig. 3.7 b**. SERCA pumps Ca^{2+} into the SR. There was also less expression of SERCA in the endocardium, which correlates with the longer half duration and slower decay of Ca^{2+} transients in this layer. Another critical protein is phospholamban (PLN). PLN regulates SERCA activity such that when PLN is not phosphorylated, SERCA's affinity for Ca^{2+} is dramatically reduced. Interestingly, PLN expression did not change. Nevertheless, the fraction of SERCA inhibited by PLN is greater in the endocardium because of the less expression of SERCA. This suggested that SERCA may be an important contributor causing alternans to appear at lower HRs in the endocardium.

Finally, Kv4.3 was used as a reference gene, which is responsible for the I_{to}. It is well known that the epicardium has a larger I_{to} and therefore, the expression of Kv4.3 is expected to be greater than in the endocardium. Quantifying the mRNA showed that indeed there is a higher expression of Kv4.3 in the epicardium (**Fig. 3.13**). The work presented in **Fig. 3.13** was published in the *Journal of Molecular and Cellular Cardiology*.[94]

Fig. 3.13

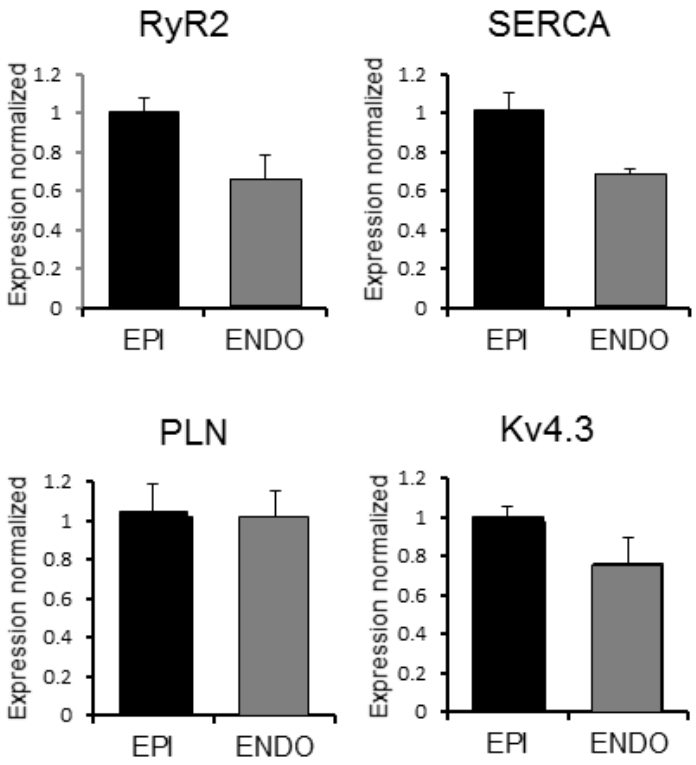

Fig. 3.13 mRNA assessment of genes encoding key Ca^{2+} handling proteins (RyR2, SERCA, and PLN) across the ventricular wall. Kv4.3, the gene responsible for the I_{to}, was used as a control based on the well known larger Ito in the epicardium. (These results have been published by Mattiazzi et al. *J. Mol. Cell Cardiol.* 2015.)

Overall, in this chapter we were able to show that increasing the HR shortened the duration of the AP repolarization. This shortening correlated with faster relaxation kinetics in the intracellular Ca^{2+} transients as the HR was increased. When we continued increasing the HR, we saw that the endocardium alternated at lower HRs than the epicardium. After assessing the differences in the Ca^{2+} transients across the ventricular wall, our results showed that the endocardium Ca^{2+} transients relax slower. Our molecular biology data revealed that these differences may be due to the endocardium having less expression of SERCA and more inhibition by PLN in comparison to the epicardium. Together, these results may point to the importance of the Ca^{2+} re-uptake mechanism into the SR, which is hindered in the endocardium making it more prone to develop alternans.

CHAPTER 4:

Assessing the temperature dependency of Ca^{2+} transient alternans

Research has focused on the mishandling of intracellular Ca^{2+} as the underlying cause of T-wave alternans.[58–62] The handling of intracellular Ca^{2+} involves many proteins that can be affected by temperature. A shift towards elevated temperatures can increase the open probability of L-type Ca^{2+} channels[69,70] through which Ca^{2+} enters myocytes to trigger CICR. The NCX, which helps in the relaxation phase of the Ca^{2+} transient, is more active at higher temperatures.[34,71,72] In addition, the reuptake of intracellular free Ca^{2+} into the SR is mediated by an ATP driven pump, SERCA, which is known to be temperature-dependent.[45] These thermodynamic effects can be seen in the relaxation kinetic differences in Ca^{2+} transients taken at two different temperatures.[58] However, the effect of temperature on Ca^{2+} transient kinetics has not been thoroughly assessed.

Additionally, physiological events that regulate the cardiac function are spatially distributed. As we already showed in the last chapter, the two layers of the ventricular wall have cardiac signals that are significantly different (i.e. Ca^{2+} transients). However, in these previous experiments it was not possible to evaluate the spatial distribution of AP and Ca^{2+} transients in the same anatomical layer. In a previous paper from our laboratory,[34] it was demonstrated that morphology of APs are unevenly distributed all over the epicardium. For example, APs recorded at the apex of the left ventricle were significantly shorter than the ones recorded at the base on the left ventricle.[34] Taking these two independent variables into account (temperature and space), we decided to evaluate the spatial distribution of Ca^{2+} transients at different temperatures. In this chapter, we aim to test the hypothesis that hypothermia (cold temperatures) promotes Ca^{2+} alternans by impairing Ca^{2+} re-sequestering into the SR. We decided to evaluate the spatial distribution of the temperature dependency using the previously described FLOM technique (see **Methods**).

4.1 What is the temperature dependency and spatial distribution of intracellular Ca^{2+} transients?

Before assessing how temperature affects Ca^{2+} alternans, it was imperative to first establish how the Ca^{2+} transients are affected by temperature. Thus, we induced global temperature changes in the heart by changing the temperature of the bath in which the heart was submerged. FLOM allowed us to image the changes in fluorescence over time to measure intracellular Ca^{2+} transients. This was done by using the Ca^{2+} sensing dye, Rhod-2, and a 532 nm laser that excited and transmitted the light through the conduit placed on the surface of the heart. (**Fig. 2.9**).

Montages of the images taken from the 3.2mm conduit of the same heart at different bath temperatures are shown in **Fig. 4.1**. One Ca^{2+} transient is depicted above the montage to help illustrate which color changes (red) correspond to the rapid rise and which colors represent the slower relaxation (orange to blue) of the transient. These colors help us follow the changes in intracellular [Ca^{2+}].

The global changes in temperature affected the fluorescent scheme seen from the montages in **Fig 4.1**. As the temperature was dropped, it was very apparent that the time to peak of the Ca^{2+} transients move to longer times and the relaxation of the series of fluorescent images looks also slower.

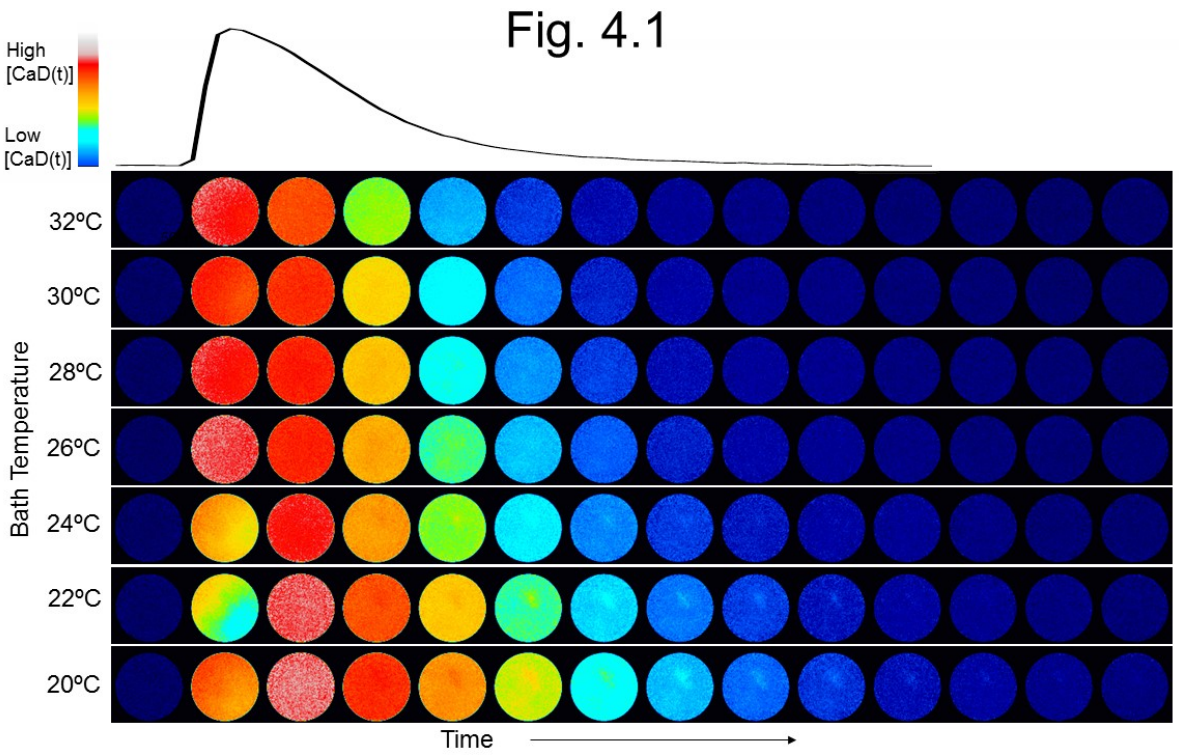

Fig. 4.1 FLOM fluorescent images from a heart loaded with Rhod-2 at decreasing bath temperatures. Color scheme was selected such that blue indicates low Ca^{2+} bound to dye (CaD) and red is high CaD. One Ca^{2+} transient is depicted above the montage to illustrate the color changes in the timecourse of the transient as Ca^{2+} binds to the dye and fluoresces. Hearts were paced at 2Hz.

At 32°C, the colors change drastically from blue (little intracellular Ca^{2+} bound to dye, CaD) to red (high CaD) indicating a fast release. However, at 20°C, there is a slower rise in colors and the blue changes to orange, light red, and finally red representing a slower rise in intracellular Ca^{2+} levels. After reaching a maximum, shown as red, the intracellular Ca^{2+} begins to drop until finally reaching low levels (blue). The relaxation phase is drastically affected by temperature. As the bath becomes colder, the montage of images also shows that more time is needed to reach a baseline of blue.

In order to assess the effects of temperature on the series of images produced by the FLOM technique, we computed global Ca^{2+} transients by space integrating the intensity

of every pixel of the recorded image. An example of this procedure is illustrated in **Fig. 4.2 a** where the computed intracellular Ca^{2+} transients at different temperatures are shown. The largest temperature effect is seen in the relaxation phase of the Ca^{2+} transient. The relaxation phase becomes progressively slower at colder temperatures.

The effects of temperature on the relaxation of the intracellular Ca^{2+} transients can be quantified by computing the derivative of the trace (**Fig. 4.2 b**). This allowed us to define the relationship between the relaxations of the Ca^{2+} transients (negative derivative) with the temperature. Thus, the negative derivative is the rate of relaxation. More than a century ago Arrhenius defined the relationship between the rate of a chemical reaction and temperature. He defined a thermodynamic framework in which the natural logarithm of a reaction rate was characterized as a function of the temperature, the change in enthalpy (ΔH) and the change in entropy (ΔS).

Fig. 4.2

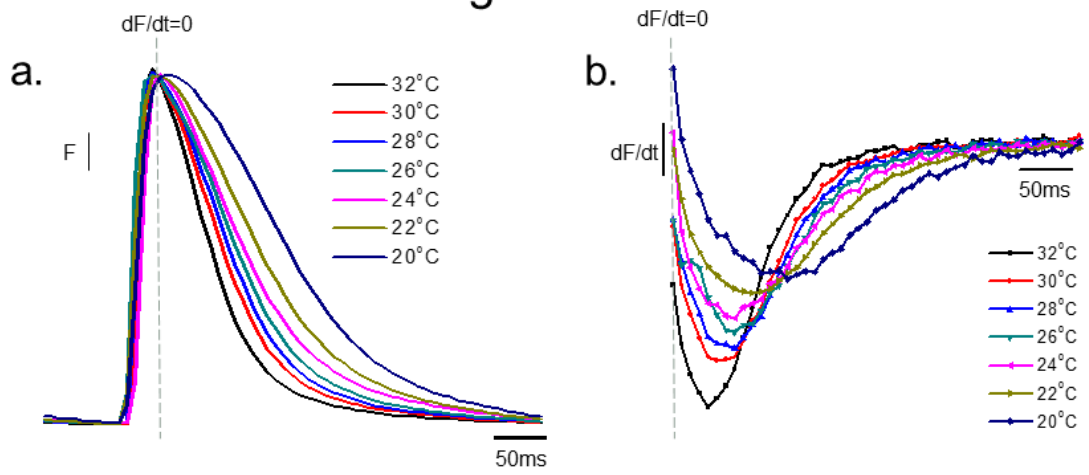

Fig. 4.2 a. Ca^{2+} transients from FLOM fluorescent images of a heart loaded with Rhod-2 and at decreasing bath temperatures. Temperature was dropped by 2°C and allowed to stabilize before every recording. Hearts were paced at 2Hz. b. The derivative of the decay (indicated by dashed line) of the Ca^{2+} transients seen in part a. This is a representation of recordings from one heart, but this experiment was repeated for 5 hearts.

In order to assess the thermodynamic effects on the relaxation of the Ca^{2+} transient, the maximum derivative of the relaxation was plotted as a function of the temperature. This will allow us to define the enthalpy and entropy of the rate of relaxation of a Ca^{2+} transient based on the temperature. **Fig. 4.3 a** shows a typical Arrhenius plot from which the thermodynamic parameters of the Ca^{2+} transient relaxation were then extracted. The fitted change in enthalpy ΔH was 9.3 Kcal/mol a number very close to the energy produced by the ATP hydrolysis (7.3 Kcal/mol). This suggested that the Ca^{2+} ATPase activity of SERCA2 is the main player in the Ca^{2+} transient relaxation. Although Ca^{2+} buffers play a role in the relaxation of the Ca^{2+} transient, SERCA is the major mechanism by which

cytosolic [Ca^{2+}] returns to diastolic levels.[26] This change in enthalpy indicates that the change in the relaxation rate for a 10 °K Q_{10} is approximately 1.6.

Although the Arrhenius formulation gives a precise relationship between the rate of a chemical reaction and temperature, the temperature range we are exploring is narrow

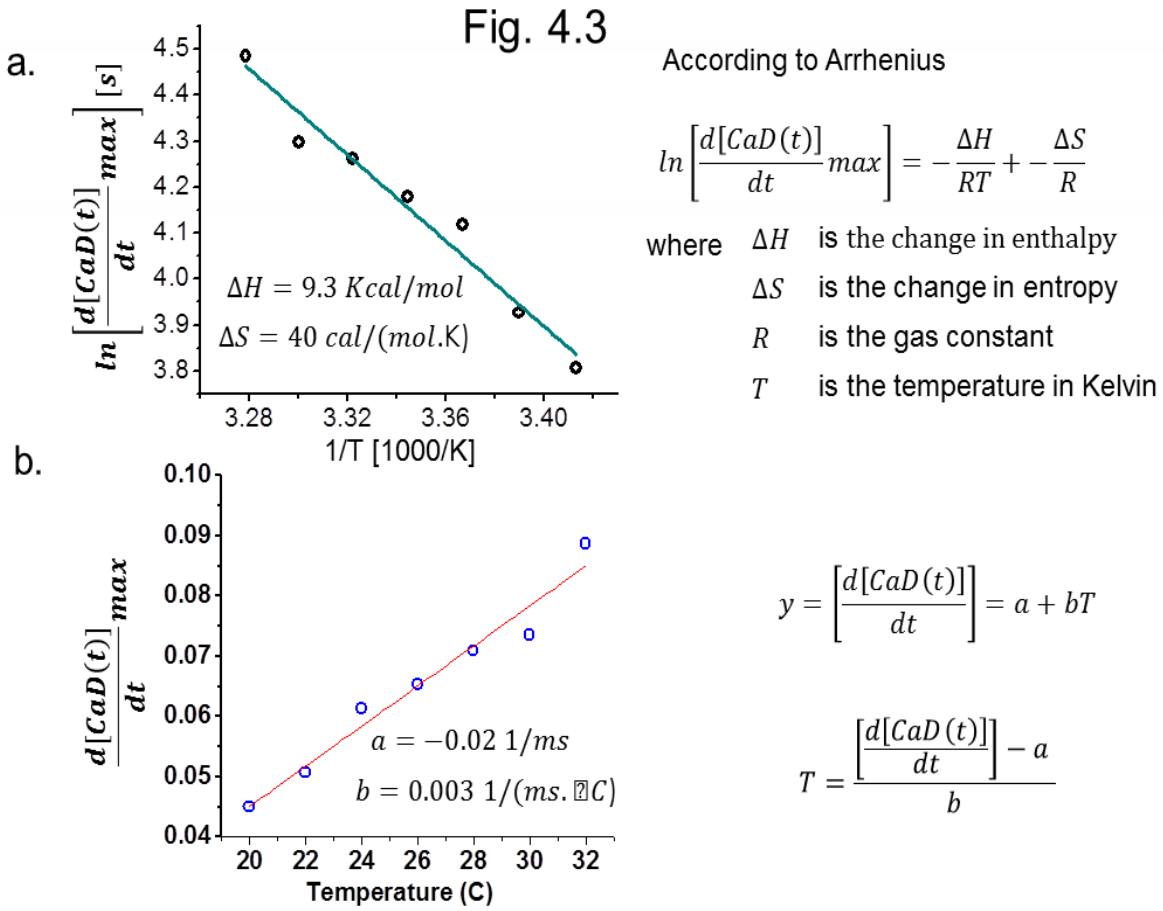

Fig. 4.3 a. Arrhenius plot of the rate of decay of the Ca^{2+} transients as a function of bath temperature. b. The relationship between the maximum rate of decay as a function of temperature indicates a linearity.

for a temperature scale in °K. This narrow temperature range made it possible to linearize the Arrhenius equation. Assuming a linear behavior for a small temperature change made it possible to plot the maximum velocity values as function of the temperature. This can be observed in **Fig 4.3 b**. By fitting a linear function, it was possible to obtain the slope (b) and the y-intercept (a). This equation allowed us to calculate Q_{10}. The Q_{10} computed value, assuming a linear behavior, is 1.63, a number very close to the one obtained using the Arrhenius formulation indicating that the linear approximation is precise enough for our experimental conditions.

This linearity provides us with a function which can be used to compute the relaxation kinetics from known temperatures. In addition, simple arithmetic can be used to invert this equation such that the temperature is computed as a function of the derivative. Thus, for any tissue in which the relaxation kinetics are quantified, the temperature can be computed. This allowed us to have a calibration of the temperature range achieved while using the cold finger.

Temperature of tissue calculated from a map of Ca^{2+} transients

As previously mentioned in the **Methods** section, a cooling apparatus or "cold finger" was built as an attachment to our FLOM instrument. This allowed us to locally change the temperature of the cardiac tissue and generate a temperature gradient in which the tissue closest to the cold finger was cold and progressively became warmer to match the temperature of the bath. In conjunction with FLOM, this attachment was important to assess the effects from temperature on the spatial distribution of intracellular Ca^{2+} transients.

Fig 4.4 a shows an illustration of the temperature gradient generated by the cold finger on the tissue of the heart. The temperature difference produced across the tissue was sufficient to affect the relaxation of the intracellular Ca^2 transients. Finally, based on the calculated map of derivatives (**Fig. 4.4 b**) from the FLOM images, we were able to compute the exact temperature gradient generated with the cold finger. Our resulting temperature map showed that our cold finger generated a temperature gradient of 5°C (**Fig. 4.4 c**).

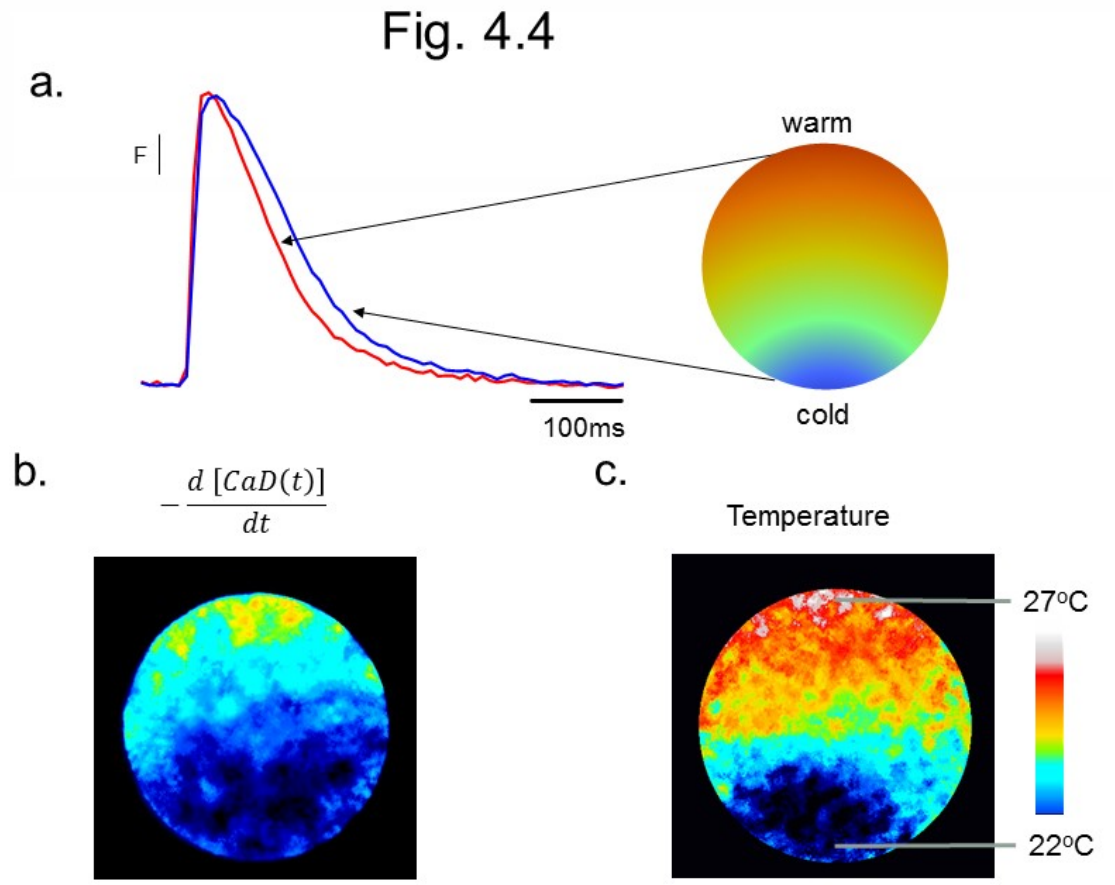

Fig. 4.4 a. Ca^{2+} transients from FLOM fluorescent images of hearts loaded with Rhod-2 in which the cold finger is generating a temperature gradient. b. A derivative map constructed from the rate of relaxation of the Ca^{2+} transients from all the regions. c. The calculated temperature map as a function of the derivative.

4.2 What is the temperature dependency of intracellular Ca^{2+} alternans spatial distribution?

As we already mentioned, T-wave alternans is an excellent predictor of ventricular arrhythmias and ventricular fibrillation. One of the factors that lead to T-wave alternans development is metabolic stress.[63] Hypothermia, for example, can produce metabolic impairments that may cause the heart to go into cardiac arrest.[63–67] In the previous chapter, we assessed how the HR affects the handling of intracellular Ca^{2+}. In this chapter, we evaluated the temperature dependency of the Ca^{2+} transient at a fixed HR. Finally, in this section, we will bring these two variables together and simultaneously evaluate how HR and temperature modulate Ca^{2+} alternans.

In order to understand the interplay between the HR and temperature, we assessed the spatial distribution of alternans at increasing frequencies and under a region where a temperature gradient was imposed. This was achieved with our FLOM imaging technique (see **Methods**). FLOM can record a series of images from the epicardial surface of the heart exposed to different temperatures at increasing HRs. During the Ca^{2+} transient alternans, one of the transients has a higher amplitude and is followed by one with a lower amplitude. After selecting the images at the time where the high alternans reached a maximum and where the low amplitude alternans peaked, we processed both images to compute a map of the degree of alternans under the 3.2 mm conduit region (see **Methods**).

Fig. 4.5 showed the alternans maps at increasing frequencies from a region with different surface temperatures. The transients illustrated above and below each map are from the warm and cold regions, respectively. Black was set to indicate no alternans and grey to represent high alternans. At 4Hz, the alternans map was completely black, indicating no alternans in the warm nor in the colder regions. At 5Hz, we saw no alternans

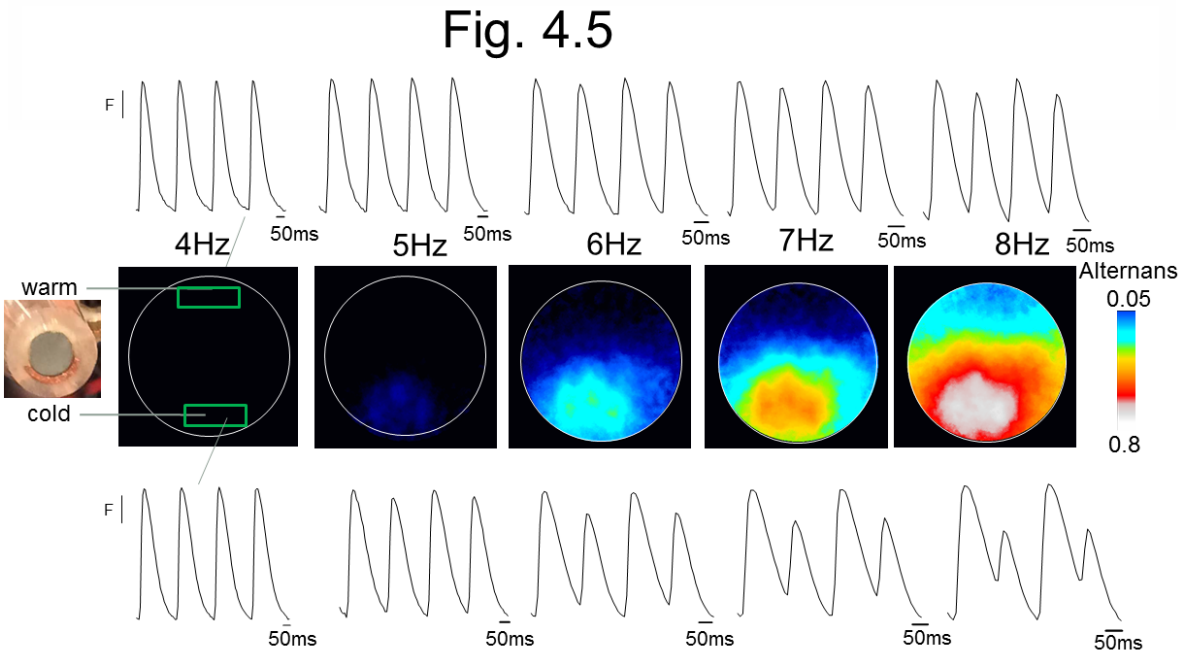

Fig. 4.5 The spatial distribution of alternans at increasing HRs shows that alternans are greater at lower HRs in the cold region. Alternans maps computed as described in Methods section. Hearts were maintained in a bath at 32ºC and the metallic cold finger set to 18ºC.

in the warm region, but a slight presence of alternans in the cold region where the metallic cold finger rested on the surface of the epicardium. Increasing the frequency to 6Hz produced a greater degree of Ca^{2+} transient alternans in the cold region as seen by the appearance of a cyan color. Regions farther from the cold finger did not alternate at this frequency. Increasing the frequency to 7Hz, made the distribution of alternans extend to

warmer regions. At 8Hz, the alternans are present in both cold and warm regions, but are greatest in the tissue with colder temperatures.

The pattern of Ca^{2+} transient alternans distribution shown in **Fig 4.5** was the same for all the hearts tested (N=5). The colder regions presented a greater degree of alternans than the warmer surfaces of the epicardial region of the heart. Also, the alternans appeared at lower frequencies in the colder areas than in the warmer regions.

In order to understand how the relationship between HR and temperature modulated Ca^{2+} alternans, we determined the alternans distribution as a function of the temperature of the tissue. This was done by taking the alternans map with the cold finger in place and the temperature map produced from the derivatives of the relaxations. The two maps were obtained in the same heart and exactly at the same spatial position of the conduit over the epicardial layer. With the two maps, we determined the degree of alternans at a position and plotted it as a function of the temperature of that same position (**Fig. 4.6**). We proceeded to do the same for all the positions (pixels) in the window recorded by the

Fig. 4.6

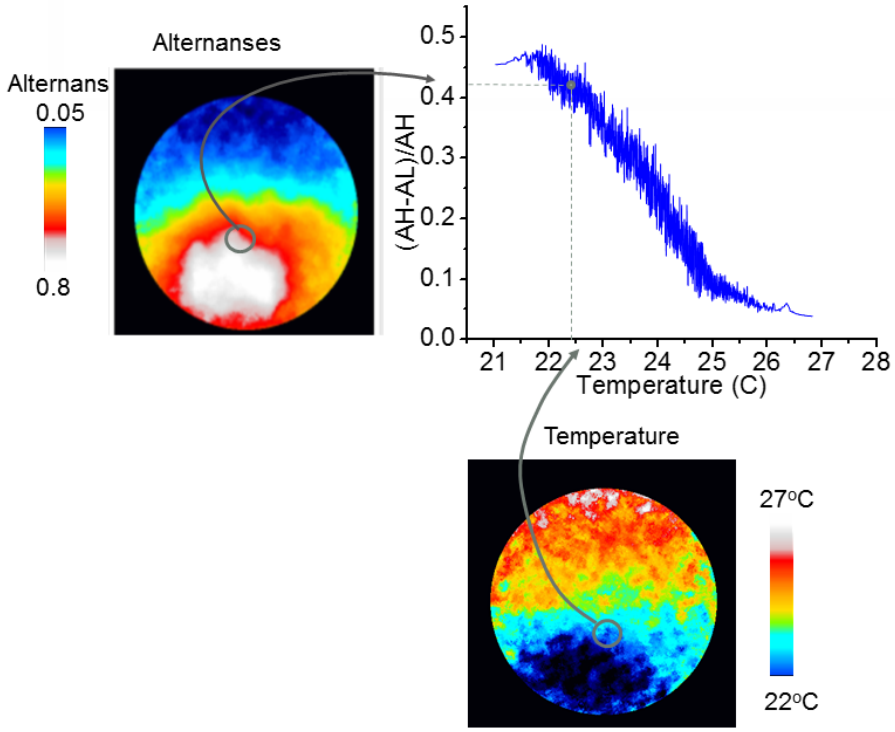

Fig. 4.6 The alternans distribution as a function of temperature was computed mapping the Ca^{2+} alternans value in one pixel vs. the temperature value at the same pixel on the temperature map. We did the same for all the positions on both maps to generate a graph of Ca^{2+} alternans vs. temperature.

camera, and plotted the alternans distribution as a function of temperature. **Fig. 4.6** showed that at colder temperatures, the tissue had a greater degree of Ca^{2+} transient alternans. The degree of alternans dropped as the regions became progressively warmer. This alternans map was obtained from a heart paced at 7Hz.

In the same manner, we plotted the Ca^{2+} transient alternans distribution as a function of temperature for different frequencies. **Fig. 4.7** showed the Ca^{2+} transient alternans versus tissue temperature for 5-8Hz. We observed that at higher HRs, the temperature dependency of the Ca^{2+} alternans was amplified.

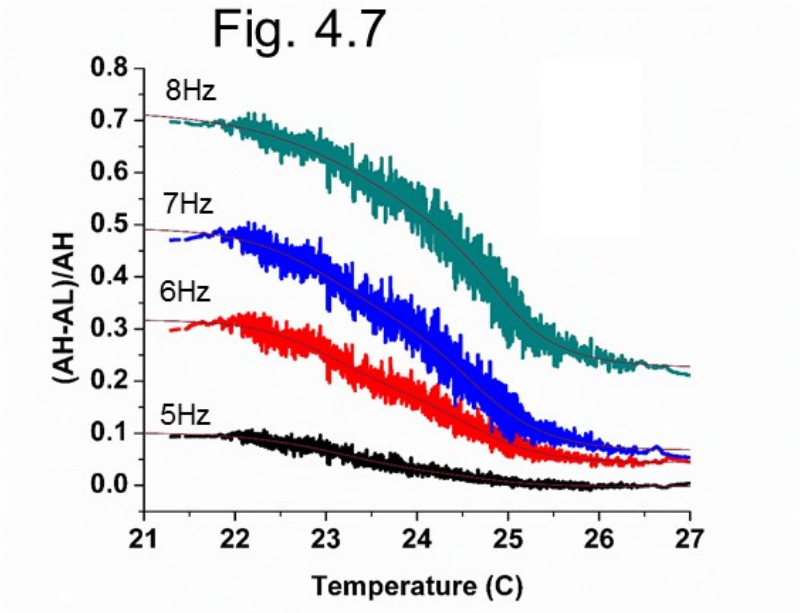

Fig. 4.7 Temperature dependency of Ca^{2+} alternans at different HR. It is possible to observe that at higher HR it is more likely that a metabolic impairment induced by hypothermia will be able to induce larger Ca^{2+} alternans.

Defining the temperature dependency of Ca^{2+} alternans is a complex process. In order to obtain the Q10 of the alternanses at different heart rates we calculate the ratio A_L/A_H. A graph of the ratio A_L/A_H as a function of the temperature is shown in **Fig 4.8 a**. Contrary to what happened with alternans, this ratio value increased as function of the temperature allowing as to use it as a standard procedure to calculate Q_{10}. The first step was to calculate two different ratios A_L/A_H at two different temperatures. In this case the temperatures used for calculating the ratio A_L/A_H were 21.5 °C (T_1) and 26.5 °C (T_2). The ratio at 21.5 °C $(A_L/A_H)_{21.5}$, we named it R_1 and the ratio at 26.5 °C $(A_L/A_H)_{26.5}$ we named it R_2. **Fig 4.8 b** illustrates the HR dependency of R_2/R_1. Finally, the Q_{10} at different HRs was calculated using the generalized expression seen in **Fig. 4.8**.

The value of Q10 at different HRs are shown in **Fig 4.8 c**. It is interesting to notice that Q_{10} increased as a function of the HR. Moreover, at several heart rates (6 ,7 and 8Hz), the Q_{10} calculated was higher than the one obtained for the Ca^{2+} transient relaxation process (Q_{10}~1.6). This indicated that the temperature dependency of the SERCA2 pump is not the only factor governing the development of Ca^{2+} alternans (see **Discussion**).

Fig. 4.8

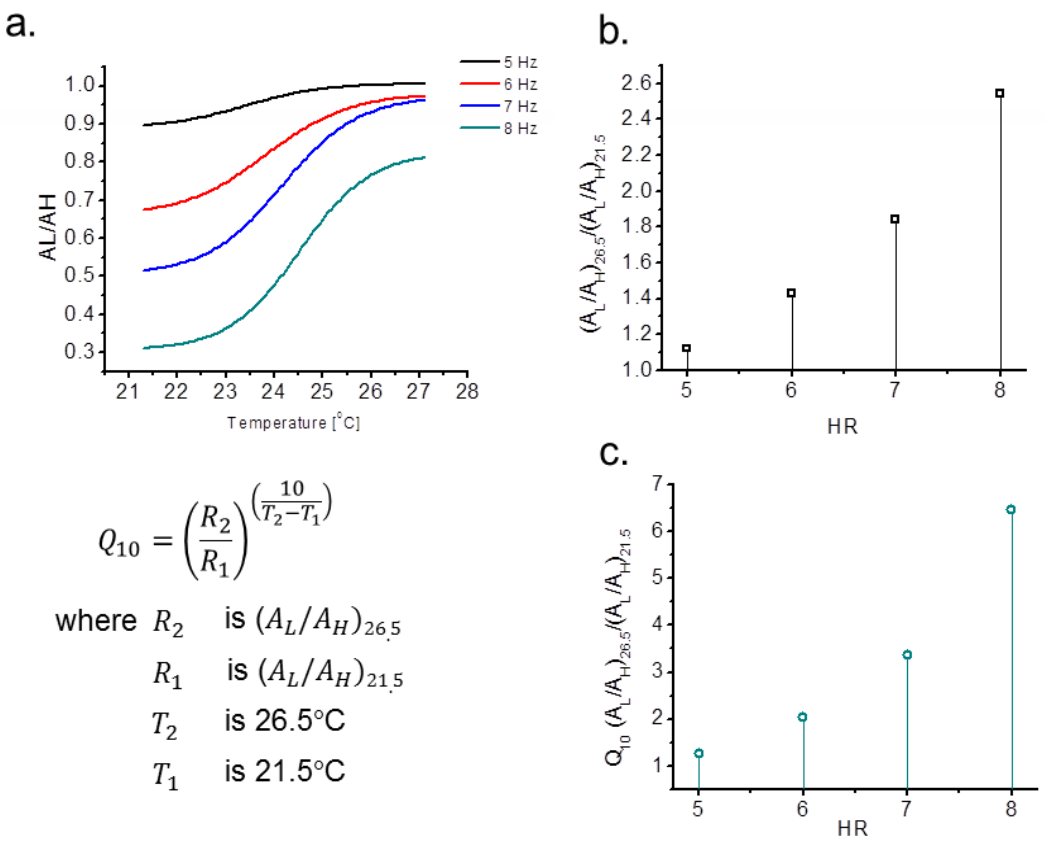

$$Q_{10} = \left(\frac{R_2}{R_1}\right)^{\left(\frac{10}{T_2 - T_1}\right)}$$

where R_2 is $(A_L/A_H)_{26.5}$

R_1 is $(A_L/A_H)_{21.5}$

T_2 is 26.5°C

T_1 is 21.5°C

Fig. 4.8 a. Ratio between the amplitude of the low (AL) and high (AH) Ca^{2+} transient as a function of the temperature for the different frequencies. b. The ratio of the rates R2/R1 was calculated for each frequency from the two temperatures (26.5ºC and 21.5ºC) in panel a. b. Using the R2/R1 ratio calculated in panel b for the two temperatures, the Q_{10} was computed at 5-8Hz.

To conclude, FLOM experiments indicate that Ca^{2+} alternans have a very steep temperature dependency. At cold temperatures, Ca^{2+} reuptake (SERCA activity) is slower promoting Ca^{2+} alternans. We saw that at low HRs, the temperature dependency observed may be due to SERCA's activity (Q_{10}~1.6). However, the temperature dependency was amplified at higher HRs. This indicated that other proteins/mechanisms aside from SERCA reuptake are involved in the genesis of Ca^{2+} alternans.

CHAPTER 5:

Intrinsic sympathetic NS activity and effect on alternans

The heart is an organ that is highly regulated. Most of this regulation is driven by the influence of the autonomic nervous system (ANS). The activation of this house keeping neural network affects some key properties of the pumping heart. Some of these effects include the control of the heart rate (chronotropism), the regulation of the cardiac contractility (inotropism), the adjustment of the speed at which the cardiac muscle mechanically relaxes (lusitropism) and, finally, the velocity by which the electrical signal propagates all over the heart (dromotropism).

In particular, the control of the heart rate is achieved by the action of two divisions of the ANS: the sympathetic NS and the parasympathetic NS. In this chapter, we will focus on the role the sympathetic NS plays in regulating this circulatory organ. In the following chapter (Chapter 6), we will analyze how the other branch of the ANS, the parasympathetic NS, influences the organ.

The sympathetic NS acts on a large variety of organs inducing very different effects. However, the way the sympathetic NS communicates with the target organ is the same, the release of chatecholamines. Neurons from the sympathetic NS innervate the heart and release a neurotransmitter, norepinephrine, also called noradrenaline. All of the sympathetic postganglionic nerves (with exception to the ones innervating the sweat glands) release norepinephrine. Locally released norepinephrine binds to adrenergic receptors and triggers a cascade of events that involve the activation of G-protein coupled receptors (for details see **Chapter 1**).

In the heart, adrenergic receptors are not only activated by the local release of norepinephrine but also by the systemic action of a hormone that mimics norepinephrine. This hormone is named epinephrine and is massively released into the circulation by the adrenal medulla. The adrenal medulla is a gland located on the superior part of the kidney and can produce a steady state release of epinephrine. Finally, the circulating epinephrine can interact with adrenergic receptors in the heart producing effect very similar to the ones induced by the local release of norepinephrine.

The Langendorff perfusion system presents multiple advantages in comparison with methods in which myocytes are enzymatically isolated. However, one of the limitations of the Langendorff heart is that it lacks postganglionic innervation and the circulation of many physiological molecules including hormones. Outside the body, these hearts no longer have the sympathetic NS's drive or the effects of circulating catecholamines. The absence of these neurotransmitters/hormones in the *ex vivo* circulation may affect the HR. Thus, catecholamines play an essential role in keeping the heart rate sufficiently high to maintain a normal cardiac output. For example, *in vivo* the

mouse heart is capable of maintaining a heart rate that oscillated between 600 and 650 beats per minute. However, when a heart is extracted from the animal and positioned on a Langendorff system, we see that the heart rate drops to lower than 300 beats per minutes.

In **Chapter 3**, we presented extensive experimental results on perfused hearts showing that at 480 beats per minutes (8Hz) the hearts presented both Ca^{2+} and electrical alternanses. Interestingly, when the heart is still in the mouse at a heart rate of 600 beats per minutes, the animal's ECG never alternated (data not shown).

Since alternans are not a noticeable phenomenon at the basal HR of the mouse and are highly dependent on HR, it is possible that the lack of catecholamines may promote their development. In this section, we test the effects of partially restoring the circulation of catecholamines in the genesis of alternans.

The sympathetic NS stimulate beta-adrenergic receptors that activate pathways that ultimately affect the intracellular Ca^{2+} cycling of the cardiomyocytes. At the organ level, sympathetic NS stimulation causes a positive inotropic effect that involves Ca^{2+} handling and, consequently, contractility. Since APD alternans are a consequence of intracellular Ca^{2+} disturbances,[60–62,151] then beta-adrenergic agonists may affect the APD and intracellular Ca^{2+} transient alternans. However, the exact effect of sympathetic NS stimulation on the Ca^{2+} handling across the ventricular wall is unknown. In this chapter, we want to test the hypothesis that beat-adrenergic stimulation reduces Ca^{2+} alternans by accelerating Ca^{2+} reuptake into the SR.

In **Chapter 3**, we showed that the alternans appear at different frequencies in the two layers of the ventricular wall. The Ca^{2+} cycling, as seen from the cytosolic Ca^{2+} transient, has different kinetics in the endocardium and epicardium. Consequently, we want to determine if beta-adrenergic agonists affect Ca^{2+} transients differentially across the ventricular wall.

5.1 How does the sympathetic drive regulates the HR of the Langendorff mouse heart?

In the body, the mouse heart functions at a basal rate of 600 beats/min or at a frequency ranging from 9-11Hz. However, in **Chapter 3**, we showed that at these frequencies, the hearts presented both APD and Ca^{2+} transient alternans. Thus, it is very important to assess the basal HRs of hearts that have been physically extracted from their physiological environment within the thoracic cavity. Although the isolated heart lacks the circulation of catecholamines, it continues to have its intrinsic ANS regulation. The heart has its local innervation of sympathetic and parasympathetic neurons as part of the intrinsic cardiac plexus.[87] We also want to determine if the local sympathetic NS neurons are active and stimulating beta-adrenergic receptors.

To assess these HRs, hearts were placed in the Langendorff set-up carefully and with minor handling. The APs were recorded under the natural rhythm set by the intact SA

node. Results showed that the basal HRs of hearts in the Langendorff set-up were at lower frequencies (4±0.4Hz) (**Fig. 5.1 a**) than inside the body.

Fig. 5.1

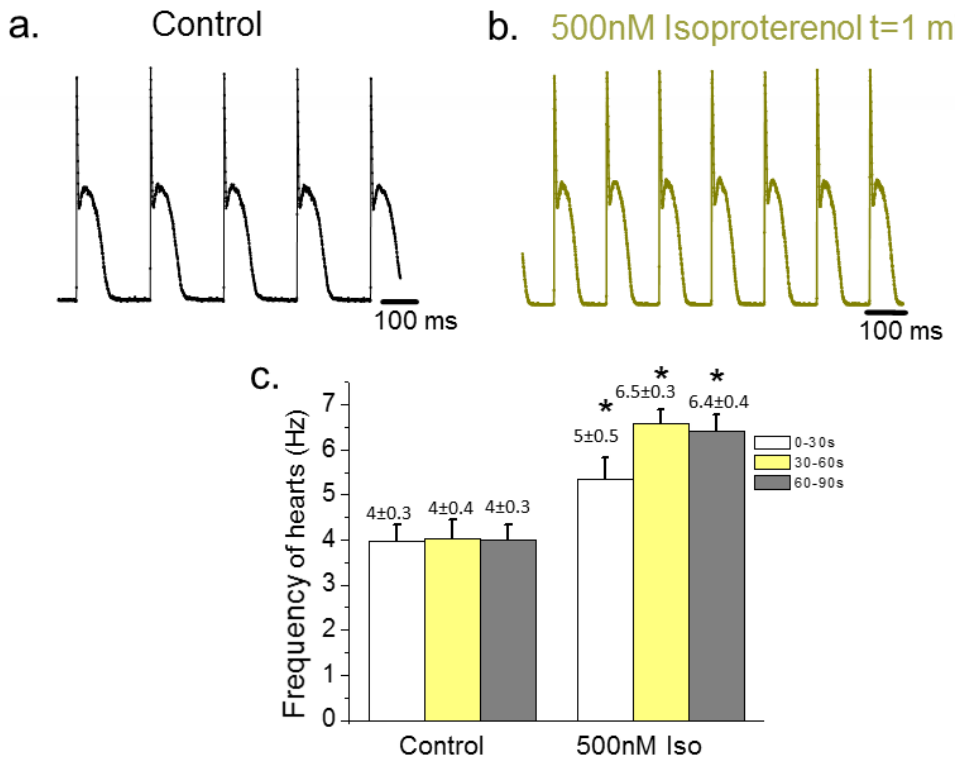

Fig. 5.1 a. A Langendorff heart's AP spontaneous frequency. b. The frequency increases upon isoproterenol perfusion. c. Over a period of 90 s, the control HR stayed around 4Hz, but this increased to as high as 6.5Hz with 500nM isoproterenol. (N=5 hearts, p<0.05, mean±SD)

These hearts were partially missing the ANS regulation. First, the somas of the postganglionic neurons were no longer present because the afferent nerves were cut from the heart during the dissection process to remove the organ from the animal. Secondly, the ANS's regulation is missing due to the absence of circulating catecholamines in the bloodstream. In the Langendorff set-up, the hearts are being perfused with Tyrode solution containing all ions similar to those found in blood at physiological pH. However, this solution lacks catecholamines, antibodies, plasmatic proteins, CO_2 and other physiological molecules circulating in the bloodstream. If we partially restore the catecholaminergic drive by perfusing a beta-adrenergic agonist (**Fig. 5.1 b**), isoproterenol (500nM), we were able to significantly ($P<0.05$) increase the HR within a minute of the time the agonist was applied (6.5±0.3 Hz) (**Fig. 5.1 c**). Interestingly, after a minute, the effect of isoproterenol began to drop, which may be due to the desensitization of the beta-adrenergic receptor.

In addition to the circulation of catecholamines in the blood, the sympathetic NS also has local innervation by post-ganglionic fibers originating from the sympathetic chain and the T1-L2 preganglionic fibers. Although the postganglionic somas were removed, sympathetic terminals could be still be present in the tissue. We wanted to determine if these terminals are active in the Langendorff heart.

In order to explore this idea, we assessed the effect of beta-adrenergic antagonist on the HR. Hearts were extracted and with very minor handling were placed in the Langendorff set-up. Using a sharp glass microelectrode, the epicardial AP firing was monitored. The APs during each 30s period were counted. The beta-adrenergic antagonist bisoprolol (15.8µM) was perfused for six minutes. **Fig. 5.2** showed how, relative to the control (4Hz), the frequency of AP firing within 30s intervals began to drop within 30s and then stabilized after 3 minutes (~3Hz). To assess if this drop in HR was due to blocking of

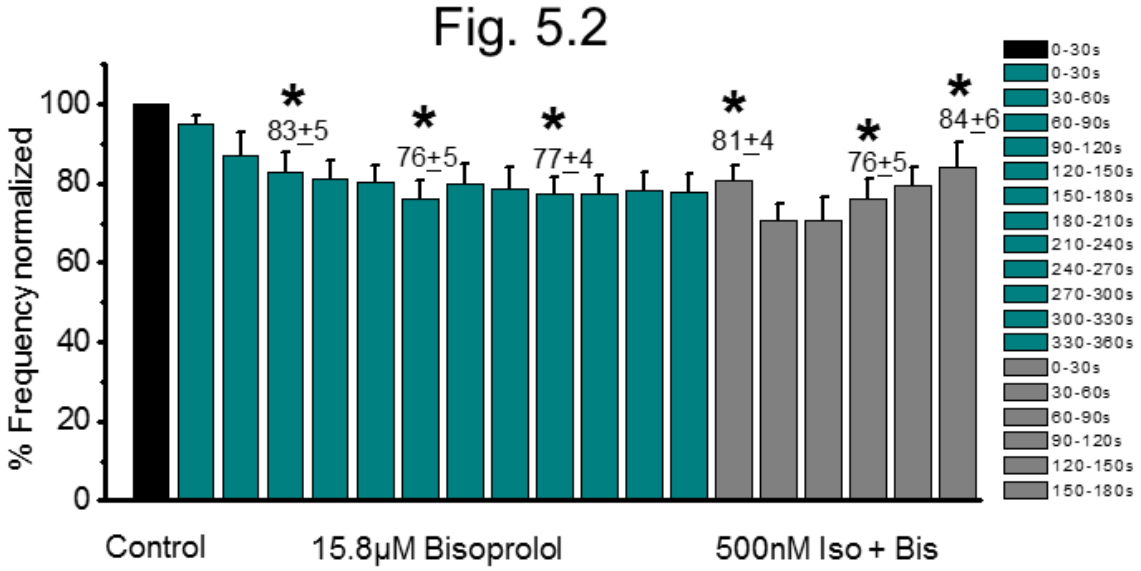

Fig. 5.2 The beta-adrenergic antagonist, bisoprolol, causes the HR to drop over time. Perfusion with isoproterenol does not increase the frequency indicating the beta-adrenergic blockade. *P<0.05. N=5 hearts.

beta-adrenergic receptors, the beta-adrenergic agonist isoproterenol was perfused in conjunction with bisoprolol. There was no increase in frequency. This indicated that the beta-adrenergic receptors were blocked. Together, these results point to the constitutive release of neurotransmitters from the terminal of local sympathetic NS neurons that are still active.

5.2 How does the sympathetic NS agonist affect APD and Ca^{2+} dynamics across the ventricular wall?

The different layers within the heart present very dissimilar AP waveforms. This is due to the disparity in the underlying density of ion channels. For example, phase 1 in the endocardium is known to be slower due to less I_{to} than the epicardium.[29] The less I_{to} is due to the decreased presence of K^+ channels.[29,30] Indeed, when recording across the ventricular wall using a potentiometric dye and the PLFFM technique, we saw that the morphology of the AP is particularly different in phase 1 for the epicardium and endocardium (**Fig. 5.3 a**).

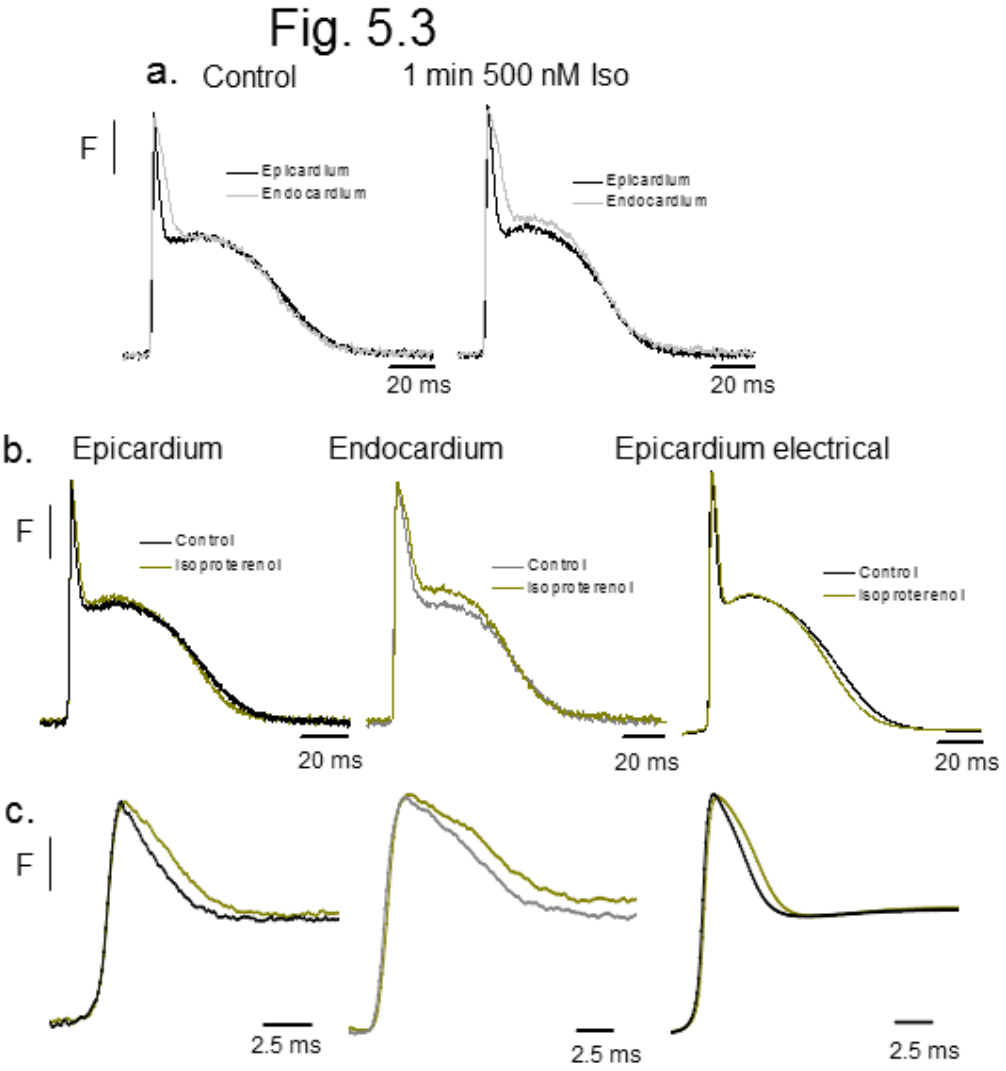

Fig. 5.3 a. Transmural optical AP recordings before and after 500nM isoproterenol obtained with di-8-ANEPPS. Although the morphology of the AP from the epicardium (black) and endocardium (grey) are very different, both respond similarly to isoproterenol. b. Relative to their controls, the epicardium and endocardium have an increase in phase 2 and in phase 1 (c) with isoproterenol (green). c. Expanded view of phase 1 from panel b showing the effect with isoproterenol. Hearts were paced at 7Hz and 37°C.

The endocardium AP depolarizes sooner, but for comparison purposes, these traces have been overlapped.

Since the T-wave is associated with the transmural electrical repolarization, we wanted to understand specifically, how the beta-adrenergic agonist isoproterenol affected the morphology of the AP. Any changes seen in the morphology of the AP may result from the regulation of ionic currents. In addition, isoproterenol may be having a differential effect between the epicardium and endocardium layers so it was important to assess any differential regulation across the ventricular wall.

In order to measure the APs in the epicardium and endocardium, we used the potentiometric dye, di-8-ANEPPS in conjunction with epicardial electrical recordings by using sharp microelectrodes. We recorded traces before and after perfusion with the beta-adrenergic agonist. After retro-perfusion with 500nM isoproterenol, there are modifications in several phases of the action potential (**Fig. 5.3 b**). There are changes that can be observed during phase 2. If the AP traces are expanded, it is possible to observe a significant increase in the duration of phase 1 (**Fig. 5.3 c**). A summary of these results can be appreciated in **Fig. 5.4**.

The most salient features of the activation of beta-adrenergic receptors are a shortening of the late phases of the AP and an increase in the duration of phase 1. **Fig. 5.4 a and b** shows that relative to their controls, isoproterenol caused the fractional change of half phase 2 to repolarize significantly ($P<0.05$) faster for both the epicardium (**Fig. 5.4 a)** (87.2 $\pm$ 5.7%) and the endocardium (**Fig. 5.4 b)** (90.9 $\pm$ 4.5%). The APD90 of both the epicardium (**Fig. 5.4 c)** (85 $\pm$ 5.5%) and endocardium (**Fig. 5.4 d)** (88 $\pm$ 4%) also repolarize faster than their controls. Interestingly, although the APD 30 is larger in the endocardium as compared to the epicardium, the relative change produced by isoproterenol respective to their control is larger in the epicardium (**Fig. 5.4 e)** (122±19%) in comparison with endocardium (**Fig. 5.4 f)** (119±9%) (**Fig. 5.4 c**).

Fig. 5.4

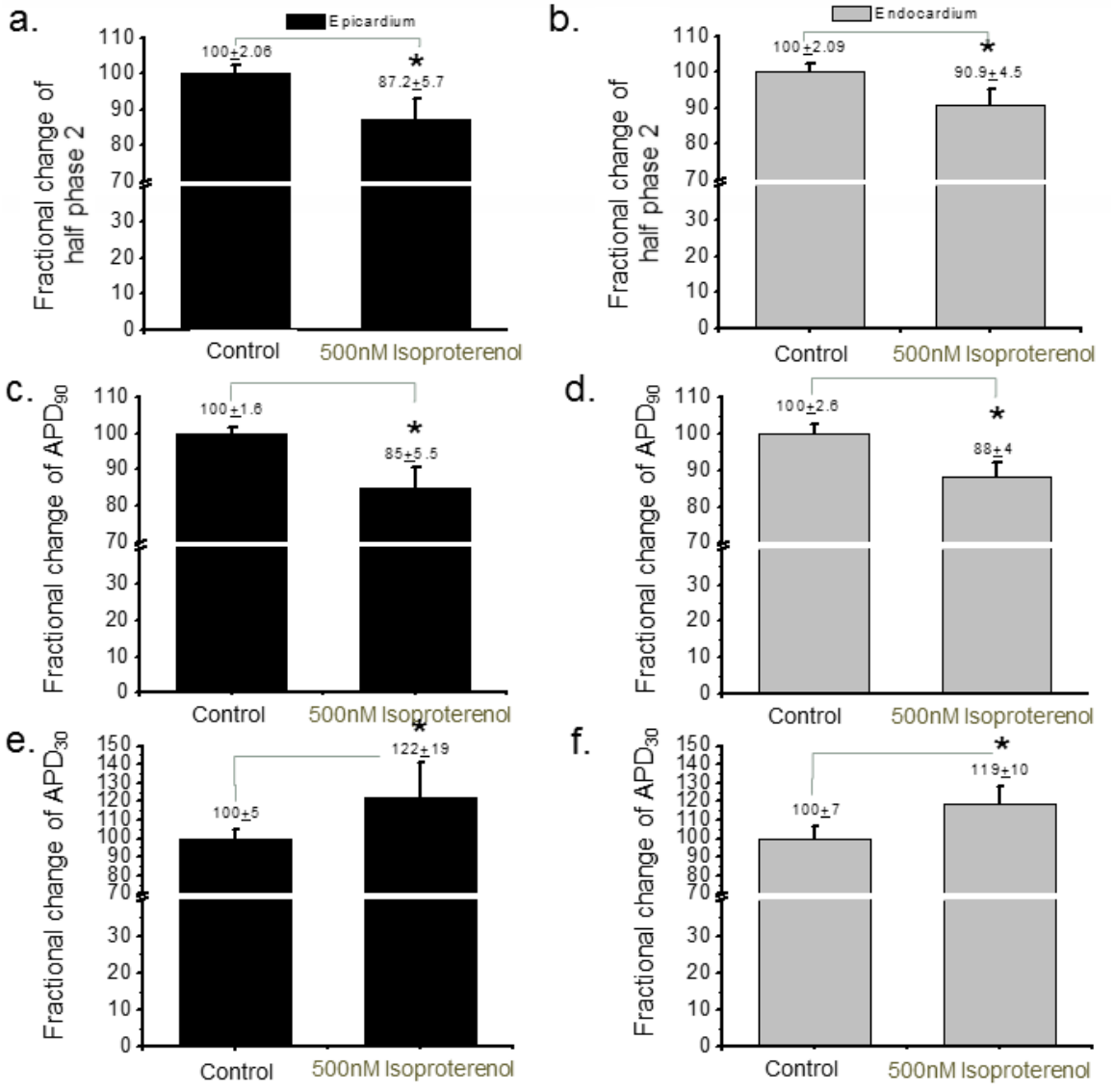

Fig. 5.4 a. Fractional change of half of phase 2 effect with 500nM isoproterenol in the epicardium (black) and (b) endocardium (grey). Isoproterenol shortens the AP repolarization time (N=4 hearts). c. Fractional change of APD 90 before and after retro-perfusion with isoproterenol (N=4) in the epicardium and (d) endocardium. e. Fractional change of APD30 shows a significant increase after isoproterenol (N=3) in the epicardium and (f) endocardium. Hearts were paced at 7Hz and 37 °C. *P<0.05, mean ± SD.

The decrease in the rate of relaxation of phase 1 can be attributed to an increase in the amplitude of L-type Ca^{2+} currents. Indeed, in our recent publication we demonstrate that most of the Ca^{2+} influx that triggers CICR occurs during phase 1.[31] On the other hand, the shortening of the late duration of the APs could be associated with the impact of beta-adrenergic stimulation on the relaxation properties of Ca^{2+} transients (positive lusitropic effect). Briefly, in the presence of isoproterenol, Ca^{2+} transients may relax faster due to the phosphorylation of PLN. Thus, it is imperative to evaluate the effect of beta-adrenergic stimulation on the kinetic properties of Ca^{2+} transients in epicardium and endocardium.

Based on the effect over the AP, it is likely that isoproterenol affects the cycling of Ca^{2+} across the ventricular wall. After isoproterenol addition, the AP showed changes in phase 2 possibly due to both an increase in the amplitude and a faster relaxation of the Ca^{2+} transients. Together, these changes in the Ca^{2+} transient may contribute to the faster repolarization of phase 2. Moreover, the slower repolarization of phase 1 may indicate a larger Ca^{2+} influx through L-type Ca^{2+} channels.

In order to address how the activation of a beta-adrenergic pathway modifies the properties of Ca^{2+} transients transmurally, we performed PLFFM experiments in hearts loaded with a Ca^{2+} indicator. Since we expected to see an increase in the amplitude of Ca^{2+} transients, we were concerned that Rhod-2 would saturate under beta adrenergic stimulation conditions. To address this difficulty we perfused the hearts with the low affinity indicator X-Rhod-5F. This lower affinity dye has a dissociation constant K_d of 1.6 μM, less affinity than Rhod-2. Using a low affinity dye has several advantages including a faster Ca^{2+} unbinding and a lower Ca^{2+} buffering effect.

However, a big drawback of a low affinity indicator is that only a small fraction of the dye will be complexed with Ca^{2+}. As the florescence emitted by the dye is a function of how much Ca^{2+} is bound to the dye, the reported signals will be small and the signal to noise ratio low. Thus, Ca^{2+} transients recorded with this dye would have lower amplitudes and higher noise levels.

Typical recording using X-Rhod-5F are presented in **Fig. 5.5**. Simultaneous recording in epicardium and endocardium using this dye are shown in **Fig. 5.5 a**. As we already showed in previous chapters, Ca^{2+} transients recorded in the epicardial layer display a smaller time to peak and a faster relaxation. This difference between epicardium and endocardium is maintained in hearts perfused with 500 nM Isoproterenol **Fig. 5.5 b**.

Fig. 5.5 c and **d** shows the effect of perfusing the heart with isoproterenol on the Ca^{2+} transients recoded in the epicardium and the endocardium. In both cases, it is possible to appreciate an increase in the amplitude of the Ca^{2+} transients. This is consistent with the positive inotropic effect of catecholamines. As we already stated it was expected that isoproterenol will not only modify the amplitude of Ca^{2+} transients but modify their kinetic profile. **Fig. 5.5 e** and **f** also increases the maximum rate of relaxation of Ca^{2+} transient in the presence of isoproterenol (positive lusitropism).

Fig. 5.5

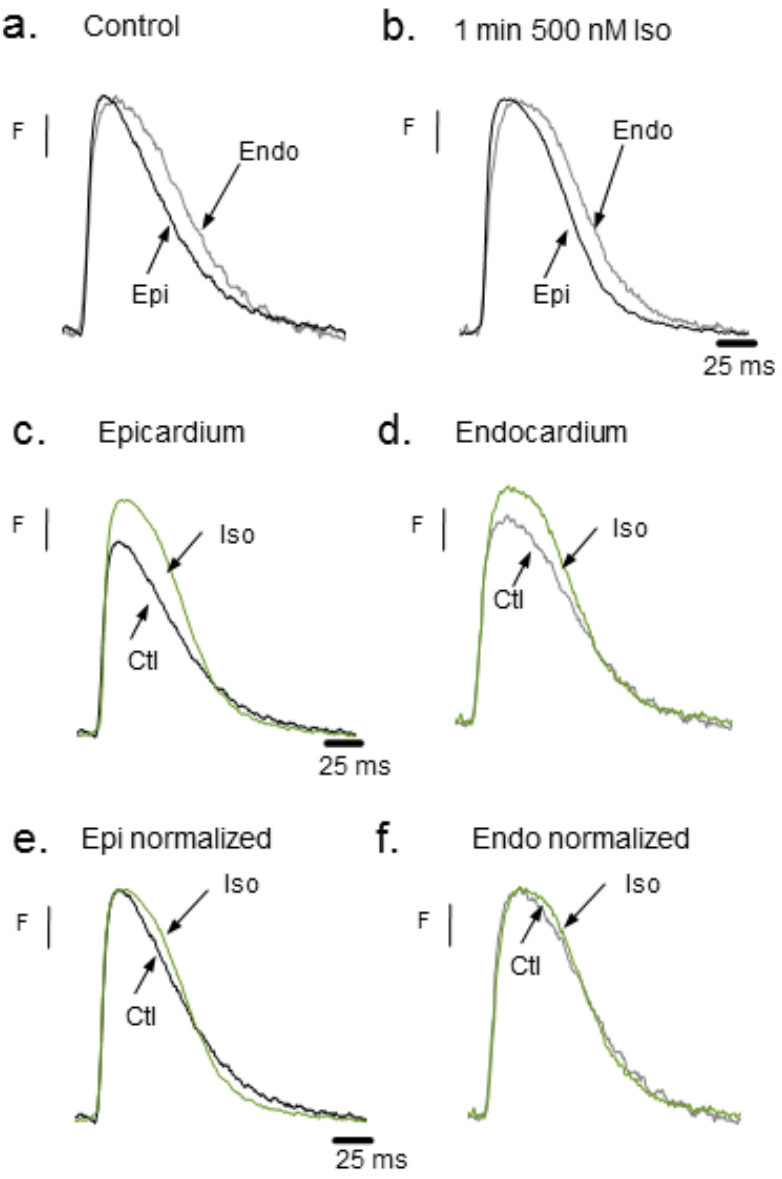

Fig. 5.5 a. X-Rhod-5F fluorescence recording of the normalized Ca^{2+} transients from the endocardium (grey) and epicardium (black) at 6Hz show different rise and relaxation kinetics that persist (b) after 500nM isoproterenol. c. The Ca^{2+} transients before (black) and after isoproterenol (green) show an increase in amplitude for the epicardium and (d) endocardium (grey). e. Normalizing Ca^{2+} transients before and after isoproterenol show faster relaxation kinetics induced in both the epicardium and (f) endocardium with isoproterenol (green).

A summary of the results is presented in **Fig. 5.6** where it is possible to observe that isoproterenol does not have a significant effect on the time to peak and rise time of Ca^{2+} transients recorded in the epicardial (**Fig. 5.6 a and c**) and endocardial layers (**Fig. 5.6 b and d**). Although statistically significant, the activation of a beta-adrenergic pathway modified the half time duration of the Ca^{2+} transients by only 8% (92±5% for the epicardium and 94±5% for the endocardium, **Fig. 5.7 c and d**). Furthermore, the greatest effect seen was on the decay time which was significantly accelerated in the presence of isoproterenol (76±3% for the epicardium and 83±4% for the endocardium, **Fig. 5.7 a and b**). Altogether, isoproterenol induced a large lusitropic action on the systolic Ca^{2+} signaling.

Fig. 5.6

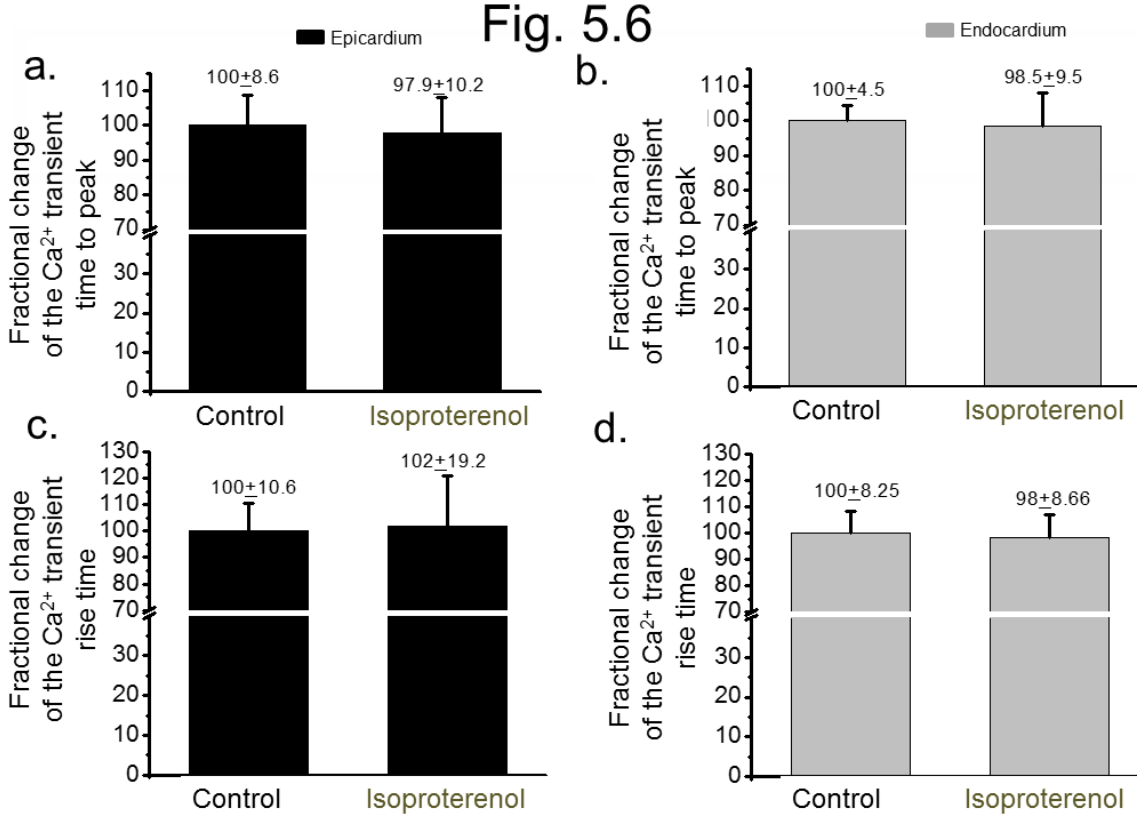

Fig. 5.6 a. Fractional change of the intracellular Ca^{2+} transient time to peak showed no significant changes after 500nM isoproterenol for epicardium (black) and (b) endocardium (grey). c. Fractional change of the intracellular Ca^{2+} transient rise time was not significantly changed after isoproterenol in epicardium and (d) endocardium. Mice hearts were paced at 6Hz and temperature set to 37°C. *P<0.05, N=4 hearts, mean±SD.

The changes in the Ca^{2+} signaling will affect the time course of the epicardial and endocardial APs. This is due to the interconnectivity between intracellular [Ca^{2+}] and the activity of the NCX which affects the membrane potential (phase 2). Thus far we have seen

that with a beta-adrenergic agonist there is a larger influx of Ca^{2+} in phase 1 which may trigger the SR to release more Ca^{2+} into the cytosol (higher Ca^{2+} transient amplitude). The larger cytosolic [Ca^{2+}] activates the NCX in the forward mode.[31] Therefore, the effect seen of isoproterenol in phase 2 (representing the greater NCX activity) may be due to the underlying effect of Ca^{2+} increase induced by SR Ca^{2+} release. In addition, the faster relaxation of the Ca^{2+} transient that we saw may be due to PKA's phosphorylation of PLN, relieving the SERCA to re-sequester Ca^{2+} faster into the SR.

Fig. 5.7

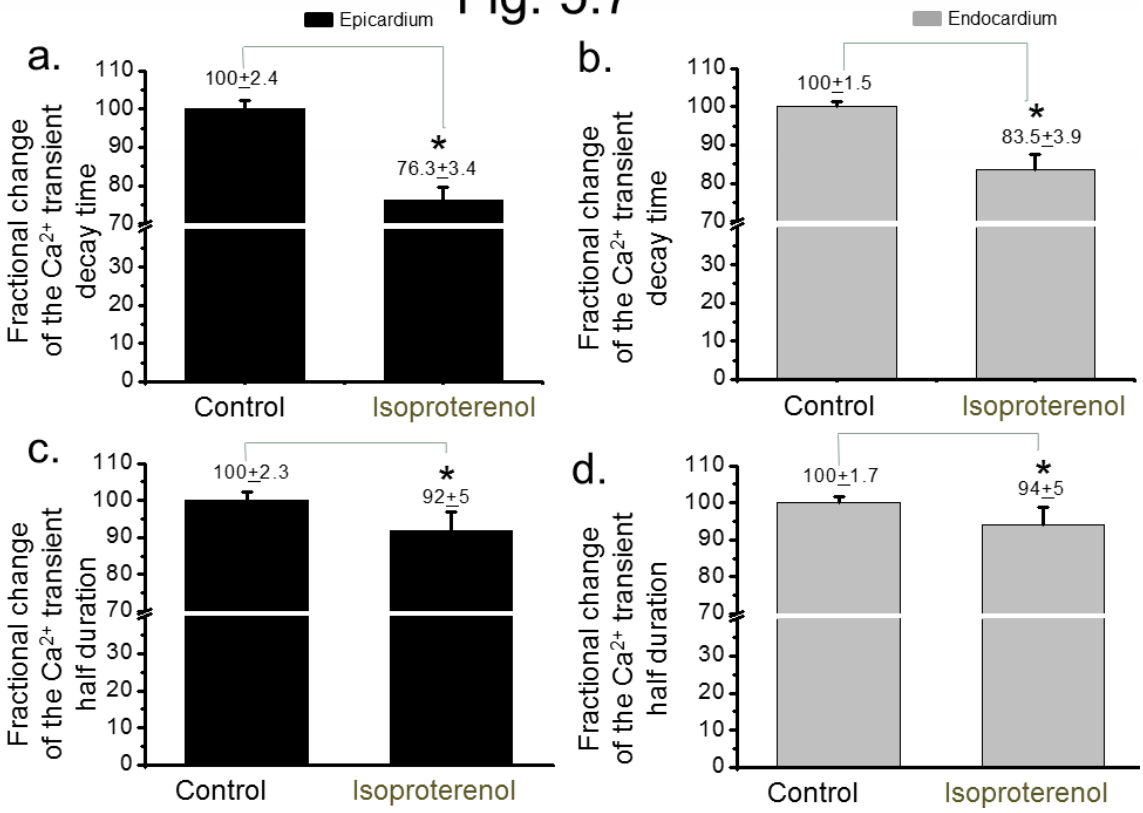

Fig. 5.7 a. Fractional change of the intracellular Ca^{2+} transient decay time indicated a faster relaxation after 500nM isoproterenol for epicardium (black) and (b) endocardium (grey). c. Fractional change of the intracellular Ca^{2+} transient half duration also became faster after isoproterenol in epicardium and (d) endocardium. Mice hearts were paced at 6Hz and temperature set to 37°C. *P<0.05, N=4 hearts, mean±SD.

5.3 How are the Ca^{2+} currents affected after sympathetic NS agonist?

In the last section, we saw that the stimulation of beta-adrenergic receptors induced changes in the AP that correlated with changes in the intracellular Ca^{2+} transients. Particularly, across the ventricular wall, sympathetic NS stimulation via beta-adrenergic receptors produced a longer phase 1 and increased amplitude of phase 2 (**Fig. 5.3**). The intracellular Ca^{2+} transients, in the epicardium and endocardium, also showed an increase in Ca^{2+} transient amplitude (**Fig. 5.5**).

The downstream activation of PKA and phosphorylation of key Ca^{2+} handling proteins may be responsible for the increased cycling of Ca^{2+}. However, PKA phosphorylates multiple proteins. In order to try to understand the specific proteins producing the phase 1 and 2 changes, we assessed the Ca^{2+} currents across the membrane. Our lab has shown that, aside from an outward K^+ current, phase 1 is mediated by an inward Ca^{2+} current that enters the cell through the L-type Ca^{2+} channel.[31] Phase 2 is also affected by Ca^{2+} current across the membrane by the activity of the NCX.

In order to directly evaluate any changes in the $I_{L\text{-}Ca}$, we used a UV sensitive compound (nifedipine) that blocks this channel in conjunction with a patch to measure current changes. Our newly developed LPP technique was used to measure membrane currents at the intact heart level.[31] We placed a UV laser to photolyze the UV compound (nifedipine) (**Fig. 5.8**) at the loose patch site. Initially, the L-type Ca^{2+} channels are blocked by nifedipine and after the UV flash the inhibition is removed allowing the channels to permeate Ca^{2+}. Upon a UV flash, the immediate changes in the current can be measured by taking the difference between the recording before and after the flash (ΔIm) (see **Methods** for details). Since the only current changing after the flash is Ca^{2+}, then the resulting signal is from Ca^{2+} moving across the membrane.

The Ca^{2+} current produced by the UV flash consists of an early and late component (**Fig. 5.8 b**). Our lab has published that the early component is Ca^{2+} current through the L-type Ca^{2+} channel, while the late is produced from Ca^{2+} extrusion by the NCX after SR release.[31] In order to only evaluate the changes in the current through the L-type Ca^{2+} channel and not those produced by the NCX, we recorded currents in which the fraction of nifedipine breakdown increased by increasing the intensity of UV energy used. Ryanodine (Ry, 10μM) was retro-perfused in conjunction with thapsigargin (Tg, 2μM). Ry keeps open the RyRs located in the membrane of the SR. Tg inhibits the SERCA pump from sequestering Ca^{2+} into the SR. Together, these two drugs impair the myocytes from having a full SR Ca^{2+} release. Thus, our currents recorded from UV pulses of increasing intensities had no i-late components (**Fig. 5.9 a**). This allowed us to solely assess the changes in L-type Ca^{2+} currents under increasing UV pulse duration. At increasing pulses, more nifedipines are broken and thus, more current is produced through L-type Ca^{2+} channels (**Fig. 5.9 a**). **Fig. 5.9 b** shows how i-early, or the current through the L-type Ca^{2+} currents,

increased more with 500nM isoproterenol. Plotting the amplitudes, we can see that the i-early was larger for isoproterenol conditions than control at increasing energy of the UV pulses (**Fig. 5.9 c**).

These results indicated that the beta-adrenergic stimulation (with isoproterenol) increased the L-type Ca^{2+} current likely by the activation of PKA. Since the Ca^{2+} that triggers CICR enters the cell during phase 1, then $I_{L\text{-}Ca}$ can be attributed to the longer phase 1 which we saw in **Fig. 5.3**. If more Ca^{2+} enters the cell, then a larger SR Ca^{2+} may be released, which explains the greater Ca^{2+} transient amplitude seen in **Fig. 5.5** after isoproterenol.

Fig. 5.8

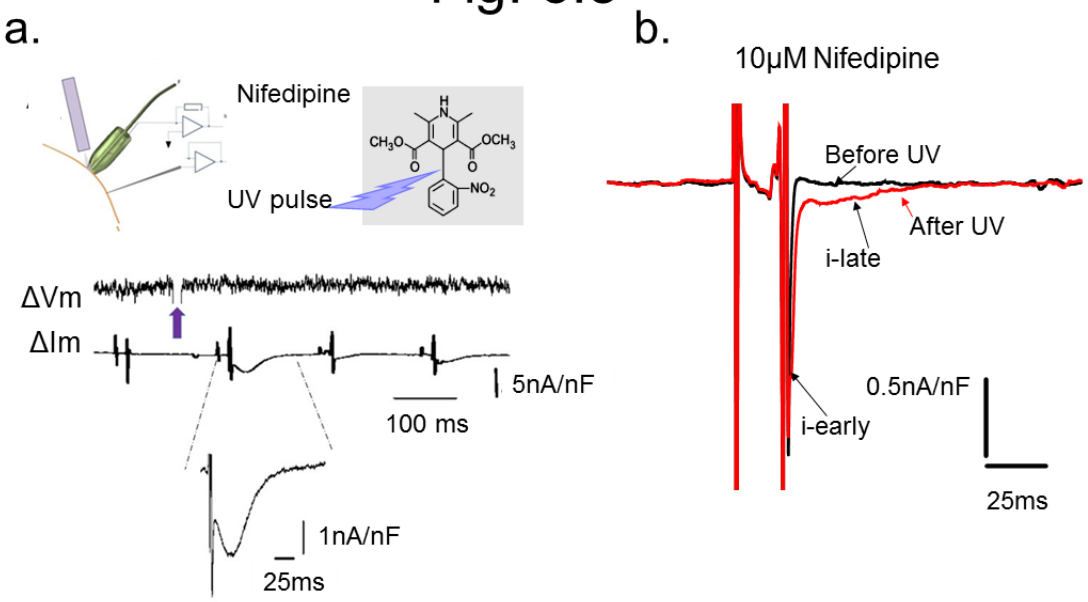

Fig. 5.8 a. The LPP technique uses a UV laser to break UV sensitive compounds (nifedipine) to induce immediate Ca^{2+} currents across the membrane. The recording with a UV pulse is subtracted from the current without the pulse and the result is the change in current (ΔIm). b. The current (red) after nifedipine inhibition is removed by a UV flash consists of two components: i-early and i-late.

Fig. 5.9

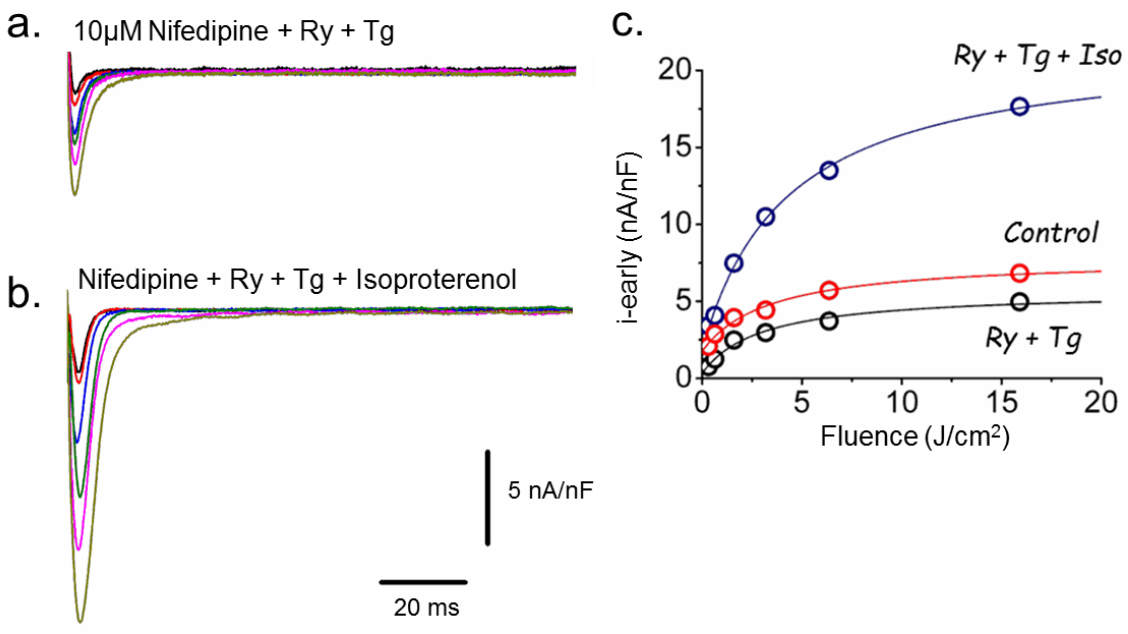

Fig. 5.9 a. UV induced currents at increasing laser energies show increasing i-early from the greater fraction of nifedipine breakdown. Ry and Tg prevent SR release, which is responsible for the i-late, not seen here. b. Isoproterenol causes the i-early currents to be larger indicating a beta-adrenergic stimulation effect on the L-type Ca^{2+} channels. c. Increasing energy of UV pulses increased the i-early more with isoproterenol.

5.4 Are there molecular differences in beta-adrenergic receptor distribution across the ventricular wall?

The differences across the ventricular wall of the effect of isoproterenol can be due to molecular disparities associated with the population of beta-adrenergic receptors across the ventricular wall. If there are more receptors in one region of the ventricular wall, then this region will report a greater response to isoproterenol. The adrenergic receptor agonist, isoproterenol, is highly specific in stimulating the beta-1-adrenergic receptor (β1AR). It presents a larger affinity for β1AR than beta-2-adrenergic receptor (β2AR).

In order to assess the molecular differences across the ventricular wall, we measured the expression level of the β1AR. Using a vibrotome, we cut 200μm thick slices from the endocardium and epicardium of mice hearts. The whole ventricular wall of the mouse is approximately 1.2 mm thick. These were then processed for RT-PCR (refer to **Methods** section for details). RT-PCR is able to measure the mRNA expression of proteins. The expression was relative to a housekeeping gene that is important in the function of a cell such that its expression will not vary. It is a conserved gene. Additionally, the expression of the β1AR gene in the endocardium was normalized to the epicardium expression level. RT-PCR showed an increased expression (but not significant) of β1AR in the endocardium (1.78 ± 1.09) relative to the epicardium (1.03 ± 0.3) (**Fig. 5.10 a**).

β2AR was also assessed in the epicardium and endocardium to evaluate if the different sensitivity to adrenergic agonist between epicardium and endocardium could be related with differential expression of β2AR. As shown in **Fig. 5.10 b**, the expression level of mRNA coding for this receptor was not significantly different in the two regions of the ventricular wall.

Fig. 5.10

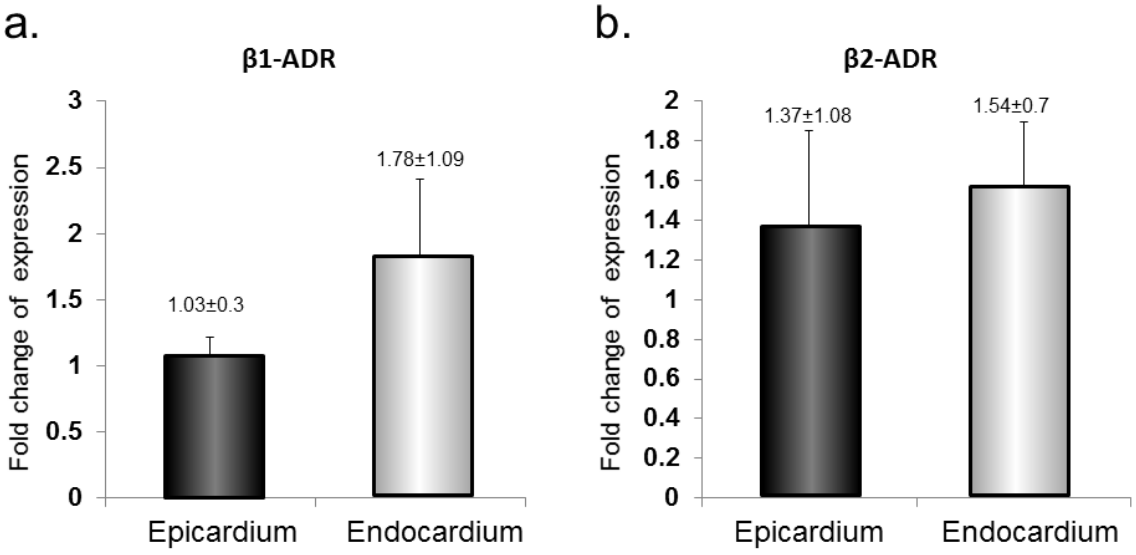

Fig. 5.10 a. mRNA expression of beta-1-adrenergic receptors in the epicardium and endocardium layer of the mouse heart. The expression of the genes was relative to that of the housekeeping gene, GAPDH. Additionally, the expression of genes in the endocardium were normalized to the expression of the same genes in the epicardium. b. mRNA expression of beta-2-adrenergic receptor was not different between the epicardium and endocardium. *P<0.05, N=5 hearts, mean±SD.

5.5 Does sympathetic NS agonist affect epicardial electrical alternans?

The mouse naturally increases its HR by the action of the sympathetic NS. A fraction of the sympathetic control of the HR is due to circulation of epinephrine through the blood**.** The catecholamines affect EC coupling and CICR by activating a beta adrenergic receptor couple to a stimulatory G-protein G_s. Downstream Gs can activate an adenyl cyclase (AC) that promotes the conversion of ATP into cAMP. An increase of cAMP will induce the dissociation of the catalytic subunit of PKA from the regulatory one. Finally, the downward cascade of PKA activation leads to the phosphorylation and subsequent stimulation of multiple Ca^{2+} handling proteins including the RyR, SERCA by PLN phosphorylation, and the L-type Ca^{2+} channel. Therefore, if alternans are due to failures in the underlying cycling of Ca^{2+}, then the sympathetic NS's effects over Ca^{2+} dynamics may affect Ca^{2+} alternans.

In order to understand how the sympathetic NS affects the alternans, we externally paced Langendorff perfused hearts and increased the HR until alternans appeared. At this

point, isoproterenol was perfused. Interestingly, the alternans were drastically reduced. **Fig. 5.11 a** showed how the large degree of APD alternans at 10Hz (black) disappeared after perfusion with 500nM isoproterenol. By measuring APD70 (**Fig. 5.11 b**), the alternans was calculated as 0.28 (±0.09, SD). This was significantly reduced to 0.01 (±0.09) after treatment with isoproterenol. The alternans at APD90 was also reduced (data not shown to avoid repetitive results), but not as much as APD70.

We already showed the close relationship between action potential alternans and Ca^{2+} alternans. Thus, we expect that the activation of a beta-adrenergic pathway also will have a significant effect on the development of Ca^{2+} alternans. The rational is as follows: if Ca^{2+} transient alternans are a result of the underlying Ca^{2+} mishandling, then isoproterenol may affect these alternans across the ventricular wall. Since the alternans

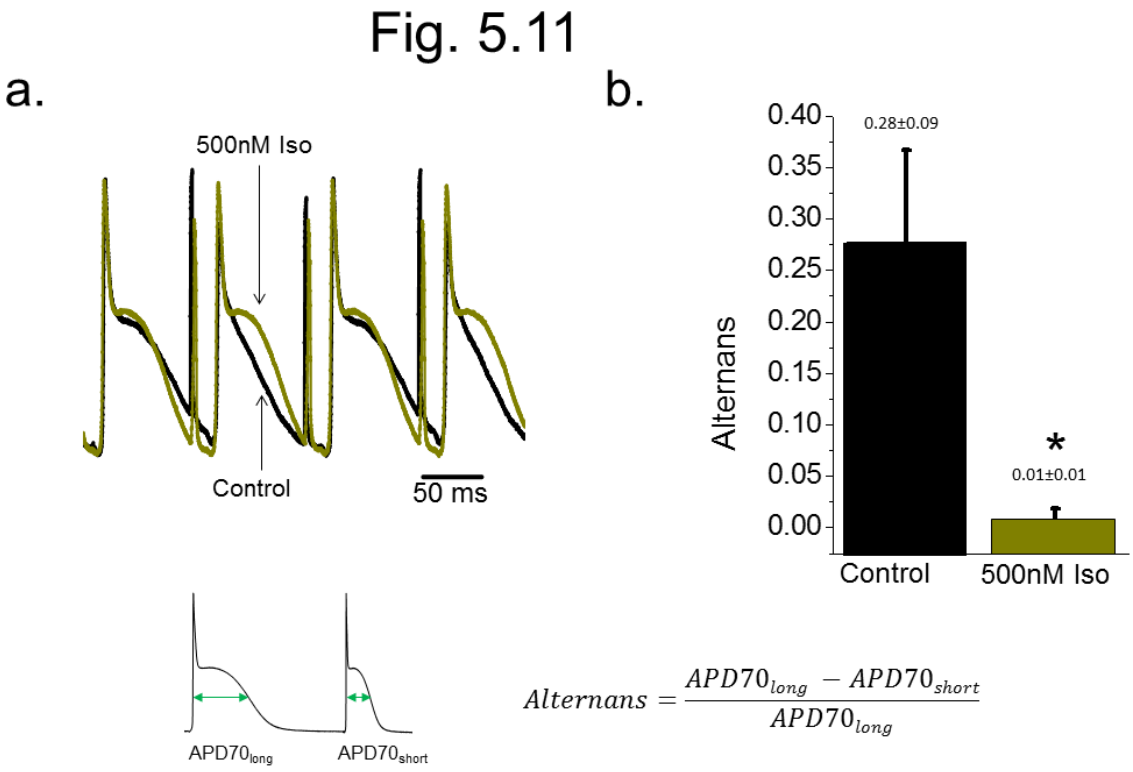

Fig. 5.11 a. Electrically recorded AP traces at 10Hz alternate, but perfusion with 500nM Iso (green) eliminated the alternans. The magnitude of the pacing stimulus (seen in between consecutive APs) was increased in order for the heart to follow the 10Hz HR. b. APD70 alternans are significantly reduced with isoproterenol. *P<0.05. N=4 hearts. mean±SD.

were found to be non-homogeneous in the epicardium and endocardium, then the effect of beta-adrenergic stimulation on the Ca^{2+} transient alternans could be heterogeneous. To test the effect of isoproterenol on the Ca^{2+} transient alternans, we externally paced an isolated

mouse heart at increasing frequencies until alternans were produced. This was done because alternans are frequency dependent. Once the alternans were produced, Tyrode with isoproterenol was retro-perfused. **Fig. 5.12** showed the Ca^{2+} transient alternans at 7Hz. At this frequency, the endocardium alternated more than the epicardium. Retro-perfusion with 500nM isoproterenol greatly reduced the alternans of both the endocardium and epicardium.

Fig. 5.12

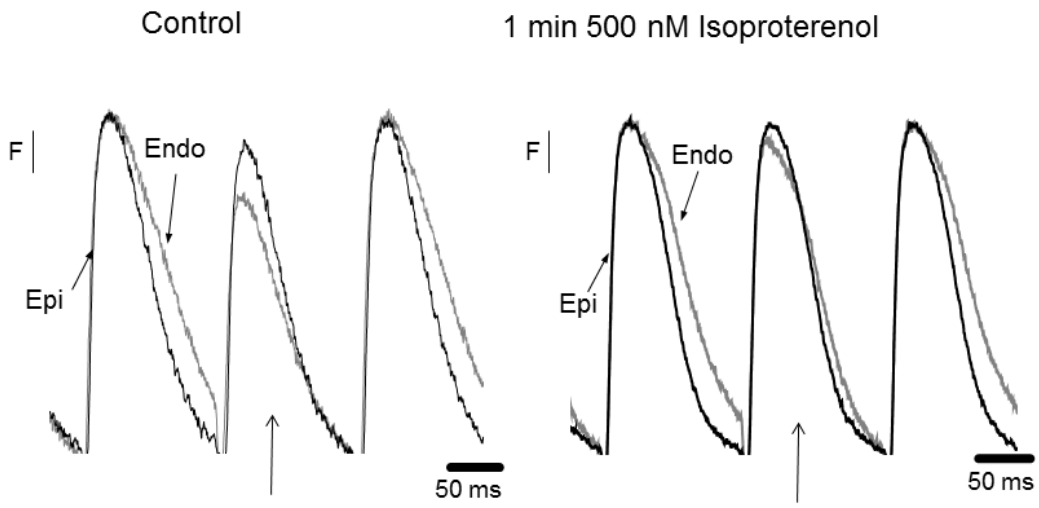

Fig. 5.12 Ca^{2+} transient alternans of the epicardium (black) and endocardium (gray) at 7Hz showed different degrees of alternans (arrow). At this HR, some hearts alternated in the epicardium while others did not, but what was consistent was that the endocardium alternated more than the epicardium in all the hearts. Retro-perfusion of 500nM isoproterenol drastically reduced the alternans in both regions of the ventricular wall.

The effect of beta-adrenergic agonist on Ca^{2+} alternans is shown in **Fig. 5.13**. Upon retro-perfusion with isoproterenol, the alternans significantly ($P<0.05$) decreased for the epicardium and endocardium layers. It is very interesting to see how the activation of a sympathetic NS agonist affects the cycling of intracellular Ca^{2+} in a manner that improves the Ca^{2+} dynamics and reduces alternans. Although the ventricular wall has differences in the handling of intracellular Ca^{2+}, the effect of isoproterenol was the same for both regions.

Overall, this chapter assessed whether restoring the circulation of catecholamines by retro-perfusion with a beta-adrenergic agonist affected the electrical properties and Ca^{2+} dynamics. We demonstrated that across the ventricular wall, the time course of the AP had a decrease in total repolarization time, but a longer phase 1. Since phase 1 and the repolarization of the dome is associated with Ca^{2+} handling, we assessed the intracellular

Ca^{2+} transient changes upon retro-perfusion of a beta-adrenergic agonist. Indeed, there was an increase in the Ca^{2+} transient amplitude as well as a faster relaxation of the transient. The larger amplitude and the faster relaxation of the and Ca^{2+} transient correlate with the increase in phase 1 duration, due to more Ca^{2+} entering the cell and producing a larger release from the SR. In other words, beta-adrenergic stimulation causes more Ca^{2+} influx during phase 1 that leads to a greater magnitude of CICR. Additionally, the faster repolarization of the AP correlates with the faster relaxation of the intracellular Ca^{2+} transient. Thus, a beta-adrenergic agonist may be able to significantly decrease Ca^{2+} alternans by improving the rate and efficiency of Ca^{2+} cycling (release and re-uptake) to be on par with the increased HR.

Fig. 5.13

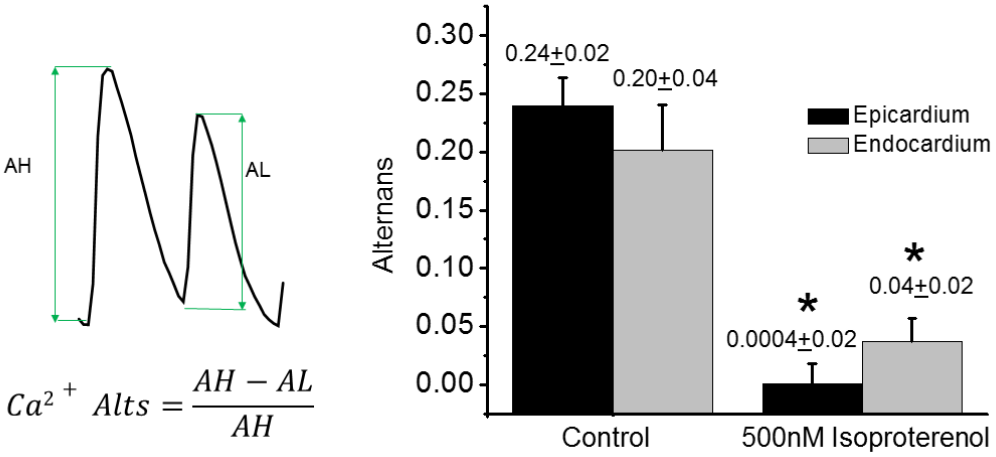

Fig. 5.13 Ca^{2+} transient alternans of the epicardium (black) and endocardium (gray) at 10Hz and 32ºC. Retro-perfusion of 500nM isoproterenol significantly reduced the alternans. *P<0.05, N=3, mean±SEM.

CHAPTER 6:

Intrinsic parasympathetic NS activity and effect on alternans

Hearts in the Langendorff set-up beat at lower frequencies outside the body. We found that these intact mice hearts have a frequency of 4Hz. However, in their physiological setting inside the thoracic cavity, they beat at 9-11Hz. As we show in Chapter 5, the circulation of catecholamines is responsible for maintaining this rhythm. The Langendorff heart lacks the circulation of neurotransmitters released as part of the extrinsic ANS regulation. Nevertheless, the heart has its own local innervation from the cardiac plexus. As part of this "mini-brain", there are local releasing sympathetic NS neurons as well as parasympathetic NS neurons. We saw that the sympathetic NS neurons are active by assessing the beta-adrenergic activity. When blocked, the HR dropped further, indicating release of neurotransmitters from the sympathetic NS neurons still exist in the isolated heart. However, despite the activity of the beta-adrenergic receptors, the HR is not as high as in physiological settings. Interestingly, the sympathetic NS downstream activity at the cellular level is closely regulated by the activity of the parasympathetic NS agonists. Thus, it is possible that the parasympathetic NS is overdriving dominantly the chronotropism in the isolated mouse heart.

6.1 Are the parasympathetic NS neurons active in the Langendorff heart?

As we already mentioned in Chapter 5, the heart is innervated by the two branches of the ANS. The sympathetic NS acts by releasing catecholamines and defines a typical systemic response named "fight or flight". On the other hand, the parasympathetic NS releases the neurotransmitter ACh and is involved in the defining a systemic response named "rest and digest". Indeed, when we are resting (i.e sleeping) the parasympathetic NS releases ACh in order to reduce our HR.

The action of ACh in the heart has a mirror opposite effect than the relase of catecholamines. Activation of parasympathetic NS reduces the HR (negative chronotropic action), reduces contractility (negative inotropic action), slows down the rate of the mechanical relaxation (negative lusitropic action) and finally modifies the velocity at which APs propagate in the heart (negative dromotropic action). In order to achieve these cardiac responses, the ACh released by the parasympathetic NS needs to bind to a muscarinic (M2) receptor. This receptor is coupled to a G-protein, specifically, G_i. The activation of G_i has two separate downstream pathways. On one hand, it dissociates into a $G\alpha_i$ subunit that inhibits AC. This action will reduce AC's ability to convert ATP into cAMP, which affects PKA. It results in a reduction in the level of phosphorylation mediated by PKA.[152,153]

On the other hand, the activation of G_i will lead to the dissociation of the $G\beta\gamma_i$ subunit. The dissociated $G\beta\gamma_i$ subunit can interact with an inward rectifier K^+ channel (Girk 3.4) producing an increase of the open probability of the channel named I_K ACh (I_{KAch}).

Both actions, the inhibition of the AC and the activation of I_{KAch} will lead to a strong negative chronotropic action.[86]

The molecular selectivity is not the only difference between the sympathetic and parasympathetic NS. The somas of the postganglionic neurons from the sympathetic NS are located outside the heart, principally on the cervical ganglia. In contrast, the parasympathetic NS postganglionic neurons are located in intracardiac ganglia within the heart structure. This last feature lead to the possibility that in the Langendorff perfused heart a parasympathetic tone will still be present.

In order to test the activity of the local innervation of parasympathetic NS neurons, we cannulated intact mouse hearts and retro-perfused Tyrode, while we monitored the frequency of AP firing. Physiologically, the local increase of ACh can be achieved in two ways. One is a constitutive release of ACh from the postganglionic terminals. The second is by inhibiting the pathways by which the clearance of ACh is produced. Contrary of what happened with most of the neurotransmitter, ACh cannot be reuptaken by the pre-synaptic terminal. The main way the local increase in ACh is dissipated is by the activation of an enzyme that degrades ACh. This enzyme is called Acetylcholine esterase (AChE). AChE is an enzyme that cleaves ACh and as a product of the reaction produces choline, a molecule that can be reuptaken by the presynaptic terminal. Thus, inhibiting AChE will increase the ACh concentration in the cleft between the terminal and the myocyte.

To evaluate this idea, we retro-perfused with an AChE inhibitor. AChE is usually inhibited by organophosphates. Paraoxon is an organophosphate with a big selectivity for AChE. Inhibiting the AChE with paraoxon will allow us to see if there is activity from the parasympathetic NS neurons releasing ACh. Indeed, it there is a constitutive basal release of ACh, paraoxon will enhance the action of this spontaneous ACh release. If ACh is released and it is not being degraded, then there will be an accumulation of ACh, which will affect the HR.

This was tested by measuring the spontaneous AP firing frequency before and after paraoxon. **Fig. 6.1** showed that within 30 s of retro-perfusion with 5μM of paraoxon, the frequency of AP dropped 3% (97.4$\pm$1.8) in comparison to the control frequency. After 1 min, the frequency significantly dropped ($P<0.05$) to 91.8% ($\pm$3) of the control frequency and continued decreasing. Between 60-90s and 240-270s of paraoxon retro-perfusion all the frequencies are significant. The frequency fell as low as 66% ($\pm$5) of the initial HR after 240-270s of paraoxon. This indicated the constitutive release of ACh and its accumulation upon AChE inhibition. The accumulated ACh dropped the frequency of AP firing. Thus, the neurons are active in the isolated heart resulting in a vagal tone. This correlates with the basal HR of the intact heart *ex vivo*.

ACh is the neurotransmitter of the synapse between a preganglionic neuron and postganglionic neuron of the sympathetic and parasympathetic NS. AChE could be causing an effect by having the ACh build in the synapse between pre and post-ganglionic neurons and stimulating the nicotinic receptors. At the synapse between the post-ganglionic neuron

Fig. 6.1

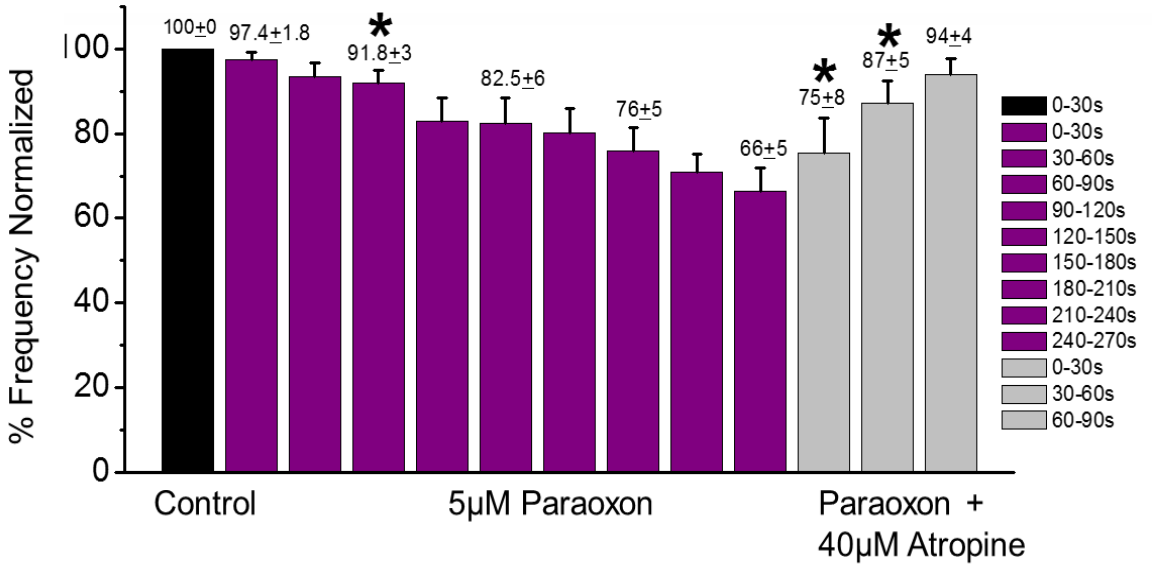

Fig. 6.1 The AChE inhibitor, paraoxon, caused the AP firing frequency to drop over time indicating a constitutive release of ACh from the local innervation of parasympathetic NS neurons. Retro-perfusion with the muscarinic specific blocker, atropine, reversed the decrease in HR. Hearts were not externally paced and temperature was set to 37ºC. *P<0.05. N=5 hearts, mean±SEM.

and the myocytes, parasympathetic NS neurons release ACh which binds to muscarinic receptors. To verify that the effect of paraoxon was muscarinic specific and not nicotinic, we retro-perfused the heart with the muscarinic antagonist, atropine. The retro-perfusion of 5μM paraoxon and 40μM atropine caused an increase in HR as seen in **Fig. 6.1**. Atropine reversed the effect of paraoxon indicating that the accumulation of ACh caused by paraoxon was stimulating muscarinic receptors. The stimulation of the muscarinic receptors resulted in a decrease in the HR, which was reversed when the muscarinic receptors were blocked by atropine.

Since the parasympathetic NS neurons are active in the isolated heart, then they could be affecting cardiac properties including intracellular [Ca^{2+}] levels and membrane potential. In order to study effects of parasympathetic NS stimulation on cardiac properties, we used a muscarinic receptor agonists, carbachol. Carbachol is synthetic analog of ACh with improved long term stability properties. Before testing the effects of parasympathetic NS over AP and Ca^{2+} transients, first we set-out to evaluate if the heart would respond to the circulation of carbachol in the Langendorff set-up.

In the case of the sympathetic NS's circulation of catecholamines, the Langendorff system efficiently simulated this circulation by retro-perfusion. However, the neurons from

the parasympathetic NS locally release ACh. ACh is not released through the bloodstream. Therefore, in the Langendorff set-up, the retro-perfusion of carbachol through the coronaries may not produce a response.

To assess if the Langendorff system was a good set-up to study effects of parasympathetic NS agonists on multiple physiological variables in the intact heart, we tested if it responded accordingly to the retro-perfusion with carbachol. We measured the frequency of AP firing before and after retro-perfusion with carbachol. **Fig. 6.2 a** showed sample trace from a heart that has been retro-perfused with Tyrode solution at physiological

Fig. 6.2

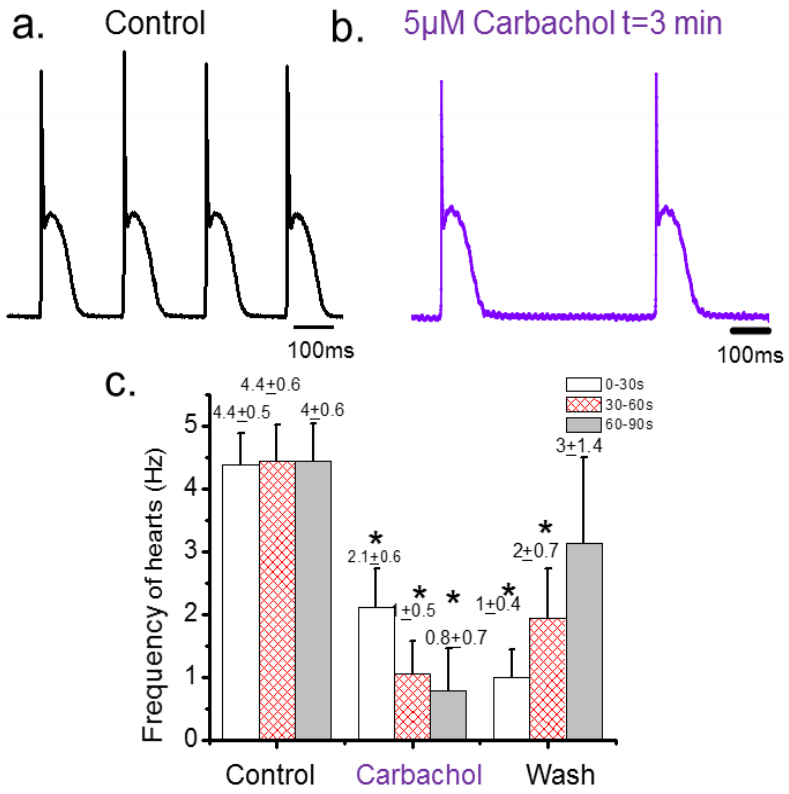

Fig. 6.2 Typical APs show a frequency of 4Hz. b. The AP firing frequency dropped to 2Hz after retro-perfusion with 5μM carbachol. c. The AP frequency was consistently around 4Hz and dropped within 1 min of carbachol retro-perfusion. Washing for about 1.5 mins restored the frequency to 3Hz. *P<0.05. N=5 hearts.

temperature, 37 °C. These hearts are not externally paced; instead, the intact atriums set the HR. We then retro-perfused with 5μM carbachol for more than 3 min, the spontaneous AP frequency dropped (**Fig. 6.2 b**). Assessing the AP firing frequency over a period of 90 s showed that these isolated hearts have a frequency around 4.4Hz (±0.6). These results were very consistent with what was seen for the AP frequency of hearts with Tyrode solution before retro-perfusion with isoproterenol. Compared to 4.4Hz for the control, the HR dropped significantly ($P<0.05$) to 1Hz (±0.5) within a minute of retro-perfusion with

5μM of carbachol (**Fig. 6.2 c**). In the Langendorff set-up, the heart is able to respond to the retro-perfusion of carbachol. **Fig. 6.2 b** showed how carbachol decreased the frequency of AP firing, acting accordingly as a negative chronotropic agent. Using retro-perfusion with Tyrode, we saw that the effect on the frequency was washed progressively over a period of 1.5 mins.

In summary, the isolated heart had a vagal tone. In addition, despite the non-physiological method by which we are perfusing carbachol, the heart responded by decreasing its HR. Although the Langendorff set-up does not simulate the local neurotransmitter release of the parasympathetic NS neurons, the HR was affected by the systemic perfusion with muscarinic agonists. Next, we want to understand how the vagal tone may affect physiological parameters across the ventricular wall.

6.2 How does the parasympathetic NS agonist affect AP morphology across the ventricular wall?

The constitutive release of ACh from the local innervation of parasympathetic NS neurons in the isolated heart stimulates the muscarinic receptor. This affects the heart in a negative chronotropic, ionotropic, and lusitropic effect by blocking the downward cascade of sympathetic NS agonist and/or the activation of I_{KACh}.

The direct action of muscarinic stimulation on the electrical properties of the ventricular AP has been controversial.[154] Therefore, we want to understand how the AP morphology and intracellular Ca^{2+} transients change upon muscarinic stimulation with carbachol. Assessing the AP morphology is an indicator of the underlying ionic currents affected. Therefore, we measured the AP before and after carbachol retro-perfusion. Knowing that the Langendorff heart responds accordingly to the circulation of muscarinic agonist, we retro-perfused with carbachol and assessed the epicardial AP electrically using sharp glass microelectrodes. **Fig. 6.3 a** shows the epicardial AP recorded with glass sharp microelectrodes before and after the retro-perfusion with 5 μM carbachol at 6Hz and physiological temperature of 37˚C. Retro-perfusion with carbachol (purple trace) makes the repolarization of phase 2 and 3 faster. Phase 2 is associated with the Ca^{2+} release from the SR and the subsequent activation of the NCX current. Phase 3 is mediated by K^+ channels that help restore the membrane potential. Therefore, it is important to assess intracellular Ca^{2+} transients, as well, to determine if the faster repolarization is due to the Ca^{2+} handling.

Since the heart had a strong vagal tone, we wanted to understand how the ventricular wall's AP morphology was affected by muscarinic stimulation. In order to

Fig. 6.3

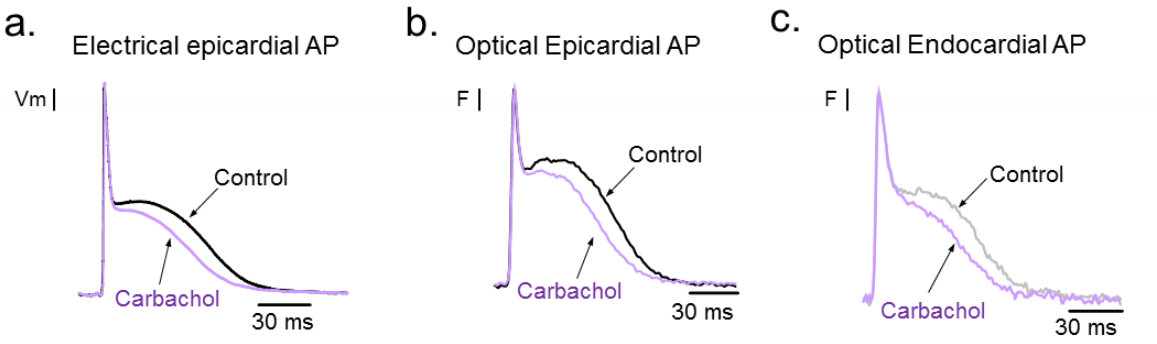

Fig. 6.3 a. Sharp microelectrode AP measurement before (black) and after (purple) retro-perfusion with 5µM carbachol at 6Hz, 37°C. b. Optical recording from the epicardial region with di-8-ANEPPs before (black) and after (purple) retro-perfusion with carbachol at 5Hz. c. Optical endocardial AP before (grey) and after (purple) retro-perfusion with carbachol.

record APs across the ventricular wall, we retro-perfused with the potentiometric dye, di-8-ANEPPs. The optically recorded epicardial APs presented the same morphological changes after retro-perfusion with 5µM carbachol (**Fig. 6.3 b**). Although the control waveform of the AP of the endocardium was very different to the epicardium, the response to carbachol was the same (**Fig. 6.3 c**). Across the ventricular wall, retro-perfusion with carbachol shortened the AP.

Both layers across the ventricular wall showed an effect in the phase 2 and 3 of the AP. To quantify the effect, we assessed the APDs associated with these phases. Since the dome was affected, we measured an APD of half of the dome (Half Phase 2). APD Half Phase 2 tells the time it takes for 50% of the dome to repolarize. APD90 is the time taken for the AP to be 90% repolarized. After 5µM carbachol, the epicardium (black) took 22% less time (78±2 %) to repolarize half of phase 2, relative to its control (**Fig. 6.4 a**). The APD90 also took less time for the epicardium (82 ± 2 %) (**Fig. 6.4 b**). Interestingly, the endocardium (grey) showed less of an effect with carbachol by repolarizing half of phase 2 in only 14% (86 ± 2 %) less time than its control (**Fig. 6.4 c**). After carbachol, the APD90 repolarized in 15% (85 ± 1 %) less time than the control (**Fig. 6.4 d**).

Fig. 6.4

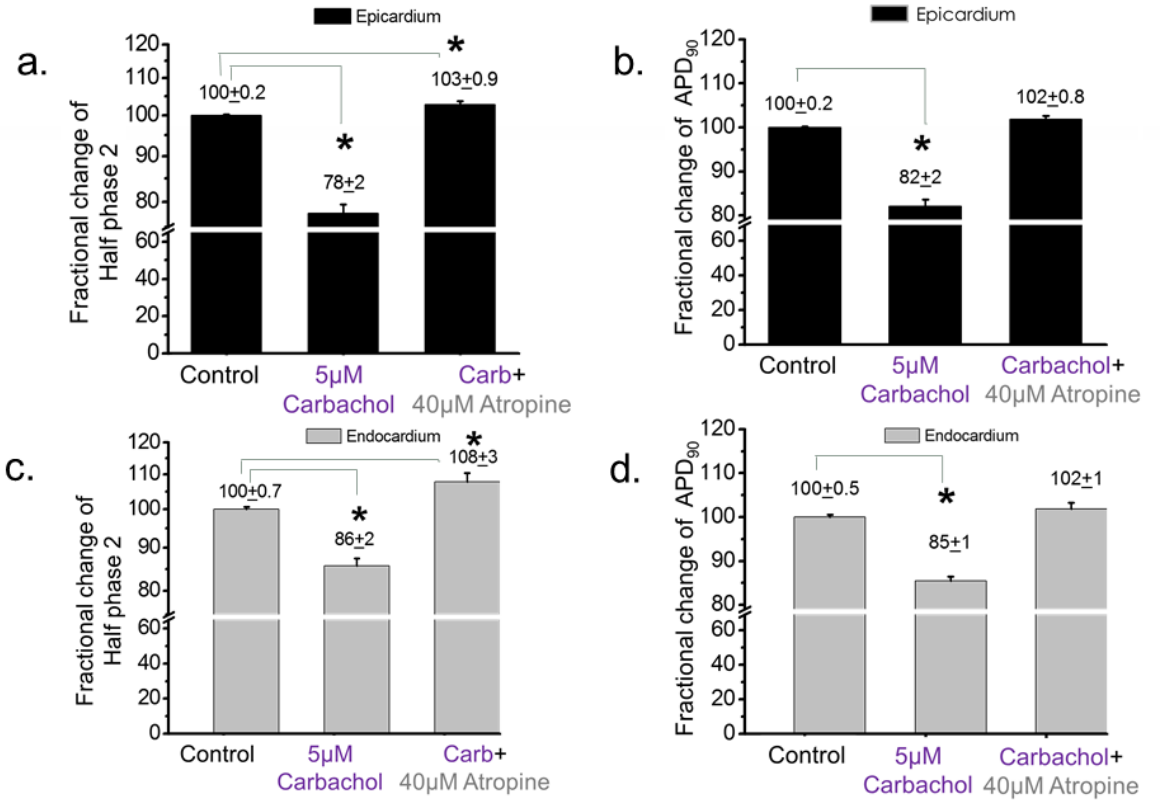

Fig. 6.4 a. Fractional change of half phase 2 effect after 5µM carbachol and carbachol with atropine in the epicardium. The effect was normalized to the control. b. Fractional change of APD 90 in the epicardium. Carbachol shortened the AP repolarization time, an effect reversed with the simultaneous retro-perfusion of carbachol and atropine. c. Fractional change of half phase 2 in the endocardium with carbachol. d. Fractional change of APD 90 after carbachol retro-perfusion in the endocardium. *P<0.05. N=5 hearts, ± SEM.

These effects were reversed for both layers after retro-perfusion with carbachol and atropine. The simultaneous retro-perfusion of a muscarinic agonist and antagonist assured that the effect of faster repolarization seen was due to a muscarinic specific binding. Overall, carbachol had a larger effect on the repolarization of the epicardium compared to the endocardium.

6.3 Are the AP morphology changes induced by parasympathetic NS agonist due to the stimulation of I_{KACh}?

The faster repolarization effect produced by the muscarinic agonist, carbachol, can also be due to a K^+ conductance. The activation of M2 receptors by ACh stimulates the G_i protein which dissociates into α and βγ subunits. The α subunit of G_i interacts in an inhibitory manner towards AC. The βγ subunit is known to interact with an inward rectifier K+ channel that produces the I_{KACh}. I_{KACh} is more prevalent in the atrium than the ventricle.[155–157] The ventricle expression of the genes responsible for the ACh-sensitive K^+ channel, Kir3.1 and 3.4, are barely detected in rat hearts,[155] thus little is known of the presence of this current in the ventricle. This current repolarizes the membrane and therefore can be producing the faster repolarization effect seen with carbachol.

In order to assess if the parasympathetic NS stimulation of M2 receptors was activating I_{KACh}, we retro-perfused hearts with a blocker of this ACh-sensitive K^+ channel. The ACh-sensitive K^+ channels were blocked with the bee venom, tertiapin. The tertiapin was retro-perfused into the hearts for 10 min. This amount of time ensured that the ACh-sensitive K^+ channels were blocked. The AP was recorded electrically from the epicardium before and after 100nM tertiapin.

There were no significant changes in the AP morphology with tertiapin (**Fig. 6.5 a**). Afterwards, we retro-perfused simultaneously with tertiapin and carbachol. We expected that if the AP shortening was being produced by the activation of I_{KACh}, then the blocking of this channel would result in no effect after parasympathetic stimulation with simultaneous perfusion of carbachol and tertiapin. It was important to retro-perfuse these simultaneously to ensure that the tertiapin did not wash out during carbachol retro-perfusion. If the tertiapin washed out, then the effect seen would be due to the non-inhibited ACh-sensitive K^+ channels being stimulated by the interaction of the βγ subunit. After 1 min, epicardial APs were electrically recorded (**Fig. 6.5 a**). The effect of carbachol desensitizes after 1 min, therefore in order to see any effect produced by the M2 agonist on the AP, we recorded at 1 min. The faster repolarization induced by carbachol alone did not occur in the presence of the I_{KACh} blocker (**Fig. 6.5 a** and **b**). The simultaneous retro-perfusion of tertiapin and carbachol showed a significant increase in the duration of half phase 2. This is probably due to the inhibition of a K^+ current, which slows repolarization.

To ensure that these hearts indeed responded to carbachol, we washed the tertiapin and carbachol with tyrode solution for 20 mins. We recorded the AP at the 20 min wash time and then retro-perfused with 5μM carbachol. The effect of carbachol still produced a faster repolarization effect relative to the control (**Fig. 6.5 c**). However, the faster

repolarization was not as low as those seen in **Fig 6.4 d** where the optically recorded APs with carbachol were 78 ± 2%. This could be due to the presence of tertiapin even after a 20 min retro-perfusion with Tyrode solution without carbachol or tertiapin.

These results indicate that the activation of I_{KACh} is highly involved in speeding up the relaxation of the ventricular action potential. However, other mechanisms may also contribute to this change in repolarization rate including changes in the systolic Ca^{2+} dynamics.

Fig. 6.5

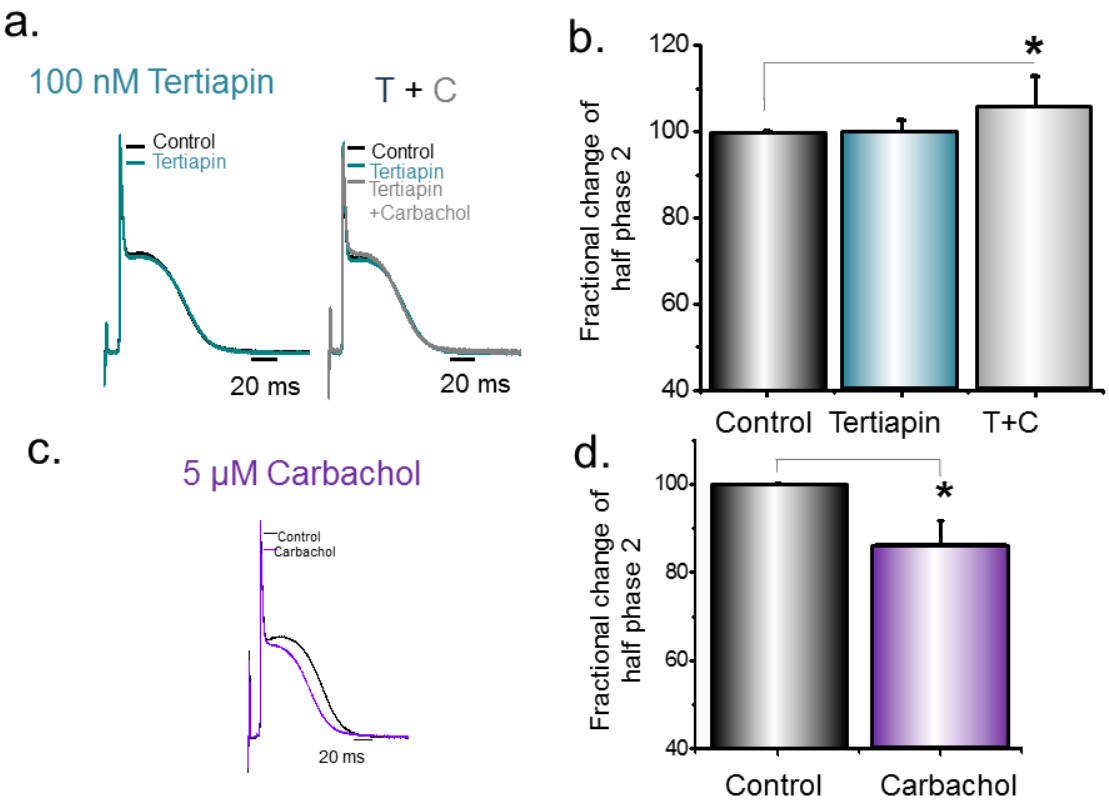

Fig. 6.5 a. Blocking I_{KACh} produced no changes in the morphology of the AP when perfusig with carbachol. b. The APD of half of phase 2 was not shortened when using 100nM tertiapin. The only significant effects were after the simultaneous retro-perfusion of tertiapin and carbachol c. After a long wash, hearts were perfused with carbachol. d. Alone, carbachol shortened the duration of half phase 2. T=37°C. N=5 hearts, ± SEM. *P<0.05.

6.4 Parasympathetic NS agonists and Ca^{2+} transient kinetics

The mechanism by which the muscarinic agonists affects the AP repolarization is not very clear. However, morphological changes associated with phase 2 may be a result of the underlying Ca^{2+} handling. SR Ca^{2+} release or rise in intracellular [Ca^{2+}] can affect phase 2 by the activation of the NCX. The faster repolarization seen with carbachol on the AP can be produced by a decrease in the intracellular [Ca^{2+}] such that the NCX is activated less and a net charge of +1 does not enter the cell to depolarize the membrane. Thus, a decreased activity of the NCX may contribute to the faster repolarization.

In order to assess whether the phase 2 changes induced by carbachol are a result of intracellular [Ca^{2+}] changes, we monitored the Ca^{2+} transients across the ventricular wall with Rhod-2. **Fig. 6.6** shows the Ca^{2+} transients before and after 5μM carbachol (purple) for the epicardium and endocardium. The epicardium (black) Ca^{2+} transient trace (**Fig. 6.6 a**) before and after carbachol (purple) are overlapping, indicating no morphological changes between the two in the epicardium. The same occurred in the endocardium (**Fig. 6.6 b**). The endocardium control Ca^{2+} transient trace overlapped with the trace recorded after carbachol (purple) was retro-perfused into the heart.

Fig. 6.6

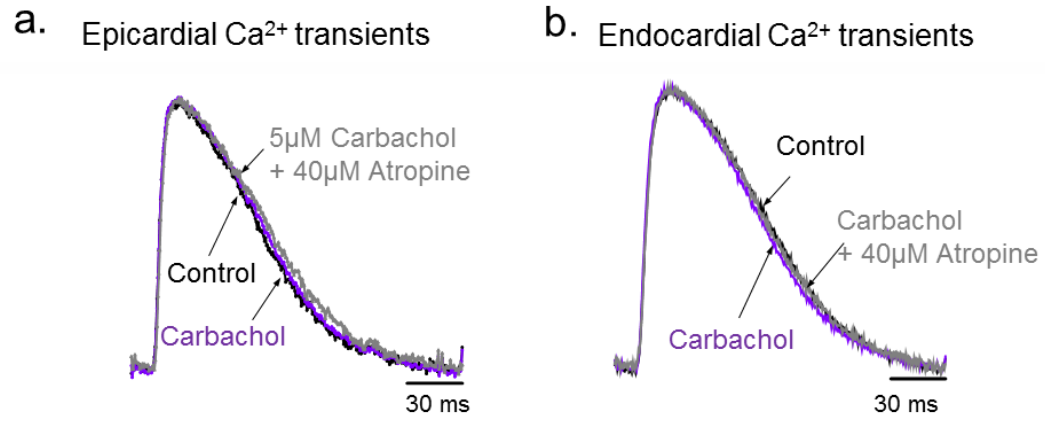

Fig. 6.6 a. Ca^{2+} transients from the epicardium before (black), after carbachol (purple), and with simultaneous retro-perfusion of carbachol and atropine. b. Endocardial Ca^{2+} transients do not change with retro-perfusion of carbachol nor after the simultaneous retro-perfusion of carbachol and atropine.

Overall, both the endocardium and epicardium showed Ca^{2+} transients that appear to not be altered by carbachol. Additionally, after retro-perfusion with carbachol, the heart was retro-perfused simultaneously with carbachol and 40μM atropine to ensure any effect seen was due to M2 specific stimulation.

Fig. 6.7

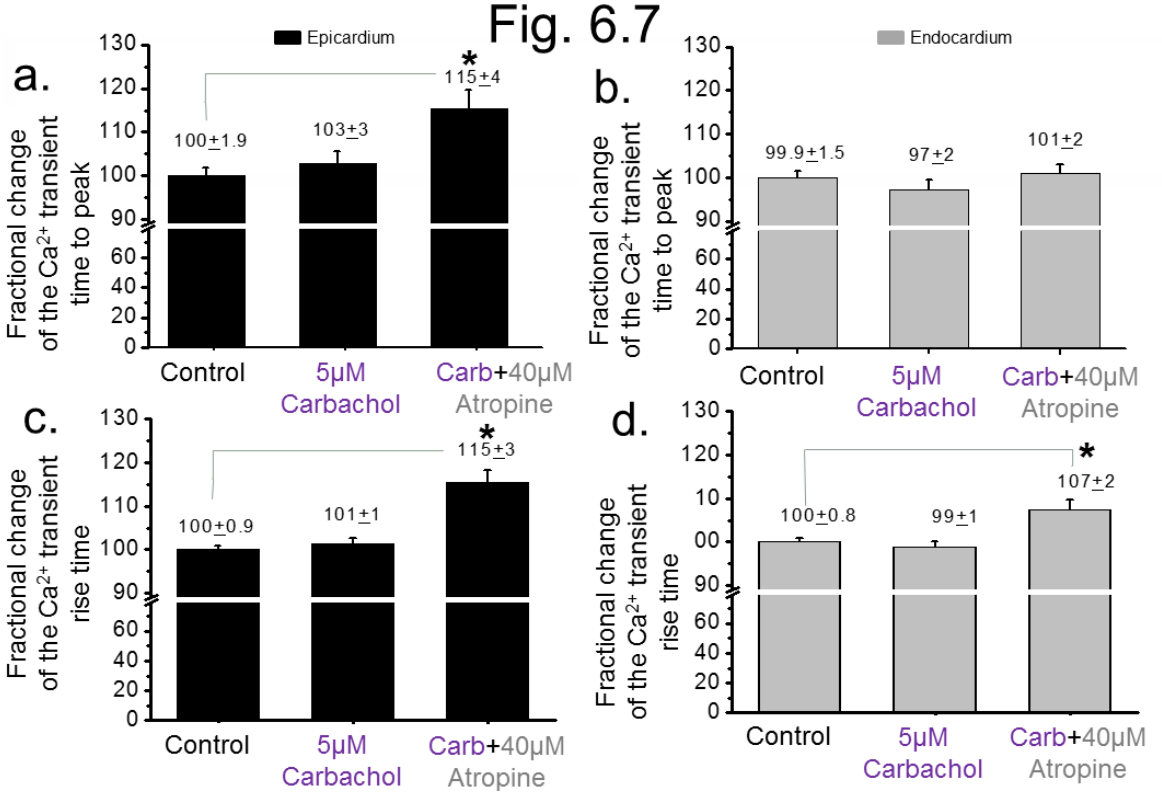

Fig. 6.7 a. Time to peak kinetics of the Ca^{2+} transients with 5μM carbachol and then carbachol with atropine after 2 mins measured in the epicardium and (b) endocardium. These hearts were paced at 6Hz and temperature set to 37°C. c. Rise time kinetics of the epicardium (black) and (d) endocardium (grey) before and after 5μM carbachol. N=5 hearts, ± SEM. *P<0.05.

In order to quantify any kinetic changes induced by carbachol on the Ca^{2+} transients, we measured well-defined parameters mentioned in the **Methods** section including: TTP, RT, DT, HD. **Fig. 6.7 and 6.8** (**a-d**) show that across all parameters of Ca^{2+} transient kinetics, there were no significant changes with carbachol. Based on a one-way ANOVA, the results were not significant.

Interestingly, the Ca^{2+} transient TTP, RT, DT and HD of the simultaneous retro-perfusion with carbachol and atropine were significantly longer for both the epicardium and endocardium, relative to their individual controls. This could be due to the desensitization effect produced by carbachol since these traces were assessed after 2 min of retro-perfusion and we previously saw that carbachol effect desensitized after 1 min. Desensitization caused the AP traces to take more time to repolarize (data not shown).

Fig. 6.8

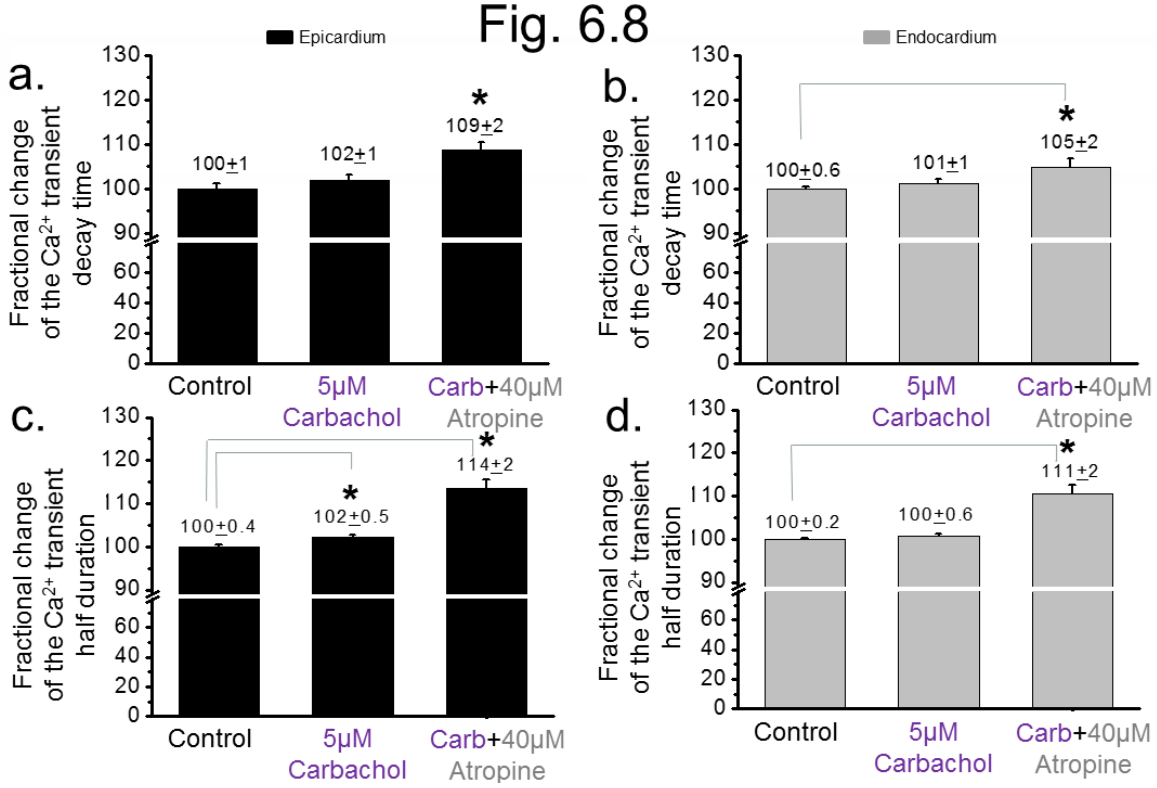

Fig. 6.8 a. Decay time kinetics of the Ca^{2+} transients with 5μM carbachol and then carbachol with atropine after 2 mins measured in the epicardium and (b) endocardium. c. Half duration kinetics of the epicardium (black) and (d) endocardium (grey) before and after 5μM carbachol. These hearts were paced at 6Hz and temperature set to 37°C. N=5 hearts, ± SEM. *P<0.05.

Overall, the parameters of the Ca^{2+} transient kinetics measured showed slight changes that were not significant with carbachol. Although the simultaneous retro-perfusion with carbachol and atropine significantly lengthened the kinetics measured, these effects may be produced by desensitization to carbachol, Therefore, the faster repolarization effect seen in the AP phase 2 and 3 is not mediated by changes in intracellular [Ca^{2+}].

Although the G_i protein dissociates from M2 after muscarinic stimulation and inhibits the activity of AC, the Ca^{2+} dynamics do not change if AC was not on. These experiments were conducted on isolated mice hearts that lack the circulation of catecholamines, which turn AC on. Therefore, in the absence of a sympathetic NS stimulation, a parasympathetic NS stimulation affects the AP morphology in a Ca^{2+}-independent pathway.

6.5 How are the Ca^{2+} currents affected after parasympathetic NS agonist?

In the last section, we saw that the intracellular Ca^{2+} transients are unaffected by the stimulation of muscarinic receptors in the intact heart. The changes in the AP morphology were a consequence of I_{KACh}. This was a very interesting finding because we expected to see changes in the Ca^{2+} dynamics produced by the downstream inhibition of PKA. As previously mentioned, ACh stimulation of muscarinic receptors produces the inhibition of AC by G_i and this affects cAMP levels which are needed for PKA activation. Thus, we expected that if PKA is not active, then it would be unable to phosphorylate key Ca^{2+} handling proteins in myocytes. One of these proteins is the L-type Ca^{2+} channel. When phosphorylated by PKA, this channel has an increase in the open probability allowing it to pass a larger Ca^{2+} current, $I_{L\text{-}Ca}$. Under AC inhibition, PKA is unable to phosphorylate the L-type Ca^{2+} channel and consequently less current passes through it. The less current would then have implications on CICR because Ca^{2+} entering through this channel is highly responsible for triggering the SR Ca^{2+} release. However, in the last section, we saw no changes in the Ca^{2+} transients.

In order to reaffirm our findings in the last section, we tested any changes in the $I_{L\text{-}Ca}$ before and after muscarinic stimulation with carbachol. Our novel technique, LPP (described in **Methods**), is able to measure membrane currents in the intact heart where all the cells continue to be coupled. **Fig. 6.9 a** shows the currents induced after a UV flash on hearts perfused with nifedipine. After recording the currents (black), a solution containing

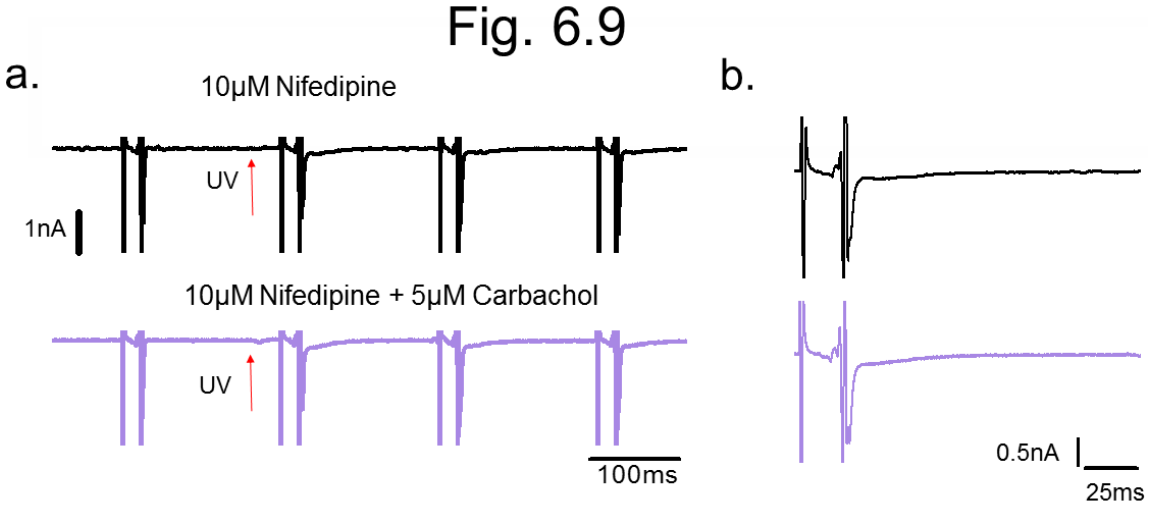

Fig. 6.9 Ca^{2+} currents measured with LPP using the UV sensitive L-type Ca^{2+} channel blocker (nifedipine) after a UV flash. Currents induced by photolysis under the simultaneous perfusion of nifedipine and carbachol (purple). b. Closer view of the UV induced currents with nifedipine and after (purple) simultaneous retro-perfusion of nifedipine (10μM) with carbachol.

both nifedipine and carbachol was retro-perfused and the currents were re-evaluted (purple). **Fig. 6.9 b** demonstrated that the currents were very similar and were not significantly different. When overlapped, the currents are identical (**Fig. 6.10 a**). To

quantify if there are any changes not easily seen when overlapped, we measured the amplitude of the peaks of the i-early and i-late before and after carbachol (**Fig. 6.10 b**). Interestingly, i-late increased relative to its control, but changes were not significant.

These findings indicated that the inhibition of PKA, in the isolated heart, has no noticeable changes in the downstream Ca^{2+} currents. In particular, these sets of experiments reveal that in the isolated heart, which lacks sympathetic NS stimulation, PKA is not actively phosphorylating L-type Ca^{2+} channels. Consequently, inhibition by carbachol's activation of G_i does not affect currents through these channels (see **Discussion**).

Fig. 6.10

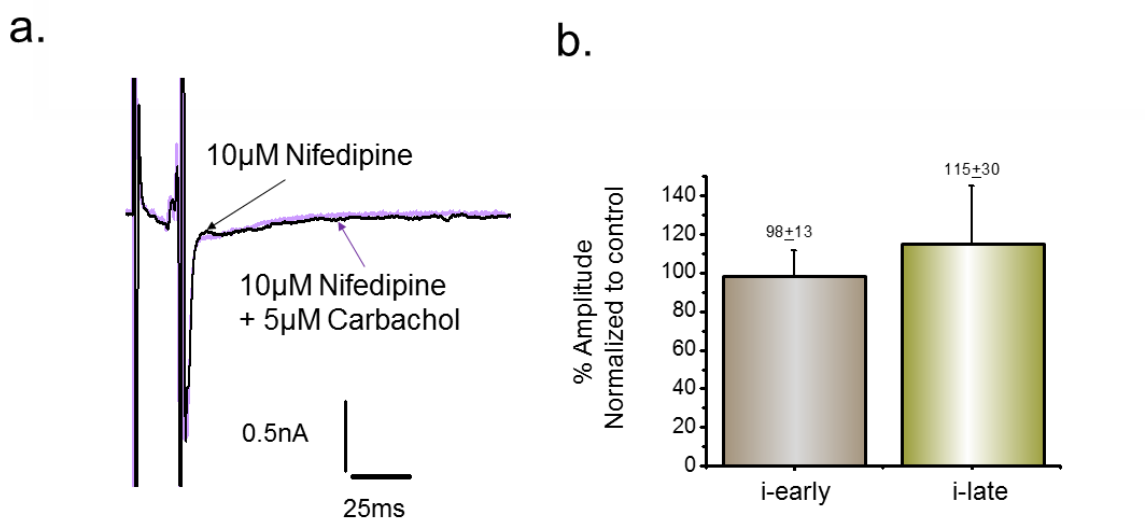

Fig. 6.10 Ca^{2+} currents measured with LPP before and after (purple) simultaneous retro-perfusion of nifedipine (10μM) with carbachol. b. Amplitude changes in the i-early and i-late with carbachol. *P<0.05. N=6 hearts, ± SD.

6.6 What are the molecular heterogeneities associated with parasympathetic NS stimulation across the ventricular wall?

The faster carbachol-induced repolarization of the epicardium vs the endocardium could be due to the heterogeneous distribution of muscarinic receptors in the different layers of the ventricular wall. Therefore, RT-PCR was used to assess the expression levels of the M2 receptors in the endocardium and epicardium layer. Instead of homogenizing the whole heart and assessing the overall expression of the M2 receptors, we took 200µm slices from the epicardium and endocardium layers to assure the expression was from these individually processed tissues. **Fig. 6.11** shows the expression from the epicardium and endocardium of the cholinergic muscarinic receptor 2 (CHMR2). These were normalized to GAPDH and processed using the Pfaffl method.[158] The endocardium showed a larger mRNA expression of the CHMR2 gene associated with M2 receptors.

Fig. 6.11

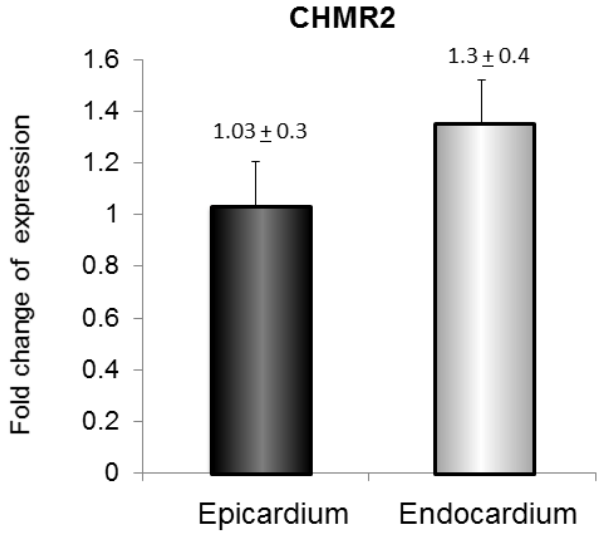

Fig. 6.11 Relative expression of the cholinergic muscarinic receptor 2 in the endocardium and epicardium. Normalized to GAPDH. *P<0.05. N=5 hearts, ± SD.

Despite the greater expression of the muscarinic receptors in the endocardium, the effect of the muscarinic agonist is less in this layer (**Fig. 6.4 c and d**). The increase in the amount of receptors does not necessarily indicate a greater response. More receptors also results in a faster desensitization, which could be the case for the endocardium. When we conducted experiments measuring the effect of carbachol on the electrically recorded AP, we saw that the faster repolarization decreased after 1 min. The effect was at a maximum at 1 min and then it was not present. The experimental conditions where this desensitization

was observed was when the hearts were externally paced. However, the effect of carbachol over hearts that had atriums intact and were not paced continued to have a decreased HR after 1 min.

6.7 How does the parasympathetic NS agonist affect epicardial electrical alternans?

Results in the last chapter showed that isolated intact hearts have a lower HR than in the animal's body. In addition, in the beginning of this chapter we saw that inhibition of AChE decreased the HR even more. This suggested that the low HR correlated with a constitutive release of ACh from the local innervation of the parasympathetic NS neurons. Thus, the isolated hearts may have a vagal tone which produces lower HRs and a faster repolarization by the activation of I_{KACh}.

Since the alternans are highly dependent on HR, we wanted to understand if the vagal tone may affect the alternans. The vagal tone was shown to be mediated by the stimulation of muscarinic receptors by retro-perfusion with carbachol. In order to test if the

Fig. 6.12

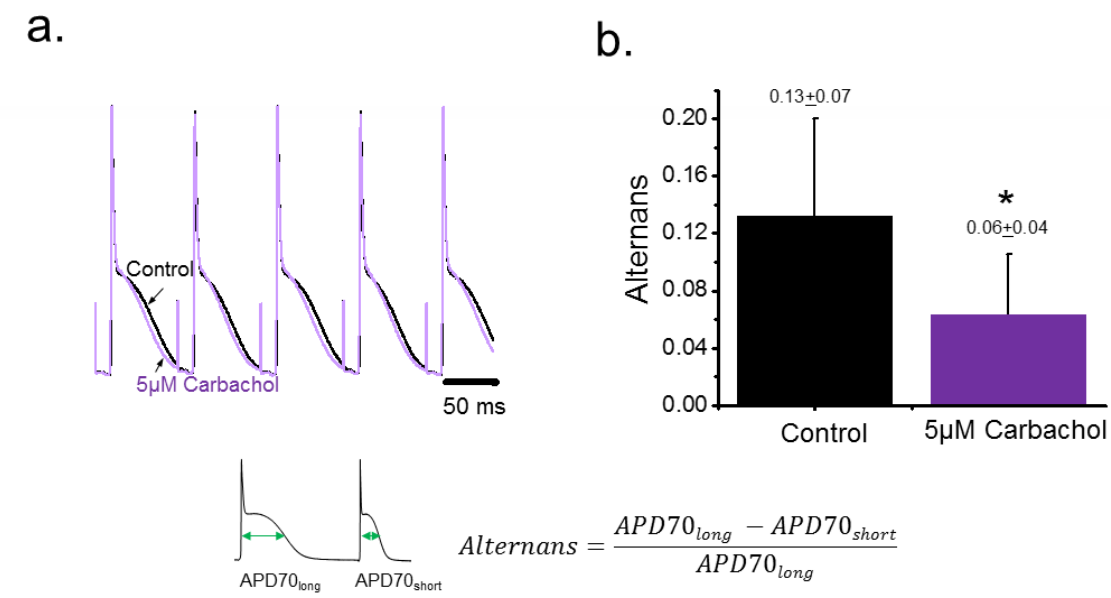

Fig. 6.12 Electrically recorded APs before (black) and after retro-perfusion with carbachol. Carbachol significantly reduced the APD70 alternans. *P<0.05. N=5 hearts, ± SD.

vagal tone affected the APD and Ca^{2+} transient alternans, we increased the external pacing frequency of the heart to induce alternans and then retro-perfused with 5μM carbachol and assessed the effect on the alternans.

Fig. 6.12a shows the APD alternans produced at a pacing rate of 12Hz (black trace) and modifications to the repolarization caused by carbachol. It was difficult to visually

evaluate the effects of the carbachol on APD alternans. Thus, to quantify any changes in the repolarization, we measured the duration at 70% repolarization for each AP and computed the alternans based on the equation (**Fig. 6.12 b**).

Retro-perfusion with carbachol significantly reduced the APD alternans. One reason is that in the presence of carbachol the activation of I_{KACh} accelerates the AP repolarization. Indeed, it is important to remember that phase 2 is a result of the balance between an influx of Na^+ through NCX and a K^+ efflux through several K^+ channels. Following this line of arguments, if the myocytes increase a K^+ conductance it will be more difficult for the NCX to impact the AP repolarization. Then, APD alternans will be damped by the increased K^+ conductance.

The second possibility is that the activation of muscarinic receptors could have an impact in the genesis of Ca^{2+} alternans. To test this idea PLFFM experiments were performed at different HR in order to induce alternans. A summary of this experiment is presented in **Fig. 6.13.** Interestingly, the degree of Ca^{2+} alternans was reduced by the

Fig. 6.13

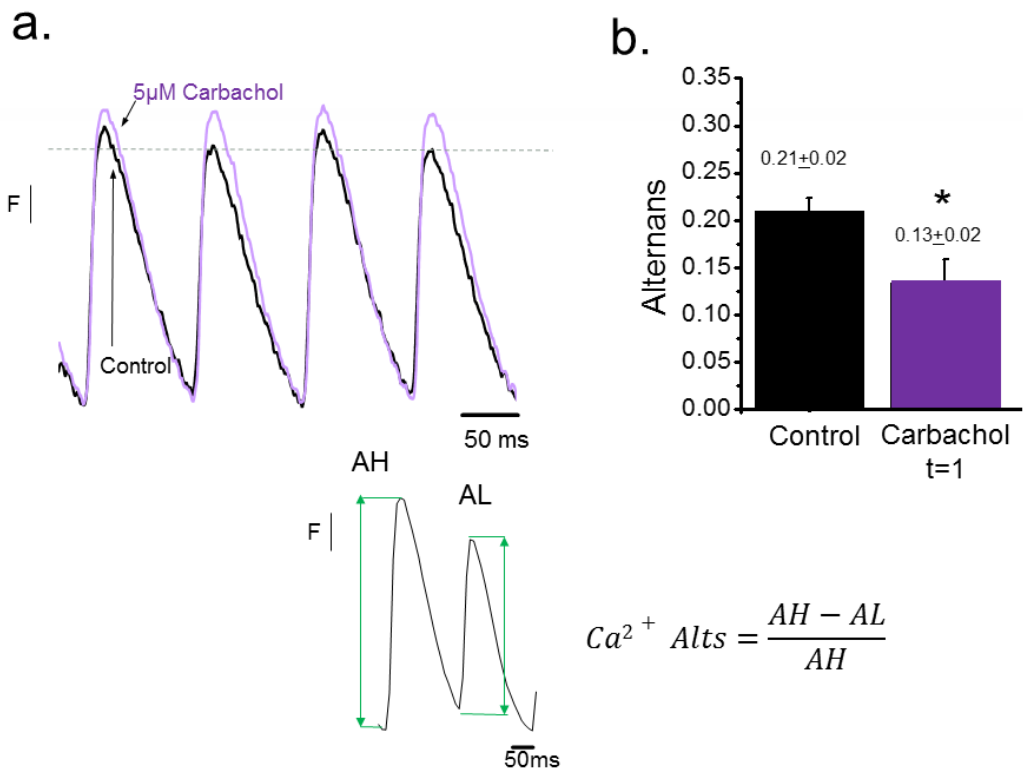

Fig. 6.13 Ca2+ transients recorded before (black) and after retro-perfusion with carbachol (purple). Carbachol significantly reduced the Ca2+ alternans. *P<0.05. N=4 hearts, ± SEM.

perfusion with 5 μM of carbachol (**Fig. 6.13a** and **b**). This result was highly unexpected since alternans are mediated by Ca^{2+} mishandling and in another section of this chapter, we found that carbachol produced no changes in the Ca^{2+} kinetics.

In the presence of carbachol, the repolarization of the AP is faster due to the activation of I_{KACh}, based on results in an earlier section. The faster repolarization may cause the activity of the NCX to increase. Under these conditions the driving force for the Na^{+} influx through the exchanger will be larger and will promote a larger Ca^{2+} efflux from the cytosol. This condition will tend to slightly (which is probably why we did not see any effects in the fast Ca^{2+} transients) reduce the steady state diastolic Ca^{2+} level in the cytosol and inside the SR. Our assessment of the Ca^{2+} transients would be unable to capture these gradual, steady state changes in diastolic Ca^{2+} levels because we did not measure Ca^{2+} changes over a larger time span and in conditions that reduced bleaching of the dye. We primarily focused on changes that occurred within the first minute of retro-perfusion with carbachol to prevent desensitization. Finally, this steady state SR Ca^{2+}reduction will decrease the gain of the CICR process leading to Ca^{2+} alternans reduction. Thus, instead of having a direct effect over the Ca^{2+} dynamics, by inhibiting PKA activation, the repolarization changes produced by a completely different ion (K^{+}) can affect the Ca^{2+} dynamics through changes in the membrane potential.

To summarize this chapter, we found that there is a big scene for a parasympathetic regulation in the ventricular free wall. There is not only a constitutive release of ACh from the synaptic terminals of the post ganglionic parasympathetic neurons but also a very significant effect of the muscarinic receptor activation on the ventricular AP repolarization. Finally, the results here suggest that parasympathetic drive can attenuate alternans by two mechanisms: decreasing the HR (alternans are less prevalent at lower HRs) and by increasing the NCX extrusion of Ca^{2+} (possibly lowering the diastolic level of Ca^{2+} in the cytosol and SR) due to the I_{KACh} induced faster action potential repolarization.

CHAPTER 7: Discussion

SCD kills about 300,000 people every year in developed countries and the underlying cellular events leading to its manifestation are not clear.[1] The only medical speculation of possible SCD is the appearance of alternating beat-to-beat changes in the morphology of the T-wave (T-wave alternans) from a patient's ECG.[52,150] T-wave alternans are a high indicator of ventricular fibrillation (VF) leading to SCD. This thesis presents medical implications for understanding SCD due to the link between T-wave alternans and ventricular fibrillation (VF). The central goal of this thesis was to evaluate the molecular mechanisms involved in the genesis of T-wave alternans.

The heart is a very dynamic organ that is able to function as an electromechanical pump by coordinating the movement of ions at the cellular level. These ionic changes are the underlying causes of the electrical signal (Na^+, K^+) and contractile properties (Ca^{2+}). In order to understand the organ level phenomenon of T-wave alternans, in this thesis, we evaluated the cellular dynamics across the ventricular wall where T-wave alternans manifest.

We assessed the effects over the electrical properties and intracellular Ca^{2+} dynamics of the heart under conditions that increased the risk of generating alternans. Particularly, the changes in the HR and temperature mimicked conditions of high demand on the heart that consequently produced alternans. Since T-wave alternans are associated with the repolarization of the ventricular region, we focused on the effects in the two outermost layers of the ventricular wall, the epicardium and endocardium. Additionally, the activation of receptors associated with the ANS's regulation over the heart was assessed to evaluate their effect on the cardiac properties and T-wave alternans.

The results from this thesis shed light into the molecular events impacting the genesis of T-wave alternans. It outlines effects of HR, temperature, and ANS stimulation on the underlying causes of T-wave alternans. Specifically, we were able to assess the electrical action potential duration and Ca^{2+} transient alternans from myocytes in the intact organ. This allowed us to determine the underlying ionic current effects in the AP morphology and Ca^{2+} transient kinetic effects produced across the ventricular wall as a consequence of alternans under modulations in the HR, temperature, and ANS stimulation.

The morphology of the AP and Ca^{2+} transient are rate-dependent: implications for increasing the risk of cardiac alternans

The rhythmicity of the heart is critical to its function.[159] This rhythm is maintained by the coordinated electrical pacing and its propagation throughout the heart.[41] Abnormalities in the rhythm are termed arrhythmias. High or low HRs can both lead to arrhythmic conditions. Thus, pathological conditions in which the rhythmicity is affected can greatly impair the function of the heart and its ability to pump blood.

The length of the cardiac cycle is highly dependent on the HR. Generally, the faster the HR, the shorter the cycle length. Multiple variables interplay within the cardiac cycle. For example, the propagation of the electrical signal, as seen in the ECG, occurs within a faster period at high HRs. As the timing changes, the dynamics of key cardiac properties are also expected to change accordingly. Thus, the AP morphology and the cycling of intracellular Ca^{2+} have a faster time course at increased HRs. Fig.3.3 (also 3.5) and 3.8 showed AP durations and decay time of the Ca^{2+} transient, respectively, follows the same trend where higher HRs have shorter durations.

In addition, at higher HRs, we observed the appearance of alternans in the electrocardiographic T-wave and in the APD. T-wave and APD alternans both increase in magnitude as HRs increases. This result was very similar to the one reported by Nearing et al.[160] In general, the frequency dependency of the alternans has been a well established experimental observation.[52,62,148] Pastore et al. referred to the HR in which the alternans began to appear as the alternans threshold.[161] For our experiments, this was at frequencies between 8 and 9Hz. Dynamic pacing protocols in which the heart is paced at increasing frequencies until it no longer follows the rate is generally used to induce alternans.[162,163]

Although the frequency dependency of alternans is now a days a well-established fact, it was not until Thomas Lewis (1910) showed sets of experiments where alternans were produced by high HRs in humans. Fig. 3.1 confirmed that this finding was also true for externally perfused mouse heart where T-wave alternans were recorded by a transmural ECG. Furthermore, Fig. 3.2 also showed that this was a consequence of APD alternans.

In order to address if T-wave alternans were promoted by a differential response to HR of different ventricular anatomical layers, we assessed the epicardium and endocardium APD and Ca^{2+} dynamics at increasing HRs. The duration of the epicardium and endocardium AP shortened at increasing frequencies. This behavior holds true until alternans in the duration of the AP develop.

As expected, the Ca^{2+} transient amplitudes also dropped at increasing frequency (Fig. 3.9 and 3.10). Furthermore, the endocardium began to alternate at lower HRs than the epicardium. Interestingly, the Ca^{2+} alternans appeared at lower frequencies than the APD alternans. This agreed with results from Wang et al. who showed SR Ca^{2+} alternans occurred sooner than APD alternans. [164]

Increasing the HR increases the likelihood of developing alternans. Thus, we wanted to understand how the Ca^{2+} handling changes in an intact beating heart at increasing frequencies. As the HR was increased, it was possible to observe that there were significant changes in the relaxation kinetics of the Ca^{2+} transient and not in the rising phase (Fig. 3.8). For both regions of the ventricular wall, the primary effect from increasing HRs on the Ca^{2+} transients was seen in the relaxation kinetics.

The rate of relaxation of the Ca^{2+} transient is defined by a combination of several passive and active processes. Passive processes such as diffusion from the dyadic space

and binding to cytosolic Ca^{2+} buffers (i.e. diffusible proteins, contractile proteins, ATP, etc.) are responsible for the short-term and fast relaxation of Ca^{2+} transients. Although these mechanisms are kinetically very efficient, Ca^{2+} buffers can saturate after several cardiac cycles. Active primary and secondary transport systems have a dual role. First, these extrude the Ca^{2+} ions that permeate into the cell (i.e. NCX) through L-type Ca^{2+} channels during an AP. Second, these transport systems define the reuptake of Ca^{2+} into the SR to maintain a level of free Ca^{2+} concentration (SERCA).

The SR sequestering is largely responsible for the relaxation of the Ca^{2+} transient. Thus, we concluded that increases in the HR affected SERCA activity and alternans occur when SERCA does not replenish the SR fully at higher HRs. Specifically, these conclusions can be explained by the following. 1) Tachycardia limits the time for SR Ca^{2+} refilling (refilling could also be limited by metabolic status). 2) Reduced SR Ca^{2+} load (regardless of cause) results in less Ca^{2+} -bound to intra SR Ca^{2+} binding proteins (i.e. calsequestrin (CSQ), an intra-SR Ca^{2+} binding protein). 3) Less diastolic in the SR Ca^{2+} deactivates SR Ca^{2+} release channels resulting in smaller SR Ca^{2+} release during the next beat. 4) Smaller release leaves a higher residual intra-SR Ca^{2+} level. 5) Subsequent SR refilling (on top of residual) results in higher SR Ca^{2+} load. 6) Higher SR diastolic Ca^{2+} enhances activation of SR release channels resulting in larger SR release during the next beat. 7) Larger release leaves lower intra-SR residual level and the cycle starts again.

This idea contradicts with the mechanism proposed by Wang et al.[164] They postulate that Ca^{2+} alternans are independent of the diastolic free Ca^{2+} concentration in the SR and propose that the time dependency recovery from inactivation of the RyR is the main cause of Ca^{2+} alternans. However, we did not directly measure SR Ca^{2+} content which is a better indicator of Ca^{2+} replenishment in the SR.

7.1 AP morphology and Ca^{2+} dynamics are different in the epicardium and endocardium

The ECG T-wave reflects the ventricular repolarization. More specifically, it reflects the electrical heterogeneity of repolarization across the ventricular wall. Therefore, the appearance of T-wave alternans indicated that the increased HR affected the repolarization dynamics in the tissue. Specifically, the duration of repolarization changed at higher HRs. Verrier et al. suggested that the HR amplifies the repolarization heterogeneity across the ventricular wall.[57]

In this thesis, we assessed the AP and Ca^{2+} transients across the ventricular wall. Although the left ventricular wall in the mouse heart is only 1mm thick, the different layers presented unique AP morphologies (Fig. 3.4) and Ca^{2+} dynamics (Fig. 3.7). Here, we saw that the epicardium presented shorter durations and faster kinetics in the AP and Ca^{2+} transients, respectively. For the AP, the primary difference was seen in phase 1, which is assessed by measuring the APD30. Our results agree with those presented by other researchers which showed the phase 1 differences between the epicardium and the endocardium.[20,29] They have attributed these phase 1 disparities to the underlying molecular heterogeneities in expression of proteins involve in the I_{to}. The epicardium has

a higher density of Kv. 4.3 responsible of potassium channels producing a larger I_{to} than the endocardium. Therefore, phase 1 is faster in the epicardium.

During the propagation of the electrical signal across the ventricular wall, the first structure being depolarized is the endocardium. Then, the action potential travels through the ventricular wall in an inward to outward fashion to finally depolarize the epicardium.[28] Fig. 3.4 showed this same pattern of action potential propagation where the endocardium had an earlier depolarization followed by the later depolarization of the epicardium. This delay in depolarization between the endocardium and epicardium was critical to identify which layer within the ventricular wall was the one optically recorded. Additionally, the Ca^{2+} transients also presented these same delays between the rise in intracellular Ca^{2+} of the endocardium and epicardium.

Interestingly, while the AP was primarily different in phase 1, the Ca^{2+} transients presented various kinetic differences between the epicardium and endocardium. The RT, TP, HD, and DT were all significantly different (Fig. 3.7). Overall, the time course of the endocardium transients was longer than those in the epicardium. These results from intact mice hearts are in agreement with *in silico* simulation studies conducted by Bondarenko and Rasmusson[165] and experiments on isolated canine cells[166] reported that the epicardium Ca^{2+} transients had faster rise and relaxation kinetics than the endocardium. These results were also similar to those obtained by Laurita et al. in canine hearts.[167]

The AP and intracellular Ca^{2+} dynamics are two cardiac variables that are highly interconnected. Thus, changes in Ca^{2+} can be reflected in the morphology of the AP, and vice versa. The ventricular wall presented important differences in the handling of intracellular Ca^{2+}. Consequently, the AP dissimilarities can be due to the underlying Ca^{2+} handling. Therefore, it was critical to understand the multiplicity of Ca^{2+} handling mechanisms in the heart to decipher electrical heterogeneities under physiological or pathological conditions such as T-wave alternans.

7.2 Molecular heterogeneities across the ventricular wall may underlie the differential regulation of Ca^{2+} dynamics in the epicardium and endocardium

In order to understand the kinetic differences of the recorded Ca^{2+} transients in the epicardium and endocardium, it was important to evaluate the underlying molecular differences. The molecular heterogeneities are the basis of the differential electrical properties throughout the organ,[168] and the ventricular wall is not exempt. Assessing the genetics was critical in unveiling molecular heterogeneities underlying the major differences we saw in the AP morphology and Ca^{2+} transient kinetics between the epicardium and endocardium.

We quantified the mRNA expression of the gene Kv4.3 responsible for the I_{to} current dominant in phase 1. In agreement with various researchers, there was a larger expression of the mRNA that codes for Kv4.3 in the epicardium in comparison with the endocardium.[21,22,29] This is the molecular reason behind the larger amplitude of I_{to} in this

layer. Aside from presenting evidence of the nonhomogeneous distribution of channels affecting phase 1, it was used as a control measurement for the other unknown genetic differences of the other proteins assessed in the two layers of the ventricular wall.

Additionally, in this thesis, we were able to specifically quantify the mRNA expression level of key proteins that are involved in the differential Ca^{2+} cycling in the epicardium and endocardium. The handling of intracellular Ca^{2+} is critical in the ability (or disability) of the ventricular wall to generate alternans. The idea was that if the Ca^{2+} is handled differently across the ventricular wall, this is a consequence of the differential expression of the key Ca^{2+} cycling proteins. Thus, we were able to characterize expression of genes coding for the RyR, SERCA, and PLN (Fig. 3.13). [94]

Unveiling the molecular distribution of the Ca^{2+} handling proteins allowed us to see that the slower kinetics of the endocardium (Fig. 3.7) correlated with the lower RyR and SERCA expression in this layer (Fig. 3.13). Although PLN did not change, the ratio of SERCA to PLN is larger for the endocardium, indicating a larger inhibition of the SERCA in this layer. This in turn affected and produced slower relaxation kinetics in the endocardium.

7.3 Mechanism of T-wave alternans based on HR

Together, the results in Chapter 3 point to the importance of the Ca^{2+} handling differences between the epicardium and endocardium. Since the Ca^{2+} is the source of the APD alternans, finally resulting in ECG T-wave alternans, then understanding Ca^{2+} handling is important in deciphering alternans. The endocardial layers is where Ca^{2+} alternans first develop. After assessing the differences in the Ca^{2+} dynamics across the wall, we saw that the Ca^{2+} transient has slower time course kinetics in the endocardium than the epicardium. Finally, the molecular components of this thesis allowed us to see that the primary difference between the epicardium and endocardium was the level of RyR and SERCA.

The consensus in the field is that the SR is the primary player in the genesis of alternans.[169] However, which component of the SR is not agreed upon. While some researchers have pointed to the importance of the RyR, others signal SERCA activity as the source of Ca^{2+} alternans leading to T-wave alternans. Here, we saw the RyR is less expressed in the endocardium, but also SERCA. However, when we placed the heart in conditions that increased the risk of generating alternans, we saw that the increasing HR affected the relaxation rather than the rise of intracellular Ca^{2+}. This points to an effect of HR on the relaxation kinetics, which is closely associated with the activity of the SERCA pump and not the release kinetics governed primarily by RyR activity. The endocardium has less SERCA and it also has more PLN for the SERCA present, resulting in greater fractional inhibition. Thus, we conclude that the SERCA is more inhibited in the endocardium and this contributes to the greater susceptibly of the endocardium in generating alternans.

Finally, increasing the HR compromises the activity of the SERCA to re-sequester Ca^{2+} into the SR. The SERCAs inability to replenish Ca^{2+} into the SR does not allow enough Ca^{2+} to be inside the SR for the next release. Thus, a large release is followed by a smaller one. Fortunately, the small SR Ca^{2+} content also causes the RyR to open less, inhibiting more releases and allowing Ca^{2+} content to increase and replenish the SR such that the next release is recovered (large release).

Cold temperatures predispose the tissue to generate Ca^{2+} alternans

Temperature affects many physiological processes including ECC and CICR in the heart. Hypothermia can cause the heart to go into cardiac arrest.[63–67] L-type Ca^{2+} channels,[69,70] the NCX,[34,71,72] and SERCA[45] are all temperature dependent. Consequently, alternans, which are caused by underlying Ca^{2+} handling, may be affected by temperature, as well. In Chapter 4, we simultaneously assessed the changes in the HR and temperature effects on the genesis of the Ca^{2+} alternans.

7.4 Ca^{2+} transient decay is primarily affected by changes in temperature

Global changes in the temperature affected the cycling of intracellular Ca^{2+} handling. Although the rise time was affected, as seen from the FLOM fluorescent images in Fig. 4.1, most of the effect occurred in the relaxation kinetics. These results were very similar to those obtained by Korneyeyev et al., which recorded Ca^{2+} transients at two different temperatures.[58] However, here we assessed the thermodynamic effects on the Ca^{2+} transient kinetics under several temperatures and computed the derivatives of the relaxation to quantify the changes. Like Korneyeyev et al.,[58] we saw that colder temperatures slowed the relaxation of the Ca^{2+} transients. Puglisi et al. also showed similar effects in the relaxation.[170]

Physiologically, our findings implicate that at colder temperatures, the cytosolic Ca^{2+} is elevated for a longer time. This agrees with findings from various researchers which have shown that colder temperatures result in an increase in force.[171,172] This effect is usually termed hypothermic inotropy.[41] Additionally, there is an increase in cytosolic Ca^{2+} due to the decrease in the NCX activity such that there is less Ca^{2+} extruded. Although we did not perform experiment in the APD, others have shown that the duration also increases with colder temperatures.[173] Assessing the thermodynamics of the relaxation, we calculated a Q_{10} of 1.6, a value similar to that of the ATP hydrolysis process. This led us to speculate that the effects over the relaxation produced by temperature was a result of the temperature inhibition on the SERCA pump, which requires ATP hydrolysis to function.

7.5 Cold temperatures affects Ca^{2+} alternans genesis

After seeing the effects of temperature over Ca^{2+} transients, we assessed the interplay between HR and temperature on the genesis of Ca^{2+} alternans. We imposed a temperature gradient and measured the spatial distribution of Ca^{2+} alternans. Under local

changes in temperature, regions that were colder produced alternans at lower frequencies than warmer regions (Fig. 4.5). At increasing HRs, the colder tissue was more susceptible for generating alternans. In other scenarios, despite being the same frequency, the cold tissue produced a greater degree of alternans than warmer regions.

The increase in Ca^{2+} alternans as a function of HR agrees with findings from Clusin et al.[174] Other researchers have shown that colder temperatures increase the genesis of APD and Ca^{2+} transient alternans.[173] Here, we were able to spatially map the degree of alternans as a function of tissue temperature (Fig. 4.6 and 4.7) for different frequencies. We saw that the temperature dependency of alternans was amplified at increasing frequencies. Calculating the Q_{10} allowed us to quantify the thermodynamics of the alternans dependency for the different frequencies. The Q_{10} at 5Hz was very similar to the energy produced by ATP hydrolysis, indicating that the pump was responsible for the temperature effect on alternans. However, at increasing frequencies, the Q_{10} increased. This indicated that the pump was not the only factor governing the development of the Ca^{2+} alternans. The contributing role of other proteins may be to blame at higher frequencies.[164,169] For example, the NCX is less active at colder temperatures[34,71,72] which can lead to a greater SR Ca^{2+} fill, creating a greater depletion and more alternans if the SERCA pump rate is limited by the cold temperature. It is possible that CICR amplifies the dependency of the alternans to temperature at higher frequencies.

7.6 Mechanism of T-wave alternans based on HR and Temperature

Together, the results in Chapter 3 and 4 outline the importance of the SR Ca^{2+} content in the genesis of the Ca^{2+} alternans.[175] Under situations in which the Ca^{2+} cycling kinetics are decreased, such as hypothermia, the tissue is more prone to develop alternans. The activity of the SERCA pump is decreased, resulting in slower relaxation kinetics. In addition, the NCX activity is inhibited at lower temperatures, resulting in an increase in cytosolic Ca^{2+}. Consequently, this increase in cytosolic Ca^{2+} results in an SR with a greater fill. When the SR is more full, the fraction of depletion will be greater. Therefore, a larger release will occur, but since the SERCA activity is compromised at colder temperatures, the next release will be even smaller due to a greater depletion.

Sympathetic nervous system activation eliminates alternans

The heart's activity is highly regulated by the ANS. However, one major limitation to the Langendorff set up is that the isolated hearts no longer have the ANS regulation. The action of catecholamines is the main mechanism by which the HR is elevated in the living animal. Since HR affects the genesis of alternans, we wanted to understand if sympathetic NS stimulation by acting over beta-adrenergic receptors would increase the HR without producing alternans. Additionally, sympathetic NS stimulation produces a cascade of events that ultimately affect the Ca^{2+} cycling at the myocyte level, thus we wanted to evaluate the role of the sympathetic NS on the genesis of alternans. In Chapter 5, we

assessed the effects of the sympathetic nervous system branch over the AP and Ca^{2+} dynamics and finally over the alternans across the ventricular wall.

7.7 The sympathetic NS increased phase 1 and 2 of the AP by changing Ca^{2+} dynamics across the ventricular wall

In order to understand the effect of restoring the sympathetic NS's activation cascade on the cardiac properties, we assessed the changes in the epicardium and endocardium AP and Ca^{2+} dynamics induced by beta-adrenergic stimulation. Figure 5.3 and 5.4 showed how the duration of the APD phase 1 became longer and the amplitude of phase 2 increased. However, the duration of phase 3 decreased agreeing with the faster cycle length effect produced by the "flight or flight" response.

The increase in duration of phase 1 correlated with the larger L-type Ca^{2+} currents under isoproterenol conditions (Fig. 5.9). These findings agree with previous experiments from our group in which we showed that Ca^{2+} that triggers CICR enters during phase 1.[31] The larger influx of Ca^{2+} through L-type Ca^{2+} channels is reflected in the amplitude of phase 2 increase, as well. The greater influx of Ca^{2+} into the cell may be affecting CICR to produce a larger release and thus increasing the intracellular Ca^{2+} transient during systole. Finally, this will influence the NCX activity inducing a larger depolarization during phase 2.

Across the ventricular wall, beta-adrenergic stimulation produced an increase in the amplitude of the Ca^{2+} transients (Fig. 5.5). The larger cytosolic Ca^{2+} content caused by larger release or greater influx through L-type Ca^{2+} channels helps to increase the activity of the NCX, affecting phase 2. Interestingly, the dynamics of the intracellular Ca^{2+} transients are not really affected. Although the final cascade of molecular events induced by beta-adrenergic stimulation is PKA activation and its stimulation over multiple key Ca^{2+} handling proteins, most of the effect seen here is on the decay kinetics (Fig. 5.7). These effects are primarily associated with the re-sequestering of Ca^{2+} into the SR mediated by SERCA.

7.8 Sympathetic NS stimulation eliminates alternans

Ca^{2+} mishandling is the underlying cause of APD and T-wave alternans (Blatter 2003, Clusin 2008, Rosenbaum 2001).[59,114,174] At the cellular level, the stimulation of beta-adrenergic receptors activates PKA, which phosphorylates multiple Ca^{2+} handling proteins. Thus, we assessed the APD and Ca^{2+} alternans under high HRs before and after beta-adrenergic stimulation. Figs. 5.11 to 5.13 show that the alternans are drastically reduced across the ventricular wall with beta-adrenergic stimulation. These results agree with those presented by Euler et al.[80] in canine and Florea and Blatter[82] in cat myocytes. However, others have published results in which blocking, and not stimulating, beta-adrenergic receptors actually helps reduce alternans. In the clinical setting, "pulsus alternans" are reduced by beta-blocker therapy.[176]

Although a consensus still needs to be reached, our results clearly showed that sympathetic NS stimulation affected the Ca^{2+} handling and was beneficial in reducing alternans. There is greater influx of Ca^{2+}, larger releases of Ca^{2+}, and improved SERCA activity to replenish the SR Ca^{2+} content. Together, all these effects enhanced Ca^{2+} cycling.

7.9 Mechanism of T-wave alternans based on sympathetic NS stimulation

The results in Chapter 5 outline the importance of Ca^{2+} mishandling in the genesis of Ca^{2+} alternans. The end result of the cascade of events after beta-adrenergic stimulation is PKA activation, which increases the open probability of the L-type Ca^{2+} channel and the RyR and relieves the inhibition on SERCA imposed by PLN. Sympathetic NS stimulation helps increase the cycling of Ca^{2+} at the myocyte level such that there is more Ca^{2+} entering the cell during phase 1 and consequently, a greater SR content, and after every release the SR is replenished better due to the uninhibited activity of the SERCA pump. In the mouse, the sympathetic NS can increase the HR without producing alternans by simultaneously enhancing the cycling of intracellular Ca^{2+}.

Parasympathetic nervous system activation does not affect Ca^{2+} handling directly

The regulation by the parasympathetic NS branch of the ANS is relatively unclear in the ventricular region (Coote 2013).[87] However, various studies have demonstrated the vast innervation of postganglionic parasympathetic NS neurons in the ventricles.[177–179] The parasympathetic NS exhibits important regulation over the sympathetic NS. At the cellular level, both branches interact at adenylyl cyclase (AC). The sympathetic NS activates while the parasympathetic NS inhibits the cascade of events produced by AC. We saw that the sympathetic NS, by beta-adrenergic stimulation, reduced the alternans. In this thesis, we also wanted to understand how the parasympathetic NS branch affected the regulation of key cardiac properties across the ventricular wall and whether it affected the genesis of alternans.

7.10 The parasympathetic NS is constitutively active in the isolated heart

The isolated hearts presented basal frequencies that were relatively slow (4Hz) in comparison to those in the mouse (10Hz). However, in Chapter 5, we saw that the sympathetic NS terminals were constitutively releasing neurotransmitters (Fig. 5.2). Despite this activity, the HR was low. The activity of the sympathetic NS is counteracted by the activity of the parasympathetic NS branch. Indeed, we found that the lower HR correlated with a possible constitutive release of ACh from the active parasympathetic NS neurons (Fig. 6.1). Coote[87] has described the innervation by postganglionic neurons of the parasympathetic NS. Here, we saw that these neurons are still active in the isolated heart and we conclude they are the reason why the HR is depressed.

7.11 The parasympathetic NS decreased phase 2 of the AP without changing Ca^{2+} dynamics across the ventricular wall

The isolated mouse heart in the Langendorff set up has a vagal tone and this may affect other properties in the heart. Therefore, we wanted to understand how vagal stimulation by M2 receptor activation affects various cardiac properties across the ventricular wall. We saw that the AP was shortened by perfusion of an M2 agonist (Fig. 6.3). Phase 2 and 3 repolarized faster across the ventricular wall. These results were different than those by Calloe et al.[154] which showed a significant shortening of atrial cells, but not ventricular cells after ACh. Although Calloe et al.[154] saw it as insignificant, they still observed shortening of the ventricles after ACh similar to our findings. In addition, we saw this shortening occur within one minute of perfusion with the M2 agonist and desensitize rapidly which makes it difficult to record.

Effects over the dome are usually linked to changes in the intracellular Ca^{2+} handling and the consequent effect over the NCX activity. However, when we assessed changes in the intracellular Ca^{2+} transients, we saw no changes in the kinetics (Fig. 6.6 and 6.7). Levy and Zieske[180] have shown this same interaction where the vagal stimulation does not affect Ca^{2+} dynamics unless sympathetic NS is active. The "accentuated antagonism" refers to the parasympathetic NS branch's ability to show a greater effect under sympathetic NS activity. Therefore, in the absence of a sympathetic NS stimulation, the parasympathetic NS did not affect the Ca^{2+} cycling of the isolated heart.

Since the isolated mouse heart has a vagal tone, then the sympathetic NS branch has limited effects, despite having local releases of norepinephrine. This means that the AC and its cascade of events affecting key Ca^{2+} handling proteins is not on. When we stimulated the M2 pathway, the parasympathetic NS was inhibiting a cascade of events that was not on. Therefore, we did not see changes in the Ca^{2+} dynamics. In addition, to verify this concept, we assessed ionic current changes through the L-type Ca^{2+} channels, one of the targets of PKA activity. If PKA activity is on and we turn it off by M2 stimulation, then we should have seen a reduction in the current through the L-type Ca^{2+} channel. However, Fig. 6.9 and 6.10 both show no changes in the Ca^{2+} currents indicating that PKA activity was off and its inhibition resulted in an absence of response.

Interestingly, if the Ca^{2+} dynamics were not the underlying cause of the changes in the repolarization induced by parasympathetic NS stimulation via M2 activation, we evaluated the role of another pathway involving an ACh-sensitive K^+ current (I_{KACh}). M2 stimulation inhibits AC by the dissociation of the Gα-subunit from the G_i protein. However, the G_i also dissociates into a $G_{\beta\gamma}$-subunit which is known to affect a K^+ channel.[181] When we blocked I_{KACh}, the faster repolarization effect induced by M2 stimulation was no longer seen (Fig. 6.5) indicating that the faster APD was due to a K^+ current. In line with these results, experiments conducted on the atrium have shown this same faster repolarization with parasympathetic NS stimulation and can be reversed with I_{KACh} blockade .[182]

This muscarinic effect has been highly studied because of its relation to atrial fibrillation induced by the parasympathetic branch and has been proposed as a possible inhibitor.[183,184] However, the effect over the ventricular region has not been seen[154] and this is mostly due to lower innervation of the ventricular region by parasympathetic NS and lower density of the channels responsible for I_{KACh}.[185] Nonetheless, the experiments presented in this thesis are based on intact hearts and not isolated cells which have lost all the coupling. The intact heart allows cells to be electrically coupled and since I_{KACh} affects the membrane potential, the effect may be more dramatic than in isolated cells by globally affecting the electrotone of the organ.

7.12 Parasympathetic NS stimulation reduced alternans by changing membrane potential

Despite our findings that the parasympathetic NS activity by M2 stimulation does not affect Ca^{2+} cycling in the absence of sympathetic NS stimulation, it reduced the APD alternans. These results were very interesting since alternans are due to Ca^{2+} mishandling. However, the primary effect of M2 stimulation was to increase the repolarization of the AP by changing a K^+ conductance, which affects the membrane potential. Consequently, the changes in the membrane potential indirectly affect the Ca^{2+} dynamics by altering the activity of the NCX. Specifically, I_{KACh} shortened the duration of the AP and repolarized the membrane faster which may cause the activity of the NCX to increase due to larger driving force for influx of Na^+ ions. As the NCX brings in more Na^+, it will decrease the cytosolic Ca^{2+} and also the SR Ca^{2+} content such that after every release, the SERCA is able to replenish the small depletions. Aside from the changes in the membrane potential, the parasympathetic NS is also likely to reduce alternans by decreasing the HR. This agrees with Ng et al.[186] who saw vagal stimulation decreased the ranges of HRs in which alternans occurred. We saw in Chapter 3 and 4 that lower HRs are less prone to develop alternans.

Disadvantages and Limitations:

In trying to understand the molecular causes of the pro-arrhythmic T-wave, we evaluated various cardiac properties in the epicardium and endocardium of the ventricular wall. However, the ventricular wall, where T-wave alternans manifest, has three distinct layers, not two. One of the major limitations of the work presented in this thesis was that we speculated the molecular cause of T-wave alternans by focusing on only the epicardium and endocardium. The midmyocardium is in between the epicardium and endocardium. Nonetheless, most experiments conducted on the midmyocardium have found it to have characteristics in between the epicardium and endocardium.[20,149] However, the experiments presented here are more physiological than those studying the midmyocardium because we used the intact heart and not a wedge.

The intact hearts were obtained from mice. When attempting to extrapolate findings in animal models to humans, it can prove disadvantageous. However, mice are a good model for assessing molecular mechanisms of the heart. The hearts are small and very practical to use in the Langendorff set-up. Also, loading the heart with the dyes is more cost-efficient such that the whole organ may be used to measure cardiac properties. This allows us to obtain recordings where the cells are metabolically, electrically, and mechanically coupled.

Another limitation of the experiments presented here deals with the intrinsic disadvantages of using fluorescent indicators. The AP recordings taken using di-8-ANEPPS can be calibrated with the electrically obtained AP via the microelectrode. However, the Ca^{2+} transient has no calibration method. The kinetics of the transients are associated with the fluorescent properties of the dye. If we had used other dyes, the transient would have looked different based on the dissociation properties. Additionally, the exact concentration of intracellular Ca^{2+} cannot be specified. Here, we are only able to quantify cumulative effects over the Ca^{2+} transient kinetics. Thus, we are unable to quantify if there is a larger concentration of intracellular Ca^{2+} in the epicardium relative to the endocardium which may affect the cycling.

Finally, one of the major conclusions of this project was the importance of the SR Ca^{2+} content in the genesis of Ca^{2+} alternans. However, the Ca^{2+} in the SR is not all free. It is bound to a protein, calsequestrin (CSQ). CSQ may play a critical role in the large and small releases that define Ca^{2+} alternans. The temperature dependence of this protein and others indirectly involved in CICR and ECC could be affecting the genesis of alternans. In addition, we speculated that one of the key indicators of Ca^{2+} alternans was the SR Ca^{2+} content. However, this thesis does not present direct measurements of SR Ca^{2+} which we have accomplished with a different dye, Mag-Fluo-4 (data not shown).

CONCLUSION:

The central goal of this thesis was to evaluate the molecular mechanisms leading to T-wave alternans. We assessed the effects on the two cardiac properties (electrical and Ca^{2+} dynamics) under conditions that may affect alternans including: HR, temperature, and ANS regulation. Our findings suggest that the risk for alternans rises with increasing HR, colder temperatures, and lack of sympathetic NS stimulation. The tissue is less prone to alternating at lower frequencies, warmer temperatures (within physiological ranges), and stimulation by the sympathetic NS (at a constant HR). The results presented in this thesis provide substantial evidence to support our hypothesis: **insufficient Ca^{2+} uptake by the sarcoplasmic reticulum during increased HRs, hypothermia, or autonomic nervous system dysfunction produces Ca^{2+} alternans. Ca^{2+} alternans produce beat-to-beat alterations in the AP repolarization leading to T-wave alternans.**

T-wave alternans manifest in the ventricular wall, therefore, we assessed effects of HR and ANS stimulation over the AP and Ca^{2+} dynamics in the outer and innermost regions of the ventricular wall. We found that the endocardium alternated sooner than the epicardium. This could suggest that the cells in the endocardium are not as efficient in cycling intracellular Ca^{2+} (re-sequestering) in comparison to the epicardium. Thus, the endocardium may be more at faults for the genesis of T-wave alternans. Nonetheless, the sympathetic NS stimulation of beta-adrenergic receptors eliminated alternans in both regions.

The major conclusion from this thesis is that Ca^{2+} alternans are produced primarily by the interplay between Ca^{2+} in the SR, Ca^{2+} in the cytosol, and the rate by which these two regions change $[Ca^{2+}]$. Under conditions in which the HR is changing rapidly, the rate at which the SERCA fills the SR is insufficient in maintaining Ca^{2+} levels after every release. Thus, there is a large SR release followed by a small release due to the lack of refilling by the slow SERCA pump rate at high HRs.

Under hypothermic conditions, the re-sequestering rate of the SERCA pump is compromised even at lower frequencies producing alternans. In addition, hypothermia affects other key Ca^{2+} handling proteins that change $[Ca^{2+}]$ in the cytosol. The NCX activity is decreased at low temperatures, which contributes to a larger cytosolic $[Ca^{2+}]$. Consequently, the SR is able to fill with more Ca^{2+} and produces a larger release (Ca^{2+} transient with high amplitude). Since the release is larger, the next release will be even smaller (Ca^{2+} transient with low amplitude) because the rate of the SERCA pump is unable to compensate for the greater depletion. However, the "third" Ca^{2+} transient, or the repetition of the first Ca^{2+} transient, can recover to a high amplitude. This recovery is due to the RyR's open probability decreasing when the SR is depleted such that it is able to fill once again and produce a larger Ca^{2+} release.

Finally, the two branches of the ANS help reduce alternans by two different mechanisms. The sympathetic NS increases the cycling of intracellular Ca^{2+} allowing more Ca^{2+} to enter the cell via the L-type Ca^{2+} channel producing greater releases. SERCA is

able to compensate for the large releases because the cascade of beta-adrenergic stimulation releases the inhibition of the SERCA pump allowing it to re-fill the SR more efficiently. The parasympathetic NS affects the repolarization kinetics of the membrane potential (I_{KACh}), which increases the driving force for Na^+ influx via the NCX. We speculate that the faster NCX activity causes less [Ca^{2+}] in the cytosol, producing less filling of the SR such that the releases are not large. Since the depletions are not large, the SERCA activity is sufficient to replenish the SR Ca^{2+} content, thus reducing alternans.

REFERENCES:

1. European Heart Rhythm Association *et al.* ACC/AHA/ESC 2006 guidelines for management of patients with ventricular arrhythmias and the prevention of sudden cardiac death: a report of the American College of Cardiology/American Heart Association Task Force and the European Society of Cardiology Committee for Practice Guidelines (Writing Committee to Develop Guidelines for Management of Patients With Ventricular Arrhythmias and the Prevention of Sudden Cardiac Death). *J. Am. Coll. Cardiol.* **48,** e247-346 (2006).

2. WRITING GROUP MEMBERS *et al.* Heart disease and stroke statistics--2010 update: a report from the American Heart Association. *Circulation* **121,** e46–e215 (2010).

3. Clapham, D. E. & Kim, D. G protein activation mechanisms of the cardiac K+ channel, iK.ACh. *Soc. Gen. Physiol. Ser.* **44,** 55–68 (1989).

4. Breitwieser, G. E. & Szabo, G. Mechanism of muscarinic receptor-induced K+ channel activation as revealed by hydrolysis-resistant GTP analogues. *J. Gen. Physiol.* **91,** 469–493 (1988).

5. Kurachi, Y., Ito, H., Sugimoto, T., Katada, T. & Ui, M. Activation of atrial muscarinic K+ channels by low concentrations of beta gamma subunits of rat brain G protein. *Pflüg. Arch. Eur. J. Physiol.* **413,** 325–327 (1989).

6. Bolter, C. P. & English, D. J. The effects of tertiapin-Q on responses of the sinoatrial pacemaker of the guinea-pig heart to vagal nerve stimulation and muscarinic agonists. *Exp. Physiol.* **93,** 53–63 (2008).

7. Whitteridge, G. William Harvey on the circulation of the blood and on generation. *Am. J. Med.* **65,** 888–890 (1978).

8. Da Vinci, Leonardo. Heart of an ox. (1907v).

9. Jones, R. Leonardo da Vinci: anatomist. *Br. J. Gen. Pract.* **62,** 319–319 (2012).

10. Hamilton, S. *Animal Welfare & Anti-vivisection 1870-1910: Frances Power Cobbe*. (Taylor & Francis, 2004).

11. Duke, W. W. THE RATE OF REGENERATION OF BLOOD PLATELETS. *J. Exp. Med.* **14,** 265–273 (1911).

12. Hall, W. S. & Eubank, M. D. THE REGENERATION OF THE BLOOD. *J. Exp. Med.* **1,** 656–676 (1896).

13. Gensini, G. F., Conti, A. A., Lippi, D. & Conti, A. [The historical bases of a super-specialty: electrocardiography]. *Med. Secoli* **16,** 595–602 (2004).

14. de Micheli, A. [On the first studies of electrophysiology]. *Arch. Cardiol. Mex.* **81,** 337–342 (2011).

15. Eranti, A. *et al.* 12-Lead electrocardiogram as a predictor of sudden cardiac death: from epidemiology to clinical practice. *Scand. Cardiovasc. J. SCJ* **50,** 253–259 (2016).

16. Priori, S. G. & Blomström-Lundqvist, C. 2015 European Society of Cardiology Guidelines for the management of patients with ventricular arrhythmias and the prevention of sudden cardiac death summarized by co-chairs. *Eur. Heart J.* **36,** 2757–2759 (2015).

17. Anttonen, O., Väänänen, H., Junttila, J., Huikuri, H. V. & Viitasalo, M. Electrocardiographic transmural dispersion of repolarization in patients with inherited short QT syndrome. *Ann. Noninvasive Electrocardiol. Off. J. Int. Soc. Holter Noninvasive Electrocardiol. Inc* **13,** 295–300 (2008).

18. Brugada, P. & Brugada, J. Right bundle branch block, persistent ST segment elevation and sudden cardiac death: a distinct clinical and electrocardiographic syndrome. A multicenter report. *J. Am. Coll. Cardiol.* **20,** 1391–1396 (1992).

19. DiFrancesco, D. The role of the funny current in pacemaker activity. *Circ. Res.* **106,** 434–446 (2010).

20. Sicouri, S. & Antzelevitch, C. A subpopulation of cells with unique electrophysiological properties in the deep subepicardium of the canine ventricle. The M cell. *Circ. Res.* **68,** 1729–1741 (1991).

21. Sicouri, S. & Antzelevitch, C. Afterdepolarizations and triggered activity develop in a select population of cells (M cells) in canine ventricular myocardium: the effects of acetylstrophanthidin and Bay K 8644. *Pacing Clin. Electrophysiol. PACE* **14,** 1714–1720 (1991).

22. Antzelevitch, C. *et al.* Heterogeneity within the ventricular wall. Electrophysiology and pharmacology of epicardial, endocardial, and M cells. *Circ. Res.* **69,** 1427–1449 (1991).

23. Bezanilla, F. The Nerve Impulse. (1998). Available at: http://nerve.bsd.uchicago.edu/med98a.htm. (Accessed: 16th May 2016)

24. Nattel, S. & Carlsson, L. Innovative approaches to anti-arrhythmic drug therapy. *Nat. Rev. Drug Discov.* **5,** 1034–1049 (2006).

25. Grant, A. O. Cardiac ion channels. *Circ. Arrhythm. Electrophysiol.* **2,** 185–194 (2009).

26. Opie, L. H. *The heart: physiology, from cell to circulation*. (Lippincott-Raven, 1998).

27. Guo, W., Xu, H., London, B. & Nerbonne, J. M. Molecular basis of transient outward K+ current diversity in mouse ventricular myocytes. *J. Physiol.* **521 Pt 3,** 587–599 (1999).

28. Nerbonne, J. M. & Kass, R. S. Molecular physiology of cardiac repolarization. *Physiol. Rev.* **85,** 1205–1253 (2005).

29. Litovsky, S. H. & Antzelevitch, C. Transient outward current prominent in canine ventricular epicardium but not endocardium. *Circ. Res.* **62,** 116–126 (1988).

30. London, B., Wang, D. W., Hill, J. A. & Bennett, P. B. The transient outward current in mice lacking the potassium channel gene Kv1.4. *J. Physiol.* **509 (Pt 1),** 171–182 (1998).

31. Ramos-Franco, J., Aguilar-Sanchez, Y. & Escobar, A. L. Intact Heart Loose Patch Photolysis Reveals Ionic Current Kinetics During Ventricular Action Potentials. *Circ. Res.* **118,** 203–215 (2016).

32. Beeler, G. W. & Reuter, H. The relation between membrane potential, membrane currents and activation of contraction in ventricular myocardial fibres. *J. Physiol.* **207,** 211–229 (1970).

33. Reuter, H. The dependence of slow inward current in Purkinje fibres on the extracellular calcium-concentration. *J. Physiol.* **192,** 479–492 (1967).

34. Ferreiro, M., Petrosky, A. D. & Escobar, A. L. Intracellular Ca2+ release underlies the development of phase 2 in mouse ventricular action potentials. *Am. J. Physiol. Heart Circ. Physiol.* **302,** H1160-1172 (2012).

35. Santana, L. F., Gómez, A. M., Kranias, E. G. & Lederer, W. J. Amount of calcium in the sarcoplasmic reticulum: influence on excitation-contraction coupling in heart muscle. *Heart Vessels* **Suppl 12,** 44–49 (1997).

36. Banyasz, T., Horvath, B., Jian, Z., Izu, L. T. & Chen-Izu, Y. Profile of L-type Ca(2+) current and Na(+)/Ca(2+) exchange current during cardiac action potential

in ventricular myocytes. *Heart Rhythm Off. J. Heart Rhythm Soc.* **9,** 134–142 (2012).

37. Fabiato, A. & Fabiato, F. Contractions induced by a calcium-triggered release of calcium from the sarcoplasmic reticulum of single skinned cardiac cells. *J. Physiol.* **249,** 469–495 (1975).

38. Fabiato, A. Calcium release in skinned cardiac cells: variations with species, tissues, and development. *Fed. Proc.* **41,** 2238–2244 (1982).

39. Niggli, E. & Lederer, W. J. Voltage-independent calcium release in heart muscle. *Science* **250,** 565–568 (1990).

40. Bers, D. M. Cardiac excitation-contraction coupling. *Nature* **415,** 198–205 (2002).
41. Bers, D. M. *Excitation-contraction coupling and cardiac contractile force*. (Kluwer, 2001).

42. Näbauer, M., Callewaert, G., Cleemann, L. & Morad, M. Regulation of calcium release is gated by calcium current, not gating charge, in cardiac myocytes. *Science* **244,** 800–803 (1989).

43. Shannon, T. R. & Bers, D. M. Assessment of intra-SR free [Ca] and buffering in rat heart. *Biophys. J.* **73,** 1524–1531 (1997).

44. Tada, M., Kirchberger, M. A., Repke, D. I. & Katz, A. M. The stimulation of calcium transport in cardiac sarcoplasmic reticulum by adenosine 3':5'-monophosphate-dependent protein kinase. *J. Biol. Chem.* **249,** 6174–6180 (1974).

45. Shigekawa, M., Finegan, J. A. & Katz, A. M. Calcium transport ATPase of canine cardiac sarcoplasmic reticulum. A comparison with that of rabbit fast skeletal muscle sarcoplasmic reticulum. *J. Biol. Chem.* **251,** 6894–6900 (1976).

46. Litovsky, S. H. & Antzelevitch, C. Rate dependence of action potential duration and refractoriness in canine ventricular endocardium differs from that of epicardium: role of the transient outward current. *J. Am. Coll. Cardiol.* **14,** 1053–1066 (1989).

47. Cutler, M. J. & Rosenbaum, D. S. Risk stratification for sudden cardiac death: is there a clinical role for T wave alternans? *Heart Rhythm Off. J. Heart Rhythm Soc.* **6,** S56-61 (2009).

48. Abdelghani, S. A., Rosenthal, T. M. & Morin, D. P. Surface Electrocardiogram Predictors of Sudden Cardiac Arrest. *Ochsner J.* **16,** 280–289 (2016).

49. Stein, P. K., Sanghavi, D., Sotoodehnia, N., Siscovick, D. S. & Gottdiener, J. Association of Holter-based measures including T-wave alternans with risk of sudden cardiac death in the community-dwelling elderly: the Cardiovascular Health Study. *J. Electrocardiol.* **43,** 251–259 (2010).

50. Ikeda, T. *et al.* T-wave alternans as a predictor for sudden cardiac death after myocardial infarction. *Am. J. Cardiol.* **89,** 79–82 (2002).

51. Gold, M. R. *et al.* A comparison of T-wave alternans, signal averaged electrocardiography and programmed ventricular stimulation for arrhythmia risk stratification. *J. Am. Coll. Cardiol.* **36,** 2247–2253 (2000).

52. Rosenbaum, D. S. *et al.* Electrical alternans and vulnerability to ventricular arrhythmias. *N. Engl. J. Med.* **330,** 235–241 (1994).

53. Narayan, S. M. T-wave alternans and the susceptibility to ventricular arrhythmias. *J. Am. Coll. Cardiol.* **47,** 269–281 (2006).

54. Qu, Z., Xie, Y., Garfinkel, A. & Weiss, J. N. T-wave alternans and arrhythmogenesis in cardiac diseases. *Front. Physiol.* **1,** 154 (2010).

55. Zile, M. A. & Trayanova, N. A. Rate-dependent force, intracellular calcium, and action potential voltage alternans are modulated by sarcomere length and heart failure induced-remodeling of thin filament regulation in human heart failure: A myocyte modeling study. *Prog. Biophys. Mol. Biol.* **120,** 270–280 (2016).

56. Bayer, J. D., Narayan, S. M., Lalani, G. G. & Trayanova, N. A. Rate-dependent action potential alternans in human heart failure implicates abnormal intracellular calcium handling. *Heart Rhythm Off. J. Heart Rhythm Soc.* **7,** 1093–1101 (2010).

57. Verrier, R. L. *et al.* Combined actions of ivabradine and ranolazine reduce ventricular rate during atrial fibrillation. *J. Cardiovasc. Electrophysiol.* **26,** 329–335 (2015).

58. Kornyeyev, D., Reyes, M. & Escobar, A. L. Luminal Ca(2+) content regulates intracellular Ca(2+) release in subepicardial myocytes of intact beating mouse hearts: effect of exogenous buffers. *Am. J. Physiol. Heart Circ. Physiol.* **298,** H2138-2153 (2010).

59. Blatter, L. A. *et al.* Local calcium gradients during excitation-contraction coupling and alternans in atrial myocytes. *J. Physiol.* **546,** 19–31 (2003).

60. Walker, M. L., Wan, X., Kirsch, G. E. & Rosenbaum, D. S. Hysteresis effect implicates calcium cycling as a mechanism of repolarization alternans. *Circulation* **108,** 2704–2709 (2003).

61. Sipido, K. R. Understanding cardiac alternans: the answer lies in the Ca2+ store. *Circ. Res.* **94,** 570–572 (2004).

62. Lab, M. J. & Lee, J. A. Changes in intracellular calcium during mechanical alternans in isolated ferret ventricular muscle. *Circ. Res.* **66,** 585–595 (1990).

63. Smith, J. M., Clancy, E. A., Valeri, C. R., Ruskin, J. N. & Cohen, R. J. Electrical alternans and cardiac electrical instability. *Circulation* **77,** 110–121 (1988).

64. Furukawa, Y., Kobayashi, M. & Chiba, S. Cardiac arrest and reactivation by changes of temperature in the isolated, blood-perfused canine heart. *Jpn. Heart J.* **21,** 837–844 (1980).

65. Badeer, H. Ventricular fibrillation in hypothermia; a review of factors favoring fibrillation in hypothermia with and without cardiac surgery. *J. Thorac. Surg.* **35,** 265–273 (1958).

66. Mouritzen, C. V. & Andersen, M. N. Mechanisms of ventricular fibrillation during hypothermia. Relative changes in myocardial refractory period and conduction velocity. *J. Thorac. Cardiovasc. Surg.* **51,** 585–589 (1966).

67. Adam, D. R. *et al.* Fluctuations in T-wave morphology and susceptibility to ventricular fibrillation. *J. Electrocardiol.* **17,** 209–218 (1984).

68. Kurihara, S. & Sakai, T. Effects of rapid cooling on mechanical and electrical responses in ventricular muscle of guinea-pig. *J. Physiol.* **361,** 361–378 (1985).

69. Kohlhardt, M. [Transmembrane inward currents during excitation of the heart (author's transl)]. *Klin. Wochenschr.* **53,** 1089–1099 (1975).

70. Klöckner, U., Schiefer, A. & Isenberg, G. L-type Ca-channels: similar Q10 of Ca-, Ba- and Na-conductance points to the importance of ion-channel interaction. *Pflugers Arch.* **415,** 638–641 (1990).

71. Bersohn, M. M., Vemuri, R., Schuil, D. W., Weiss, R. S. & Philipson, K. D. Effect of temperature on sodium-calcium exchange in sarcolemma from mammalian and amphibian hearts. *Biochim. Biophys. Acta* **1062,** 19–23 (1991).

72. Blaustein, M. P. & Lederer, W. J. Sodium/calcium exchange: its physiological implications. *Physiol. Rev.* **79,** 763–854 (1999).

73. Berg, J. M., Tymoczko, J. L. & Stryer, L. *Biochemistry, 6th Edition*. (W. H. Freeman, 2006).

74. Brum, G., Osterrieder, W. & Trautwein, W. Beta-adrenergic increase in the calcium conductance of cardiac myocytes studied with the patch clamp. *Pflüg. Arch. Eur. J. Physiol.* **401,** 111–118 (1984).

75. Huke, S. & Bers, D. M. Ryanodine receptor phosphorylation at Serine 2030, 2808 and 2814 in rat cardiomyocytes. *Biochem. Biophys. Res. Commun.* **376,** 80–85 (2008).

76. Xiao, B. *et al.* Isoform-dependent formation of heteromeric Ca2+ release channels (ryanodine receptors). *J. Biol. Chem.* **277,** 41778–41785 (2002).

77. Marks, A. R. Novel therapy for heart failure and exercise-induced ventricular tachycardia based on 'fixing' the leak in ryanodine receptors. *Novartis Found. Symp.* **274,** 132-147-155, 272–276 (2006).

78. Liao, Z., Lockhead, D., Larson, E. D. & Proenza, C. Phosphorylation and modulation of hyperpolarization-activated HCN4 channels by protein kinase A in the mouse sinoatrial node. *J. Gen. Physiol.* **136,** 247–258 (2010).

79. Noma, A., Kotake, H. & Irisawa, H. Slow inward current and its role mediating the chronotropic effect of epinephrine in the rabbit sinoatrial node. *Pflugers Arch.* **388,** 1–9 (1980).

80. Euler, D. E., Guo, H. & Olshansky, B. Sympathetic influences on electrical and mechanical alternans in the canine heart. *Cardiovasc. Res.* **32,** 854–860 (1996).

81. Hüser, J. *et al.* Functional coupling between glycolysis and excitation-contraction coupling underlies alternans in cat heart cells. *J. Physiol.* **524 Pt 3,** 795–806 (2000).

82. Florea, S. M. & Blatter, L. A. Regulation of cardiac alternans by β-adrenergic signaling pathways. *Am. J. Physiol. Heart Circ. Physiol.* **303,** H1047-1056 (2012).

83. Paterson, D. J., Rogers, J., Powell, T. & Brown, H. F. Effect of catecholamines on the ventricular myocyte action potential in raised extracellular potassium. *Acta Physiol. Scand.* **148,** 177–186 (1993).

84. Callewaert, G., Cleemann, L. & Morad, M. Epinephrine enhances Ca2+ current-regulated Ca2+ release and Ca2+ reuptake in rat ventricular myocytes. *Proc. Natl. Acad. Sci. U. S. A.* **85,** 2009–2013 (1988).

85. Harvey, R. D. Muscarinic receptor agonists and antagonists: effects on cardiovascular function. *Handb. Exp. Pharmacol.* 299–316 (2012). doi:10.1007/978-3-642-23274-9_13

86. Clapham, D. E. & Kim, D. G protein activation mechanisms of the cardiac K+ channel, iK.ACh. *Soc. Gen. Physiol. Ser.* **44,** 55–68 (1989).

87. Coote, J. H. Myths and realities of the cardiac vagus. *J. Physiol.* **591,** 4073–4085 (2013).

88. *Neural regulation of the heart*. (Oxford University Press, 1977).

89. Shimizu, W. & Antzelevitch, C. Cellular and ionic basis for T-wave alternans under long-QT conditions. *Circulation* **99,** 1499–1507 (1999).

90. Mitra, R. & Morad, M. A uniform enzymatic method for dissociation of myocytes from hearts and stomachs of vertebrates. *Am. J. Physiol.* **249,** H1056-1060 (1985).

91. Severs, N. J. Gap junction alterations in the failing heart. *Eur. Heart J.* **15 Suppl D,** 53–57 (1994).

92. Escobar, A. L. *et al.* Developmental changes of intracellular Ca2+ transients in beating rat hearts. *Am. J. Physiol. Heart Circ. Physiol.* **286,** H971-978 (2004).

93. Beyer, E. C., Davis, L. M., Saffitz, J. E. & Veenstra, R. D. Cardiac intercellular communication: consequences of connexin distribution and diversity. *Braz. J. Med. Biol. Res. Rev. Bras. Pesqui. Medicas E Biol.* **28,** 415–425 (1995).

94. Mattiazzi, A., Argenziano, M., Aguilar-Sanchez, Y., Mazzocchi, G. & Escobar, A. L. Ca2+ Sparks and Ca2+ waves are the subcellular events underlying Ca2+ overload during ischemia and reperfusion in perfused intact hearts. *J. Mol. Cell. Cardiol.* **79,** 69–78 (2015).

95. Mejía-Alvarez, R. *et al.* Pulsed local-field fluorescence microscopy: a new approach for measuring cellular signals in the beating heart. *Pflugers Arch.* **445,** 747–758 (2003).

96. Kornyeyev, D. *et al.* Calsequestrin 2 deletion shortens the refractoriness of Ca^{2+} release and reduces rate-dependent Ca^{2+}-alternans in intact mouse hearts. *J. Mol. Cell. Cardiol.* **52,** 21–31 (2012).

97. Valverde, C. A. *et al.* Transient Ca2+ depletion of the sarcoplasmic reticulum at the onset of reperfusion. *Cardiovasc. Res.* **85,** 671–680 (2010).

98. Furukawa, T., Myerburg, R. J., Furukawa, N., Bassett, A. L. & Kimura, S. Differences in transient outward currents of feline endocardial and epicardial myocytes. *Circ. Res.* **67,** 1287–1291 (1990).

99. Tande, P. M., Mortensen, E. & Refsum, H. Rate-dependent differences in dog epi- and endocardial monophasic action potential configuration in vivo. *Am. J. Physiol.* **261,** H1387-1391 (1991).

100. Taylor, D. G., Parilak, L. D., LeWinter, M. M. & Knot, H. J. Quantification of the rat left ventricle force and Ca2+ -frequency relationships: similarities to dog and human. *Cardiovasc. Res.* **61,** 77–86 (2004).

101. Wettwer, E., Amos, G. J., Posival, H. & Ravens, U. Transient outward current in human ventricular myocytes of subepicardial and subendocardial origin. *Circ. Res.* **75,** 473–482 (1994).

102. Malo, M. E. & Fliegel, L. Physiological role and regulation of the Na+/H+ exchanger. *Can. J. Physiol. Pharmacol.* **84,** 1081–1095 (2006).

103. Javadov, S. *et al.* NHE-1 inhibition-induced cardioprotection against ischaemia/reperfusion is associated with attenuation of the mitochondrial permeability transition. *Cardiovasc. Res.* **77,** 416–424 (2008).

104. Di Lisa, F. A female way to protect the heart: say NO to calcium. *Circ. Res.* **98,** 298–300 (2006).

105. Ferdinandy, P., Schulz, R. & Baxter, G. F. Interaction of cardiovascular risk factors with myocardial ischemia/reperfusion injury, preconditioning, and postconditioning. *Pharmacol. Rev.* **59,** 418–458 (2007).

106. Halestrap, A. P. & Richardson, A. P. The mitochondrial permeability transition: a current perspective on its identity and role in ischaemia/reperfusion injury. *J. Mol. Cell. Cardiol.* **78,** 129–141 (2015).

107. Di Lisa, F., Schulz, R. & Murphy, E. Preface to mitochondria and cardioprotection. *Biochim. Biophys. Acta* **1813,** 1261–1262 (2011).

108. Olejnickova, V., Novakova, M. & Provaznik, I. Isolated heart models: cardiovascular system studies and technological advances. *Med. Biol. Eng. Comput.* **53,** 669–678 (2015).

109. Zimmer, H.-G. The Isolated Perfused Heart and Its Pioneers. *News Physiol. Sci. Int. J. Physiol. Prod. Jointly Int. Union Physiol. Sci. Am. Physiol. Soc.* **13,** 203–210 (1998).

110. Dou, Y., Arlock, P. & Arner, A. Blebbistatin specifically inhibits actin-myosin interaction in mouse cardiac muscle. *Am. J. Physiol. Cell Physiol.* **293,** C1148-1153 (2007).

111. Farman, G. P. *et al.* Blebbistatin: use as inhibitor of muscle contraction. *Pflugers Arch.* **455,** 995–1005 (2008).

112. Fedorov, V. V. *et al.* Application of blebbistatin as an excitation-contraction uncoupler for electrophysiologic study of rat and rabbit hearts. *Heart Rhythm Off. J. Heart Rhythm Soc.* **4,** 619–626 (2007).

113. Molecular Probes Handbook: A Guide to Fluorescent Probes and Labeling Technologies, 11th Edition [Hardcover]. Available at: http://www.thermofisher.com/order/catalog/product/H37126. (Accessed: 2nd December 2016)

114. Rosenbaum, D. S. & Jalife, J. *Optical mapping of cardiac excitation and arrhythmias*. (Futura, 2001).

115. Ringer, S. A further Contribution regarding the influence of the different Constituents of the Blood on the Contraction of the Heart. *J. Physiol.* **4,** 29–42.3 (1883).

116. Fabiato, A. Calcium-induced release of calcium from the cardiac sarcoplasmic reticulum. *Am. J. Physiol.* **245,** C1-14 (1983).

117. Fabiato, A. Time and calcium dependence of activation and inactivation of calcium-induced release of calcium from the sarcoplasmic reticulum of a skinned canine cardiac Purkinje cell. *J. Gen. Physiol.* **85,** 247–289 (1985).

118. Minta, A., Kao, J. P. & Tsien, R. Y. Fluorescent indicators for cytosolic calcium based on rhodamine and fluorescein chromophores. *J. Biol. Chem.* **264,** 8171–8178 (1989).

119. Tsien, R. Y. New calcium indicators and buffers with high selectivity against magnesium and protons: design, synthesis, and properties of prototype structures. *Biochemistry (Mosc.)* **19,** 2396–2404 (1980).

120. Escobar, A. L. *et al.* Role of inositol 1,4,5-trisphosphate in the regulation of ventricular Ca(2+) signaling in intact mouse heart. *J. Mol. Cell. Cardiol.* **53,** 768–779 (2012).

121. Sanchez, J. A. & Vergara, J. Modulation of Ca2+ transients by photorelease of caged nucleotides in frog skeletal muscle fibers. *Am. J. Physiol.* **266,** C1291-1300 (1994).

122. Escobar, A. L. *et al.* Kinetic properties of DM-nitrophen and calcium indicators: rapid transient response to flash photolysis. *Pflugers Arch.* **434,** 615–631 (1997).

123. Gurney, A. M., Nerbonne, J. M. & Lester, H. A. Photoinduced removal of nifedipine reveals mechanisms of calcium antagonist action on single heart cells. *J. Gen. Physiol.* **86,** 353–379 (1985).

124. Morad, M., Goldman, Y. E. & Trentham, D. R. Rapid photochemical inactivation of Ca2+-antagonists shows that Ca2+ entry directly activates contraction in frog heart. *Nature* **304,** 635–638 (1983).

125. Roberts, W. M. & Almers, W. An improved loose patch voltage clamp method using concentric pipettes. *Pflugers Arch.* **402,** 190–196 (1984).

126. Almers, W., Roberts, W. M. & Ruff, R. L. Voltage clamp of rat and human skeletal muscle: measurements with an improved loose-patch technique. *J. Physiol.* **347,** 751–768 (1984).

127. Zhang, H., Iijima, K., Huang, J., Walcott, G. P. & Rogers, J. M. Optical Mapping of Membrane Potential and Epicardial Deformation in Beating Hearts. *Biophys. J.* **111,** 438–451 (2016).

128. Boukens, B. J. & Efimov, I. R. A century of optocardiography. *IEEE Rev. Biomed. Eng.* **7,** 115–125 (2014).

129. Efimov, I. R. Innovation in optical imaging: looking inside the heart. *Heart Rhythm Off. J. Heart Rhythm Soc.* **4,** 925–926 (2007).

130. Antzelevitch, C. & Fish, J. Electrical heterogeneity within the ventricular wall. *Basic Res. Cardiol.* **96,** 517–527 (2001).

131. Boyett, M. R. A study of the effect of the rate of stimulation on the transient outward current in sheep cardiac Purkinje fibres. *J. Physiol.* **319,** 1–22 (1981).

132. Cranefield, P. F., Wit, A. L. & Hoffman, B. F. Genesis of cardiac arrhythmias. *Circulation* **47,** 190–204 (1973).

133. Lujan, H. L., Rivers, J. P. & DiCarlo, S. E. Complex and interacting influences of the autonomic nervous system on cardiac electrophysiology in conscious mice. *Auton. Neurosci. Basic Clin.* **201,** 24–31 (2016).

134. Nchimi, A., Davin, L., Georgiopoulos, A. & Lancellotti, P. Value of cardiac MRI to evaluate ischemia-related ventricular arrhythmia substrates. *Expert Rev. Cardiovasc. Ther.* **13,** 565–576 (2015).

135. Manning, A. S. & Hearse, D. J. Reperfusion-induced arrhythmias: mechanisms and prevention. *J. Mol. Cell. Cardiol.* **16,** 497–518 (1984).

136. Manning, A. S., Coltart, D. J. & Hearse, D. J. Ischemia and reperfusion-induced arrhythmias in the rat. Effects of xanthine oxidase inhibition with allopurinol. *Circ. Res.* **55,** 545–548 (1984).

137. Corr, P. B. & Witkowski, F. X. Potential electrophysiologic mechanisms responsible for dysrhythmias associated with reperfusion of ischemic myocardium. *Circulation* **68,** I16-24 (1983).

138. Lazzerini, P. E., Capecchi, P. L., Acampa, M., Galeazzi, M. & Laghi-Pasini, F. Arrhythmic risk in rheumatoid arthritis: the driving role of systemic inflammation. *Autoimmun. Rev.* **13,** 936–944 (2014).

139. Gabriel, S. E. Cardiovascular morbidity and mortality in rheumatoid arthritis. *Am. J. Med.* **121,** S9-14 (2008).

140. Maradit-Kremers, H., Nicola, P. J., Crowson, C. S., Ballman, K. V. & Gabriel, S. E. Cardiovascular death in rheumatoid arthritis: a population-based study. *Arthritis Rheum.* **52,** 722–732 (2005).

141. Wållberg-Jonsson, S., Johansson, H., Ohman, M. L. & Rantapää-Dahlqvist, S. Extent of inflammation predicts cardiovascular disease and overall mortality in seropositive rheumatoid arthritis. A retrospective cohort study from disease onset. *J. Rheumatol.* **26,** 2562–2571 (1999).

142. Gillis, R. A. Role of the nervous system in the arrhythmias produced by coronary occlusion in the cat. *Am. Heart J.* **81,** 677–684 (1971).

143. Shen, M. J. & Zipes, D. P. Role of the autonomic nervous system in modulating cardiac arrhythmias. *Circ. Res.* **114,** 1004–1021 (2014).

144. Zell, S. C. & Kurtz, K. J. Severe exposure hypothermia: a resuscitation protocol. *Ann. Emerg. Med.* **14,** 339–345 (1985).

145. Cohen, H. C., D'Cruz, I., Arbel, E. R., Langendorf, R. & Pick, A. Tachycardia and bradycardia-dependent bundle branch block alternans: clinical observations. *Circulation* **55,** 242–246 (1977).

146. Cardinal, R. *et al.* Mapping of ventricular tachycardia induced by thoracic neural stimulation in dogs. *Can. J. Physiol. Pharmacol.* **64,** 411–418 (1986).

147. Cohen, H. C., D'Cruz, I. A. & Pick, A. Effects of stable and changing rates and premature ventricular beats on transient tachycardia-, pseudobradycardia-, and bradycardia-dependent bundle branch block alternans. *J. Electrocardiol.* **12,** 151–156 (1979).

148. Pham, Q., Quan, K. J. & Rosenbaum, D. S. T-wave alternans: marker, mechanism, and methodology for predicting sudden cardiac death. *J. Electrocardiol.* **36 Suppl,** 75–81 (2003).

149. Yan, G. X. & Antzelevitch, C. Cellular basis for the normal T wave and the electrocardiographic manifestations of the long-QT syndrome. *Circulation* **98,** 1928–1936 (1998).

150. Gehi, A. K., Stein, R. H., Metz, L. D. & Gomes, J. A. Microvolt T-wave alternans for the risk stratification of ventricular tachyarrhythmic events: a meta-analysis. *J. Am. Coll. Cardiol.* **46,** 75–82 (2005).

151. Kanaporis, G. & Blatter, L. A. The mechanisms of calcium cycling and action potential dynamics in cardiac alternans. *Circ. Res.* **116,** 846–856 (2015).

152. Kang, M., Chung, K. Y. & Walker, J. W. G-protein coupled receptor signaling in myocardium: not for the faint of heart. *Physiol. Bethesda Md* **22,** 174–184 (2007).

153. Scott, J. D. & Pawson, T. Cell signaling in space and time: where proteins come together and when they're apart. *Science* **326,** 1220–1224 (2009).

154. Calloe, K., Goodrow, R., Olesen, S.-P., Antzelevitch, C. & Cordeiro, J. M. Tissue-specific effects of acetylcholine in the canine heart. *Am. J. Physiol. Heart Circ. Physiol.* **305,** H66-75 (2013).

155. Dobrzynski, H. *et al.* Distribution of the muscarinic K+ channel proteins Kir3.1 and Kir3.4 in the ventricle, atrium, and sinoatrial node of heart. *J. Histochem. Cytochem. Off. J. Histochem. Soc.* **49,** 1221–1234 (2001).

156. McMorn, S. O., Harrison, S. M., Zang, W. J., Yu, X. J. & Boyett, M. R. A direct negative inotropic effect of acetylcholine on rat ventricular myocytes. *Am. J. Physiol.* **265,** H1393-1400 (1993).

157. Corey, S., Krapivinsky, G., Krapivinsky, L. & Clapham, D. E. Number and stoichiometry of subunits in the native atrial G-protein-gated K+ channel, IKACh. *J. Biol. Chem.* **273,** 5271–5278 (1998).

158. Pfaffl, M. W. A new mathematical model for relative quantification in real-time RT-PCR. *Nucleic Acids Res.* **29,** e45 (2001).

159. Fozzard, H. A. Excitation-contraction coupling in the heart. *Adv. Exp. Med. Biol.* **308,** 135–142 (1991).

160. Nearing, B. D., Oesterle, S. N. & Verrier, R. L. Quantification of ischaemia induced vulnerability by precordial T wave alternans analysis in dog and human. *Cardiovasc. Res.* **28,** 1440–1449 (1994).

161. Pastore, J. M., Girouard, S. D., Laurita, K. R., Akar, F. G. & Rosenbaum, D. S. Mechanism linking T-wave alternans to the genesis of cardiac fibrillation. *Circulation* **99,** 1385–1394 (1999).

162. Osadchii, O. E. Effects of ventricular pacing protocol on electrical restitution assessments in guinea-pig heart. *Exp. Physiol.* **97,** 807–821 (2012).

163. Kalb, S. S. *et al.* The restitution portrait: a new method for investigating rate-dependent restitution. *J. Cardiovasc. Electrophysiol.* **15,** 698–709 (2004).

164. Wang, L. *et al.* Optical mapping of sarcoplasmic reticulum Ca2+ in the intact heart: ryanodine receptor refractoriness during alternans and fibrillation. *Circ. Res.* **114,** 1410–1421 (2014).

165. Bondarenko, V. E. & Rasmusson, R. L. Transmural heterogeneity of repolarization and Ca2+ handling in a model of mouse ventricular tissue. *Am. J. Physiol. Heart Circ. Physiol.* **299,** H454-469 (2010).

166. Cordeiro, J. M., Greene, L., Heilmann, C., Antzelevitch, D. & Antzelevitch, C. Transmural heterogeneity of calcium activity and mechanical function in the canine left ventricle. *Am. J. Physiol. Heart Circ. Physiol.* **286,** H1471-1479 (2004).

167. Laurita, K. R., Katra, R., Wible, B., Wan, X. & Koo, M. H. Transmural heterogeneity of calcium handling in canine. *Circ. Res.* **92,** 668–675 (2003).

168. Dumaine, R. & Antzelevitch, C. Molecular mechanisms underlying the long QT syndrome. *Curr. Opin. Cardiol.* **17,** 36–42 (2002).

169. Escobar, A. L. & Valdivia, H. H. Cardiac alternans and ventricular fibrillation: a bad case of ryanodine receptors reneging on their duty. *Circ. Res.* **114,** 1369–1371 (2014).

170. Puglisi, J. L., Bassani, R. A., Bassani, J. W., Amin, J. N. & Bers, D. M. Temperature and relative contributions of Ca transport systems in cardiac myocyte relaxation. *Am. J. Physiol.* **270,** H1772-1778 (1996).

171. Sumbera, J., Kruta, V. & Bravený, P. Influence of a rapid change of temperature on the mechanical response of mammalian myocardium. *Arch. Int. Physiol. Biochim.* **74,** 627–641 (1966).

172. Langer, G. A. & Brady, A. J. The effects of temperature upon contraction and ionic exchange in rabbit ventricular myocardium. Relation to control of active state. *J. Gen. Physiol.* **52,** 682–713 (1968).

173. Egorov, Y. V., Glukhov, A. V., Efimov, I. R. & Rosenshtraukh, L. V. Hypothermia-induced spatially discordant action potential duration alternans and arrhythmogenesis in nonhibernating versus hibernating mammals. *Am. J. Physiol. Heart Circ. Physiol.* **303,** H1035-1046 (2012).

174. Clusin, W. T. Mechanisms of calcium transient and action potential alternans in cardiac cells and tissues. *Am. J. Physiol. Heart Circ. Physiol.* **294,** H1–H10 (2008).

175. Díaz, M. E., O'Neill, S. C. & Eisner, D. A. Sarcoplasmic reticulum calcium content fluctuation is the key to cardiac alternans. *Circ. Res.* **94,** 650–656 (2004).

176. Kobayashi, S. *et al.* Low-dose β-blocker in combination with milrinone safely improves cardiac function and eliminates pulsus alternans in patients with acute decompensated heart failure. *Circ. J. Off. J. Jpn. Circ. Soc.* **76,** 1646–1653 (2012).

177. Jacobowitz, D., Cooper, T. & Barner, H. B. Histochemical and chemical studies of the localization of adrenergic and cholinergic nerves in normal and denervated cat hearts. *Circ. Res.* **20,** 289–298 (1967).

178. Ulphani, J. S. *et al.* Quantitative analysis of parasympathetic innervation of the porcine heart. *Heart Rhythm Off. J. Heart Rhythm Soc.* **7,** 1113–1119 (2010).

179. Napolitano, L. M., Willman, V. L., Hanlon, C. R. & Cooper, T. INTRINSIC INNERVATION OF THE HEART. *Am. J. Physiol.* **208,** 455–458 (1965).

180. Levy, M. N. & Zieske, H. Effect of enhanced contractility on the left ventricular response to vagus nerve stimulation in dogs. *Circ. Res.* **24,** 303–311 (1969).

181. Logothetis, D. E., Kurachi, Y., Galper, J., Neer, E. J. & Clapham, D. E. The beta gamma subunits of GTP-binding proteins activate the muscarinic K+ channel in heart. *Nature* **325,** 321–326 (1987).

182. Brodde, O. E. & Michel, M. C. Adrenergic and muscarinic receptors in the human heart. *Pharmacol. Rev.* **51,** 651–690 (1999).

183. Machida, T. *et al.* Effects of a highly selective acetylcholine-activated K+ channel blocker on experimental atrial fibrillation. *Circ. Arrhythm. Electrophysiol.* **4,** 94–102 (2011).

184. Ravens, U. & Christ, T. Atrial-selective drugs for treatment of atrial fibrillation. *Herzschrittmachertherapie Elektrophysiologie* **21,** 217–221 (2010).

185. Gaborit, N. *et al.* Regional and tissue specific transcript signatures of ion channel genes in the non-diseased human heart. *J. Physiol.* **582,** 675–693 (2007).

186. Ng, G. A., Brack, K. E., Patel, V. H. & Coote, J. H. Autonomic modulation of electrical restitution, alternans and ventricular fibrillation initiation in the isolated heart. *Cardiovasc. Res.* **73,** 750–760 (2007).